THE UNIVERSITY OF QUEENSLAND

AUSTRALIA

Biophysical and Structural Studies of *Escherichia coli* Mechanosensitive Channel of Large Conductance in Lipid Bilayers

Gamma Chi

Bachelor of Science (Honours), First Class

A thesis submitted for the degree of Doctor of Philosophy at

The University of Queensland in 2016

Institute for Molecular Biosciences

Abstract

A major challenge of drug development is maximising specificity and efficacy at the lowest possible dose to minimise toxic side effects (Basile *et al.*, 2012). Not only are the pharmaceutical windows small for both drug candidates and approved drugs alike, but they can also vary between individuals, making a dose level safe for one individual potentially harmful for another. One strategy for overcoming this problem is to develop new drug delivery methods where the drug is preferentially concentrated at the site of disease (Basile *et al.*, 2012). In this respect, liposomal drug delivery systems have been used with success in topical applications in skin cancer treatment, and there is significant research interest in engineering similar systems for intravenous administration (Al-Jamal & Kostarelos, 2011; Fan & Zhang, 2013). Incorporating nanovalves into liposomes with controllable gating properties would further enhance the usefulness of liposomal drug delivery systems, providing a method to further regulate the release of liposome-encapsulated drugs from liposomes at the target site (Martinac *et al.*, 2014).

The mechanosensitive channel of large conductance (MscL) has been identified as a major candidate for the development of a protein-based nanovalve (Martinac *et al.*, 2014). More generally, MscL is a prototype for the class of ion channels primarily gated by membrane tension, which includes medically significant proteins such as Piezo channels and TRP-type sodium channels (Martinac, 2011). As a well-expressing protein from *Escherichia coli*, MscL has been extensively studied both structurally and biophysically (Martinac, 2011). However, the channel gating mechanism of MscL, and by extension of mechanosensitive channels in general, remains poorly understood at the molecular level.

This thesis aims to investigate the relationship between *E. coli* MscL and phospholipids both in the context of its structure and its behaviour in a lipid bilayer environment. While much has been studied on the channel gating properties of MscL in various phospholipid environments (Anishkin *et al.*, 2005; Iscla *et al.*, 2004; Iscla *et al.*, 2011; Levin & Blount, 2004; Powl *et al.*, 2008b; Tsai *et al.*, 2005; Yoshimura *et al.*, 2004), there remains a limited understanding of the behaviour and distribution of MscL in the bilayer. These are not only important from academic perspective as well as in the context of nanovalve development, but also for example, to identify factors which may limit the functional studies on MscL. More specifically, this thesis has focused on the identification of phospholipids closely associating with MscL, the distribution of MscL in phospholipid bilayers, and the incorporation of MscL into liposomes with heterogeneous phospholipids.

The first research chapter (Chapter 2) outlines the optimisation of MscL expression and purification system for biophysical and structural studies. The original MscL construct had problems of

heterogeneous expression and being not well-suited to reliable quantification by routine methods. New constructs were successfully designed to overcome these issues, and the results have been published in European Biophysical Journal.

Chapter 3 investigates the interaction between MscL and phospholipids at the biophysical level. At the start of the project, it was hypothesised that there were functionally relevant native phospholipids associating with *E. coli* MscL. Thin layer chromatography of purified MscL showed a different lipid profile from native *E. coli* lipid and confirmed the presence of tightly-associating lipids. The same technique was then employed to purify these phospholipids for identification by lipid mass spectrometry. MscL was also reconstituted back into heterogeneous phospholipid liposome samples in order to identify any preference of its incorporation as well as any effects of these factors on its channel gating function and distribution within liposomes. Lastly, MscL was reconstituted into liposomes prepared from pure phospholipids and studied with electron microscopy in order to further identify the lipid effects on MscL function.

Chapter 4 outlines the efforts to experimentally determine a high-resolution structure of *E. coli* MscL. A wide range of techniques were employed, including 2D crystallisation, 3D crystallisation, and single particle electron microscopy. For 2D crystallisation experiments, both the traditional crystallisation experiments based on the successful attempt by (Saint *et al.*, 1998) and monolayer-assisted method described by (Landsberg *et al.*, 2010) have been employed and described in this thesis. In parallel, 3D crystallisation of detergent-solubilised *E. coli* MscL has been attempted, with some promising initial outcome.

Declaration by author

This thesis is composed of my original work, and contains no material previously published or written by another person except where due reference has been made in the text. I have clearly stated the contribution by others to jointly-authored works that I have included in my thesis.

I have clearly stated the contribution of others to my thesis as a whole, including statistical assistance, survey design, data analysis, significant technical procedures, professional editorial advice, and any other original research work used or reported in my thesis. The content of my thesis is the result of work I have carried out since the commencement of my research higher degree candidature and does not include a substantial part of work that has been submitted to qualify for the award of any other degree or diploma in any university or other tertiary institution. I have clearly stated which parts of my thesis, if any, have been submitted to qualify for another award.

I acknowledge that an electronic copy of my thesis must be lodged with the University Library and, subject to the policy and procedures of The University of Queensland, the thesis be made available for research and study in accordance with the Copyright Act 1968 unless a period of embargo has been approved by the Dean of the Graduate School.

I acknowledge that copyright of all material contained in my thesis resides with the copyright holder(s) of that material. Where appropriate I have obtained copyright permission from the copyright holder to reproduce material in this thesis.

Publications during candidature

B. Martinac, T. Nomura, **G. Chi**, E. Petrov, P. R. Rohde, A. R. Battle, A. Foo, M. Constantine, R. Rothnagel, S. Carne, E. Deplazes, B. Cornell, C. G. Cranfield, B. Hankamer and M. J. Landsberg (**2014**). "*Bacterial mechanosensitive channels: models for studying mechanosensory transduction*." Antioxid Redox Signal 20(6): 952-969.

G. Chi, P. R. Rohde, P. Ridone, B. Hankamer, B. Martinac and M. J. Landsberg (**2015**). "*Functional similarities between heterogeneously and homogenously expressed MscL constructs.*" Eur Biophys J 44(7): 589-598.

A. Foo, A. R. Battle, **G. Chi**, B. Hankamer, M. J. Landsberg and B. Martinac (**2015**). "*Inducible release of particulates from liposomes using the mechanosensitive channel of large conductance and L-alpha-lysophosphatidylcholine.*" Eur Biophys J 44(7): 521-530.

Publications included in this thesis

Incorporated as part of Chapter 2:

G. Chi, P. R. Rohde, P. Ridone, B. Hankamer, B. Martinac and M. J. Landsberg (**2015**). "*Functional similarities between heterogeneously and homogenously expressed MscL constructs.*" Eur Biophys J 44(7): 589-598.

Contributor	**Statement of contribution**
Gamma Chi (Candidate)	Designed experiments (60 %) Performed experiments (70 %) - Construct design, synthesis, and sequence verification - Protein expression and purification - Protein quantification - SDS-PAGE Analysed data (60 %) - Analysis of MscL constructs - Review of statistical analysis of patch clamp data Wrote the paper draft (80 %) Reviewed the paper draft (40 %)

Paul R. Rohde	Performed experiments (5 %) - Prepared samples for patch clamp experiments
Pietro Ridone	Performed experiments (10 %) - Performed patch clamp experiments Analysed data (10 %) - Performed statistical analysis of patch clamp data Wrote the paper draft (5 %) - Patch clamp subsection of the Methods section
Ben Hankamer	Chief investigator for the project grant (50 %) Reviewed the paper draft (10 %)
Boris Martinac	Chief investigator for the project grant (50 %) Analysed data (10 %) - Performed statistical analysis of patch clamp data Wrote the paper draft (5 %) - Patch clamp subsection of the Methods section Reviewed the paper draft (10 %)
Michael Landsberg	Designed experiments (40 %) Performed experiments (15 %) - Mass spectrometry of N-terminal MscL fragment Analysed data (20 %) - Mass spectrometry of N-terminal MscL fragment - Analysis of MscL constructs Wrote the paper draft (10 %) - Mass spectrometry of N-terminal MscL fragment - General guidance with paper writing Reviewed the paper draft (40 %)

Contributions by others to the thesis

Prof. Ben Hankamer (Institute for Molecular Biosciences, University of Queensland) and Dr. Michael Landsberg (School of Chemistry and Molecular Biosciences, University of Queensland), who are my supervisors, have made significant contributions to the project design and data analysis throughout the thesis. They have also made significant contributions to the publications in my PhD candidature, one of which is included in this thesis.

Dr. Alexander Foo (IMB, UQ) has made minor contributions to the project design and data analysis throughout the thesis. He has given significant assistance with sucrose gradient experiment (section 3.3.2.), and has also assisted with dynamic light scattering experiment (section 3.3.2.). He has also provided the data on MscL's sensitivity to lysophosphatidylcholine, from which a figure was derived and used in the discussion in section 3.3.2.

Prof. Boris Martinac (Victor Chang Cardiac Research Institute), Pietro Ridone (VCCRI), and Paul Rohde (VCCRI) have made significant contributions with the patch clamp experiments in Chapter 2. The details are listed in the publication section above.

Prof. Stephen Blanksby (Queensland University of Technology) has provided significant contributions to the lipid mass spectrometry in section 3.3.1. and 3.3.2.

Dr. Jennifer Yarnold (IMB, UQ) has made a minor contribution to the Matlab script design in section 3.3.3. of Chapter 3.

Dr. Suzanne Norwood (IMB, UQ), Irene Chassagnon (IMB, UQ) and Jannah Jeon (SCMB, UQ) have provided minor assistance with 3D crystallisation (section 4.3.2.).

Statement of parts of the thesis submitted to qualify for the award of another degree

No part of the thesis has been submitted for the award of another degree.

Acknowledgements

My first acknowledgement goes to my supervisors, Prof. Ben Hankamer and Dr. Michael Landsberg. Both were incredibly supportive and helpful with my PhD candidature, and I cannot thank them enough for their assistance. Their involvement with all aspects of my degree, ranging from project design and data analysis to more personal support such as advice on what I wanted to out of my years in PhD, cannot be understated. They have been a tremendous influence on me as a scientist, and of course, for the better.

I would also like to thank the collaborators for this project, Prof. Boris Martinac and Prof. Stephen Blanksby. Their research contributions and assistance with data analysis were critical to my PhD project. In particular, I would like to thank Boris and his research group for the kind hospitality during the week-long visit for training on automated patch clamp experiments at the Victor Chang Cardiac Research Institute.

A special mention goes to Dr. Alexander Foo, who also worked on MscL for his PhD. He made my project much easier simply by being the student who worked on MscL before me, as it would have taken an extra year to produce the works in this thesis had it not been for his optimisation trials on sucrose gradient experiments. His advice with experiment design and data analysis was also invaluable to my research project.

In addition, I thank the members and alumni of the Hankamer group and the spin-off Landsberg group for the assistance both in and out of the laboratory. Their experiences with the PhD greatly helped me guide through my own PhD course, and the many trips with them, both literal and figurative, will be some of the fondest memories of my life. For this I cannot thank them enough.

I also thank the administrative staff at the Institute for Molecular Biosciences. They made operations of the institute, by extension my candidature as well, as seamless as it could realistically be. In particular, the floor manager, Mikiko Miyagi, did an excellent job looking after the equipments; Dr. Amanda Carozzi, a truly irreplaceable figure without whom many of the PhD students at the institute would have had mental breakdown; and the financial staff, who really helped me out with the sometimes confusing paperwork.

The many friends outside of the research circle were also critical to my candidature. Oftentimes it was not easy to get my mind off the project, and they were really helpful to getting me to do it.

The level of support my parents and my only sibling, Ben (not my supervisor), throughout my candidature and beyond cannot be overstated. Nothing that I have achieved would have been possible without them. It is truly a blessing to have them as my parents and have him as my brother.

I thank my girlfriend Jannah Jeon for the support in and out of the laboratory. Not only did she provide assistance as a fellow protein biologist, but she also enriched my life in many regards. I would like to acknowledge her family for also being incredibly supportive, as well.

I thank the Australian government for the Australian Postgraduate Award, which covered much of my living stipend, the National Health and Medical Research Committee for the research funding, and the University of Queensland for the beautiful campus and their services.

In a special mention, I would like to thank myself for persevering through the arduous course the PhD has been. In the last count, over 12,000 work hours were invested in this project, and this dedication was made possible by my conviction that this research would be a small but meaningful contribution to the mankind. And with this acknowledgement, I have to state that it was humbling experience to firsthand learn the level of effort that goes into every paper we often read without second thought.

Lastly but not in the least, I would like to thank the examiners in advance for reviewing this thesis. Their critical input to this thesis will be greatly appreciated regardless of the verdict.

Keywords

mscl, mechanosensitive channel, biophysics, nanovalves, protein crystallography, construct design, escherichia coli, membrane protein, channel proteins

Australian and New Zealand Standard Research Classifications (ANZSRC)

ANZSRC code: 029901, Biological Physics, 70 %

ANZSRC code: 060112, Structural Biology, 10%

ANZSRC code: 060199, Biochemistry and Cell Biology not elsewhere classified, 20%

Fields of Research (FoR) Classification

FoR code: 0299, Other Physical Sciences, 70 %

FoR code: 0601, Biochemistry and Cell Biology, 20%

FoR code: 0699, Other Biological Sciences, 10%

List of Figures

List of Tables

List of Abbreviations

β-DDM	N-dodecyl-β-D-Maltopyranoside
2D	Two dimensional
3D	Three dimensional
Abs	Absolute value
AFM	Atomic force microscopy
BCA assay	Bicinchoninic acid assay
C:M:W	Chloroform:Methanol:Water
C1	Cytoplasmic domain 1
C2	Cytoplasmic domain 2
CCD	Charge-coupled Detector
CFTR	Cystic fibrosis transmembrane conductance regulator
CMC	Critical micelle concentration
CV	Column volume
DM	N-decyl-β-D-Maltopyranoside
DMPC	1,2-dimyristoyl-sn-glycero-3-phosphocholine
DNA	Deoxyribonucleic acid
DOPC	1,2-dioleoyl-sn-glycero-3-phosphocholine
DOPE	1,2-dioleoyl-sn-glycero-3-phosphoethanolamine
DOPS	1,2-dioleoyl-sn-glycero-3-phospho-L-serine
DPPC	1,2-dipalmitoyl-sn-glycero-3-phosphocholine
E. coli	*Escherichia coli*
EM	Electron microscopy
Fr1	DNA fragment 1
Fr2	DNA fragment 2
Fr3	DNA fragment 3

Fr4	DNA fragment 4
Fr5	DNA fragment 5
Fr6	DNA fragment 6
Fr7	DNA fragment 7
FRET	Förster resonance energy transfer
FTIR	Fourier-transform infrared spectroscopy
GPCR	G-protein coupled receptor
His	Histidine
IPTG	Isopropyl β-D-1-thiogalactopyranoside
IR	Infrared
K2P	Two-pore domain potassium channel
kDa	kilodalton
keV	kiloelectron volt
kHz	Kilohertz
LB	L-broth
LC-MS/MS	Liquid chromatography-mass spectrometer
LPC	Lysophosphatidylcholine
M. acetivorans	*Methanosarcina acetivorans*
M. tuberculosis	*Mycobacterium tuberculosis*
MscL	Mechanosensitive channel of large conductance
MscL^{G22C}	MscL with G22C substitution mutation
MscL^{L-7W}	MscL with leucine-to-tryptophan substitution at 7 residues upstream of the wild-type MscL region
MscL^{L-7Y}	MscL with leucine-to-tyrosine substitution at 7 residues upstream of the wild-type MscL region
MscL^{M1A}	MscL with M1A substitution mutation

MscL^{TEVc}	MscL with the substitution of methionine-1 of the wild-type MscL region and six residues upstream of this residues with TEV protease recognition sequence
MscS	Mechanosensitive channel of small conductance
MTSET	[2-(Trimethylammonium)ethyl] Methanethiosulfonate
MWCO	Molecular weight cut off
N/A	Not available
Ni-NTA	Nickel ion-immobilised nitriloacetic acid
OG	n-octyl-β-d-glucopyranoside
P:L	Protein-to-lipid ratio
PBS	Phosphate-buffered saline
PC	Phosphatidylcholine
PCR	Polymerase chain reaction
PD1 Buffer	PBS, β-DDM buffer (PBS pH 7.4, 1 mM β-DDM)
PD8 Buffer	PBS, β-DDM buffer (PBS pH 7.4, 8 mM β-DDM)
PDI1-15 Buffer	PBS, β-DDM, Imidazole buffer (PBS pH 7.4, 1 mM β-DDM, 15 mM Imidazole)
PDI1-300 Buffer	PBS, β-DDM, Imidazole buffer (PBS pH 7.4, 1 mM β-DDM, 300 mM Imidazole)
PE	Phosphatidylethanolamine
PEG	Poly-ethylene glycol
PG	Phosphatidylglycerol
PhD	Doctor of philosophy
PI	Phosphatidylinositol
Piezo1	Piezo1 mechanosensitive channel
Piezo2	Piezo1 mechanosensitive channel
PNK	Polynucleotide kinase

POPC	1-palmitoyl-2-oleoyl-sn-glycero-3-phosphocholine
POPG	1-palmitoyl-2-oleoyl-sn-glycero-3-phospho-(1'-rac-glycerol)
PS	Phosphatidylserine
psi	Pounds per square inch
R_f	Retention factor
RKKEE	Arginine-Lysine-Lysine-Glutamate-Glutamate motif
RP-HPLC	Reverse-phase high performance liquid chromatography
S. aureus	*Staphylococcus aureus*
S1	Soluble domain 1
SANS	Small angle neutron scattering
SDS	Sodium dodecylsulphate
SDS-PAGE	SDS-polyacrylamide gel electrophoresis
T:A:M:W	Toluene:acetone:methanol:water
TEV protease	Tobacco etch virus protease
TLC	Thin layer chromatography
TM	Transmembrane
TM1	Transmembrane helix 1
TM2	Transmembrane helix 2
TRAAK	TWIK-related arachidonic acid-stimulated potassium channel
TREK1	TWIK-related potassium channel 1
TREK2	TWIK-related potassium channel 2
Trp	Tryptophan
TRP Channel	Transient receptor potential channel
TrpA1	Transient receptor potential channel, subfamily A, member 1
TrpV1	Transient receptor potential channel, subfamily V, member 1
TrpV4	Transient receptor potential channel, subfamily V, member 4
UV	Ultraviolet

v/v	volume-to-volume
w/v	weight-to-volume
w/w	weight-to-weight
WT	Wild type

1. Introduction

1.1. Drug Delivery Methods

Globally the pharmaceutical industry is focused on developing highly effective and specific drugs with minimal side effects. However, most drug candidates act on non-targeted tissues through either specific or nonspecific interactions, causing side effects. The levels at which many drugs are both safe enough for administration and effective for the intended use, called pharmaceutical window, are often too narrow or too variable between individuals to be used. Lack of efficacy at the safe level of dose has led to the failure of a third of Phase II clinical trials in 2004-2010 (Ledford, 2011), with another quarter of drug candidates in Phase III trials not approved for this reason (Fig. 1.1) (Hay *et al.*, 2014; Ledford, 2011). In response to this, pharmaceutical companies often raise the price of new drugs to recoup the loss, and ultimately develop new agents or techniques which limit the side effects of active compounds. Such methods add financial burden and uncertainty to both the companies and the patients, contributing to the rise in health care costs.

One of the reasons for drugs affecting non-target tissues is the fact that both oral and intravenous administration typically results in an even distribution of the drug throughout the body via the circulatory system (Egusquiaguirre *et al.*, 2012). Non-target tissues are therefore exposed to similar drug concentrations as target tissues, resulting in unpredictable and potentially undesirable

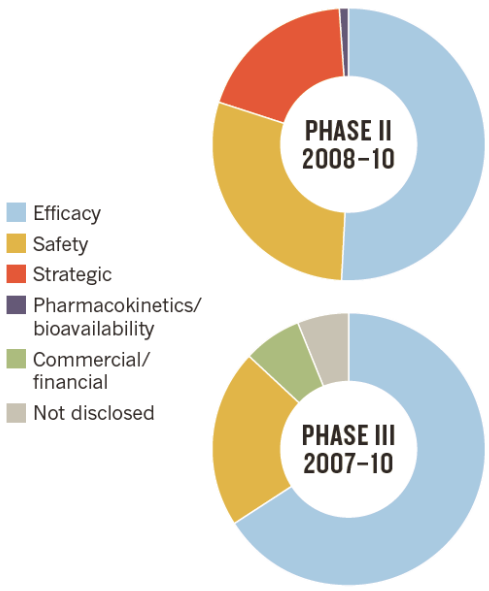

Figure 1.1. Causes of Product Failures in Phase II and Phase III Clinical Trials. Figure courtesy of (Ledford, 2011)

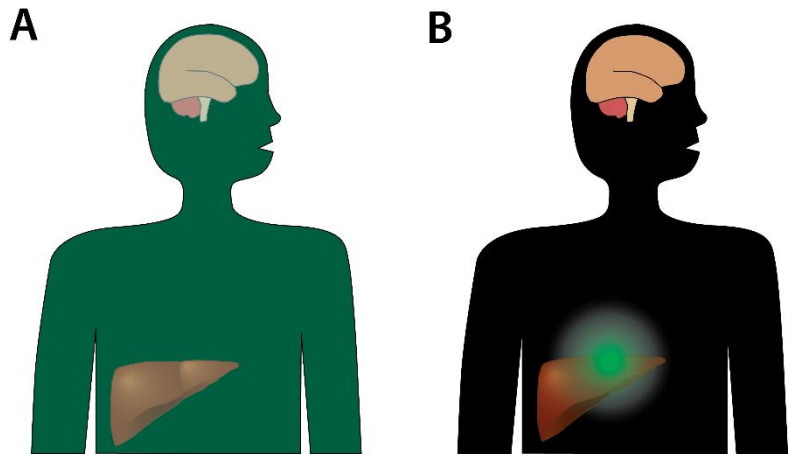

Figure 1.2. Schematic Diagram of Targeted Drug Delivery system. **A**) In a standard drug administration, drug (green) will be evenly distributed across the body and affect both target and non-target tissues. **B**) In a targeted drug delivery system, drug will localise to the target tissue, and non-target tissues will be less affected.

consequences. This is of particular concern for anti-cancer and hormonal drugs (Kubek *et al.*, 2009; Montemurro *et al.*, 2012; Nicolas *et al.*, 2013), in which target proteins are often expressed in both target and non-target tissues. These classes of drugs account for a large portion of both existing drugs and those in development (Hay *et al.*, 2014; Ledford, 2011), so there have been significant efforts to address this simple but serious issue.

A solution to this problem is to increase localisation of drugs to the target tissue, thereby minimising side effects on the healthy tissue (Basile *et al.*, 2012) (Fig. 1.2). In the case that excess drug is administered at the target tissue, the concentration will become diluted to levels below the toxic threshold once the excess or non-adsorbed molecules are in circulation. An added advantage of this approach is that the overall required dose to be administered to the patient becomes much lower as a result of more efficient delivery. This is beneficial not only for drugs with high toxicity but also for expensive ones such as biologics where cost is often a major factor limiting patient access (Kubek *et al.*, 2009). Consequently, targeted drug delivery systems can reduce cost while increasing safety and efficacy of drugs.

There are two main approaches to develop targeted drug delivery systems. The first method is to directly apply drugs at the target tissue. Examples of this strategy include the treatment of superficial infections with topical drugs which are poorly absorbed through the skin, hence remaining at the intended site of action without reaching the circulatory system (Tomalik-Scharte *et al.*, 2005). Physically immobilised drugs are also commonly used in bone fracture repair and surgery of atherosclerotic blood vessels, where implants are often coated with drugs to prevent infection, induce repair and reduce inflammation without affecting the whole body (Hussain, 2012; Trajkovski *et al.*, 2012; Weinberg *et al.*, 2008). Currently related strategies such as carmustine

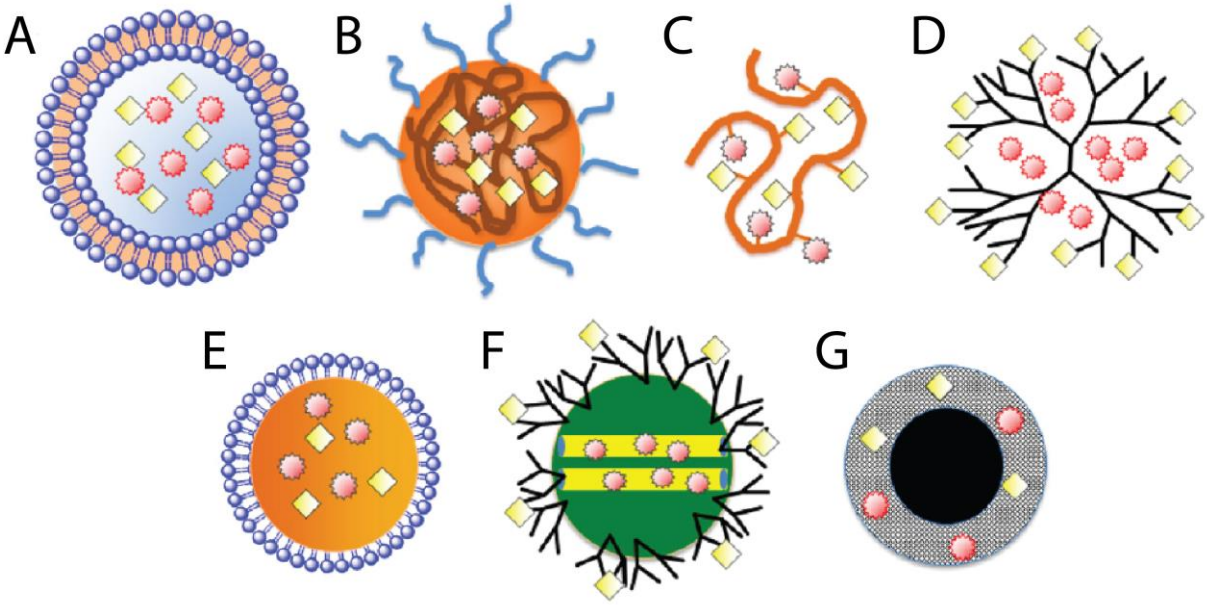

Figure 1.3. Schematic figures of various nanoparticle drug carriers. Yellow particles represent hydrophilic drug molecules, and pink particles represent hydrophobic drug molecules. **A**) liposome; **B**) polymeric micelle; **C**) polymer-drug conjugate; **D**) dendromer; **E**) oil nanoemulsion; **F**) mesoporous silica nanoparticle; **G**) iron oxide nanoparticle. Courtesy of (Hu & Zhang, 2012)

implants for brain tumours are undergoing clinical trials on cancer chemotherapies with positive results (Allhenn *et al.*, 2012), opening up new avenues for advanced healthcare.

In the second approach, drugs or drug delivery vehicles, which either are coated with, encapsulate, or otherwise internalise the drugs, are designed to be bioavailable only at the target site (Fig. 1.3) (Hu & Zhang, 2012). They can be injected into the bloodstream, and are designed to accumulate at the intended site of drug release using various mechanisms. This method has an advantage over physical implants in that surgical operation is not needed, as well as that cessation or modification of the therapy is more flexible. Several established systems, such as liposomal doxorubicin and cisplatin (Slingerland *et al.*, 2012), rely on nanoparticles for delivery to target sites with reduced off-target effects on healthy tissues. More advanced forms of nanoparticles for improved drug localisation need to overcome several problems before deployment. A major condition for clinically safe nanoparticles is that they must be hypoimmunogenic, biodegradable, and without toxicity (Nicolas *et al.*, 2013). This excludes a number of organic polymers and inorganic particles such as fullerene derivatives, gold particles and silica nanobeads, although the last of the three is still under consideration due to their high drug absorptivity (Dreaden *et al.*, 2012; Hu & Zhang, 2012). Remaining candidates include biopolymers such as polysaccharides and lipid-based nanoparticles such as niosomes and liposomes. The choice of drug carriers between them is likely to be both disease and drug-specific: drugs that require slow release will be more compatible with biopolymer systems while those requiring rapid release will be more suited to liposome encapsulation; and

lipid-based systems will be preferred for hydrophobic drugs.

1.2. Nanovalve-based Liposomal Drug Delivery System

1.2.1. Liposomal drug delivery system

A liposome is an approximately spherical nanoparticle with its interior separated from the outside by a lipid bilayer similar to a cell membrane. Liposomal drug delivery systems have advantages over other drug delivery methods in three areas. First, they can carry a range of cargo molecules (H. I. Chang & Yeh, 2012). Both small molecules and much larger ones such as proteins can be contained in liposomes, and hydrophobic molecules can be dissolved and carried in the lipid bilayer (Hu & Zhang, 2012). In addition, liposomes are capable of carrying polynucleotides, allowing their potential use in gene therapy (Caracciolo & Amenitsch, 2012). Second, liposomes are easily modifiable to accommodate various properties/function (Levchenko *et al.*, 2012; Slingerland *et al.*, 2012). For example, antibodies and polyethylene glycols can be added to improve their target specificity as well as reduced immunogenicity (Garnier *et al.*, 2012; Wolff *et al.*, 2010), and lipid composition has also been varied for improved solubility of specific drugs (Slingerland *et al.*, 2012). Third, liposomes can be easily adsorbed by tissues, as evidenced by topical liposomes commonly used by the cosmetic industry (Betz *et al.*, 2005; Posner, 2002) as well as for topical nystatin formulations (Torchilin, 2005).

Liposomal drug delivery systems have already found use as a drug administration strategy, particularly in cancer chemotherapy (H. I. Chang & Yeh, 2012; Fan & Zhang, 2013; Slingerland *et al.*, 2012). For example, doxorubicin is commonly encapsulated in liposomes, often coated with polyethylene glycol prior to intravenous delivery which achieves a minor targeting effect in treatment of skin cancers (H. I. Chang & Yeh, 2012). This strategy not only reduces doxorubicin's cardiotoxic effect, but also keeps concentration at the target site more consistent over time due to slower clearance from circulation. Such benefits make possible combined use with trastuzumab (Theodoulou & Hudis, 2004), another cardiotoxic anticancer agent, which has recently been use in chemotherapy (Gavila *et al.*, 2015; Tahover *et al.*, 2015; Uriarte-Pinto *et al.*, 2016), and several variations of the formulations are currently in clinical trials as well (Pircher *et al.*, 2015; Tuxen *et al.*, 2014). Successful uses of liposomes in drug formulations are expanding to other agents such as cisplatin, whose cytotoxicity and hydrophobicity have limited its use until now (Fan & Zhang, 2013).

1.2.2. Delivery Strategies for Liposomal Drug Delivery Systems

Despite these successes, there are also limitations to be overcome in order for this technology to become more widely applicable. Major disadvantages of liposomes are their relative instability compared to other nanoparticles, the large size which restricts their access to certain tissues (Heneweer *et al.*, 2012), and inefficient release of the drug molecules from the liposomes at the target site. With the first problem, there is active research to improve liposomes' stability through the use of synthetic lipids as well as establishing a scaffold within the liposomes and coating them with stabilising molecules (Al-Jamal & Kostarelos, 2011; H. I. Chang & Yeh, 2012; Egusquiaguirre *et al.*, 2012). With the second, it is possible to produce stable modifiable liposomes smaller than 100 nm, which is small enough to cross the blood-brain barrier. With the third challenge, liposomes which directly release drugs at the target site via nanovalves and those which undergo receptor-mediated fusion to the target cells are currently under development (Garnier *et al.*, 2012; Nakayama *et al.*, 2015).

1.2.2.1. Passive Targeting

There are three main ways for liposomes to accumulate in diseased tissues. Current successes rely heavily on passive targeting methods, where adsorption of liposomes relies largely on leaky vasculature (Fig. 1.4B) (Sawant & Torchilin, 2012). Liposomes usually have diameters of 100 - 300 nm, which are too large to pass through the walls of blood vessels (Fig. 1.4A) (Lammers *et al.*, 2012). In diseased tissues like tumours, however, inflammation and active angiogenesis make the vessel walls more permeable, allowing liposomes to pass through (Lammers *et al.*, 2012). Diseased tissues consequently become far more accessible to liposomes than healthy tissues, and are as a result subject to much higher concentrations of drugs released from them. However, this method has weaknesses in that A) a significant portion of drug release in the bloodstream could still affect healthy cells, B) inflamed non-target tissues or those undergoing active angiogenesis for other reasons (e.g. regeneration of uterus lining) will be exposed to similar levels of drugs, C) this strategy will be ineffective if the target tissue does not have liposome-permeable vasculature, and D) a slow and inconsistent rate of accumulation make the dosage at the target difficult to control (Lammers *et al.*, 2012; Sawant & Torchilin, 2012). Hence, other methods for targeting are desirable if liposomes are to find a broader use as a drug delivery system.

1.2.2.2. Active Targeting

More recent developments have seen successes in concentrating liposomes at targeted sites by embedding molecules with specific affinity to target cells on the liposomal membrane (Fig. 1.4C) (Basile *et al.*, 2012; Garnier *et al.*, 2012; Lammers *et al.*, 2012; Sawant & Torchilin, 2012). The

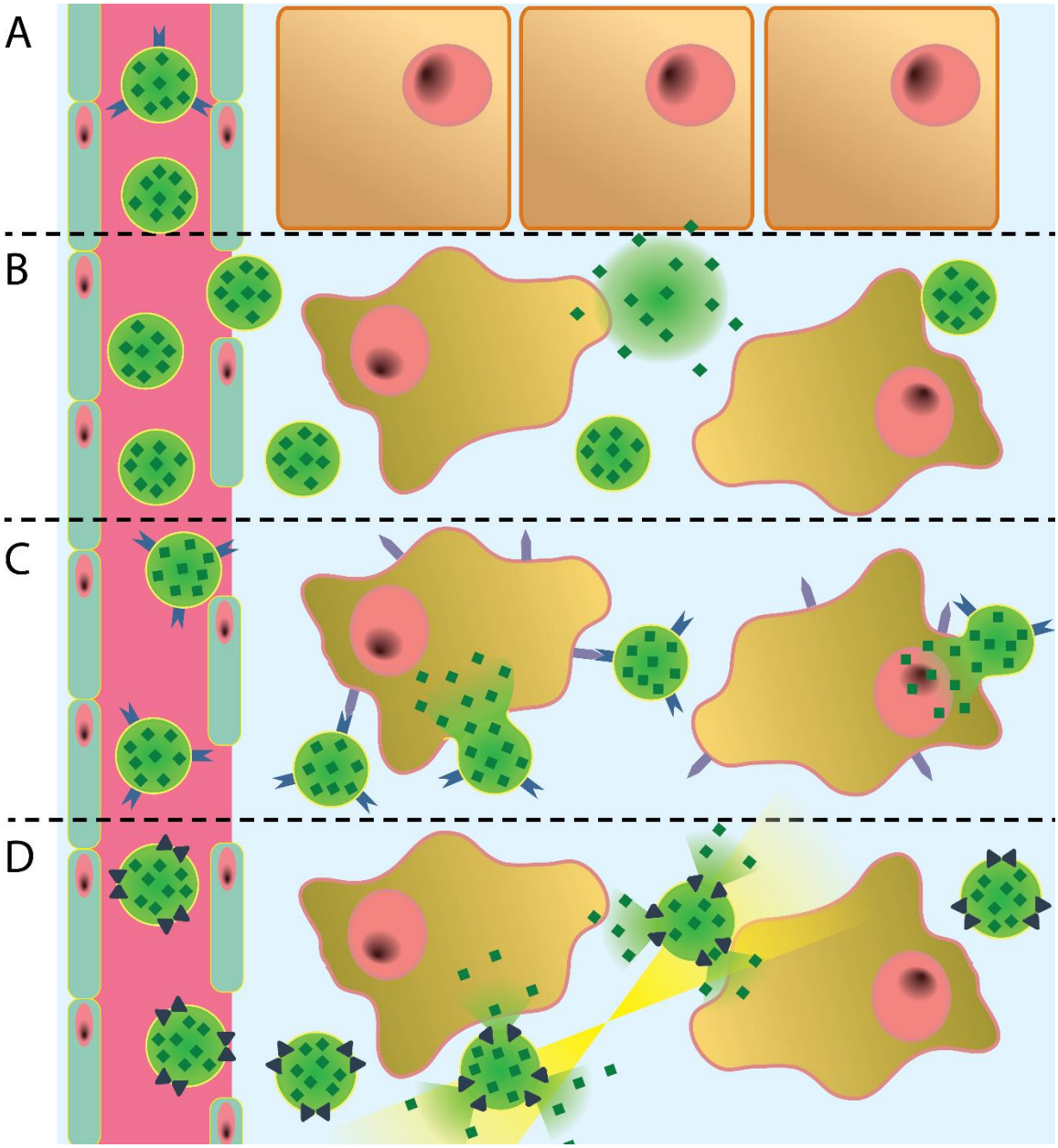

Figure 1.4. Schematic diagram of delivery strategies for liposomal drug delivery system. **A**) in healthy tissues, liposomes are too large to pass through the blood vessels (red); **B**) in diseased tissues, blood vessel walls are often more porous, allowing liposomes to deliver their cargo by passive diffusion; **C**) ligands such as antibodies on liposomes actively target diseased cells, and potentially release drugs directly into them; **D**) nanovalves on liposomes are induced to open by external triggers, releasing drugs at the target tissue.

specificity of these affinity tags can range from fairly low (e.g. polyethylene glycol and ionic tags) to highly specific (e.g. ligands) (Basile *et al.*, 2012; Fan & Zhang, 2013; Levchenko *et al.*, 2012). They can also facilitate fusion of liposomes with cell surface membranes depending on the tags used, releasing the cargo directly into the cell. This has the potential to effectively deliver drugs at effective doses even at a very low level of overall dose, and has also opened up the possibility of exploiting liposomes as potential delivery systems for gene therapy (Heneweer *et al.*, 2012; Levchenko *et al.*, 2012). Moreover, in the case of metastatic cancer, active targeting allows

liposomes to target cancer cells which have metastasised to other tissues. A basic form of active targeting strategy is already used for a chemotherapy formulation, where Doxil™ has polyethylene glycol on the liposomal surface to facilitate not only immune surveillance avoidance but also its accumulation in skin tissues in Kaposi's sarcoma (Northfelt *et al.*, 1996). A few cationic lipid-based liposomes are in clinical trials and ligand-based systems, particularly those using antibodies, are also subjects of intense research efforts, making the active targeting method a highly promising strategy for liposomal drug delivery and imaging systems (Heneweer *et al.*, 2012; Lammers *et al.*, 2012).

Active targeting strategies have a few significant disadvantages (Lammers *et al.*, 2012). Most affinity tags cannot be truly specific to the diseased tissue, as in most cases surface antigens and ligand receptors expressed by diseased cells are also expressed by at least some healthy cells, making them vulnerable to exposure of highly damaging concentrations of drugs (Lammers *et al.*, 2012). Ionic lipids will also be attracted to any surface with an opposing charge. Hence, while active targeting can be expected to contribute to greatly reduced side effects, those which remain may become exacerbated due to higher dosage to the affected cells. For example, Doxil has lower maximum tolerated dose than free doxorubicin injection (Gabizon, 2001), and it has greatly increased skin toxicity due to accumulation in healthy skin cells (Torchilin, 2006). This safety concern may therefore require additional clinical trials on each tagged liposome; i.e. since the safety and efficacy of actively targeting liposomes is additionally dependent on the affinity tag used, another clinical trial to assess them will be required in addition to trials establishing the safety and efficacy of the cargo drug. Moreover, different affinity tags would usually be required for different, significantly influencing the current versatility of generalised liposomal and likely increasing the number of clinical trials. Considering the time and cost of clinical trials, such active targeting methods may result in the rise of potentially effective drugs that either fail to enter or are permanently pulled from clinical trials for strategic reasons, which already accounted for a fifth of "failed" stage II trials in the 2008-2010 period. In addition, for highly mutagenic diseases such as cancer, there is a risk of the cells developing mutations which reduce affinity to the tags, which will make the targeting less effective (Ledford, 2011).

1.2.2.3. External Targeting Through Localised Release

An alternative strategy for liposomal targeting involves the use of external forces to trigger the release of cargo from liposomes specifically at the target tissue (Fig. 1.4D) (Egusquiaguirre *et al.*, 2012; Lammers *et al.*, 2012; Preiss & Bothun, 2011). In this system, liposomes are embedded with nanovalves or nanoparticles responsive to external stimuli such as magnetic field (Hughes *et al.*, 2008; Preiss & Bothun, 2011). When liposomes reach the site of an applied stimulus, drugs are

released, through the opening of nanovalves or by destruction of the liposomes with vibrating nanoparticles for example. This method is unique in that it is not dependent on the accumulation of liposomes at the target tissue. Additionally, it has the advantage of not necessarily having to have liposomes pass physical barriers, as drugs (which are generally small enough to pass through such barriers) can still be released at the targeted site for adsorption to the targeted tissues. Therefore, it can be used either independent of passive or active targeting strategies, or in conjunction with them to achieve a synergistic effect (Egusquiaguirre *et al.*, 2012; Lammers *et al.*, 2012).

This strategy, while still in early development, has found success in proof-of-concept experiments that have demonstrated its viability (Pradhan *et al.*, 2010). One of the approaches, the use of nanoparticles to disrupt liposomal architecture, has shown particular promise in part due to the simplicity of operation. For example, photothermal release of doxorubicin from nanoparticle-embedded liposomes has successfully been demonstrated *in vivo* in a mouse study (Preiss & Bothun, 2011). There are still a number of areas in need of further research, such as the practicality of applying magnetic pulses to patients for extended periods, but these experiments do show that external targeting is a possible strategy.

Another focus of external targeting systems is the use of nanovalves to release cargo from liposomes without destroying them. An ideal nanovalve system might possess the ability to be opened in response to e.g. an externally applied magnetic field (Hughes *et al.*, 2008). This would allow controlled release of drugs over time by restricting both the size of the valve pore and the duration of its opening. In addition, nanovalves which are biodegradable organic compounds would be highly favoured over, for example, those that incorporate gold nanoparticles (potentially nephrotoxic). In this regard, the use of gated transmembrane protein channels as liposomal nanovalves has been investigated. Hughes *et al.* (2008) successfully attached magnetic particles to an engineered potassium channel and opened the channel by applying magnetic force to it. Recently, the mechanosensitive channel of large conductance from *Escherichia coli*, has been studied as a potential nanovalve (Kocer, 2010; Kocer *et al.*, 2005; Nakayama *et al.*, 2015). Mutational studies have demonstrated the ability to control its pore size as well as the activation energy required for the conformational change between open and closed states (Blount *et al.*, 1996; Iscla *et al.*, 2013; Kocer *et al.*, 2005; L. M. Yang & Blount, 2011). Being a protein, MscL is less likely to cause toxicity issues than inorganic nanoparticles such as silica nanoparticles (Duan *et al.*, 2013). Proof-of-concept studies have also demonstrated release of reporter molecules and small peptides in response to various stimuli, including a light-activated chromophore attached to the channel gate, ferromagnetic nanoparticle also attached to the channel gate, and the use of lysophosphatidylcholine to induce channel opening (A. Foo *et al.*, 2015; Kocer-Sagiroglu *et al.*,

2005; Nakayama *et al.*, 2015; Perozo, Kloda, *et al.*, 2002). The first two examples, which are mixed nanoparticle-nanovalve approaches, have successfully been demonstrated *in vitro* so far.

1.3. Mechanosensitive Channels

Mechanosensitive channels are integral membrane channel proteins whose primary opening trigger is membrane tension (Martinac, 2011; Pivetti *et al.*, 2003). When the membrane bilayer is stretched or curved, it imparts a negative pressure on the mechanosensitive channels, which forces open the channels via a conformation change. For this reason, mechanosensitive channels are commonly present in unicellular organisms, where they serve as a protective mechanism against hyposmotic shock (Fig. 1.5) (Haswell *et al.*, 2011). When the organism swells due to the hyposmotic environment, the cell surface membrane becomes stretched, triggering channel opening (Haswell *et al.*, 2011). As a result, intracellular contents escape the cell through the channels and the turgor pressure is relieved. Due to their importance, a number of organisms have redundant mechanosensitive channels opening at different tension thresholds to provide some level of regulation of the hyposmotic shock response (Haswell *et al.*, 2011; Kung *et al.*, 2010). This phenomenon is well characterised in *E. coli* where only mechanosensitive channels of small conductance (MscS) open to control osmotic pressure releasing intracellular ions in mild hyposmotic environments, whereas in severe hyposmotic environments, mechanosensitive channels of large conductance (MscL) additionally open to rapidly balance the osmotic gradient across the cell surface membrane at the cost of a wide range of intracellular molecules such as adenosine triphosphate (ATP) and peptides being released into the extracellular milieu (Haswell *et al.*, 2011; Kung *et al.*, 2010; Martinac, 2011). Biophysics of MscS and MscL have been extensively studied, as they serve as prototypes not only for their own structural families, but also for mechanosensitive

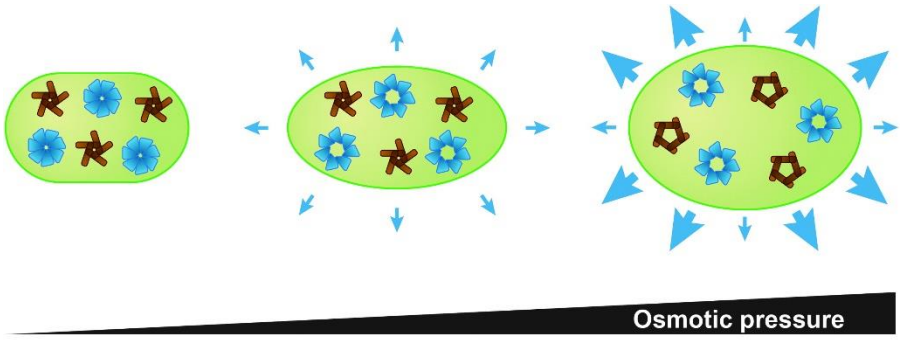

Figure 1.5. Schematic diagram of MscS (blue heptamers) and MscL (brown pentamers) channel activation with osmotic pressure. In a weakly hyposmotic environment, stretched membrane induces MscS to open to relieve the osmotic stress. In a major hyposmotic shock, MscL opens in addition to MscS to more quickly release intracellular contents through its larger channel pore. Courtesy of (Martinac *et al.*, 2014)

channels and mechanosensitive membrane proteins in general.

Mechanosensitive channels are also found in higher-order organisms, where they have a variety of roles (Martinac, 2011; Martinac *et al.*, 2014). Members of the MscS-family of proteins are found in plants in addition to unicellular organisms, with the mechanosensitive function retained in some, but not all, members. Different families of mechanosensitive channels are also found in animals, with the most notable examples being Piezo, transient receptor potential (Trp) channels, and the two-domain potassium channel (K2P) families of proteins (Brohawn, 2015; Corey, 2003; Gottlieb & Sachs, 2012). They have recently attracted significant research interest due to their medical significance, such as Piezo1 channels implicated in hereditary xerocytosis (Bae *et al.*, 2013), TrpV4 and TREK2 channels in cancer (K. S. Park *et al.*, 2013; Thoppil *et al.*, 2015), and TrpV4 and TrpA1 in inflammatory pain. Owing to this and the technological advancement in methods for studying the structure of eukaryotic membrane proteins, particularly cryo-electron microscopy, the structures of their members Piezo1, TRAAK, TREK1, TREK2, TrpA1, TrpV1, and TrpV4 channels, have been determined (Brohawn *et al.*, 2012; Cao *et al.*, 2013; Dong *et al.*, 2015; Ge *et al.*, 2015; Liao *et al.*, 2013; Paulsen *et al.*, 2015; Pike, 2014). In addition, membrane tension acts as a secondary trigger for a number of protein channels primarily gated by other triggers, such as the CFTR (Cystic Fibrosis Transmembrane Conductance Regulator), mutations in which are commonly responsible for cystic fibrosis (Vitzthum *et al.*, 2015). All families except MscL and Piezo channels include both mechanosensitive channels and non-mechanosensitive channels as members, and they are highly divergent in structure, suggesting multiple evolutionary origins for mechanosensation as well as diverse mechanisms of action.

1.3.1. Mechanosensitive Channels of Small Conductance

1.3.1.1. Overview of MscS-Family of Proteins

The mechanosensitive channel of small conductance is the defining member of a membrane protein family with unique membrane and carboxy-terminal domains (Pivetti *et al.*, 2003). This protein family is highly divergent in both structure and function. Examples have been found in all three domains of life, although their existence in animals has yet to be established (Fig. 1.6) (Pivetti *et al.*, 2003). It is also common for multiple MscS-family proteins to be present in a species, with good examples being *E. coli* where there are at least four channels (MscS, MscM, MscK, and YnaI), and *Arabidopsis thaliana* which has ten (MSC1-10) (Hamilton *et al.*, 2015; Martinac, 2011; Zou *et al.*, 2015). Although MscS is a non-specific channel, other members of this family are ligand-specific

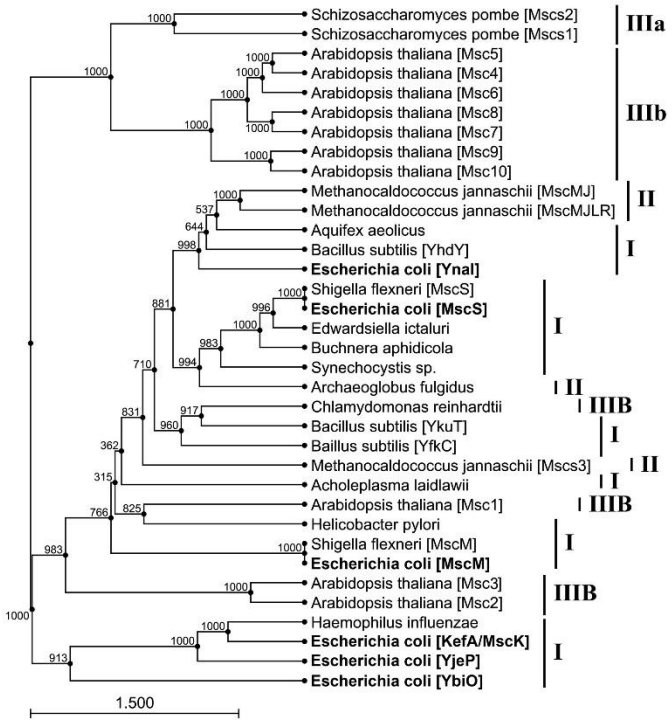

Figure 1.6. Phylogenetic tree of MscS family of mechanosensitive channels. Species with the Roman numeral I belong to bacteria, II to archaea, IIIa to yeasts, and IIIb and IIIB are different members of MscS family proteins in plant cells. Courtesy of (Martinac *et al.*, 2014)

and some of them are hypothesised not to be channel proteins at all, which explains the plurality of MscS-like proteins in a species (Gibson *et al.*, 2015; Wilson *et al.*, 2013).

1.3.1.2. MscS Structure and Function

Structures of *E. coli* MscS, the prototypical member of its family, in closed and nonconducting states as well as its functional homologs from other organisms have been determined by protein crystallography (Fig. 1.7) (Bass *et al.*, 2002; Bottcher *et al.*, 2015; Vasquez *et al.*, 2008; W. Wang *et al.*, 2008), and these, combined with simulation and biophysical studies, have provided structural and functional insights into the mechanism of MscS channel gating. MscS is a homoheptameric membrane channel of 211 kDa in size, and has a complex three-domain structure consisting of: a transmembrane domain comprised of three α-helices per subunit (TM domain); an intermediate cytoplasmic domain composed of β-strands (C1 domain); and a C-terminal cytoplasmic domain with a mix of helices and strands (C2 domain).

The N-terminus of the protein is located in the TM domain approximately 50 Å long across the membrane and has a diameter of 80 Å (Bass *et al.*, 2002). While its exterior surface is largely hydrophobic, it has arginine residues forming a positively charged ring via which MscS is thought to interact with the phospholipid head groups of the lipid bilayer. A recent mass spectrometry study

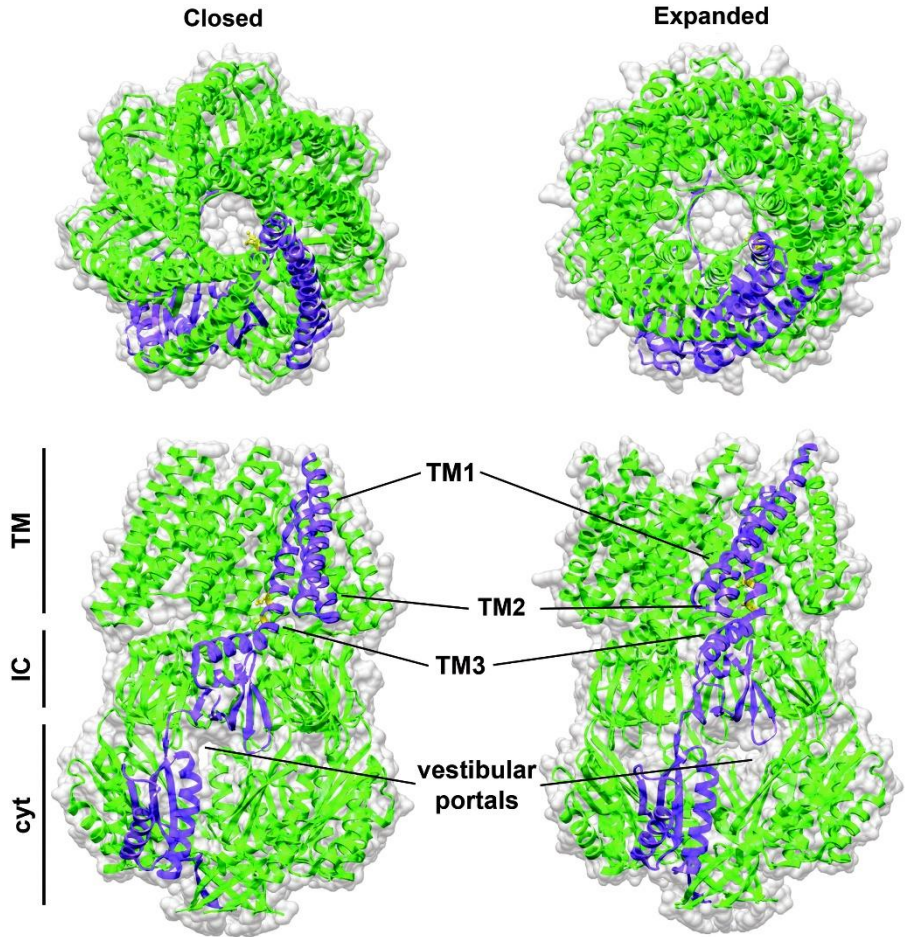

Figure 1.7. Structure of *E. coli* MscS determined by protein crystallography. The structure on the left is in closed conformation, and the one on the right is in expanded nonconducting state. Courtesy of (Martinac *et al.*, 2014)

on phospholipids identified phosphatidylglycerols, whose head group has net negative change, as the main phospholipid species interacting with MscS (Pliotas *et al.*, 2015). Molecular dynamics simulation showed them to be interacting with the arginine residues, confirming their significance in the protein-lipid interaction.

The central channel pore remains closed in the inactive state, but when there is membrane tension, equivalent to -10 mmHg pressure in patch clamp experiments, it opens in an optical diaphragm-like motion (Haswell *et al.*, 2011; Martinac, 2001). The size of the channel pore in a fully open state is somewhat debated, with early experiments observing a pore diameter of up to 16 Å, but the current consensus favouring 10 Å, as concluded from later patch clamp experiments and molecular dynamics simulations (Bass *et al.*, 2002). While the primary molecules which pass through the channel pore are thought to be water and potassium ions - the latter has sometimes led to the mislabelling of MscS as an ion channel (A. R. Battle *et al.*, 2009; Koprowski & Kubalski, 2003) - small organic molecules such as glutamate have also been observed to diffuse across the pore (Gamini *et al.*, 2011). A major factor for the lack of substrate specificity is the absence of highly selective structural elements such as those present in sodium channels.

The channel pore then leads to a spheroid internal chamber of approximately 60 Å long and 40 Å across formed by the C1 and C2 domains (Bass *et al.*, 2002). There are a total of eight pores connecting to the cytoplasmic exterior: seven pores of 7 Å at the C1 and C2 domain interface at the widest section of the chamber; and an 8 Å pore at the elongated end of the chamber, opposite the channel pore. These pores form simple sieve-like filters with mild enthalpy barrier, presumably to prevent clogging the pores while selecting for small molecules (Gamini *et al.*, 2011). The chamber reportedly expands and distorts to a more spherical shape during channel opening, with the role of this conformational change yet to be studied in detail. The cytoplasmic domain forming the chamber also has other functions such as mediating interactions with co-factors in both MscS and its structural homologues (Becker & Kramer, 2015; Koprowski *et al.*, 2015; Rowe *et al.*, 2013), which are currently subjects of further research as well.

1.3.2. Mechanosensitive Channels of Large Conductance

1.3.2.1. Overview of MscL Family of Proteins

The mechanosensitive channel of large conductance (MscL) belongs to another family of mechanosensitive channels which are structurally distinct from MscS family proteins. MscL-family proteins are characterised by a two-domain alpha-helical barrel-on-barrel structure with a relatively large retractable pore compared to the protein size (Fig. 1.9.) (G. Chang *et al.*, 1998; Steinbacher *et*

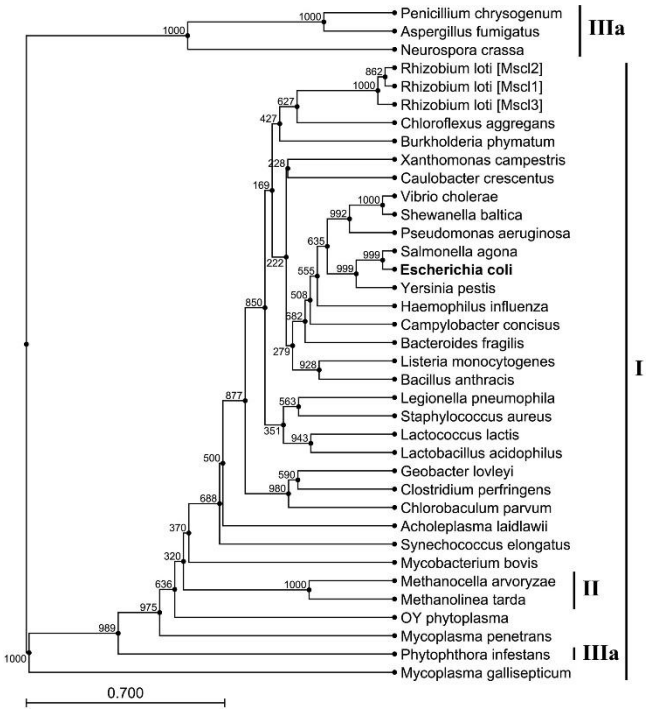

Figure 1.8. Phylogenetic tree of MscL family of mechanosensitive channels. Species with the Roman numeral I belong to bacteria, II to archaea, and IIIa to eukaryotes. Courtesy of (Martinac *et al.*, 2014)

al., 2007). They are more structurally homogenous than members of the MscS family, and all proteins identified so far are nonspecific channels, the gating of which are triggered by intense membrane tension. This lack of functional and structural diversity may account for there being only one copy of the protein in each species (Martinac, 2011). Contrary to their low diversity, this protein family is actually phylogenetically ancient, with representatives in all three domains of life (Fig. 1.8) (Martinac, 2011; Pivetti *et al.*, 2003; C. X. Wang *et al.*, 2007).

Like MscS, MscL proteins used in studies are often sourced from a range of species. While the majority of biochemical characterisation has been carried out using *E. coli* MscL, determined MscL structures are from Mycobacterium tuberculosis, *Staphylococcus aureus*, and archaeal Methanosarcina acetivorans (G. Chang *et al.*, 1998; J. Li *et al.*, 2015; Liu *et al.*, 2009). The structure and function was initially perceived to be conserved between species, leading to extrapolation of biochemical and biophysical characteristics of MscL from one species to similar proteins in other species. In addition, nearly all species expressing MscL are microorganisms (fungi being the only multicellular organisms). This has made MscL an attractive target for antibiotic development, with at least one compound targeting MscL in active development (Iscla *et al.*, 2015), and has also further encouraged characterisation of MscL across multiple species in order to facilitate design and identification of effective ligands or agonists. However, one of the drawbacks of different MscL homologues being studied is that in some aspects, there is insufficient overlapping data between channels from different organisms to enable accurate comparison. This is especially pronounced between *M. tuberculosis* and *E. coli* MscL: there are experimentally determined structures and lipid mass spectrometry data for *M. tuberculosis* MscL (Steinbacher *et al.*, 2007; Zhong & Blount, 2013), but comparatively little residue-specific data (e.g. EPR, FRET, and mutation studies) is available. For *E. coli* MscL the situation is the opposite. However, recent data (see section 1.3.2.2. and 1.3.2.3.) indicates that there is significant biophysical difference between the two species, leading to at least one paper cautioning against the extrapolation of data between them (Rui *et al.*, 2011). Hence, further experimental data will be needed to ensure that MscL provides a comprehensive model for mechanosensitive channel gating more generally.

1.3.2.2. MscL Structure and Function

Despite the challenge of being a membrane protein with a small soluble domain (less than 25 kDa in total), there has been intense research interest in the structure of MscL, with crystallographic structures now available for a number of species. The structure of *M. tuberculosis* MscL was initially determined in its closed state by Chang *et al.* in 1998, but with a major error in the model identified leading to the publication of a revised structure by the same laboratory in 2007 (Steinbacher *et al.*, 2007). Subsequently, the structure of *S. aureus* MscL in an unusual tetrameric

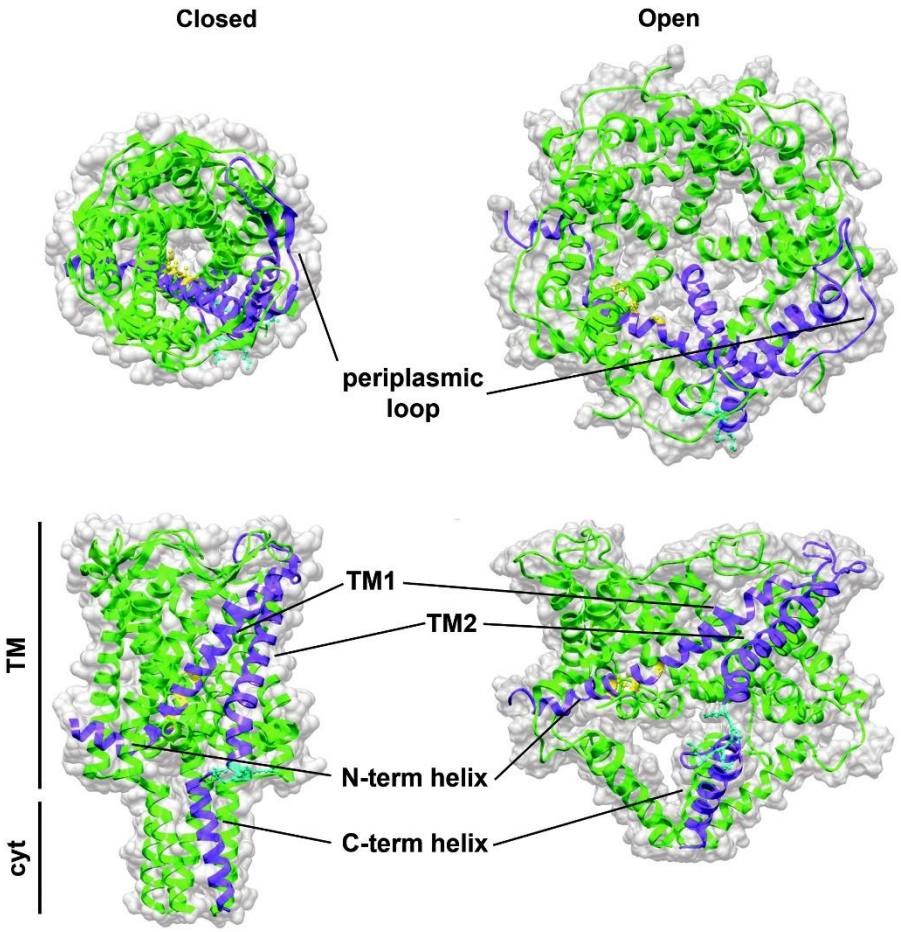

Figure 1.9. Structure of MscL. The structure on the left is *M. tuberculosis* MscL in closed state determined by protein crystallography. The structure on the right is *E. coli* MscL in open state generated by molecular dynamics simulation. Courtesy of (Martinac *et al.*, 2014)

nonconducting state was also determined by the same group (Liu *et al.*, 2009), with the change in quaternary structure concluded to be induced by the detergent environment forcing its transition away from the natural pentameric state (Dorwart *et al.*, 2010). During the course of this project, a truncated structure of the cytoplasmic domain of *E. coli* MscL became available (Walton & Rees, 2013), and another MscL structure from *M. acetivorans* was also determined (J. Li *et al.*, 2015). Notably, however, a full structure of *E. coli* MscL is not available despite decades of effort, with an attempt at two-dimensional crystallography resulting in an incorrect low-resolution structure with pseudohexameric symmetry (Saint *et al.*, 1998). Therefore, the descriptions of MscL structure in literature, in this thesis and elsewhere, needs to be viewed with a degree of caution.

E. coli MscL is a homopentameric membrane channel protein complex with a molecular weight of 80 kDa (Martinac *et al.*, 2014). MscL consists of two N-terminal transmembrane helices TM1 and TM2 forming the transmembrane domain, and a C-terminal S1 helix forming the cytoplasmic domain. Both N- and C-termini are at the cytoplasmic side while the flexible loop linking TM1 and TM2 is at the periplasmic side. Together, the larger transmembrane domain and smaller

cytoplasmic domain form a structure resembling a stack of two cylinders (Fig. 1.9).

The transmembrane domain of MscL consists of TM1 and TM2 from each subunit oriented against the bilayer plane forming an optical diaphragm-like pore similar to MscS (Fig. 1.6 and 1.7) (Martinac *et al.*, 2014). In the closed state, the pore is constricted on the cytoplasmic side and exposed on the periplasmic side with a conically shaped cavity. The pore interface is dominated by the TM1 helix, which is highly conserved across species, with a minor contribution from the N-terminal region of the TM2 helix, which is less conserved. At the cytoplasmic end of the pore, L17, V21, and T25 in *M. tuberculosis* MscL (L19, V23, and A27 in *E. coli*) line the main pore constriction (G. Chang *et al.*, 1998). While there are no strong specific interactions such as hydrogen bonds between the subunits to form strong energy barriers against channel opening, the hydrophobicity of this region stabilises MscL in the closed conformation in the absence of an external trigger (Birkner *et al.*, 2012; G. Chang *et al.*, 1998; S. Sukharev *et al.*, 2001; Yoshimura *et al.*, 2001). Substitution of these residues for hydrophilic ones such as aspartate results in an enhanced sensitivity to membrane tension (gain-of-function mutation) (Anishkin *et al.*, 2005; Yoshimura *et al.*, 1999), probably due to a reduced energy requirement for conformational change. In particular, an *E. coli* mutant with G22C substitution is frequently employed in MscL studies because 2-(trimethylammonium) ethyl methanethiosulphonate (MTSET) can induce opening of the pore through the introduction of a positive charge around the constriction when it reacts with the introduced cysteine residue (Yoshimura *et al.*, 2001). On the other hand, the periplasmic side of the MscL pore lacks distinctly charged or hydrophobic regions (G. Chang *et al.*, 1998; Iscla *et al.*, 2013; Yoshimura *et al.*, 2001; Yoshimura *et al.*, 1999), hence the absence of any associated ion selectivity function within the channel.

Although the structure of MscL in the fully open state has not been determined by X-ray diffraction analysis of protein crystals, EPR and FRET spectroscopic studies as well as computational modelling have led to a general consensus on the structural dynamics of its transmembrane domains (Fig. 1.9). According to open-state models, the interaction between TM1 and TM2 does not significantly change from the closed to the open state. However the tilt angle of the subunits with respect to the membrane plane is increased by around 20° between the two channel conformations (Perozo, Cortes, *et al.*, 2002; S. Sukharev *et al.*, 2001; Yilmaz *et al.*, 2015). In addition, the partially open structure of *M. acetivorans* MscL indicates that the L-shaped TM1 helix undergoes a minor pivot-like motion, with the angle of the bend increasing from 93° to over 140° (J. Li *et al.*, 2015). All open channel models have a similar pore diameter of ~30 Å corresponding to ~20 nm^2 in-plane protein expansion (Bavi *et al.*, 2014; Deplazes *et al.*, 2012; Gullingsrud *et al.*, 2001; Konijnenberg *et al.*, 2014; Sawada *et al.*, 2012). This is also supported by the structures of *M. acetivorans* and *S.*

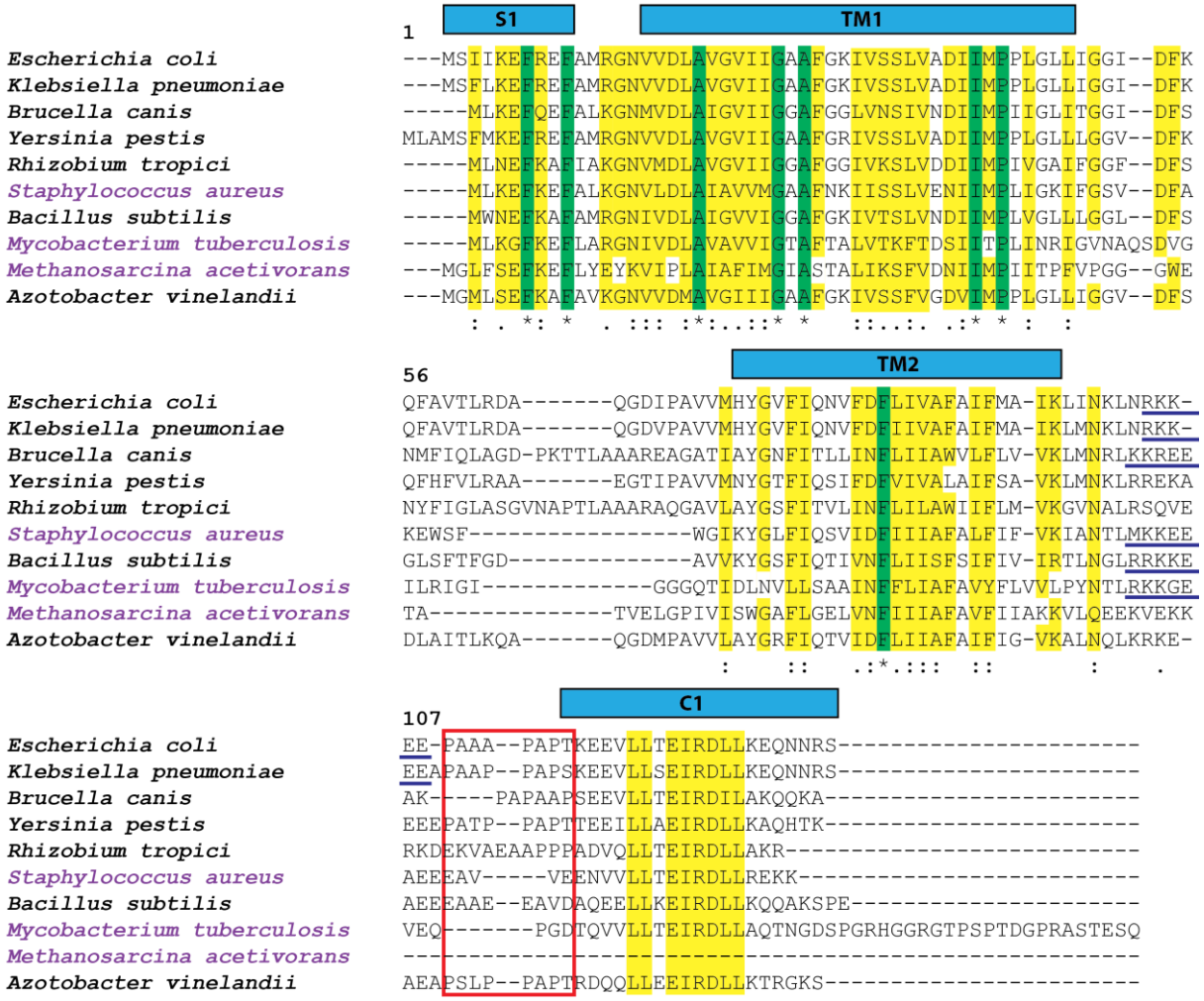

Figure 1.10. Sequence alignment of MscL family of mechanosensitive channels. Residue numbering and location of secondary structures (in cyan) are based on *E. coli* MscL. Green highlight denotes high level of sequence conservation across members. Yellow highlights denote moderate level of sequence conservation. The RKKEE motif (104 – 108) is underlined in dark blue. Proline and alanine-rich loop region is marked with a red box. Sequence data courtesy of Protein database (NIH, USA). Sequence alignment was performed with Clustal Omega (Sievers *et al.*, 2011).

aureus MscL (J. Li *et al.*, 2015; Liu *et al.*, 2009). This conformational change also decreases the length of the transmembrane domain by at least 13 Å (J. Li *et al.*, 2015; Liu *et al.*, 2009), likely more given the larger tilt of TM helices in the fully open state proposed by simulation studies.

The cytoplasmic domain consists of five TM2-S1 interhelical loops and S1 helices contributed by each subunit (Steinbacher *et al.*, 2007). Like TM1 and TM2, the S1 helices are also oriented against the bilayer plane. Between TM2 and S1 is a RKKEE motif, which is thought to be critical for the stability of MscL structure, sensitivity to pH, and synchronised conformational change of subunits during the opening of the channel (Anishkin *et al.*, 2003; Hase, Le Dain, *et al.*, 1997; Kloda *et al.*, 2006). Unlike TM1 and TM2, the function of the S1 helices is not very well understood. This is in part because it is not as well conserved across species. Its length alone is highly variable and ranges from being absent (*M. acetivorans*) to over 80 residues (*Mycoplasma gallisepticum*). Moreover,

there is often little sequence similarity between species, with negatively charged residues dominating the surface of *M. tuberculosis* MscL whereas *E. coli* MscL is rich in proline and alanine on the N-terminal end (Fig. 1.10) (G. Chang *et al.*, 1998). Given that proline's rigid structure is often used for structural and functional significance (Williamson, 1994), it is possible for this region to contribute to the functional difference between the two proteins. This is further complicated by the finding that a significant truncation of this domain does not critically compromise the function of the channel (Anishkin *et al.*, 2003), making its relationship with the transmembrane domain and functional significance unclear.

The structure of the cytoplasmic domain in the open state is also contentious with two prevalent competing models. Electron microscopy studies, together with the observed ability of MscL to allow molecules as large as insulin to pass through the pore, suggests that the C-terminal domain might dissociate and incorporate into the transmembrane domain during channel opening (Sawada *et al.*, 2012; S. Sukharev *et al.*, 2001; van den Bogaart *et al.*, 2007; Yoshimura *et al.*, 2008). At odds with this however, are molecular dynamics simulations (Corry *et al.*, 2010; Deplazes *et al.*, 2012; Zhu *et al.*, 2016), mass spectrometry (Konijnenberg *et al.*, 2014), and mutational analyses (L. M. Yang & Blount, 2011), which suggest that the C-terminal domain remains intact and undergoes only partial dissociation proximal to the TM2 helix. Complicating this issue further is that neither of the two structures of MscL in non-conducting states feature the C1 helix (J. Li *et al.*, 2015; Liu *et al.*, 2009), either by design or by nature. Moreover, many simulation experiments either fix the conformation of the cytoplasmic domain or even truncate it (Colombo *et al.*, 2003; Gullingsrud & Schulten, 2003; Y. Li *et al.*, 2009; Meyer *et al.*, 2006), probably due to the lack of experimental data. Considering that the cytoplasmic domain has the potential to restrict the pore size, this information will be important not only to understand the mechanism of mechanosensitive channel gating but also for the development of MscL as a protein-based nanovalve.

1.3.2.3. Mechanism of MscL Mechanosensation

As a protein channel primarily gated by membrane tension, MscL's interaction with phospholipids is a subject of intense research interest. There are two main areas of interest with regard to their relationship: role of phospholipids in channel activation, and the phospholipids preferentially interacting with MscL.

MscL channel opening is largely facilitated by destabilisation of the hydrophobic region of the membrane (Martinac *et al.*, 2014). This is evidenced by a large number of residues critical to channel function located at the interface with the fatty acyl chains of phospholipids (Levin & Blount, 2004; Ou *et al.*, 1998). Modifying the width of the phospholipid bilayer also affects the

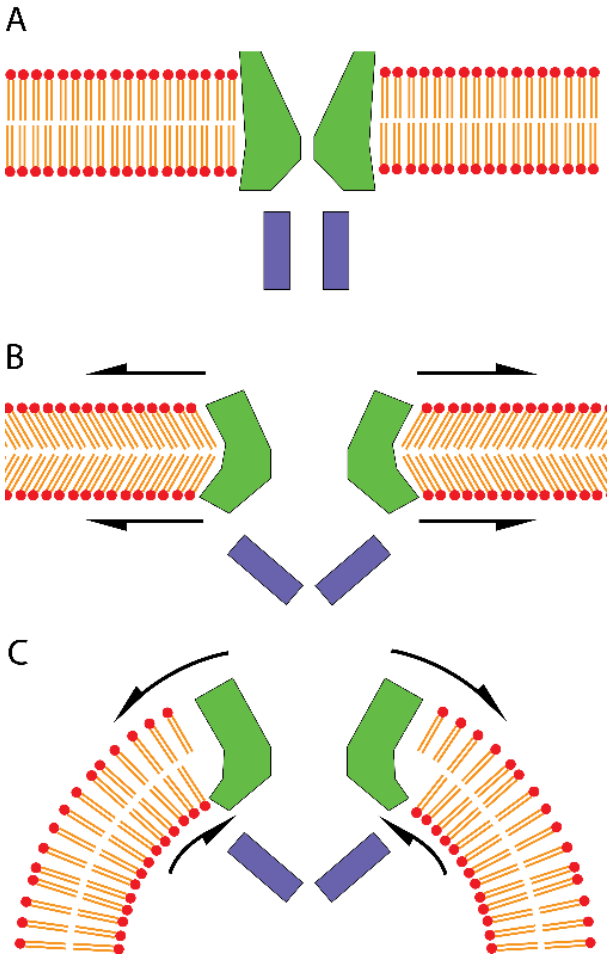

Figure 1.11. Schematic diagram of the models of MscL channel gating mechanism. **A**) MscL in closed state; **B**) In the stretch-activation hypothesis, near-even stretch on both sides of the bilayer provides energy for conformation change; **C**) In the curvature-activation hypothesis, MscL channel gating is facilitated by uneven shear force across the bilayer.

sensitivity of MscL to membrane tension (Powl *et al.*, 2007), suggesting that this is mediated by the interaction with the hydrophobic region. On the other hand, residues interacting with phospholipid head groups, especially those on the periplasmic side, are not critical for MscL channel function, even tolerating truncation (Blount *et al.*, 1996).

Less well understood is the type of stress on the membrane required to trigger channel opening. In the first hypothesis, MscL mainly senses curvature-induced stress on the membrane, defined by the discrepancy between the cross-sectional areas of the phospholipid head groups and fatty acyl chains (Fig. 1.11C) (Bavi, Cox, *et al.*, 2016; Meyer *et al.*, 2006; Powl *et al.*, 2008b). This is supported by the lowered pressure threshold for MscL opening in liposomes containing "cone-shaped" phospholipids, which have larger head groups than the tail ends and consequently favour curvature formation (Powl *et al.*, 2003). In addition, introducing lysophospholipids (LPC), which have only one fatty acyl chain (thence much smaller cross-sectional hydrophobic area), results in spontaneous "flickering" (quick opening and closing) of MscL channel, giving further credence to this

hypothesis (Perozo, Cortes, *et al.*, 2002; Perozo, Kloda, *et al.*, 2002).

In an alternative hypothesis, membrane tension simply decreases the thickness of the bilayer, with the resulting hydrophobic mismatch driving MscL's conformational change (Fig. 1.11B) (Yoshimura & Sokabe, 2010). There are several studies supporting this, such as: 1) experiments showing MscL's increased mechanosensitivity in membranes comprised of phospholipids with shorter chain length (Powl *et al.*, 2003, 2007); 2) analyses on the phospholipid head groups which indicate they have no impact on MscL channel function (P. Moe & Blount, 2005; Powl *et al.*, 2005); 3) and a patch clamp experiment testing the two hypotheses (P. Moe & Blount, 2005). This is a simpler model than the curvature-based one, and as a result has been adopted as the primary channel trigger in many simulation experiments.

1.3.2.4. Phospholipids Associating with MscL and Their Functional Significance

MscL in its native environment is speculated to preferentially interact with certain types of phospholipids, a property which will likely affect its channel gating function (Zhong & Blount, 2013). The clearest evidence of this so far has been MscL clustering in native *E. coli* membranes observed by confocal microscopy (Grage *et al.*, 2011). In addition, MscL channel gating properties are dependent on the phospholipid environment, namely those comprised of with phosphatidylglycerol (PG), phosphatidylcholine (PC), phosphatidylethanolamine (PE), phosphatidic acid (PA) and cardiolipin (CL) head groups (Andrew R. Battle *et al.*, 2011; Grage *et al.*, 2011; P. Moe & Blount, 2005; Powl *et al.*, 2008a, 2008b). CL and PG are also known to localise to certain areas of *E. coli* membrane (Andrew R. Battle *et al.*, 2011; Oliver *et al.*, 2014; Romantsov *et al.*, 2010), suggesting that *E. coli* MscL may have differing levels of affinity for these lipids. In a separate but related experiment, the pressure threshold of *M. tuberculosis* MscL differs between synthetic membranes using PG and phosphatidylinositols (PI; *M. tuberculosis* membrane contains

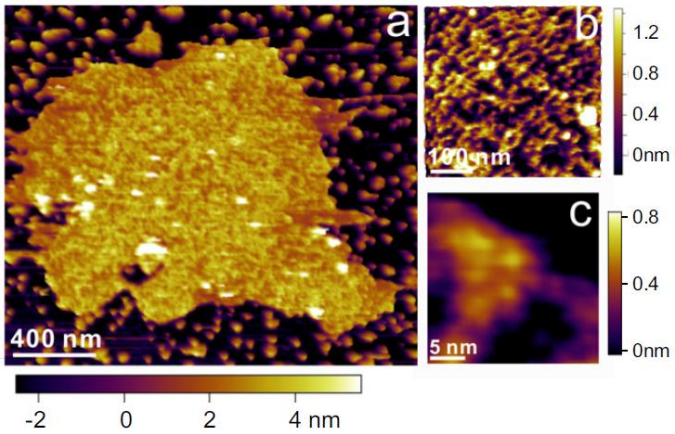

Figure 1.12. Atomic force microscopy of *E. coli* MscL cluster on DOPC membrane. **a**) Overview of MscL cluster; **b**) magnified view of the cluster which reportedly shows individual MscL particles; **c**) a further magnified view showing what could be individual particles. Image courtesy of (Grage *et al.*, 2011)

PI instead of PG) (Zhong & Blount, 2013), supporting the importance of phospholipids on the function of MscL.

MscL's relationship with phospholipids is also characterised by its distribution within the membrane. MscL clustering in both native *E. coli* membrane and DOPC has been observed in at least two separate experiments using a range of techniques such as fluorescence microscopy, small-angle neutron scattering (SANS), and atomic force microscopy (Fig. 1.12) (Grage *et al.*, 2011; Nomura *et al.*, 2012). This clustering of MscL appears to have a functional significance, as the proportion of active channels significantly decreases in this environment. Unfortunately, however, the clustering behaviour was not further studied with a wide range of phospholipids, limiting the level of information available to establish functional significance.

1.3.2.5. MscL's Potential as Nanovalve Candidate

MscL is a major protein-based nanovalve candidate due to a number of its favourable properties: it opens relatively large and non-selective pore, the trigger is purely mechanical and not ligand-dependent, it is relatively small in size, and it is stable across a range of temperature and detergent conditions (Iscla *et al.*, 2013; Martinac *et al.*, 2014). A current proposed biotechnological application for this nanovalve is for the release of cargo molecules from liposomes in a new drug delivery system. An alternative, more radical proposal might involve the direct incorporation of MscL into target cells in order to increase their permeabilisation and drug uptake (Doerner *et al.*, 2012).

Such practical applications require MscL gating to be controlled by triggers other than membrane stress, and this is an area of active development. In order to facilitate this, MscL needs to be engineered with either the addition of molecules activated by external stimuli, or by substitution of its residues to be responsive to the environment specific to the target site. Of these, there have been considerable progress on the former strategy. Two external stimuli, light and electromagnetic force, have been proposed as inducible triggers for MscL channel gating (Kocer *et al.*, 2005; Nakayama *et al.*, 2015). The system based on light was pioneered by a group at the University of Groningen, and uses *E. coli* $MscL^{G22C}$ with a molecule containing a spiropyran group, which can be reversibly charged by 366 nm ultraviolet light to induce channel opening with the repulsive force between the charged regions (Kocer *et al.*, 2007; Kocer *et al.*, 2005; Yilmaz *et al.*, 2015). The electromagnetic field-based approach was first performed on TREK1, another mechanosensitive channel, with 250 nm Fe_3O_4 particles attached (Hughes *et al.*, 2008). While inducible opening of the channel as a result of repulsive forces between the magnetic particles was achieved, this was considered impractical for medical application due to the large size of the particles used. However, a similar

result was recently achieved using MscL instead, this time with 5 nm $CoFe_2O_4$, which is not only small enough to be incorporated within liposomes without impacting their permeability to physical barriers but also non-cytotoxic (Nakayama *et al.*, 2015). While the experiment was carried out at sub-threshold membrane tension created by patch clamp, applying this strategy on an MscL construct with a lowered gating threshold may produce a nanovalve primarily activated by electromagnetic force.

A second aspect in the development of MscL as a nanovalve is controlling the specificity of the channel pore. MscL has a large pore lacking a selective mechanism for substrates. While this is an advantageous property for the nanovalve's use in liposomal drug delivery system, for other applications such as the use of MscL for increasing the permeabilisation of target cells (Doerner *et al.*, 2012), the option of being able to add a size or charge-based filter may be necessary and/or advantageous. One potential strategy is to add molecules with inducible charges to the pore constriction. The light-induced channel opening system previously described, for example, introduced charges to the channel pore, which would select against certain like-charged molecules as demonstrated in a separate experiment (Kocer *et al.*, 2005). An alternative approach is to use the cytoplasmic domain as a molecular size-based sieve, based on the observation that the dissociation of the domain is at least not necessary (if it happens at all) (L. M. Yang & Blount, 2011; L. M. Yang *et al.*, 2012). In this method, cysteine disulphide bridges would be added to the loop region linking the TM2 helix to the cytoplasmic helix, reducing the size of the gaps between the subunits. A combination of these two strategies is also a possibility, allowing the conversion of MscL into a more selective channel where desirable.

1.3.2.6. MscL as a Drug Target

MscL is widely found in microorganisms but absent in higher order organisms such as humans, making it a potential drug target. The two lead compounds are: parabens, which lower the tension threshold for mechanosensitive channels by destabilising the cell membrane, leading to the loss of ions even in mild osmotic stress (Nguyen *et al.*, 2005); and 1,3,5-tris[(1E)-2′-(4″-benzoic acid)vinyl]benzene, which is thought to bind to MscL at the channel pore, locking it in an open conformation (Iscla *et al.*, 2015). Of these, the latter has been tested successfully *in vivo* with *Caenorhabditis elegans* infected with methicillin-resistant *S. aureus*. Interestingly, this compound was not effective on *M. tuberculosis*, whose MscL served as the basis for the *in silico* docking experiment used for the drug design.

1.3.3. Mechanosensitive Channels in Higher-order Organisms

While mechanosensitive channels in prokaryotes remain best-studied, they play significant roles in higher organisms as well. Starting with the identification of TRAAK in rat atrial cells in 1992 (Kim, 1992, 1993), new eukaryotic mechanosensitive channels have steadily been identified, a trend which continues. Apart from MscL and MscS, which had already been discussed, three families have been identified as having eukaryotic mechanosensitive channels as members: K2P, Trp, and Piezo channels.

K2P channels, which include TRAAK, TREK1 and TREK2 as members gated primarily by membrane tension, are potassium channels found in various tissues in multicellular complex organisms (Fig. 1.13) (Brohawn, 2015). Whereas TRAAK is mainly found in neuronal cells, TREK1 and TREK2 are expressed in smooth muscle tissues and nociceptors, and have been implicated in pain sensation, as well as cancer, and side effects to fluoxetine, also known as Prozac© (Acosta *et al.*, 2014; Brohawn, 2015; Dong *et al.*, 2015; K. S. Park *et al.*, 2013). The structures of all three proteins have been determined by protein x-ray crystallography (Brohawn *et al.*, 2013; Brohawn *et al.*, 2012; Pike, 2014), and show a compact homodimeric structure with a potassium-selective pore in the centre. Unlike MscL and MscS, K2P channels have broad membrane tension ranges for channel activation, constantly flickering between closed and open states, but favouring the open state at higher tension (Brohawn, 2015). This is speculated to be due to a suggested relatively small conformational change required for channel activation, and probably

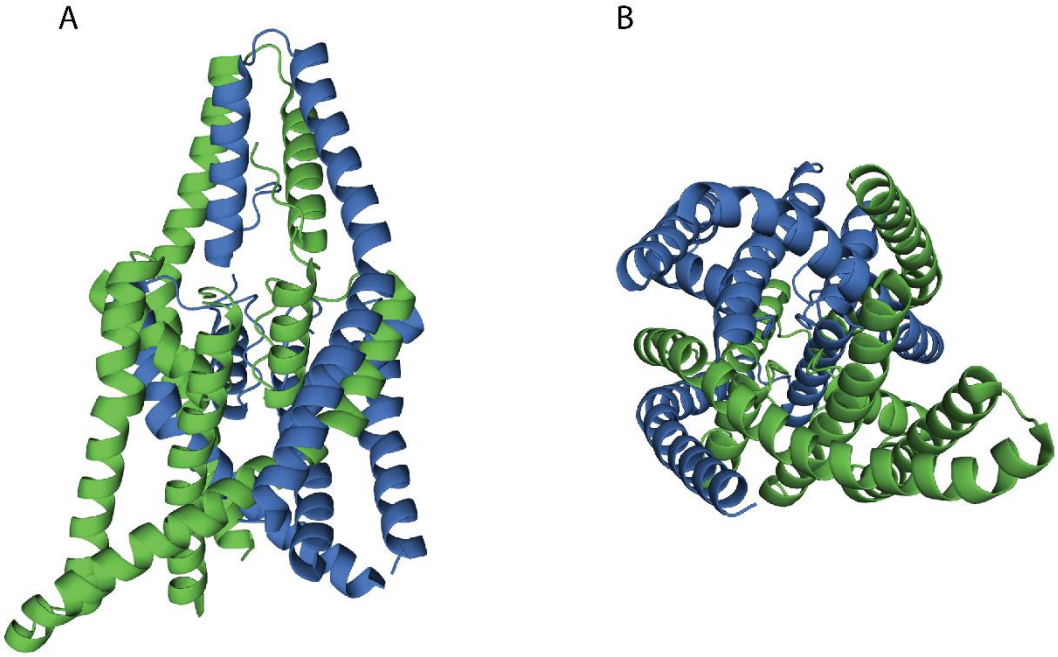

Figure 1.13. Crystal structure of human TREK2 in closed state (PDB ID: 4XDJ). **A**) Side view with the transmembrane domain at the bottom. **B**) Top view seen from the transmembrane domain. One of the two subunits has been coloured blue.

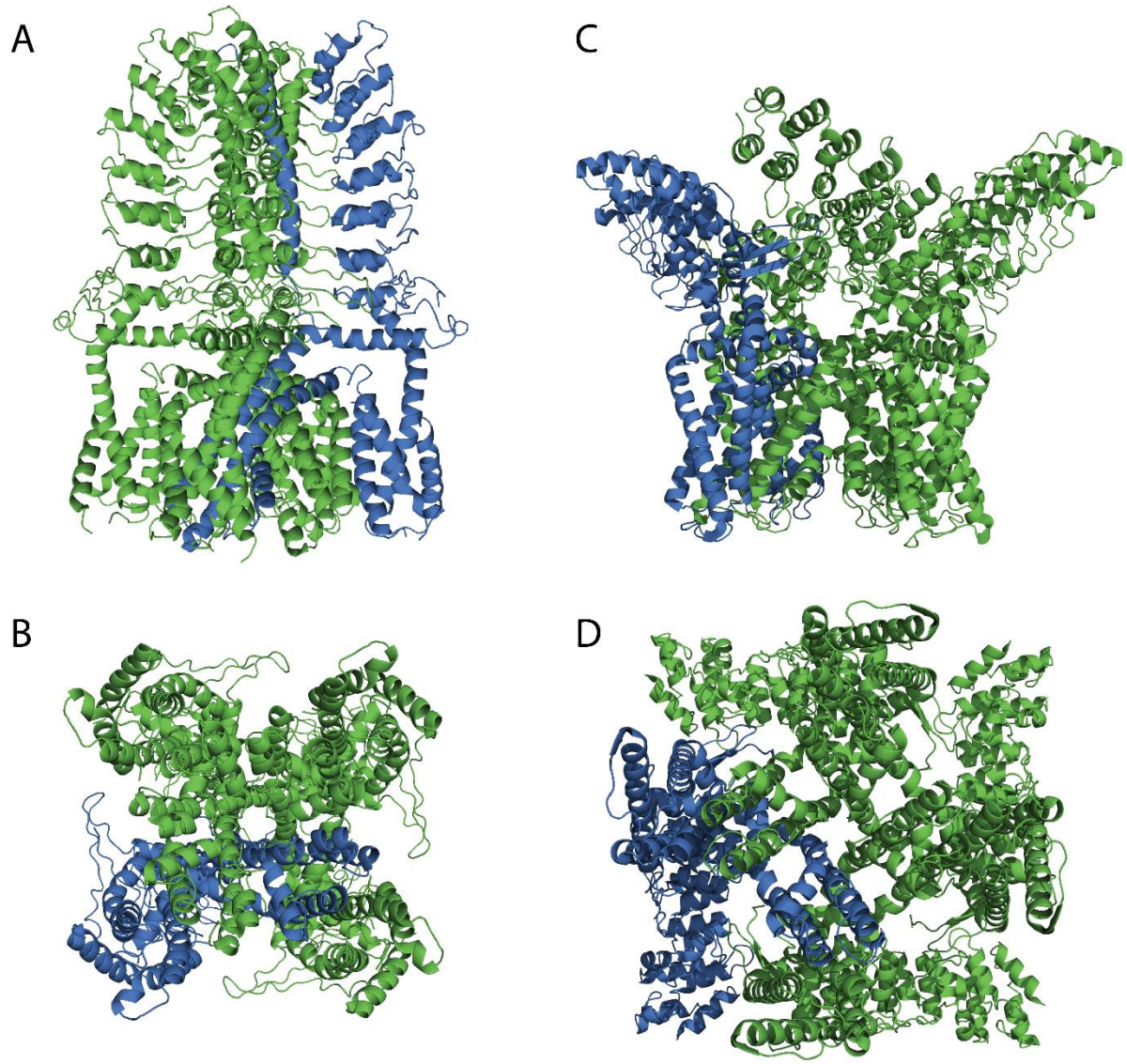

Figure 1.14. Crystal structures of human TrpA1 (PDB ID: 3J9P) and rat TrpV1 (PDB ID: 3J5R), both in closed state. **A**) Side view of TrpA1 with transmembrane domain at the bottom; **B**) Top view of TrpA1 seen from the transmembrane domain; **C**) Side view of TrpV1 with transmembrane domain at the bottom; **D**) Top view of TrpV1 seen from the transmembrane domain. One subunit from each structure has been coloured blue. Two antiparallel helices from each subunit form the channel pore in both proteins.

has a physiological role of allowing quantitative response to the stimulus. Interestingly, the TRAAK channel also activates in the presence of polyunsaturated fatty acids and arachidonic acid (Fink *et al.*, 1998; Kim, 1992), suggesting a close relationship between channel activity and phospholipids.

Trp channels are another family of ion channels with a diverse range of stimuli including mechanical stress. Of its members, TrpV1 and TrpV4 have been recognised as mechanosensitive channels (Huynh *et al.*, 2014), with TrpA1, TrpC1, and TrpC2 also reported to be mechanically activated (El Karim *et al.*, 2015; Kloda *et al.*, 2006). The closed-state structures of TrpV1 and TrpA1 have been determined by cryo-transmission electron microscopy using single particle analysis (Fig. 1.14) (Liao *et al.*, 2013; Paulsen *et al.*, 2015).

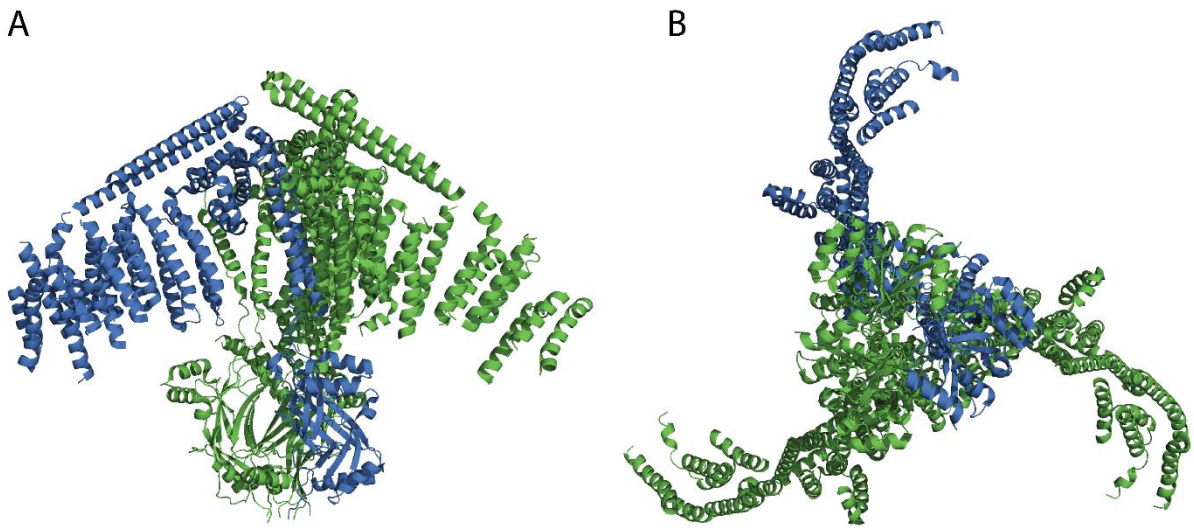

Figure 1.15. Crystal structure of mouse Piezo1 channel in the closed state (PDB ID: 3JAC). A) Side view with the transmembrane domain at the bottom; B) Top view seen from the transmembrane domain. One subunit has been coloured blue.

TrpV1 features a selectivity filter structure well-conserved in potassium channels, which is surrounded by a connected structure thought to be involved in mechanosensation. Mechanosensitive Trp channels are found in various cells such as skeletal muscle, blood vessels, sensory neurones, lens epithelial cells, and odontoblasts (Baratchi *et al.*, 2016; Corey, 2003; El Karim *et al.*, 2015; T. C. Ho *et al.*, 2012; Shahidullah *et al.*, 2015; Sharif-Naeini *et al.*, 2008), and are involved in kinase pathways while also having mechanosensitive ion channel function (El Karim *et al.*, 2015; Shahidullah *et al.*, 2015). Trp channel activity is influenced by the presence of phosphatidylinositols, which can be either stimulatory or inhibitory depending on the molecules, and this is due to both the direct interaction between them (i.e. mechanosensation) and mediated by external factors such as phosphatases (Rohacs, 2014).

Piezo channels are nonselective cation channels also found in a wide range of cells. They are characterised by a large structure comprised of three 300+ kDa subunits forming a triangular channel, which then forms 2MDa dimer structure (Coste *et al.*, 2012; Ge *et al.*, 2015). A medium-resolution structure of Piezo1 has been determined by electron microscopy, and reveals a long and narrow selectivity filter in the middle resembling P2X channels (Fig. 1.15) (Ge *et al.*, 2015). Uniquely for a mechanosensitive channel, a blade-like structure in the soluble domain has been proposed as the mechanosensor rather than the surface of the transmembrane domain (Ge *et al.*, 2015). However, this hypothesis has not been validated with biophysical experiments, and there is speculation that they might not be traditional mechanosensitive channels at all, activated by a

cytoskeletal structure instead (Soattin *et al.*, 2016). Despite their broad medical significance (Coste *et al.*, 2012; Gottlieb & Sachs, 2012; Soattin *et al.*, 2016), their biophysical and physiological properties are poorly understood and remain to be studied.

1.4. Project Overview

The first aim of this thesis was to characterise the relationship between MscL and the phospholipid membrane. MscL is primarily gated by membrane tension exerted by phospholipids, but their relationship remains poorly understood (Yoshimura & Sokabe, 2010). This problem is especially pronounced in a broader context than molecular-level interaction, as most studies have focused on the relationship between phospholipids and single MscL molecules (Bavi, Vossoughi, *et al.*, 2016; Deplazes *et al.*, 2012; Pliotas *et al.*, 2015; Yoshimura *et al.*, 2008). Therefore, this project has sought to address this gap in knowledge by studying the effect of various membrane-related variables such as curvature and phospholipid composition on MscL function. In particular, their influence on MscL aggregation was investigated, with implications on its channel gating threshold. The findings from this objective would not only help with understanding MscL function on its own right, but also aid with future biophysical experiment designs.

The second aim of this thesis was to structurally characterise *E. coli* MscL. While there are crystallographic structures of its homologues in *M. tuberculosis*, *S. aureus*, and *M. acetivorans* (G.

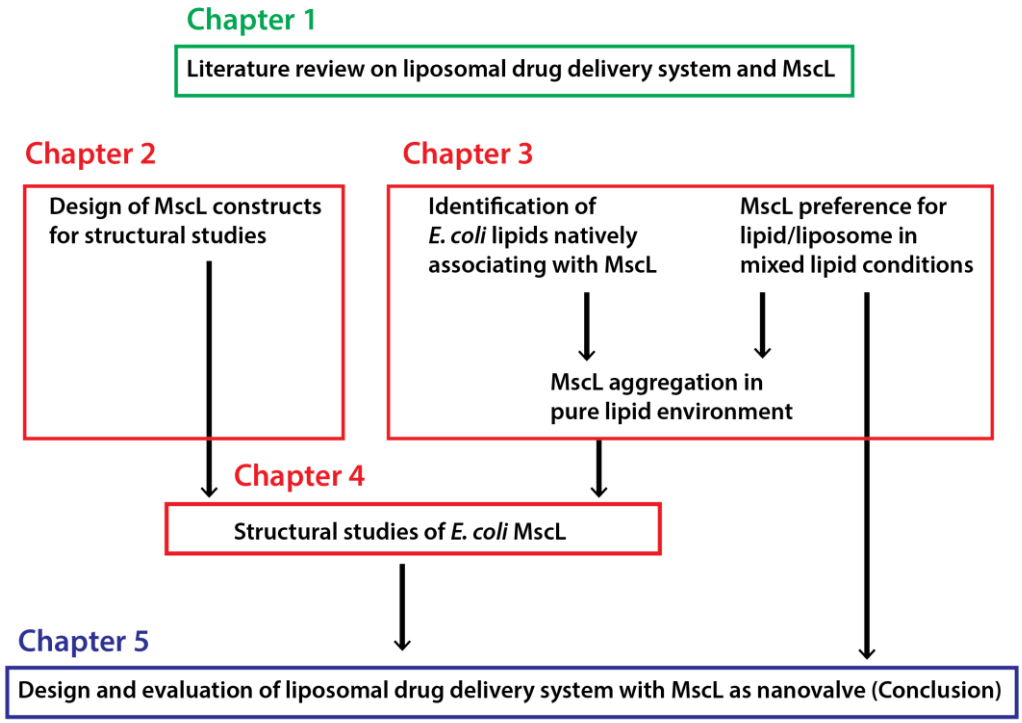

Figure 1.16. The Outline of the project "*Biophysical and Structural Characterisation of Escherichia coli MscL in Lipid Bilayers*"

Chang *et al.*, 1998; Liu *et al.*, 2009; Zhu *et al.*, 2016), the one for *E. coli* MscL, which remains biophysically the best characterised protein of this family, has still not been determined. Moreover, MscL structure was found to be sensitive to detergents, which are the environments where all MscL structures were determined, resulting in *S. aureus* MscL taking an unusual tetramer conformation (Dorwart *et al.*, 2010; Liu *et al.*, 2009). Therefore, both 2D and 3D crystallisations were attempted with *E. coli* MscL to determine its structure. In particular, MscL structure in 2D crystals would have provided unique insight into MscL's relationship with phospholipids, which was the first aim of this thesis. Ultimately, findings from these two objectives would help not only with understanding the function of mechanosensitive channels but also with the development of a new liposomal drug delivery system with MscL as the nanovalve.

2. MscL Construct Design

2.1. Introduction

One of the challenges of this project was the quality of the starting contruct of *E. coli* MscL. In particular, the MscL plasmid construct resulted in heterogeneously expressed products, producing two species of MscL monomers. Second, due to the lack of tryptophan and tyrosine in MscL, the expressed protein poorly absorbed ultraviolet light at 280 nm wavelength, which in turn made the quantification both inaccurate and imprecise. Works focused on solving these issues are detailed in this chapter, part of which have been published in an academic journal with myself as the first author.

Contributions to the publication are as described in the following:

> MscL construct design, construct production, protein expression, protein purification, concentration measurements with UV/Vis spectrometer and infrared spectrometer, and SDS-PAGE were performed by Gamma Chi (me).
>
> Mass spectrometry experiment was performed by Dr. Michael Landsberg.
>
> Sample preparation for patch clamp experiment was performed by Paul Rohde. Patch clamp experiment was performed by Pietro Ridone. The analysis was performed by Pietro Ridone and Prof. Boris Martinac.
>
> First draft for the publication was written by Gamma Chi (me), and was reviewed by Gamma Chi (me), Dr. Michael Landsberg, Prof. Ben Hankamer, and Prof. Boris Martinac.
>
> Supporting funding was provided by the NHMRC via grant 635513. *Mechanosensitive channels: Antimicrobials, channelopathies and nanovalves for drug delivery. CI Hankamer & Martinac*

There are also experiments which are not discussed or detailed in the publication relevant to this chapter, which will be explained in the following section. The most significant of these are techniques used for site-directed mutagenesis, and experiments to troubleshoot one of the produced constructs, $MscL^{TEVc}$.

2.2. Publication: Functional similarities between heterogeneously and homogenously expressed MscL constructs

Gamma Chi[1], Paul R. Rohde[2], Pietro Ridone[2], Ben Hankamer[1], Boris Martinac[2,3], Michael J. Landsberg[1,4]

[1] Institute for Molecular Bioscience, The University of Queensland, St Lucia, QLD 4072, Australia

[2] Molecular Cardiology and Biophysics Division, Victor Chang Cardiac Research Institute, Darlinghurst, NSW 2010, Australia

[3] St Vincent's Clinical School, University of New South Wales, Darlinghurst, NSW 2010, Australia

[4] School of chemistry and Molecular Biosciences, The University of Queensland, St Lucia, QLD 4072, Australia

2.2.1. Abstract

The mechanosensitive channel of large conductance MscL is a well-characterized mechanically gated non-selective ion channel, which often serves as a prototype mechanosensitive channel for mechanotransduction studies. However, there are some discrepancies between MscL constructs used in these studies, most notably unintended heterogeneous expression from some MscL expression constructs. In this study we investigate the possible cause of this expression pattern, and compare the original non-homogeneously expressing one to confirm that there is little functional difference between them. In addition, a new MscL construct has been developed with an improved molar extinction coefficient at 280 nm, enabling more accurate protein quantification.

2.2.2. Keywords

MscL, Mechanosensitive channel, Construct design, Protein quantification, Heterogeneous expression, Patch clamp

2.2.3. Introduction

Mechanosensitive channels are non- or weakly selective ion channels that are primarily gated by membrane tension, which exerts a mechanical force that opens the channel and in turn allows the passage of ion currents. The MS channels of large (MscL) and small conductance (MscS) were first identified in *Escherichia coli* as emergency valves that protect against hypoosmotic stress (Blount *et al.*, 1997; Levina *et al.*, 1999; S. I. Sukharev *et al.*, 1993). Further MS channels with various functions have been discovered since then, including medically significant mechanosensitive

channels in mammals and other higher eukaryotes, such as Piezo and transient receptor potential (TRP) channels (Coste *et al.*, 2012; Sharif-Naeini *et al.*, 2008). More recent discoveries notwithstanding, MscL and MscS remain the most extensively studied and are thus prototypes for the mechanosensitive class of ion channels, due largely to their ease of expression, purification and reconstitution into artificial membrane systems (Martinac, 2011). These characteristics have also led to particularly MscL often being used as a reference protein for the development of new experimental approaches to study other membrane proteins (Konijnenberg *et al.*, 2014; Lee & Liu, 2015; Qi *et al.*, 2014). Finally, interest in MscL has increased in recent years because of its demonstrated potential to be modified and implemented as a stimulus-triggered nanovalve in liposomal drug delivery systems (A. Foo *et al.*, 2015; Kocer *et al.*, 2007; L. M. Yang *et al.*, 2012) and for introducing cell-impermeable biomarkers and bioactive molecules into mammalian cells (Doerner *et al.*, 2012).

Since its molecular identification in 1994 (S. I. Sukharev *et al.*, 1994), the biophysical and structural properties of MscL have been the focus of intense study. The structure of MscL from Mycobacterium tuberculosis in the closed stated has been determined by X-ray crystallography (G. Chang *et al.*, 1998; Steinbacher *et al.*, 2007) revealing a homopentameric assembly comprised of an N-terminal transmembrane and C-terminal cytoplasmic domain. More recently, the structure of the C-terminal cytoplasmic domain of the *E. coli* channel was also solved by X-ray diffraction (Walton & Rees, 2013), showing little difference to the equivalent region of the *M. tuberculosis* homologue. Mutation studies and functional characterization, predominantly using patch clamp experiments, have revealed residues distributed throughout the transmembrane domain that are critical for protein channel gating (Ajouz *et al.*, 2000; Balleza & Gomez-Lagunas, 2009; Blount *et al.*, 1996; Hase, Le Dain, *et al.*, 1997; Kloda *et al.*, 2006; Maurer & Dougherty, 2001; Perozo *et al.*, 2001; Yoshimura *et al.*, 1999). In combination with these, low-resolution structures of MscL in the open state determined using spectroscopic methods such as EPR and FRET (Corry *et al.*, 2010; Corry *et al.*, 2005; Perozo, Cortes, *et al.*, 2002; Y. Wang *et al.*, 2014) have helped with building plausible models for the channel gating process, subsequently evaluated by molecular dynamics-driven simulation (Corry *et al.*, 2010; Deplazes *et al.*, 2012; Meyer *et al.*, 2006; Sawada *et al.*, 2012).

One potentially confounding factor in extrapolating these results is that many of the above studies have been conducted in different laboratories using MscL constructs that differ to varying extents. The earliest studies of MscL utilized a construct that, when expressed recombinantly, contained nine non-native amino acids plus the N-terminal methionine (Hase *et al.*, 1995), which is removed from wild-type protein *in vivo*. Extensive evidence shows that this original MscL expression construct yields two distinct species when the purified expression products are analyzed by SDS-

PAGE, indicating that it is a heterogeneously expressing construct (Hase, Le Dain, *et al.*, 1997; Kloda *et al.*, 2006; S. I. Sukharev *et al.*, 1994). Many research groups have since developed their own MscL expression constructs with differences tailored to their specific experimental needs (Arkin *et al.*, 1998; Kocer *et al.*, 2007). However, this original MscL expression construct is still widely used (Doerner *et al.*, 2012; Grage *et al.*, 2011; Yoshimura *et al.*, 2001), possibly due to inadvertent ignorance (depending on the conditions of SDS-PAGE, the two products may not be resolved), or due to the apparent lack of detectable interference with MscL expression or function.

In this paper we investigate the cause of this heterogeneous expression of MscL and directly compare the functional activity of this construct with a homogeneously expressing one derived from it. In the course of this work, we have also produced an MscL construct with improved accuracy for quantification with the standard 280 nm ultraviolet light absorption technique, with positive implications for future reproducibility of biophysical and structural observations.

2.2.4. Methods

2.2.4.1. Site-directed mutagenesis

All constructs used in this study were derived from MscL 2.1 in pQE-31 plasmid, itself derived from the MscL pGEX1.1 plasmid described in Häse *et al*. (Hase *et al.*, 1995). Numbering throughout the manuscript is relative to the wild-type sequence starting with methionine-1, which is post-translationally cleaved from the mature protein. Overlap extension PCR as described by Ho *et al.* (S. N. Ho *et al.*, 1989) was used to generate a construct with the methionine-1 substituted for alanine ($MscL^{M1A}$). A modified inverse PCR protocol was subsequently used to create a construct with a further substitution of the leucine at position (-7) to tyrosine ($MscL^{L-7Y}$) introduced into the $MscL^{M1A}$ construct (i.e., $MscL^{L-7Y}$ is strictly a $MscL^{M1A/L-7Y}$ double mutant; for simplicity we retain the $MscL^{L-7Y}$ nomenclature throughout). Introduction of point mutations was confirmed by gene sequencing at the Brisbane branch of the Australian Genome Research Facility (AGRF).

2.2.4.2. Protein expression and purification

All MscL expression constructs were purified using a modified version of the protocol described by Häse *et al.* (Hase *et al.*, 1995). Expression was in the *E. coli* AW737-KO strain (S. I. Sukharev *et al.*, 1994). The presence and purity of MscL was checked at each step by 16 or 18 % SDS-PAGE.

2.2.4.3. N-terminal sequencing and mass spectrometry

Purified MscL constructs were separated by 12 or 18 % Tris-glycine SDS-PAGE. Individual gel bands were excised, the proteins eluted overnight, washed with 0.1 % TFA and then subjected to 20

cycles of Edman N-terminal sequencing using an Applied Biosystems 494 Procise Protein Sequencing System (ABSCIEX, Concord, Canada).

LC-MS/MS was performed on a Shimadzu Nano HPLC (Kyoto, Japan) coupled to a QStar Elite mass spectrometer (ABSCIEX). Sample preparation was identical, with the exception that excised gel bands were destained, dehydrated, and then rehydrated in 40 mM ammonium bicarbonate buffer containing 10 % acetonitrile and 1 µg sequencing grade porcine trypsin (Promega). Peptides were de-salted on a 50 mm x 300 µm trap and then separated on a 150 mm 300 µm C18 column using a two-step linear gradient of 0-36 % (1.3 % min-1) then 36-72 % (7.2 % min-1) acetonitrile in the presence of 0.1 % formic acid at a flow rate of 3 µl min-1. Samples were introduced to the spectrometer via a nano electrospray ion source (3000 V, curtain gas flow 16, nebulizer gas 1 (GS1) 25 and interface heater 120 ℃). Full-scan TOF-MS data were acquired (m/z 350-1800), followed by full-scan ion data (*m/z* 100-1800) in an information-dependent acquisition mode. A threshold of 12 counts and a charge state of +2 to +5 was set to trigger collection of MS/MS data for the three most intense ions. Data were processed using Analyse QS 2.0 software (ABSCIEX).

2.2.4.4. Patch clamp experiments

Proteoliposomes were prepared following the dehydration/rehydration (D/R) method as previously described (Delcour *et al.*, 1989; Hase *et al.*, 1995). Briefly, 2 mg of soybean azolectin (Sigma) was dissolved in chloroform and then air-dried under a stream of N2 gas. The dried lipid film was resuspended in 200 µl D/R Buffer (200 mM KCl, 5 mM HEPES, pH 7.5) by brief vortexing then sonication for 10 min. Purified MscL was added to a 1:500 final protein to lipid ratio (w/w) and the volume increased to 3 ml with D/R buffer. The mixture was incubated on a rotary shaker for 1 h and then further incubated for 3 h following addition of approximately 10 mg of Biobeads (SM-2; Bio-Rad). The liquid phase was collected and centrifuged at 40,000 rpm for 30 min. The resulting pellet was resuspended in 40 µl D/R buffer, spotted onto a microscope slide and dehydrated under vacuum overnight at room temperature and stored at 4 ℃.

Dried lipid spots were rehydrated for patch-clamp recording with a 50 µl drop of D/R solution and kept at 4 ℃ for at least 3 h. MscL currents were measured in the inside-out patch configuration using an AxoPatch 1D amplifier (Axon Instruments). Data were collected at a 5-kHz sampling rate with 2-kHz filtration. Borosilicate glass pipettes (Drummond Scientific, Broomall, PA) were pulled using a Narishige puller (PP-83; Narishige) to achieve a bubble number of approximately 6.0. All recordings were collected in symmetrical bath and pipette solutions containing 200 mM KCl, 40 mM MgCl2, 5 mM HEPES (pH 7.2). Suction was applied to the patch membrane using a computer-controlled High-Speed Pressure Clamp-1 apparatus (HSPC-1; ALA Scientific Instruments). All

patch clamp experiments were repeated a minimum of three times and data shown were representative. Dwell time analyses were conducted on traces containing only single channel events (e.g., no more than one MscL firing at any time during the recording). Suction was applied to the patch gradually until single channel events could be detected, and then kept constant near the MscL opening threshold until multiple channel openings could be detected, at which point the experiment was terminated. The automated analysis tool on pClamp was used to measure the open probability (P_0) and the average dwell time of a recorded trace with minimum 500 single channel events. Each data point was plotted according to its dwell time and P0 value, grouped with similar data points and the distribution trends were compared between each experimental sample.

2.2.4.5. Protein quantification using ultraviolet and infrared light absorption

UV absorption at 280 nm was measured in triplicate using a Nanodrop UV/Vis spectrometer (Thermo Scientific). Following estimation of the protein concentration based on theoretical molar extinction coefficients (ε_0), solutions were adjusted to a theoretical concentration of 1 mg/ml and the absorbance re-measured. Absolute protein concentrations were obtained by infrared measurement using a Direct Detect spectrometer (EMD Millipore). Samples were analyzed in triplicate in a buffer free of infrared absorbance at 1650 cm^{-1} (amide bond absorbance maxima). AM2 background and NIST analysis settings were used to account for the presence of β-DDM in the solution.

2.2.5. Results and discussion

Prior to this study, repeated experiments in our hands have reproducibly shown that the original MscL expression construct (Hase *et al.*, 1995) yields two stable and distinct bands that both migrate close to a 15 kDa marker following cleavage of the recombinantly expressed fusion tag (Fig. 2.1b). This phenomenon is also observed in several publications where SDS-PAGE data of MscL are available (Hase *et al.*, 1995; Hase, Le Dain, *et al.*, 1997; Hase, Minchin, *et al.*, 1997; Kloda *et al.*, 2006; Saint *et al.*, 1998; S. I. Sukharev *et al.*, 1994). Notably, the electrophoretic mobility of the lower molecular weight band on SDS-PAGE appears unchanged, regardless of whether the N-terminal fusion tag is cleaved or not, suggesting that this lower molecular weight species may be degraded or otherwise differs at its N-terminus in a way that either removes the N-terminal fusion tag or renders it resistant to cleavage. To clarify this, we performed N-terminal sequencing. Twenty cycles of Edman degradation revealed that the N-terminal sequence of the lower molecular weight construct was Ser-Ile-Ile-Lys-Glu-Phe-Arg-Glu-Phe-Ala-Met-Arg-Gly-Asn-Val-Val-Asp-Leu-Ala-Val. This sequence matches exactly the native MscL N-terminal sequence commencing from

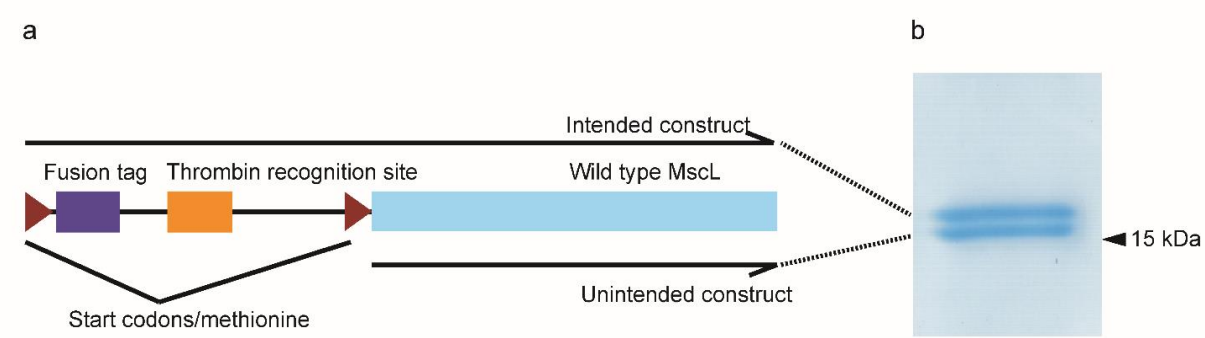

Figure 2.1. a) Schematic illustration of the original MscL2.1-pQE-31 expression construct indicates the expected expression product (intended product) as well as a secondary, unintended product which arises from translation initiation at the wild-type methionine. These constructs correspond to the upper and lower bands, respectively, as shown in Fig. 2.2. **b**) A typical SDS-PAGE showing purified MscL expressed from the widely used MscL2.1-pQE-31 plasmid, following protease cleavage to remove the plasmid-encoded fusion tag. Similar results have been observed for the parent plasmid MscL-pGEX1.1 described in Häse *et al.* (Hase *et al.*, 1995)

serine-2 (i.e. minus the initial methionine residue) (Fig. 2.2).

LC-MS/MS analyses of the higher and lower molecular bands following extraction from SDS-PAGE, destaining and trypsin hydrolysis supported the observations from N-terminal sequence analysis. A peptide with *m/z* 446.8 (z = 2) was identified in the MALDI spectrum of the lower molecular weight band and MS/MS fragmentation of this ion yielded the sequence Ser-Ile-Ile-Lys-Glu-Phe-Arg (Fig. 2.2a), an exact match for the N-terminal sequence detected by Edman degradation. For the high molecular weight band, a peptide with m/z 543.6 (z = 3) was observed and fragmentation of this ion yielded the sequence Gly-Ser-Leu-Glu-His-Arg-Glu-Asn-Asn-Met-Ser-Ile-Ile-Lys (Fig. 2.2b) with deamidation of the Asn residue at position 8 observed. This was an exact match for the expected amino acid sequence deduced from the plasmid DNA.

Since N-terminal methionine cleavage is a common post-translational modification in bacteria (Frottin *et al.*, 2006; Hirel *et al.*, 1989), these analyses suggested that the lower molecular weight band arises from expression of the native MscL sequence. Furthermore, since the AS737-KO cell line used in these studies (and many preceding studies) has the endogenous MscL sequence replaced with a chloramphenicol resistance gene, it would appear that this native sequence is plasmid-encoded with translation initiated at the native methionine-1 residue, a non-unprecedented phenomenon (Bazykin & Kochetov, 2011).

2.2.5.1. Engineering of a homogeneously expression MscL construct

Since transcription initiation in bacteria typically requires a promoter sequence located 10-30 base pairs upstream of a start codon, we hypothesized that the linker region of the MscL expression plasmid might contain a secondary promoter sequence. Furthermore, the DNA sequence of the five

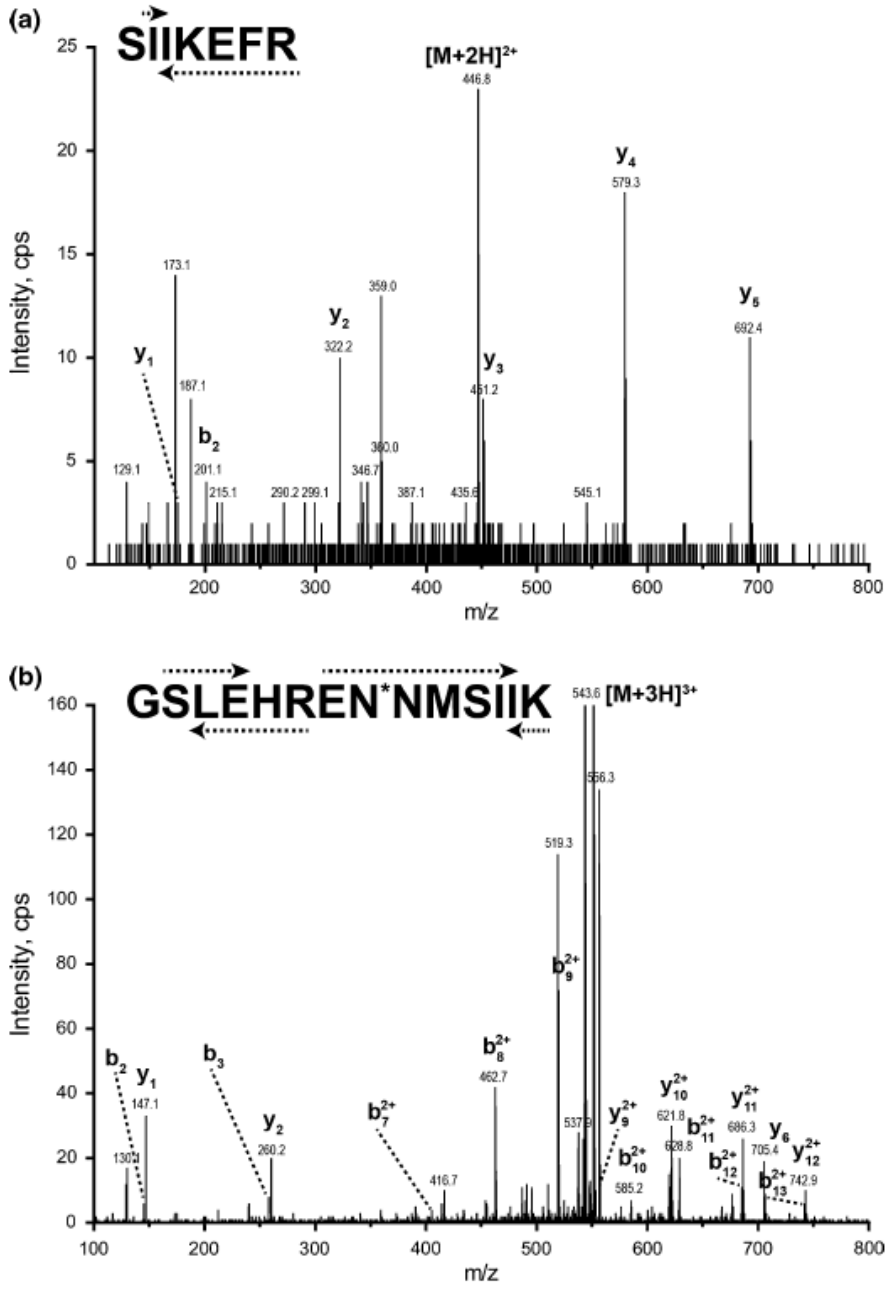

Figure 2.2. Nanospray LC-MS/MS of tryptic peptides generated from gel-purified upper and lower molecular weight band proteins shown in Fig. 2.1b. The spectra shown correspond to the N-terminal peptides of the lower band (**a**) and upper band (**b**). The double and triple charged parent ions are labelled ($[M+2H]^{2+}$ and $[M+3H]^{3+}$) along with b-series and y-series ions that give rise to the amino acid sequences shown in the *top of each panel*. Sequence coverage by the b-series and y-series ions is indicated by *dashed arrows* above and below the amino acid sequences. The parent ion and fragmentation series indicate deamidation of Asn-8

amino acid immediately preceding MscL Met-1 is derived from the original genomic cloning of MscL, and thus may contain unknown contextual translation start information. We proposed that silent mutation of either of these elements might prevent the lower molecular weight species from being expressed, however, no recognizable promoter or translation initiation sequences could be identified using either sequence analysis tools (Stano & Klucar, 2011) or by manually searching for

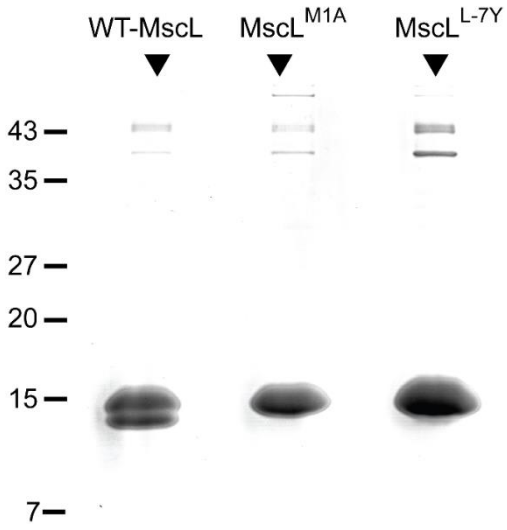

Figure 2.3. SDS-PAGE of the three purified MscL constructs described in this study. The double band resulting from heterogeneous expression can be clearly seen in the purification product of the original MscL construct (WT-MscL), while both MscL^{M1A} and MscL^{L-7Y} express as single species, coincident with the upper of the two bands observed for the original expression construct

known promoter sequences (Harley & Reynolds, 1987; Ma *et al.*, 2002). We therefore focused our initial efforts on engineering a modified MscL expression construct that introduced a TEV cleavage sequence in a manner that would produce cleaved, recombinant protein indistinguishable in sequence from the native protein. While this construct was successfully expressed and purified, it proved highly resistant to cleavage by both thrombin and TEV protease. Similarly, the introduction of the native Met-1 along with the preceding four residues to generate a thrombin cleavage site. In summary, all efforts to introduce a protease cleavage site at or near the N-terminus of the native MscL sequence resulted in a construct that could not be cleaved. We suggest that this may be due to the hydrophobic nature of the flanking sequences and/or the proximity to regions of the folded protein predicted to be membrane- or micelle-embedded.

Subsequently, we adopted a strategy that involved replacing the native start codon of the MscL-encoding region with an alanine codon. This new construct (MscL^{M1A}) also expressed well, could be cleaved (to remove the N-terminal fusion tag) and importantly, migrated as a single species on SDS-PAGE (Fig. 2.3) at a position coincident with the higher molecular weight species seen in previous analyses. The absence of the lower molecular weight band from these gels appeared to confirm that in the original construct, expression of the lower molecular weight species resulted from a secondary translation start site. The propensity for this to occur appears to be quite strong, since in our hands mutation of the native ATG to TTG does not ablate lower band expression (P. Rohde, unpublished data). Interestingly though, translation initiation at the native ATG has not been observed in cell free expression systems based on *E. coli* extracts (P. Rohde, unpublished data) and

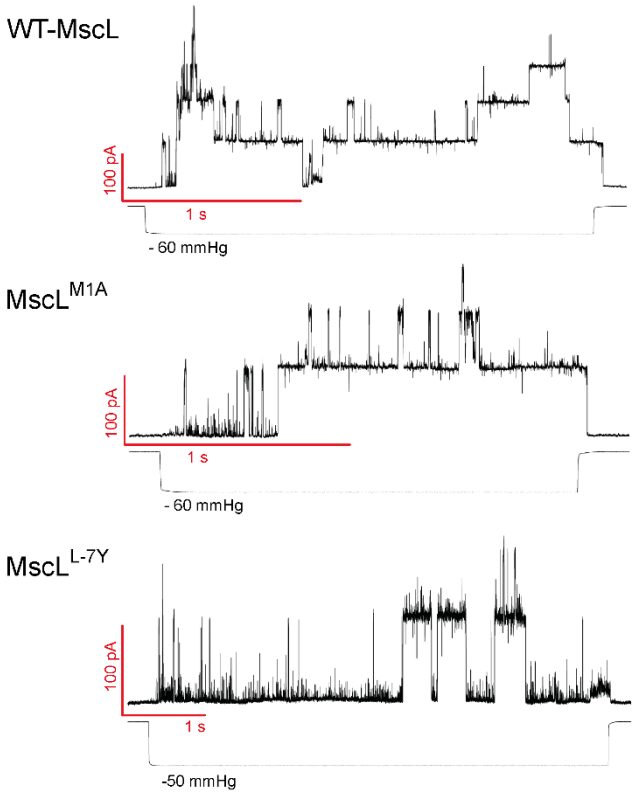

Figure 2.4. Representative patch clamp data for the original, heterogeneously expressing MscL construct (original MscL) and the new MscL^{M1A} and MscL^{L-7Y} construct. Both channels were activated at ~-60 mmHg, and have similar current amplitudes when open

so the mechanism of heterogeneous expression appears to require more than just the existence of a downstream ATG.

2.2.5.2. MscL construct with improved UV absorbance at 280 nm

An additional problem we have encountered in our studies of MscL is a difficulty with obtaining accurate, reproducible measurements of protein concentration. The capability to rapidly and accurately quantify purified MscL is desirable in many experimental situation, such as for quantitative patch clamp, functional assays which rely on accurate lipid-to-protein ratio determination, and for reproducibility of, e.g. 2D and 3D crystal screening experiments. Native MscL contains only one tyrosine and to tryptophan, which gives a hypothetical molar extinction coefficient (ε_0) of 1490 $cm^{-1}M^{-1}$ at 280 nm, approximately a tenth of its molecular mass. As a result, MscL absorbs ultraviolet light relatively poorly at this wavelength, meaning protein quantification by this technique is unreliable. Colorimetric assays are often sensitive to detergents, required to maintain solubility of MscL, and while the bicinchoninic acid (BCA) is relatively insensitive to detergents, this assay significantly underestimates MscL concentration due to its dependence on

tryptophan, tyrosine and cysteine residues (the latter is also absent from the native MscL sequence). Recently, techniques based on the absorption of infrared light at 1650 cm^{-1} by amide bonds have gained popularity for absolute protein quantitation, but organic molecules such as HEPES and ethylenediaminetetraacetic acid (EDTA) have significant overlap with the amide bond IR spectrum. Especially in the case of MscL, HEPES and TRIS are commonly used buffers in some purification steps and in biophysical experiments (K. H. Park *et al.*, 2004; Price *et al.*, 2011; Yoshimura *et al.*, 2008), and so the technique is not without its limitations.

To address this problem, we proposed introducing an extra tyrosine or tryptophan into the MscL expression construct, resulting in better absorption of UV light at 280 nm, and by extension an increased molar extinction coefficient and improved reliability of protein concentration measurement by UV absorption. We calculated that addition of one extra tyrosine would increase ε_0 of MscL to 2989 $cm^{-1}M^{-1}$, whereas an extra tryptophan would increase $\varepsilon 0$ to 6990 $cm^{-1}M^{-1}$.

Rather than modifying the MscL-encoding region, we decided to introduce either tyrosine or tryptophan within the residual N-terminal linker region, which remains after thrombin cleavage of the fusion tag. Since tyrosine is less hydrophobic than tryptophan and has a similar hydrophobicity to leucine, we chose to substitute tyrosine for a leucine located seven residues in front of the native methionine-1 residue to reduce the impact this might have on the purification process (as was seen with earlier efforts to substitute sequences close to the native N-terminus).

The new construct ($MscL^{L-7Y}$) carries both the methionine-to-alanine substitution at position 1 of the native sequence, as well as the leucine-to-tyrosine substitution and like $MscL^{M1A}$, expressed well and yielded a single band on SDS-PAGE (Fig. 2.3). The expected increase in molar extinction coefficient at 280 nm was clearly apparent when we compared the new construct to both the original MscL construct and the $MscL^{M1A}$ construct (Table 2.1). Solution concentrations for all three proteins were estimated based on absorbance at 280 nm and the same samples then had their protein concentrations analyzed by infrared spectroscopy using the amide I band at 1650 cm-1.

Table 2.1 Comparative quantitation of the original MscL expression construct, $MscL^{M1A}$ and $MscL^{L-7Y}$ via Nanodrop (UV at 280 nm) and direct detect (IR at 1650 cm^{-1})

	UV Absorbance at 280 nm			**IR absorbance at 1650 cm^{-1} mg/ml**	**Disparity (A_{280}/IR)**
	ε_0 ($cm^{-1}M^{-1}$)	**A_{280}**	**mg/ml**		
Original construct	1490	0.092	0.99	0.53	1.9
$MscL^{M1A}$	1490	0.089	0.96	0.54	1.8
$MscL^{L-7Y}$	2980	0.179	0.96	0.99	1.0

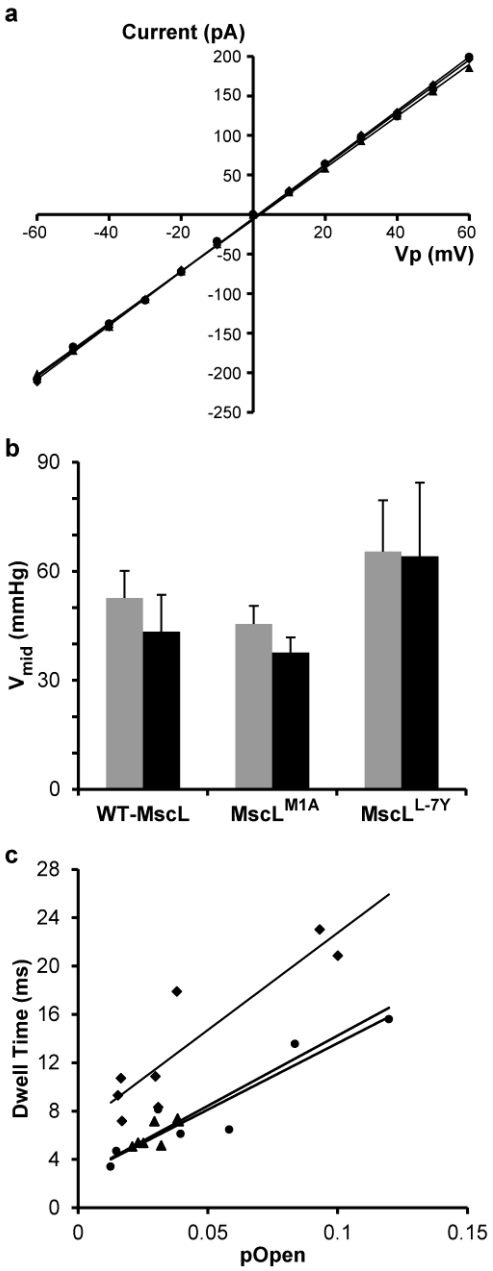

Figure 2.5. Biophysical analysis of original MscL (*filled circle*), MscL^{M1A} (*filled diamond*) and MscL^{L-7Y} (*filled triangle*) constructs via patch clamp analysis. **a** 3 individual samples were probed at 13 different voltages and a strong linear correlation independent of voltage, was established. Voltage-dependency plots of current observed through the MscL channel pore were effectively superimposed and yielded identical conductances of 3.3 nS for each construct, suggesting no detectable differences in the channel pore diameter. **b** Histogram of the opening and closing mid points of the wild-type and mutant MscL (pipette voltage V_p = + 30 mV) shows no significant difference between the wild-type and mutant channels based on the Student's t test (mean ± SD, n = 3). **c** A plot of the single channel dwell time against the channel open probability. The dwell time for MscL M1A suggests apparently longer openings compared to the wild-type and MscL^{L-7Y} mutant. However, the difference was not significant based on the t test (comparison to wild-type MscL)

While a significant discrepancy was observed in the protein concentration estimates obtained by the two techniques for both the original MscL construct and MscL^{M1A}, both techniques gave nearly identical measurements for the modified MscL^{L-7Y} construct (Table 2.1.) indicating that MscL concentration can be more accurately measured by either technique with the MscL^{L-7Y} construct.

2.2.5.3. Functional comparison of heterogeneous and homogeneous MscL constructs

Since the N-terminal region of MscL is known to be important to its function (Corry *et al.*, 2010; Iscla *et al.*, 2008), we investigated whether the homogeneously expressing $MscL^{M1A}$ and $MscL^{L-7Y}$ constructs exhibited any measurable differences in function to the original MscL construct, the latter containing a mixture of two species that vary in the length of their N-terminus. Biophysical analyses were performed on both the original MscL construct and the new $MscL^{M1A}$ and $MscL^{L-7Y}$ constructs. When reconstituted into soybean azolectin using the dehydration/rehydration reconstitution technique (Ajouz *et al.*, 2000; Delcour *et al.*, 1989; Hase *et al.*, 1995), both channels exhibited pore-forming activity, with channel activation thresholds of ~-60 mmHg (Fig. 2.4). Conductivity readings were also identical at 3.3 nS, indicating a similar channel pore size (Fig. 2.5a). This indicates that there is little if any distinguishable difference in MscL function and activity between the homogeneously and heterogeneously expressing constructs. In addition, no significant difference for midpoints of activation and deactivation thresholds was measured between the mutants compared to the wild-type MscL (Fig. 2.5b). We also performed dwell time analysis of single channel activity (Fig. 2.5c). Plotted against their respective open probability, dwell times for the $MscL^{M1A}$ mutant showed a trend towards longer openings compared to the wild-type and $MscL^{L-7Y}$ mutants, although the difference was not statistically significant.

2.2.6. Summary

The use of a heterogeneously expressing construct in some studies and homogeneously expressing constructs in others represents a potentially confounding factor in studies of MscL. Here we have identified the cause of heterogeneous expression in the original MscL expression construct developed in 1994 (Hase *et al.*, 1995; S. I. Sukharev *et al.*, 1994) and still widely used today. Despite recent studies showing that the N-terminal sequence of MscL influences the functional properties of the channel (Corry *et al.*, 2010; Iscla *et al.*, 2008), we show that this heterogeneously expressing construct is functionally indistinguishable from a newly engineered, homogeneously expressing channel, in agreement with an earlier study showing that extending the length of the N-terminal domain has no effect on the functional properties of MscL (Hase, Le Dain, *et al.*, 1997). Since the use of a homogeneously expressing construct is highly desirable (for studies of MscL structure, in particular), our work removes any uncertainty concerning the extrapolation of findings from previous studies utilizing the heterogeneously expressing construct, and recent and future studies utilizing homogeneously expressing constructs. Furthermore, we have shown that by

introducing a single residue substitution within the residual linker region of the recombinant MscL construct, protein concentration measurements can be much more reliably obtained. This represents an important variable, since accurate protein concentration measurements are essential to reliably interpret biophysical data and aid reproducibility in biophysical and structural studies.

2.2.7. Acknowledgements

N-terminal sequencing was facilitated by access to the Australian Proteome Research Facility, supported under the Australian Government's National Collaborative Research Infrastructure Strategy (NCRIS), with assistance from Gerogina Giannikopoulos and Bernie McInerney. Mass spectrometric analyses were carried out with the assistance of Alun Jones at the Institute for Molecular Bioscience Mass Spectrometry Facility. The authors additionally with to thank Dr. Honathan Beesley (QIMR Berghofer Medical Research Institute) for general advice and discussions on cloning. This work was funded in part by the National Health and Medical Research Council of Australia (APP104780).

Supplementary Information

2.3. Methods

In this section, supplementary methods not detailed in the published are provided.

2.3.1. Site-directed Mutagenesis

Site-directed mutagenesis alters nucleotide sequences in a gene in a predictable and reproducible way, making it a useful tool in protein studies. Three methods were used in this study to create new plasmid constructs with altered DNA sequences.

2.3.1.1. Cassette mutagenesis

Cassette mutagenesis involves insertion of a DNA fragment containing the desired genetic sequence to an existing construct, allowing multiple base mutations to be introduced (Fig. 2.6) (Wells *et al.*, 1985). This protocol was used in the first attempt at producing MscL^{TEVc} (in pQE-31 plasmid) construct.

The sequence of a native plasmid was analysed using Vector NTI (Invitrogen, U.S.A.), and mutation sequences were designed. Two unique restriction enzyme cutting sites were identified on

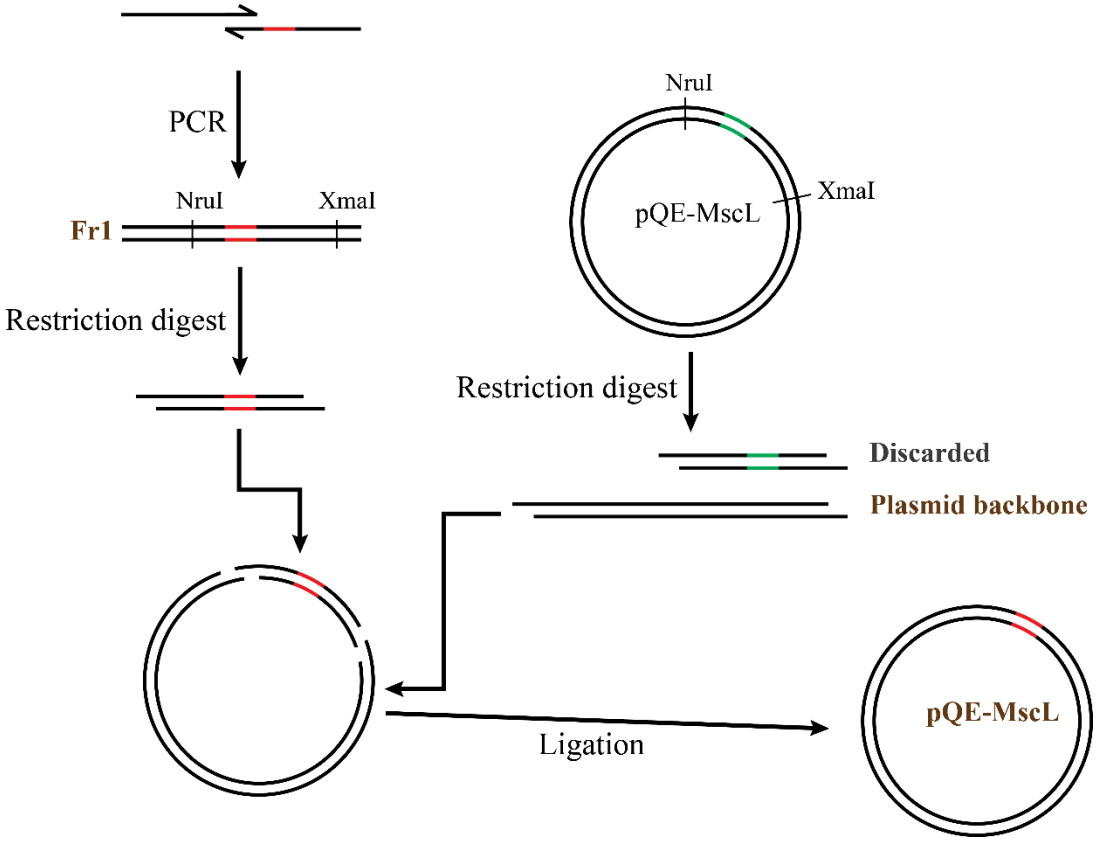

Figure 2.6. Schematic outline of cassette mutagenesis protocol. *Red* denotes the mutant sequence

either side of the target sequence, allowing cleavage of the site of interest. An insertion fragment was designed to include the recognition sites (NruI and XmaI) as well as the mutation sequence. The insertion fragment was ordered as two single-stranded primers, one direct and one complementary, with an overlapping region. They were annealed and extended by one PCR cycle (1 min denaturation at 95℃; 2 min annealing at 50℃; 5 min extension at 72℃).

A quantity of 500 ng each of the fragment (Fr1) and the native plasmid were then separately incubated with the restriction enzymes in 30 µL of solution at 37°C for 1 h. One unit of shrimp alkaline phosphatase (New England BioLabs, U.S.A.) was added to the plasmid solution, and both fragment and plasmid solutions were further incubated at 16 ℃ for 30 min. The linearised plasmid was purified by agarose gel electrophoresis (100 mL 0.8 % agarose gel; 130 V, 30 min), while the fragment was purified by polyacrylamide gel electrophoresis (PAGE) using 12% acrylamide 1 x Tris-borate-EDTA (TBE) gel with 1 mm x 85 mm x 85 mm dimension (80 V, 1 hr).

A quantity of 300 ng of the fragment and 100 ng of the linearised plasmid were combined into one tube, together with two units of T4 DNA ligase (New England Biolabs, U.S.A.) and 4 µL T4 DNA ligase buffer, with the final volume adjusted to 40 µL with sterile water. The solution was incubated at 16℃ for 4 – 6 h, after which the reaction was stopped by incubation on ice. Transformation-competent *E. coli* DH5α cells (50 µl) were transformed with 2 µL of the ligated plasmid following the methods in Section 2.3.3. Plasmids were extracted from the cultures according to Section 2.3.2., and were sequenced at the Australian Genomic Research Facility (University of Queensland, Brisbane) for confirmation.

2.3.1.2. Overlap Extension PCR

Overlap extension PCR is another method used to introduce specific genetic mutations to an existing construct. While this technique is more complicated than cassette mutagenesis, it produces larger DNA fragments which allow easier detection of problems in the case of failure. Here, the protocol described by Ho *et al.* (S. N. Ho *et al.*, 1989) was followed with research-specific modifications, and was successfully used to produce $MscL^{TEVc}$ (in pQE-31 plasmid), $MscL^{Thrombin}$ (in pQE-31 plasmid), and $MscL^{M1A}$ (in pQE-31 plasmid) constructs.

The original plasmid sequence was analysed with Vector NTI (Invitrogen, U.S.A.), and mutation sequences were designed. A forward (F2) and a reverse (R1) primer were designed, with the mutation sequences flanking them on the 5' end (Fig. 2.7). Two unique restriction sites on either end of the mutation sequences were identified. A second set of primers (forward (F1) and reverse

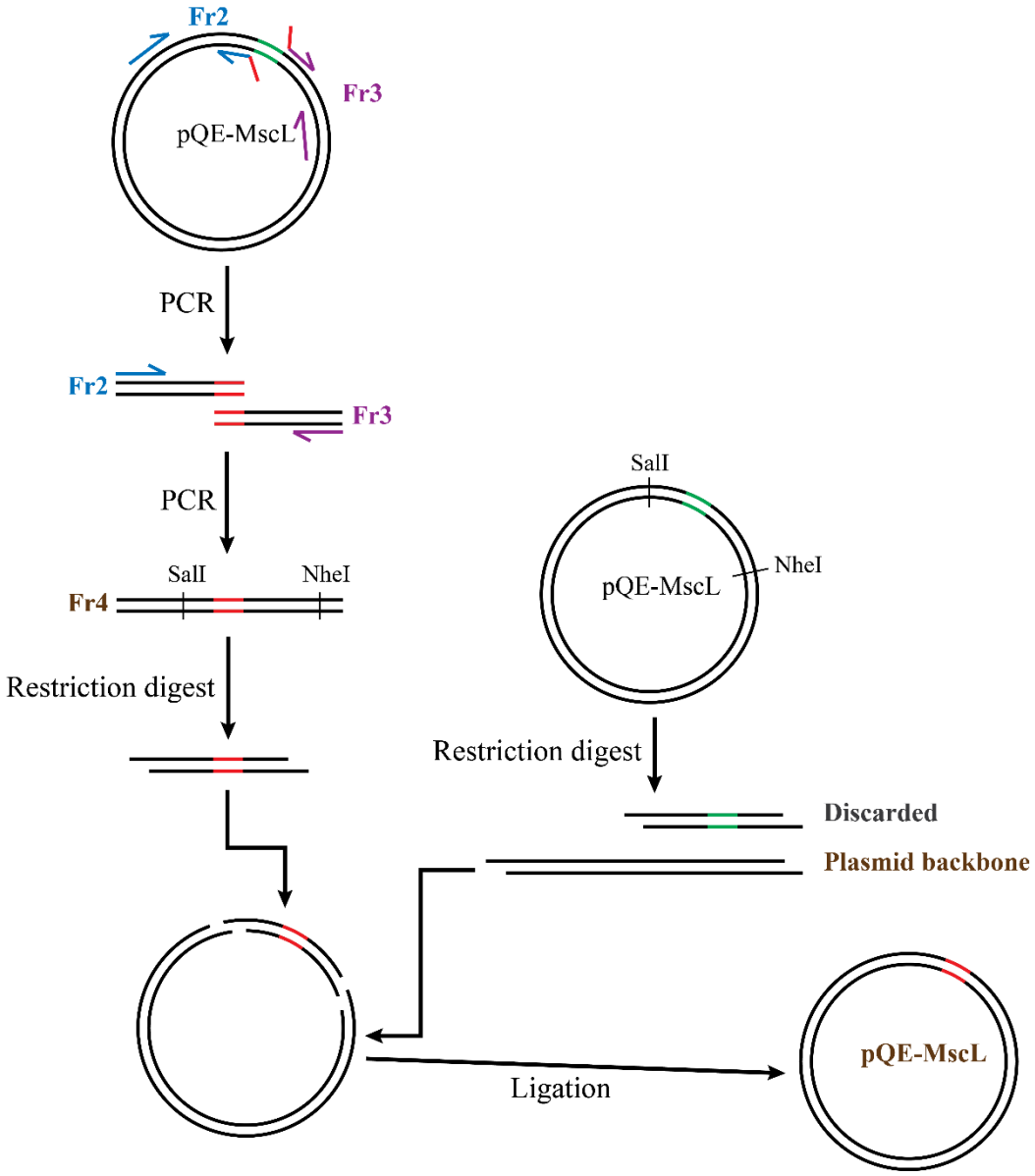

Figure 2.7. Schematic outline of overlap extension PCR protocol. *Green* indicates wild-type sequence targeted for mutation, and *Red* denotes the mutant sequence

(R2)) encompassing each restriction site (NheI and SalI) was designed. Primers were supplied by Integrated DNA Technologies (U.S.A.) and dissolved in DNase-free sterile water for a final concentration of 20 µM.

Original plasmid (20 ng), 10 µL of 5 x iProof-HF buffer, 1.5 µL of 10 mM dNTP, and 1 µL of iProof-HF DNA polymerase (Bio-rad, U.S.A.) were added to each of two PCR tubes. 1 µL each of F1 and R1 primers was added to one tube, and F2 and R2 primers to another tube. The final volume of each PCR reaction mix was adjusted to 50 µL with water. The two samples were amplified by PCR (30 cycles; conditions listed in Table 2.2). Fragments corresponding to the expected base pair (bp) size were separated by agarose gel electrophoresis (100 mL 1.2 % agarose gel; 130 V, 40 min) and extracted. The two fragments (Fr2 and Fr3) were combined in a tube, and ligated by PCR (20

cycles) as per the same protocol and conditions described above, but with F1 and R2 primers (F1/R2). The ligated fragment (Fr4) was subsequently purified with agarose gel electrophoresis (100 mL 1.0 % agarose gel; 130 V, 30 min).

The original plasmid (300 ng) and the fragment were separately incubated with the restriction enzymes in 30 μL solution at 37°C for 1 hr to create complementary ends. Both samples were run on 1.0 % agarose gel, and all unique bands were extracted. The fragment with longer base length from the plasmid sample (plasmid backbone) and the insertional fragment were combined. DNA ligation was carried out as described in Section 2.3.1.1., but using ExpressLink^{TM} T2 DNA Ligase (ThermoFisher Scientific, U.S.A.) instead of T4 DNA ligase. Competent *Escherichia coli* DH5α cells (50 μL) were transformed with 2 μL of the ligated plasmid. Plasmids were extracted from the cell culture, and were sequenced by the Australian Genomic Research Facility (AGRF) for confirmation of the correct fragment insertion.

Table 2.2. List of PCR parameters used for each sample in overlap extension PCR

PCR Condition		**Initial Denaturation**	**Denaturation**	**Annealing**	**Extension**	**Final Extension**
MscL^{TEVc}	**F1/R1**	98 ℃; 3 min	98 ℃; 30 s	52 ℃; 15 s	72 ℃; 15 s	72 ℃; 5 min
	F2/R2	98 ℃; 3 min	98 ℃; 30 s	56 ℃; 15 s	72 ℃; 15 s	72 ℃; 5 min
MscL^{Thrombin}	**F1/R1**	98 ℃; 3 min	98 ℃; 30 s	55 ℃; 15 s	72 ℃; 15 s	72 ℃; 5 min
	F2/R2	98 ℃; 3 min	98 ℃; 30 s	56 ℃; 15 s	72 ℃; 15 s	72 ℃; 5 min
MscL^{M1A}	**F1/R1**	98 ℃; 3 min	98 ℃; 30 s	55 ℃; 15 s	72 ℃; 15 s	72 ℃; 5 min
	F2/R2	98 ℃; 3 min	98 ℃; 30 s	56 ℃; 15 s	72 ℃; 15 s	72 ℃; 5 min
F1/R2 (All Constructs)		98 ℃; 3 min	98 ℃; 30 s	49 ℃; 15 s	72 ℃; 25 s	72 ℃; 5 min

2.3.1.3. Site-directed mutagenesis by Inverse PCR

Site-directed mutagenesis using an Inverse PCR method is a faster method of creating new constructs with specific mutations than the overlap extension PCR protocol, which can take up to three weeks. While this method is based on the publication by Dominy *et al.* (Dominy & Andrews, 2003), the protocol has been significantly changed to simplify the process. It was used to successfully produce the MscL^{L-7Y} (in pQE-31 plasmid) construct, and unsuccessfully for MscL^{L-7W} (in pQE-31 plasmid), and MscL^{G22C} (in pGEX 1.1 plasmid) constructs.

The original plasmid sequence was analysed with Vector NTI (Invitrogen), and mutation sequences were designed to include not only the targeted mutation but also a set of silent mutations to

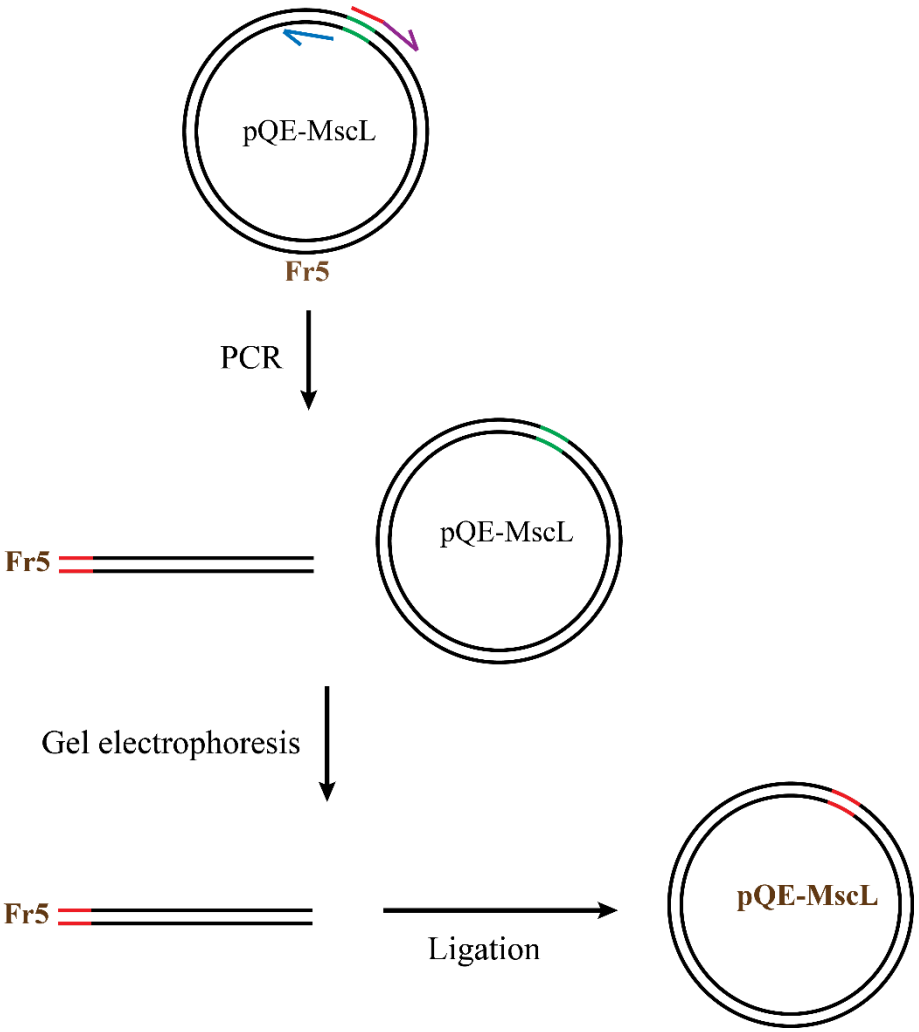

Figure 2.8. Schematic outline of inverse PCR protocol. *Green* indicates wild-type sequence targeted for mutation, and *Red* denotes the mutant sequence

introduce a sticky-end restriction site (S1) (Fig. 2.8). The forward (Fi) primer consisted of sequences containing the desired mutation, and the reverse (Ri) primer consisted of sequences complementary to the native sequence starting from the loci represented by the 5' end of the Fi primer. Primers were supplied by Integrated DNA Technologies (U.S.A.) and dissolved in DNase-free sterile water for a final concentration of 20 µM.

Original plasmid (20 ng), 1 µL each of Fi and Ri primers, 10 µL of 5 x iProof-HF buffer, 1.5 µL of 10 mM dNTP, and 1 µL of iProof-HF DNA polymerase (Bio-rad, U.S.A.) were added to a PCR tube. The final volume of each PCR reaction mix was adjusted to 50 µL with water, and the sample was amplified by PCR (30 cycles; conditions listed in table 2.3). An agarose gel electrophoresis (100 mL 0.8 % agarose gel; 130 V, 30 min) was performed with the sample to separate linear DNA from circular DNA, and the linear DNA component (Fr5) was extracted.

12 µL of the DNA solution, 2 µL T4 PNK buffer, 1 µL 20 mM ATP, 4 µL water, and 1 µL T4 polynucleotide kinase were added to a tube, which was then incubated at 37 ℃ for 30 min to

catalyse phosphate addition to the 5' terminus of the DNA fragment. The reaction was terminated by the addition of 2 µL of 0.5 M EDTA, and the DNA fragment was purified by the same ethanol precipitation method as above.

12 µL of the DNA solution, 4 µL of ligase buffer, 3.5 µL water, and 0.5 µL of ExpressLink^{TM} T2 DNA Ligase were added to a PCR tube, and was incubated at room temperature for 15 min. Competent DH5α *E. coli* cells (50 µL) was then transformed with 2 µL of the ligated plasmid as described in section 2.3.1.1. Plasmids were extracted from the culture as described in section 2.3.2.

500 ng of original plasmid, 3 µL of restriction enzyme buffer, and 1 µL of restriction enzyme for S1 site were added to a PCR tube, and water was added to a final volume of 30 µL. The restriction enzyme digestion was carried out at 37 ℃ for 1 hr, and was analysed with agarose gel electrophoresis (50 mL 0.9 % agarose gel; 130 V, 30 min), where successful digestion indicated successful mutation. The plasmid was sequenced by the Australian Genomic Research Facility (AGRF) for confirmation of the correct fragment insertion.

Table 2.2. List of PCR parameters used for each sample in inverse PCR

PCR Condition	Initial Denaturation	Denaturation	Annealing	Extension	Final Extension
MscL^{L-7W}	98 ℃; 3 min	98 ℃; 30 s	53 ℃; 20 s	72 ℃; 100 s	72 ℃; 5 min
MscL^{L-7Y}	98 ℃; 3 min	98 ℃; 30 s	52 ℃; 20 s	72 ℃; 100 s	72 ℃; 5 min
MscL^{G22C}	98 ℃; 3 min	98 ℃; 30 s	53 ℃; 20 s	72 ℃; 100 s	72 ℃; 5 min

2.3.2. Plasmid Extraction from *E. coli* DH5α

Where the purity of the sample was a concern such as for DNA sequencing, plasmids were extracted using a Miniprep® plasmid extraction kit (Bio-Rad). In most cases, however, the following method was used.

The transformed *E. coli* culture broth was incubated on a shaker at 37℃ for 12 hr. A quantity of 5 mL of culture was centrifuged at 2000 g for 10 min. The cell pellet was resuspended in 100 µL PBS and gently mixed with 500 µL of alkaline lysis buffer (1 % SDS; 0.2 M NaOH). The lysis was terminated within 5 min by adding 350 µL of 5 M potassium acetate. The solution was centrifuged at 13,000 *g* for 3 min, and the supernatant was transferred to another tube. Ethanol was added to the solution for a final concentration of 80% (v/v), and the mixture was incubated at room temperature for 5 min to precipitate the plasmid. The solution was centrifuged at 13,000 *g* for 3 min, and the supernatant was discarded. The pellet was dissolved in 200 µL water, and was re-precipitated by

adding 800 µL ethanol for cleaning. The solution was centrifuged at 13,000 *g* for 3 min, and the supernatant was discarded. The pellet was dissolved in water for a final DNA concentration of approximately 100 µg/mL.

2.3.3. Transformation of Competent *E. coli* cells with Plasmid

Plasmid solution (1 µL unless otherwise stated) was added to a tube containing 50 µL of chemically competent *E. coli* cells, and was incubated on ice for 15 min. The tube was incubated on a 42 ℃ heat block for 40 s, and then was immediately placed on ice. 500 µL of LB media was added to the tube, which was then incubated on a shaker at 37 ℃ for 1 h.

Two LB agar plates with antibiotics which the plasmid (and the competent cells' genomic DNA where relevant) have resistance genes for were prepared. LB agar with 50 mg/mL ampicillin was used for cultures intended for plasmid extraction, and LB agar with 50 mg/mL and 25 mg/mL chloramphenicol was used for cultures intended for protein expression. 200 µL of the incubated culture was evenly spread over one plate with sterile L-spreader. 20 µL of the culture was mixed with 180 µL of LB media, and was then spread over another plate with sterile L-spreader. Both plates were then incubated at 37 ℃ for a minimum of 12 h.

Colonies visible with naked eye were picked with each 200 µL pipette tip, and each of 25 mL LB media containing the antibiotics was inoculated with it. The pre-cultures were then incubated at 37 ℃ for 6-8 h or overnight.

2.3.4. Protein Expression and Purification

2.3.4.1. Protein Expression

E. coli AW737-KO strain, which has the native MscL gene substituted with chloramphenicol resistance gene, was transformed with the plasmid containing MscL gene as in section 2.3.3. Each of 500 mL LB media, 250 µL of 100 mg/mL ampicillin, and 5 mL of the pre-culture were added to a 2 L flask. In later experiments, 10 mL of a nutrient-rich solution (1 mM glucose, 100 g/L tryptone, 100 g/L yeast extract, 30% (v/v) glycerol, 100 mM Na_2HPO_4, pH 7.0) was added to each flask to reduce background expression and to increase both cell and protein yields.

The flasks were then incubated on a shaker (180 rpm) at 37 ℃ until the OD_{600} absorbance reading reached 0.7-0.8 (path length 1 cm). 400 µL of 1 M IPTG was added to each flask, and the culture was further incubated on a shaker (180 rpm) at 37 ℃ for 5 h. Cells were harvested by centrifugation with Avanti J-30i (Beckman Coulter, U.S.A.) at 7,000 *g* for 15 min. Supernatant was discarded, and

the cell pellet was used either immediately for purification or collected and stored at -20 ℃.

2.3.4.2. Protein Purification

Prior to the start of the experiment, the following solutions were prepared.

Phosphate buffered saline (PBS; 10 mM Na_2HPO_4, 1.8 mM KH_2PO_4, 2.7 mM KCl, 137 mM NaCl, adjusted to pH 7.5 with HCl) internally prepared by Queensland Biosciences Precinct (QBP) store was used as the main buffer in the experiments.

PD8 (PBS pH 7.5, 8 mM β-DDM) buffer was prepared with the volume corresponding to 15 mL per gram of cell pellet. PD1 (PBS pH 7.4, 1 mM β-DDM) buffer was prepared with PD8 buffer and PBS with the volume corresponding to 30 mL per gram of cell pellet. 50 mL of PDI1-15 (PBS pH 7.5, 1 mM β-DDM, 15 mM imidazole) and 50 mL of PDI1-300 (PBS pH 7.5, 1 mM β-DDM, 300 mM imidazole) buffer solutions were prepared with PD8 buffer, PBS, and 2 M imidazole solution. If size exclusion chromatography were to be performed, further 200 mL of PD1 buffer was prepared. For the purification of $MscL^{G22C}$, all solutions also contained 1 mM β-mercaptoethanol.

PBS was added to the cell pellet at a ratio of 9 mL per g cell, and the cell was thoroughly resuspended by vortexing for 2 min or more. The resuspended cells were then lysed with Constant Cell Disruption Systems (Thermo Scientific, U.S.A.) set to 23 kpsi pressure and passed twice. The lysate was then centrifuged at 13,000 *g* for 20 min at 4 ℃. The supernatant was collected and centrifuged with Optima L-100XP ultracentrifuge (Beckman-Coulter, U.S.A.) at 184,000 *g* (R_{av}) for 1:40 h at 4 ℃. The supernatant was discarded, and the membrane pellet was either used for further purification or stored at -20 ℃.

The membrane pellet was resuspended in PD8 buffer at a ratio of 1 g per 40 mL buffer, and was incubated for solubilisation on a rocker at 4 ℃ overnight, or 8-10 h. The solution was centrifuged with ultracentrifuge at 75,000 *g* for 30 min at 4 ℃. The supernatant was collected.

Approximately 1 mL of Talon™ resin per g membrane was prepared by repeatedly washing with water and then with PD1 buffer. The resin was then added to the supernatant and incubated on a rocker for 2 h at 4 ℃.

The combined samples were then poured into a gravity fed column. The resin was washed with 10 column volumes (CV) of PD1 buffer, followed by 50 mL of PDI1-15 (PBS, 1 mM β-DDM, 15 mM Imidazole) buffer to remove nonspecifically bound proteins and then with 10 CV PD1 buffer again to wash out residual imidazole.

To collect the His-tagged MscL, 0.5 CV of PDI1-300 buffer was added to the column and the eluent collected. 2 CV of PDI1-300 buffer was then added again and the eluent was collected again a

second time.

Alternatively to cleave the linker region with His-tag from the MscL construct, the resin was resuspended in 2 CV of PD1 buffer and transferred to a 50 mL Falcon tube instead of eluting with PDI1-500 buffer. 20 U thrombin per g membrane was added to the sample, which was incubated on a rocker at room temperature for 4 h followed by overnight incubation on a rocker at 4 ℃. The resin was transferred to the gravity flow column, and the eluent was collected. 2 CV of PD1 buffer was then added to the column and the eluent was collected a second time.

The eluent fractions were combined and concentrated with a 100,000 molecular weight cut-off (MWCO) concentrator either to a final volume of 1 mL, or to a concentration of 10 mg/mL. In the case of His-tagged MscL, the buffer condition was exchanged from PDI1-300 to PD1 by repeated dilution with PD1 followed by concentration. Alternatively, a PD10 desalting column (GE Life Sciences, U.S.A.) was used for the buffer exchange. The sample was either used for experiments or further purified.

For structural studies (Chapter 4), thin-layer chromatography (Chapter 3) and for experiments in the publication (section 2.2.), MscL samples with higher purity were obtained by size exchange chromatography. Superdex 200 10/300 GL column (GE Life Sciences) was connected to AKTA Purifier (GE Life Sciences), and was equilibrated in PD1 buffer. 500 µL of sample was injected onto the column, and the chromatography experiment was carried out with 0.5 mL/min flow rate at 4 ℃. All fractions were collected, and of these, the peak fractions presumed to contain MscL were combined and concentrated to 5 mg/mL protein concentration with 100,000 MWCO concentrator.

15 µL of sample was collected at each purification step detailed above, and they were run on SDS-PAGE (15 % acrylamide gel; 80 V, 1 h) to check expression level and purity of MscL sample in the experiment.

2.4. Results and Discussion

As most of the results from this chapter are already detailed in the publication (section 2.2.), this section will focus on the site-directed mutagenesis experiments, and MscL expression and purification protocol optimisation.

2.4.1. Site-Directed Mutagenesis

The first proposed solution to address the problem of heterogeneous expression of MscL was to substitute methionine-1 and the preceding linker region with TEV protease recognition site. The rationale for this was that 1) substituting methionine-1 would remove the second initiation site where the unintended MscL species was translated, and 2) cleavage with TEV protease would produce MscL with no linker region overhang, which was the case with the initial construct.

2.4.1.1. Cassette Mutagenesis

The first few attempts at producing this $MscL^{TEVc}$ construct used cassette mutagenesis method. This involved ligating two long primers to create a fragment containing mutation sequences (Fr1), which was then used to replace the original sequence with restriction enzymes and ligase (Fig. 2.6). The primer ligation step was successful (Fig. 2.9A) as well as the restriction digest of the main plasmid with NruI and XmaI which yielded the plasmid backbone with sticky-end restriction site on either end (Fig. 2.9B). However, the restriction digest of the Fr1 fragment could not be confirmed due to the small change in base pair size. The ligation of the Fr1 fragment to the plasmid backbone did not appear to work, as the same number colonies (4) grew on LB agar with ampicillin (LB/Amp) for both *E. coli* transformed with the plasmid and the untransformed cells (as negative control). When the plasmids from the cells were extracted and sequenced, they were found to match the original

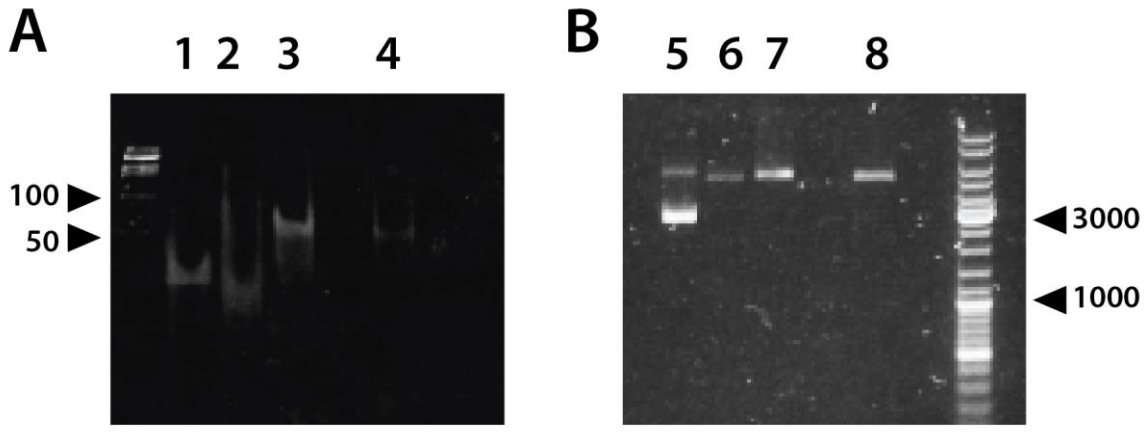

Figure 2.9. A) Polyacrylamide gel electrophoresis of starting primers (*1* and *2*), Fr1 fragment (*3*), and Fr1 cut with restriction enzymes (*4*). **B**) Agarose gel electrophoresis of original MscL2.1-pQE-31 plasmid (*5*), plasmid cut with NruI (*6*), plasmid cut with XmaI (*7*), and plasmid cut with both enzymes (*8*)

plasmid rather than the one with mutated sequence, confirming that the experiment was not successful.

2.4.1.2. Overlap-Extension PCR

The next attempt at producing the MscL^{TEVc} construct used a different strategy called overlap-extension PCR. In this method, the first round of PCR produced two fragments containing mutated sequences (Fr2 and Fr3), which were then joined by a second round of PCR to produce a larger fragment (Fr4). Then this fragment replaced the original sequence using restriction enzymes and ligase (Fig. 2.7). The first round of PCR was successful, producing Fr2 fragment of 230 bp in size, and 600 bp Fr3 fragment (Fig. 2.10A). The second round of PCR was also successful, producing Fr4 fragment larger than Fr3 in agarose gel electrophoresis (Fig. 2.10B). Restriction enzyme digestion of F4 fragment with NheI and SalI was also successful.

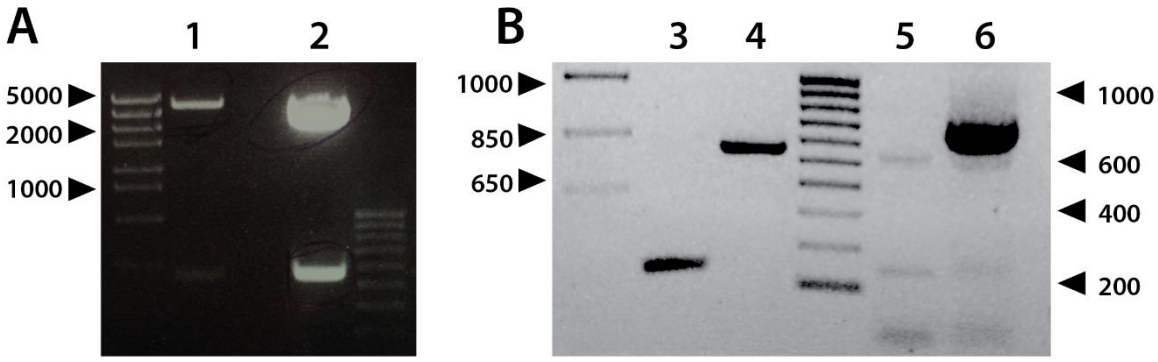

Figure 2.10. A) Agarose gel electrophoresis of original MscL plasmid (*1*), and pBlunt with mutant sequence insertion (*2*). **B**) Agarose gel electrophoresis of Fr2 (*3*), Fr3 (*4*), Fr4 fragment produced with Platinum Taq polymerase (*5*), and Fr4 fragment produced with iProof DNA polymerase (*6*).

However, similarly to the cassette mutagenesis, ligation of Fr4 fragment to the plasmid backbone did not appear to work in the first few attempts, as *E. coli* cells transformed with the ligated plasmid did not grow on LB/Amp agar plate. A different set of restriction enzymes (NruI and SalI) was also tried, as were longer ligation times (24 h instead of 4-6 h), however the ligation still did not appear to work.

In the third attempt, the same protocol for the first attempt (described in the first paragraph of this section) was used, except that the ligase used was changed from T4 DNA ligase to ExpressLink^{TM} T2 DNA Ligase. The latter, while more expensive, had higher ligation efficiency and so is often used in the ligation of blunt end fragments. This experiment was successful, with 10 colonies growing on the LB/Amp agar plate with *E. coli* transformed with the ligated plasmid, whereas none grew on the plate with untransformed *E. coli*. All 10 colonies were picked for plasmid extraction, and 4 of them were sent to AGRF for sequencing. All four sequences matched the designed mutant sequence.

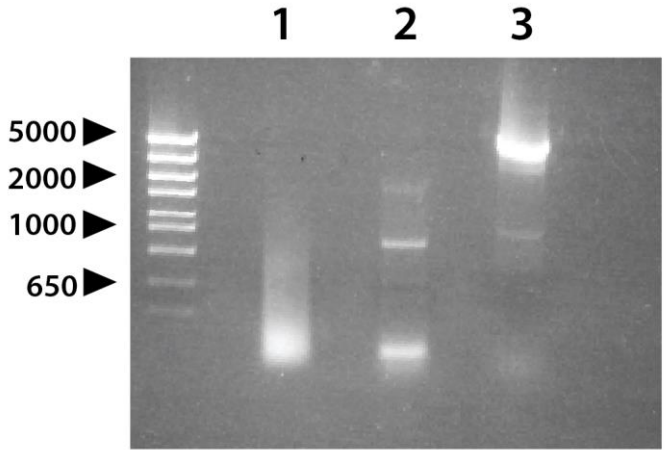

Figure 2.11. Agarose gel electrophoresis of Fr5 fragments of MscL^{G22C} (1), MscL$^{L\text{-}7W}$ (2), and MscL$^{L\text{-}7Y}$ (3)

This strategy was later repeated to produce MscL^{Thrombin} construct, which contained the thrombin cleavage site instead of the TEV protease recognition site, as well as MscL^{M1A} construct, which substituted methionine-1 with alanine. These experiments were also successful.

2.4.1.3. Site-directed Mutagenesis Using Inverse PCR

Inverse PCR method was used to produce MscL$^{L\text{-}7W}$, MscL$^{L\text{-}7Y}$, and MscL^{G22C} constructs for two reasons: first, this strategy took as little as three days, making it considerable shorter than overlap-extension PCR; and second, this experiment was not critical to the thesis at the time, so a quick approach which would not take too much time and resources was preferred.

A major disadvantage of Inverse PCR was that, unless there was a native restriction site close to the sequence targeted for mutation, a new restriction site overhang would have to be produced in the PCR step, which would then have to be removed in additional steps. Therefore, a simpler approach was developed, wherein the whole plasmid would be amplified with PCR with one of the primers containing mutated sequences, followed by blunt-end ligation of the Fr5 fragment.

The fragment amplification with PCR was successful on the second attempt, but only for MscL$^{L\text{-}7Y}$ and not for MscL$^{L\text{-}7W}$ and MscL^{G22C} (Fig. 2.11). While the reason for this is unclear, it might have been due to the inherent problems with amplifying a whole plasmid with PCR. The fragment was

Table 2.4. The number of DH-5α *E. coli* colonies transformed with the ligated plasmid (for MscL$^{L\text{-}7Y}$) grown on LB/Amp agar

Plasmid used	**No plasmid used (negative control)**	**Untreated MscL$^{L\text{-}7Y}$**	**MscL$^{L\text{-}7Y}$ treated with PNK**
Number of colonies	0	47	130

split into two, and one was treated with T4 polynucleotide kinase (PNK).

Both fragments were ligated and then used to transform *E. coli* cells, where the sample treated with PNK produced significantly more colonies on the LB/Amp agar plate than untreated one, but it was shown not to be a critical step (Table 2.4). Plasmids were extracted from the colonies and sent to AGRF for sequencing, where all of their sequences matched the mutated sequence.

2.4.2. MscL Expression and Purification Protocol Optimisation

The MscL expression and purification protocol based on Häse *et al.* (Hase *et al.*, 1995) and modified by Dr. Michael Landsberg (unpublished) was mostly followed. A more nutrient-rich culture was used instead of LB media, which improved the cell yield from 4 g/L culture to over 6 g/L, as well as MscL yield from 0.5 mg/L culture to 1 mg/L. In addition, MscL at the end of purification was kept in PD1 buffer instead of exchanging it to 20 mM Tris (pH7.5), 1 mM β-DDM buffer. Tris buffer's relatively large pH sensitivity to temperature change (0.028 per °C) was speculated to affect MscL stability, as it could be concentrated to over 10 mg/mL in PD1 buffer but only up to approximately 1 mg/mL in Tris/β-DDM buffer.

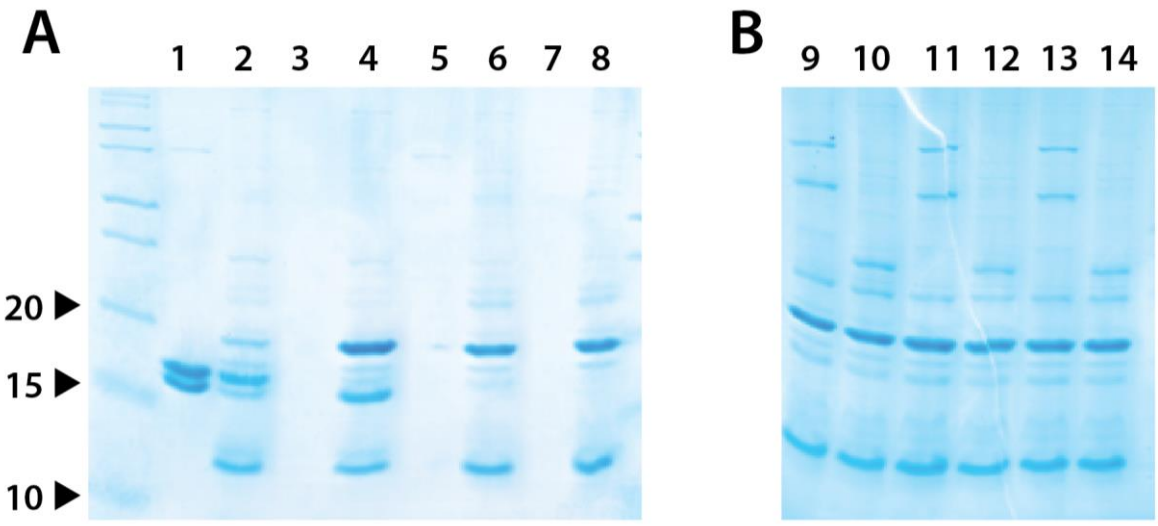

Figure 2.12. A) SDS-PAGE of various MscL samples treated with proteases. *1* – Original MscL eluent after thrombin treatment of Talon resin; *2* – Talon resin after thrombin treatment; *3* – Original MscL eluent after TEV protease treatment of Talon resin; *4* – Talon resin after TEV protease treatment; *5* – $MscL^{TEVc}$ eluent after thrombin treatment of Talon resin; *6* – Talon resin after thrombin treatment; *7* – $MscL^{TEVc}$ eluent after TEV protease treatment of Talon resin; *8* – Talon resin after TEV protease treatment. **B**) SDS-PAGE of Talon resin-bound MscLTEVc treated with heat and proteases. *9* – Thrombin with no heat treatment; *10* – TEV protease with no heat treatment; *11* – Thrombin after 70 ℃ incubation; *12* – TEV protease after 70 ℃ incubation; *13* – Thrombin after 95 ℃ incubation; *14* – TEV protease after 95 ℃ incubation

2.4.2.1. Affinity tag cleavage of MscL^{TEVc} with TEV protease and Thrombin

MscL^{TEVc} construct has two protease recognition sites in the C-terminal linker region: TEV protease site at the C-terminal end of the MscL region, and thrombin site at 8 residues upstream of the MscL region. While this construct could be homogeneously expressed and purified, it was resistant to cleavage by both proteases (Fig. 2.12). As it was thought at the time that the linker region could interfere with protein crystallisation, and because His-tag is known to affect channel gating, attempts were made to find a condition for the protease cleavage to be successful.

In the first approach, a much larger amount of protease (100 U per g membrane instead of 20 U) was added for tag cleavage, which was not successful (Fig. 2.12A). In the second attempt, MscL sample was split into three aliquots and they were incubated at room temperature (22 ℃), 75 ℃, and 90 ℃ respectively for 5 min. It was hypothesised that the linker region but not MscL would denature at 75 °C, hence improving the proteases' access to the recognition site, and 90 °C incubation was used as a positive control where MscL as a whole would become denatured. This approach was not successful either, as neither thrombin nor TEV protease could cleave the linker region of the construct in any of the samples (Fig. 2.12B).

The exact cause of this problem is not known, and has not been investigated beyond these two attempts. However, it is reasonable to speculate that the result may be due to the hydrophobic nature of the thrombin and TEV protease recognition sites (Fig. 2.13). The substituted region in the original construct was largely hydrophilic, and by replacing this with the more hydrophobic TEV protease recognition sequence, the linker region becomes more hydrophobic. As a result, the N-terminal linker region may have formed its own hydrophobic core with a propensity to bury itself

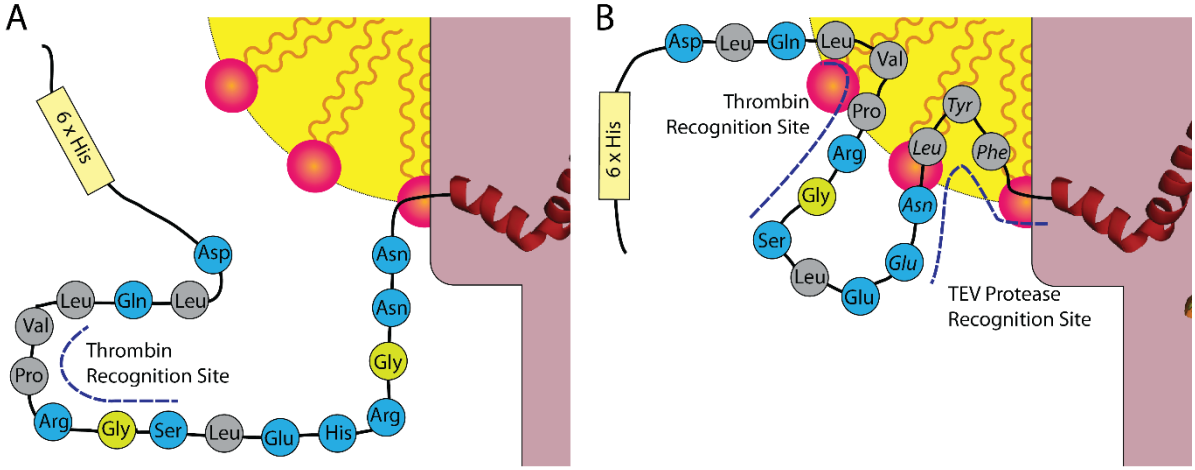

Figure 2.13. Schematic representation of the hypothesis on the resistance of MscL^{TEVc} to protease cleavage. Hydrophilic residues are highlighted with blue; neutral residues are in light green, and hydrophobic residues are highlighted with grey. **A**) The linker region of original MscL construct is largely hydrophilic with the exception of thrombin recognition site, so it is stable in solution. **B**) Both thrombin and TEV protease recognitions sites of MscL^{TEVc} are buried in the detergent micelle core due to the hydrophobicity. This prevents access by the proteases.

within the detergent micelles, hindering access by proteases. In order to address this problem, another construct ($MscL^{M1A}$) was designed so that there would be little change to the linker region, whose product could be cleaved by thrombin like the original construct.

2.5. Conclusion

I have detailed in this chapter the site-directed mutation experiments to produce new MscL constructs which express homogeneously and which is also reliably quantified. Clearly a homogeneous protein preparation is highly desirable for crystallisation experiments, and accurate and precise quantification allows these experiments to be carried out with the protein using concentration as a controllable variable. The new constructs, especially $MscL^{M1A}$ and $MscL^{L-7Y}$, were used in the experiments in the third and fourth chapters.

Patch clamp experiments (by Pietro Ridone and Dr. Yoshimura Nakayama at Victor Chang Cardiac Research Institute, Sydney) have also demonstrated that the mutations did not significantly change the channel gating properties, which makes it possible to extrapolate data between commonly used MscL constructs. For example, a heterogeneous MscL complex containing both wild-type and recombinant species having similar channel gating properties to homogeneous constructs show that the C-terminal linker region has little influence on the protein function (Chi *et al.*, 2015).

In addition, to simplify the site-directed mutagenesis protocol, a modified method based on Inverse PCR was developed and successfully used to produce a new MscL construct.

2.6. Supplementary Figures

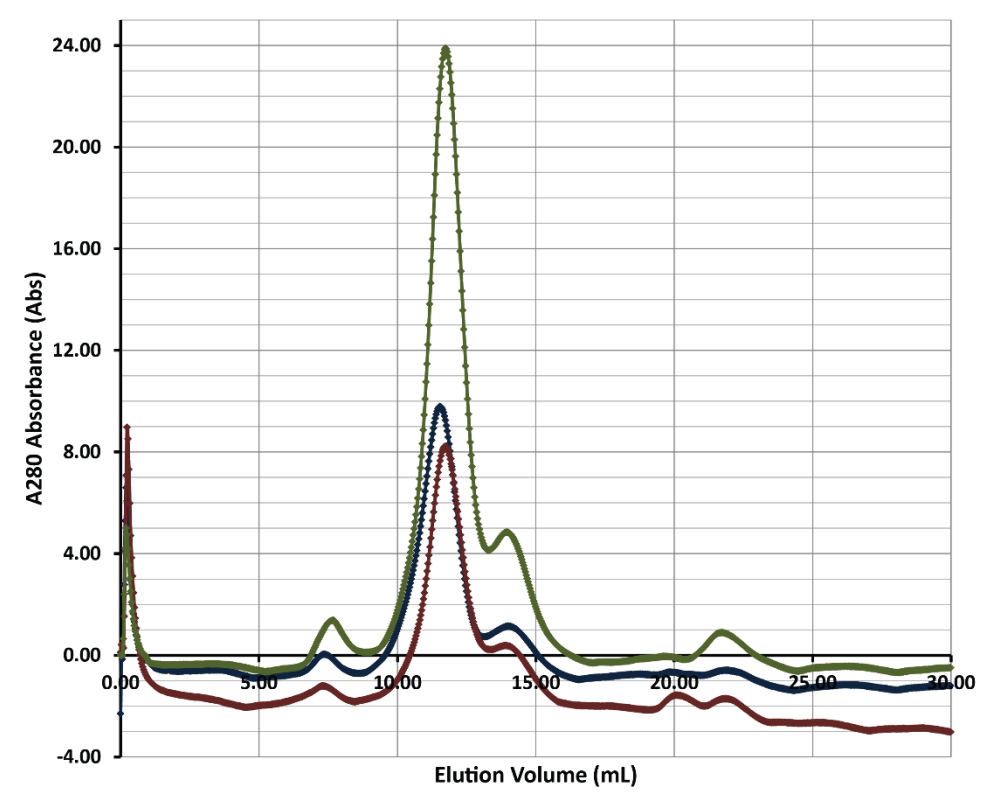

Figure 2.S1. Size exclusion chromatography of 0.5 mg of original MscL construct (blue), MscL^{M1A} (red), and MscL^{L-7Y} (green).

3. Biophysical Characterisation of Interaction Between MscL and Phospholipid

3.1. Introduction

Membrane protein function is dependent on the membrane environment, and there is a growing research interest into their relationship. As protein channels primarily gated by membrane tension, this is especially significant for mechanosensitive channels. For example, MscS localises to the poles of bacterial cells where relatively high concentrations of negative phospholipids phosphatidylglycerols (PG) and cardiolipins alter both its aggregation and channel function (Andrew R. Battle *et al.*, 2011; Nomura *et al.*, 2012; Romantsov *et al.*, 2010). The cleft between TM domain and C1 domain is thought to be a binding site for certain phospholipids (Pliotas *et al.*, 2015). Some non-mechanosensitive TRP channels are regulated by phosphoinositides in membrane, providing indirect evidence for phospholipid interaction with mechanosensitive TRP channels (Rohacs, 2014). Therefore, it is important that the function of mechanosensitive channels be understood in the context of the membrane environment they are studied with.

There is growing evidence that the membrane environment is a factor in MscL function, but their relationship remains poorly understood and is not taken into account in many experimental designs. This has led to several misinterpretation of data in the past: the channel gating threshold of *M. tuberculosis* MscL was initially thought to be significantly higher than *E. coli* MscL (P. C. Moe *et al.*, 2000). This later turned out to be due to *M. tuberculosis* MscL in membrane containing phosphatidylinositol, which is found in native *M. tuberculosis* membrane but not in *E. coli* (Zhong & Blount, 2013). Such lack of information on the relationship between MscL and phospholipids continues to be a confounding factor. The majority of research on MscL is conducted with membranes dominated by phosphatidylcholines (PC) (Corry *et al.*, 2010; Grage *et al.*, 2011; Iscla *et al.*, 2013; Kocer, 2015; Meyer *et al.*, 2006; Rui *et al.*, 2011; Sawada *et al.*, 2012; Yoshimura *et al.*, 2008) despite PC not being a native component of *E. coli*'s inner membrane. However, *E. coli* MscL's gating threshold is significantly lower in pure PC membrane than in one with the addition of phosphatidylethanolamine (PE) (Kamaraju & Sukharev, 2008; P. Moe & Blount, 2005), calling into question the validity of a number of studies. Other membrane environment factors are often not given serious consideration in experimental design or data analysis either: global curvature's influence on MscL function has not been explored beyond simulations (Bavi, Cox, *et al.*, 2016; Meyer *et al.*, 2006); the distribution pattern of MscL within membranes remains poorly understood apart from the observed clustering in DOPC (Grage *et al.*, 2011; Nomura *et al.*, 2012); and there

have been few studies investigating protein-to-protein interaction, focusing on MscS (Andrew R. Battle *et al.*, 2011; Nomura *et al.*, 2012). However, there is increasing evidence that these have significant impact on MscL function as observed in both past publications (Grage *et al.*, 2011; Nomura *et al.*, 2012) and in this thesis (sections 3.3.2. and 3.3.3.).

The information on the relationship between MscL and the membrane is relevant not only from an academic perspective but also for the development of MscL as nanovalve in a liposomal drug delivery system. Smaller liposomes are generally favoured for drug delivery because they tend to be more permeable to physiological barriers such as blood vessels (Garnier *et al.*, 2012). There are conflicting hypotheses, both based on molecular dynamics studies, on the influence of global curvature in small liposomes on MscL function (Bavi, Cox, *et al.*, 2016; Meyer *et al.*, 2006), making an experimental confirmation of whether MscL is to be engineered for gating threshold (Iscla *et al.*, 2013; Nakayama *et al.*, 2015). Likewise, the relationship between MscL and lipids (including but not limited to phospholipids) needs to be better understood, since phospholipids used for liposome formulation can be dependent on the type of target tissues or objectives (H. I. Chang & Yeh, 2012; Fan & Zhang, 2013; van den Hoven *et al.*, 2011).

In this chapter, I have investigated three aspects of the MscL/phospholipid relationship. First phospholipids' association with *E. coli* MscL in the native environment, mainly employing thin layer chromatography. It was hypothesised that MscL may interact strongly with certain lipids in the native environment, and that the interaction would be relevant to MscL function. Hence, this information had the potential to help explain the observed behaviour of MscL in various liposomal environments.

Second, MscL function in liposomes consisting of different phospholipids was studied to determine whether they were influenced by certain liposomal environments such as phospholipid composition and the liposome size. Using heterogeneous phospholipid mixtures allowed multiple variables such as liposome size, phospholipid types and the method of liposome preparation, to be studied at once and at a much lower cost than would be possible if homogeneous phospholipids were used. Electron microscopy of the liposomes was carried for structural analysis and to observe the aggregation pattern. Dynamic light scattering was used for quantitative measurement of the liposome size.

Lastly, the arrangement of MscL within lipid bilayers was investigated as a function of membrane lipid composition. Mainly employing electron microscopy, the tendency of MscL to aggregate or cluster within liposomes was investigated in the presence of multiple different lipid species. The results are later used to help with the optimisation of 2D crystallisation experiments performed and detailed in Chapter 4.

3.2. Methods

3.2.1. Phospholipid Preparation for Liposome Production

Phospholipids purchased as lyophilised powders from either Avanti Polar Lipids (U.S.A.) or Sigma Aldrich (U.S.A.) were dissolved in chloroform at a final concentration of 10 mg/mL. Aliquots were either used immediately or stored at -80 ℃ for subsequent use. The list of phospholipids used is detailed in Table 3.1.

500 µL of the phospholipid solution was added to a 5 mL glass tube pre-cleaned with chloroform, and chloroform was evaporated under a nitrogen gas stream while rotating the tube along the tube axis to produce a thin layer of phospholipid on its wall. 1 mL of water (section 3.2.3.1.) or buffer (section 3.2.2.1.) was added to the tube. The tube was vortexed for 1 min, followed by 5 min sonication in a bath sonicator to produce a dispersion of vesicles. The solution was either aliquoted in 1.5 mL microtubes and stored at -20 ℃ or used immediately in the following steps.

3.2.2. Size Fractionation of MscL Proteoliposome

The method for preparing and size fractionating MscL proteoliposomes is based on a method developed by Dr. Alexander Foo and described in (Alexander Foo, 2014).

3.2.2.1. MscL Proteoliposome Preparation by Extrusion

2 mL of 5 mg/mL liposome solution in carboxyfluorescein buffer (5 mM HEPES pH 7.2, 100 mM

Table 3.1. List of phospholipids used in Chapter 3

Phospholipid	Head Group	Tail Group	Product Source
***E. coli* Lipid**	Mixed (58 % PE; 15 % PG)	Mixed	Avanti Polar Lipids
Soy Azolectin	Mixed (30 – 40 % PC)	Mixed	Sigma-Aldrich
DOPC	Zwitterionic	18:1/18:1	Avanti Polar Lipids
POPC	Zwitterionic	16:0/18:1	Avanti Polar Lipids
DPPC	Zwitterionic	16:0/16:0	Avanti Polar Lipids
DMPC	Zwitterionic	14:0/14:0	Avanti Polar Lipids
DOPE	Zwitterionic	18:1/18:1	Avanti Polar Lipids
Cardiolipin	Negative	18:1/18:1,18:1/18:1	Avanti Polar Lipids
DOPS	Negative	18:1/18:1	Avanti Polar Lipids
POPG	Negative	16:0/18:1	Avanti Polar Lipids

KCl, 50 mM 5,6-carboxyfluorescein) was extruded using a LiposoFast-Basic System (Avestin, Canada) by passing it through a 400 nm membrane (Whatman, U.S.A.) eleven times. The solution was then re-extruded using a 100 nm membrane (Whatman). Approximately half of the phospholipid by mass is lost during the extrusion step due to factors including less than 100 % solution recovery and adherence of lipid to the membrane; this loss is taken into account in calculations in the following steps.

1 mg/mL MscL solution in PD1 buffer (PBS pH 7.4, 1 mM β-DDM) was added to the liposome solution to obtain a desired protein-to-lipid ratio (w/w; 1:10, 1:20, and 1:100 were used in this thesis), and incubated on a rocker at room temperature for 30 min. 100 mg of Bio-Beads^{TM} SM-2 (Bio-Rad) prepared by sequential wash with methanol and water was added to the solution, and further incubated on a rocker at room temperature for 4 – 6 h. This solution was either directly used in the following steps, or was used after dialysis with 3,500 MWCO SnakeSkin^{TM} (ThermoFisher Scientific, U.S.A.) dialysis membrane in 100 mL PD1 buffer overnight to remove free carboxyfluorescein.

3.2.2.2. Size Fractionation of Proteoliposome by Continuous Sucrose Gradient

12 mL of sucrose gradient solution (10 mM HEPES pH 7.4, 300 mM sucrose, 100 mM KCl) was prepared in a thin-wall UltraClear^{TM} ultracentrifuge tube (Beckman-Coulter, U.S.A.). The tube was frozen at -80 ℃ and then thawed for 3-5 h at 4 ℃ before use. 200 µL of the proteoliposome solution was gently added to the top of the tube so as not to disturb the gradient. The sample was centrifuged at 114,000 *g* (R_{av}) at 4 ℃ for 14 – 16 h. 200 – 500 µL fractions from the sucrose gradient were collected by puncturing the tube wall on the side with a syringe fitted with a needle.

Liposome fractions were characterised by dynamic light scattering using a Zetasizer Nano ZS (Malvern, United Kingdom). The peak liposome diameter, mean liposome diameter, and the polydispersity index (PdI), a measure of the size distribution were recorded for each fraction.

3.2.2.3. Lipid Mass Spectrometry

Phospholipid analysis by mass spectrometry was performed in collaboration with Prof. Stephen Blanksby (Queensland University of Technology, Australia). The samples were directly injected to a LC-ESI-MS/MS system with precursor ion scan followed by collision energy scans for individual phospholipids (phosphatidylcholine, phosphatidylethanolamine and phosphatidylinositol).

3.2.3. Electron Microscopy of MscL Proteoliposomes

3.2.3.1. Pure Phospholipid Proteoliposome Preparation

6 µL of a 5 mg/mL liposome solution, 0.5 µL 200 mM $MgSO_4$, and either 6 µL or 0.6 µL of 5 mg/mL MscL were combined in a tube resulting in a protein-to-lipid ratio (w/w) of 1:1 or 1:10 respectively. PD1 buffer was added to a final volume of 30 µL. The solution was incubated on a rocker at room temperature for 30 min. The solution was then transferred to another tube containing 2.0 – 2.5 mg of Biobeads, and further incubated on a rocker at room temperature for 4 – 6 h. During the optimisation of this protocol, solutions which did not contain $MgSO_4$ as well as those which contained $MgCl_2$ instead were also tried.

3.2.3.2. Negative Staining of MscL Proteoliposome on EM Grid

Electron microscopy (EM) grids used in this study were prepared in the laboratory. 400-mesh copper grids (Electron Microscopy Sciences, U.S.A.) were coated with a thin layer of Formvar resin (ProSciTech, Australia). A thin carbon film was then evaporated onto the Formvar layer using graphite threads in a Q150T E carbon evaporator (Quorum Technologies, United Kingdom). Grids were glow-discharged immediately prior to use.

5 µL of proteoliposome solution was applied to the grid, incubated for 2 min, and subsequently blotted with filter paper. The grid was washed twice with water, and was stained with 1 % uranyl acetate solution by incubation on the drop for 1 min, followed by blotting with filter paper.

Alternatively to tag MscL with 5 nm Ni-NTA-Nanogold (Nanoprobes, U.S.A.), 5 µL of proteoliposome solution was incubated on the grid for 5 min followed by blotting with filter paper. A 6 µL drop of Nanogold solution was then applied to the grid for 30 min, following which the grid was washed with 20 µL of PBS pH 7.4 solution containing 10 mM imidazole for 1 min. The grid was twice washed with water, and was stained with 1 % uranyl acetate solution by incubation for 1 min followed by blotting with filter paper.

Grids were imaged using a JEOL 1011 transmission electron microscope (JEOL, Japan) coupled to a Morada charge-coupled device (CCD) imaging system (Olympus Soft Imaging Solutions, Germany). The microscope was operated at a high-tension voltage of 100 keV and images were recorded at nominal magnifications of 5,000x, 25,000x, 50,000x, and 100,000x.

3.2.3.3. Quantitative Analysis Based on Gaussian Distribution and Cluster Size Distribution

Clustering of Nanogold particles in electron micrographs was modelled in Matlab® (Mathworks, U.S.A.) using a protocol developed together with Dr. Jennifer Yarnold (Institute for Molecular

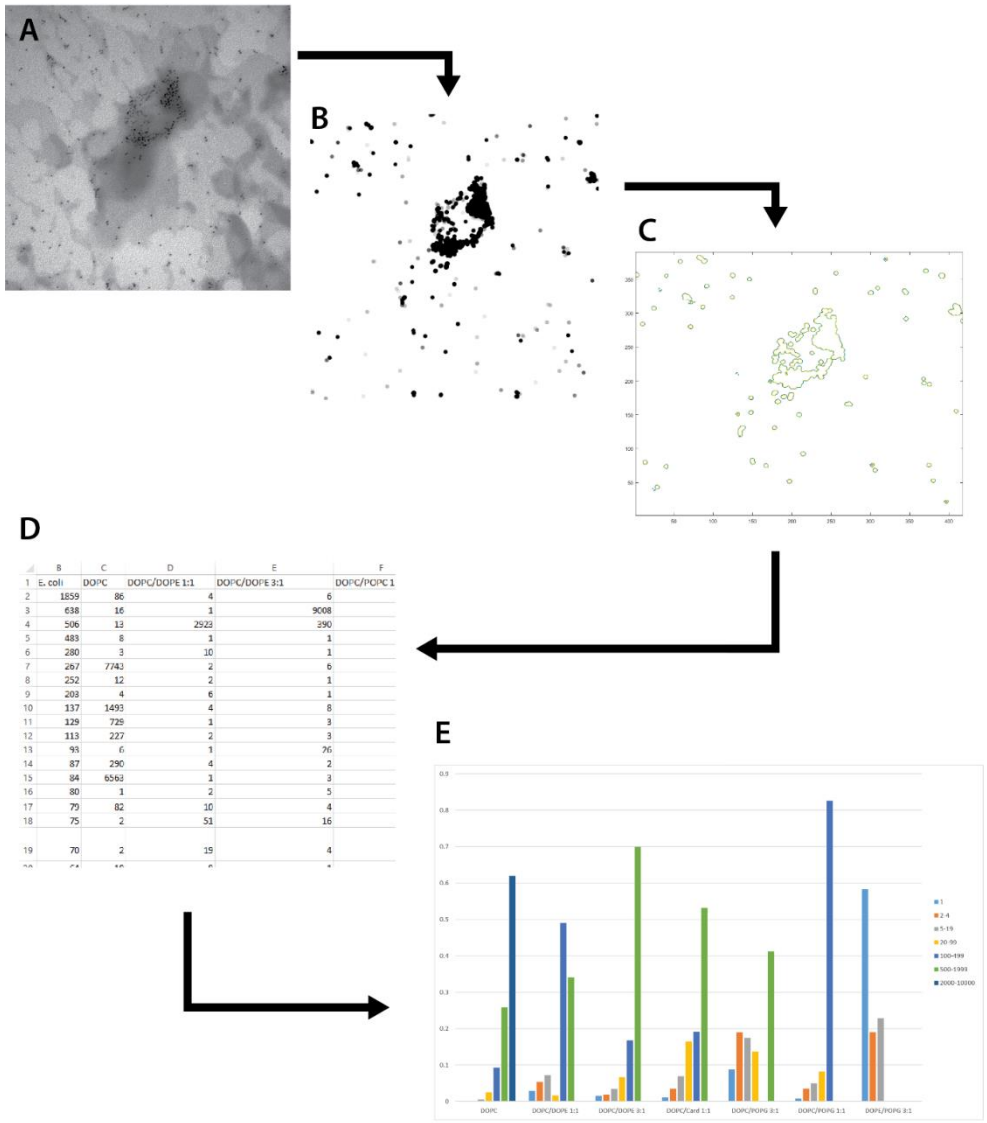

	B	C	D	E	F
1	E. coli	DOPC	DOPC/DOPE 1:1	DOPC/DOPE 3:1	DOPC/POPC 1
2	1859	86	4	6	
3	638	16	1	9008	
4	506	13	2523	390	
5	483	8	1	1	
6	280	3	10	1	
7	267	7743	2	6	
8	252	12	2	1	
9	203	4	6	1	
10	137	1493	4	8	
11	129	729	1	3	
12	113	227	2	3	
13	93	6	1	76	
14	87	290	4	2	
15	84	6563	1	3	
16	80	1	2	5	
17	79	82	10	4	
18	75	2	51	16	
19	70	2	19	4	

Figure 3.1. The schematic diagram of the protocol for semi-quantitative MscL cluster analysis. **A**) Raw micrograph. **B**) Image with contrast enhanced with Photoshop. **C**) Calculation of the area of each cluster with Matlab. **D**) Data processing with Excel. **E**) Data conversion into chart with Excel.

Bioscience, Australia). Clustering was modelled using a multi-component Gaussian mixture model, based on approaches described in the Matlab tutorials published on the Mathworks website (Mathworks, 2016).

Electron micrographs recorded at 100,000x magnification (Fig. 3.1A) were first processed (only) for improved contrast with Photoshop® CS6 (Adobe, U.S.A.). After initial processing, Nanogold particles were the darkest pixels in the image and could be readily detected (Fig. 3.1B). Where overstaining of liposomes was a problem, parts of the liposomes were masked so that only Nanogold-tagged MscL could be identified as black pixels on Matlab.

A multi-component Gaussian mixture model was applied to the imported electron micrographs and the cluster groups analysed. Initially, two protocols were run with the number of components set to

two (much fewer than the actual number of clusters) and seven (usually more than the actual number of clusters) respectively to gauge the number of clusters recognised by the program. The number of defined components in the protocol was then changed to be one more than the number of suspected clusters (the extra component accounting for non-clustered Nanogold particles). The protocol was run iteratively and checked for convergence. If the iterations failed to reach convergence, the number of components was increased by one, and the protocol was rerun. If there was convergence, triplicate analyses were performed as a control to check whether non-clustered particles were consistently grouped into a single component as they should. The proportion of this component in the scatter was recorded and compared across micrographs.

Additionally, the size of each cluster/particle was measured to estimate the number of particles in the cluster. Electron micrographs with improved contrast were again analysed with Matlab, this time using a protocol that returned the area of each Nanogold (black pixel) cluster (Fig. 3.1C). The dataset was then transferred to Excel 2013 (Microsoft, U.S.A.) (Fig. 3.1D), where noise was filtered out by removing areas smaller than 10 pixels, the average size of a single Nanogold particle at 100,000x magnification. The number of particles in each area was also estimated from this, and a histogram of the number of clustering particles was produced for each liposomal condition (Fig. 3.1E). The Matlab script for one of the processed images and the chain of Excel commands are listed in the supplementary information (section 3.6.).

3.2.4. Thin Layer Chromatography

Purified MscL at a concentration of more than 2 mg/mL concentration was transferred into a glass tube, and acetone was added to give a final concentration of 80 % (v/v). The tube was vortexed for 30 s several times, and was then incubated at room temperature for 5 min, followed by centrifugation at 1,000 *g* for 5 min. The supernatant was transferred to another glass tube.

120 mL of mobile phase solution for thin layer chromatography was prepared by mixing the components together. Early experiments used toluene, acetone and water mixed at ratios of 4:12:1 and 7:9:1 (v/v) respectively. In later experiments, the mobile phase consisted of chloroform, methanol, and water at 13:5:1 (v/v) ratio respectively.

The mobile phase solution was shaken well, and 60 mL was poured into a TLC chamber. 0.2 m x 0.2 m plain drawing paper and 0.2 m x 0.2 m glass-backed silica gel matrix plate (Sigma-Aldrich, U.S.A.) were placed in the chamber. The wash step was run until the mobile phase had migrated to the top of the silica plate. The chamber was emptied, and the plate was dried in an incubator at 50 ℃ for at least 15 min.

60 mL of fresh mobile phase solution and 0.2 m x 0.2 m of drawing paper were added to the TLC chamber, and left to equilibrate. MscL and phospholipid samples were loaded onto the silica plate with a minimum of a 2 cm gap between them. The plate was then placed in the equilibrated TLC chamber, and the chromatography was run until the mobile phase approached the top of the plate.

The plate was dried in an incubator at 50℃. Lipids were visualised using one of three different approaches. In early experiments, 45 % H_2SO_4 was sprayed on the plate, which was then charred in an incubator at 70 ℃ until the stains developed, usually for 15 min. Alternatively, the TLC plate and approximately 1 g of iodine granules were placed in a cleaned TLC chamber until lipid spots were visible. In later experiments, 0.05 % primuline solution was sprayed on the plate, and was visualised under UV light with a Gel Imaging System (Bio-rad, U.S.A.). The two latter methods have the advantages of staining non-destructively, hence allowing further analyses of the lipids such as mass spectrometry.

3.2.5. Extraction of Compounds from Silica Gel for Subsequent Analysis

The first extraction method used the main components of the mobile phase (chloroform and methanol) and the original solvent (acetone) used to extract the compounds from MscL. Locations and sizes of bands on a TLC plate with non-destructive stains (iodine or primuline) were clearly marked with pencil. Silica gel in each marked area was gently scraped from the plate with a clean spatula, and was transferred to a glass tube. The gel was mixed with 1 mL chloroform by vortexing, and was incubated on a shaker at room temperature for 10 min. The tube was centrifuged at 100 *g* for 5 min to pellet silica gel, and the chloroform was transferred to another glass tube.

The gel was then resuspended in 1 mL acetone by vortexing and incubated on a shaker at room temperature for 10 min. The tube was centrifuged at 100 *g*, and acetone was transferred to the glass tube containing the chloroform extract. Both the washed silica gel and extract solution were then stored at 80 ℃.

In an alternative method, a protocol by Bligh and Dyer (Bligh & Dyer, 1959) was followed. 1 mL water, 2.5 mL methanol, and 1.25 mL chloroform were mixed with the silica gel scraped from TLC plates by vortexing for 10 min. 1.5 mL chloroform was added to the sample, and was further vortexed for 1 min. 1.5 mL water was then added to the sample, and was vortexed for 1 min. The sample was centrifuged at 500 *g* for 10 min to separate hydrophobic (chloroform) and hydrophilic (water) phases. The hydrophobic phase was transferred to a new glass tube, and was evaporated under a stream of nitrogen gas. Once all solvent was evaporated, 100 µL chloroform and 200 µL methanol were added to the tube, and the sample was vortexed to solubilise the compounds. The

sample was then stored at -80 ℃ prior to analysis.

3.2.6. Silver Staining of PAGE gels

This protocol was based on Blum silver staining protocol described in (Mortz *et al.*, 2001).

15 µL of protein and/or proteoliposome samples were mixed with 5 µL loading solution, and were run on SDS-PAGE (15 % acrylamide gel; 80 V, 1 h). The gel was then incubated in water at room temperature for 1 min, followed by incubation in fixer solution (40 % ethanol, 10 % acetic acid, and 50 % water; v/v) at room temperature for 1 h. The gel was then incubated in water at room temperature for 6-8 h, replacing the water at least three times.

The gel was incubated in 0.02 % $Na_2S_2O_3$ solution for 1 min, and was washed with water at least three times for 20 s each. It was then incubated in staining solution (1 g/L $AgNO_3$, and 0.2 g/L formaldehyde) on ice for 20 min. The gel was washed with water at least 3 times for 20 s each. The gel was then transferred to a new container, and was incubated in developing solution (30 g/L Na_2CO_3, 0.5 g/L formaldehyde) on ice until the stain had sufficiently developed.

Once the stain had developed, the gel was washed with water, and incubated in 5 % acetic acid (v/v) for 5 min.

3.3. Results and Discussion

3.3.1. *E. coli* Phospholipids Natively Associating with MscL

3.3.1.1. Thin-Layer Chromatography

The main objective of this experiment was to identify any native *E. coli* lipids strongly associating with MscL. At the start of this project, it was hypothesised that MscL might exhibit a strong preference for particular lipids in the native environment. Different aggregation patterns and channel gating thresholds were observed for MscL reconstituted in phosphatidylcholine-only liposomes as opposed to mixed lipid liposomes. Hence, reasoning that the phospholipids preferentially interacting with MscL would also have high affinity to it and may potentially be of functional significance, experiments to identify them were carried out.

In the first set of trials, thin-layer chromatography (TLC) was performed with an organic solvent extract of purified MscL alongside a number of detergent and lipid controls. The initial objective was to identify a suitable mobile phase (i.e. solvent) and sample loading. As it was not clear at this point if detergents and phospholipids would separate well, and if other lipids such as cholesterol and

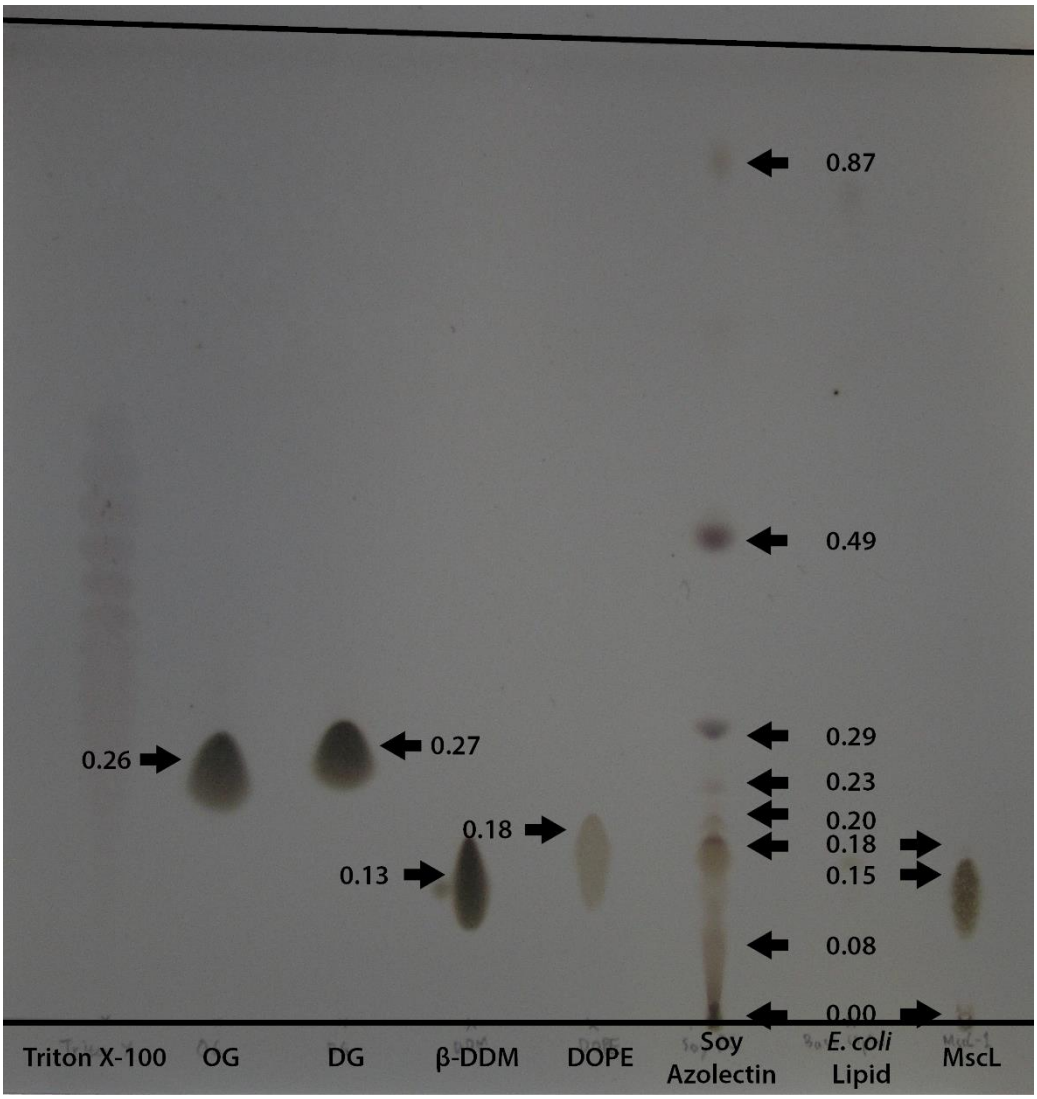

Figure 3.2. Thin layer chromatography of MscL and reference samples. The numbers next to arrows are R_f values.

lysophospholipid would be detected, a mobile phase developed by Dr. Eugene Zhang (IMB, Australia) which can screen for a broad range of organic molecules was used. This solvent contained toluene, acetone, methanol, and water (T:A:M:W, v/v), and the ratios were changed with each experiment to optimise the separation.

In the initial experiment, (T:A:M:W = 6:7:1:1), detergents and phospholipids had similar levels of movement, making them hard to separate (Fig. 3.2). Most problematic was that β-DDM, the detergent used to purify MscL, and phosphatidylethanolamine (PE), the main lipid constituent of *E. coli* membranes, had similar migration profiles under these initial solvent conditions. However, this experiment still yielded some interesting results. Soy azolectin was found to contain a range of compounds instead of being largely phosphatidylcholine as suggested in the manufacturer's description. Three constituents were detected in the purified MscL sample. The first component had a retention factor (R_f) of 0, likely residual MscL which remained in the acetone fraction. The second

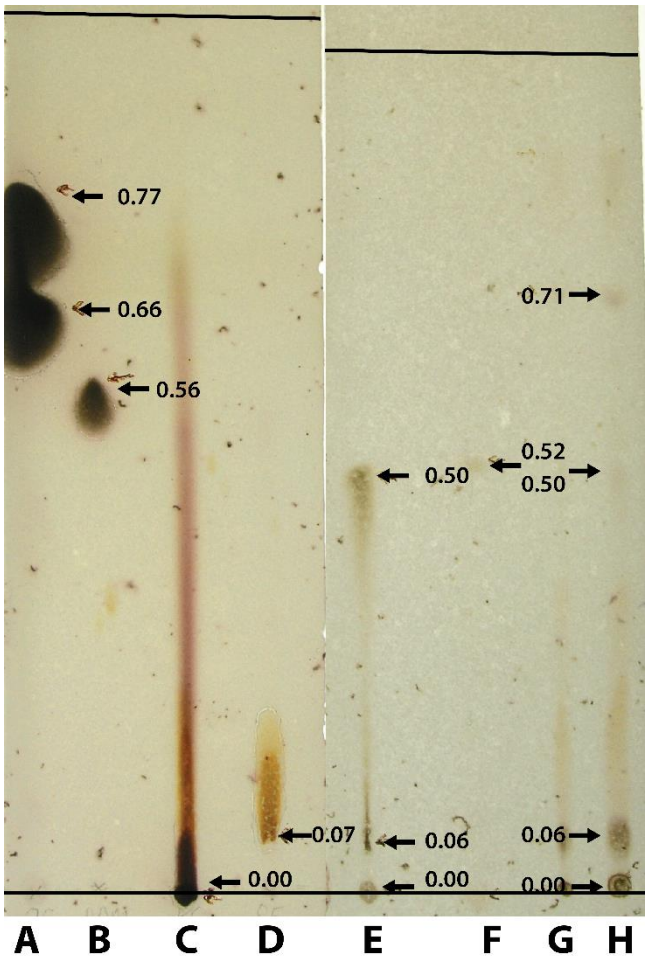

Figure 3.3. TLC of MscL and various reference samples. The numbers next to arrows are R_f values. **A**) OG; **B**) β-DDM; **C**) Soy Azolectin (5 mg); **D**) DOPE; **E**) MscL (1 mg); **F**) β-DDM; **G**) Soy Azolectin (0.1 mg); **H**) Soy Azolectin (0.5 mg)

component (R_f = 0.15), stained quite strongly, and given its location compared to the standards, was hypothesised to be β-DDM (R_f = 0.13). The third component (R_f = 0.18) was clearly visible only immediately after charring with H_2SO_4 and faded within minutes, but it appeared distinct from the much larger β-DDM band. While the chance of this band still being from β-DDM could not be discounted, there was also a possibility that this was a native *E. coli* membrane lipid (or lipids). Due to it running slightly higher than the β-DDM band, it was speculated that this could be PE (R_f = 0.18).

A more hydrophobic solvent (T:A:M:W = 7:9:0:1) was trialled in the second experiment, with the hypothesis that this could make phospholipids travel further on the TLC plate while having the opposite effect on detergents (Fig. 3.3A-D). Interestingly, the outcome was reversed relative to the expected effect, with detergents migrating further (R_f = 0.58) whereas DOPE standard remained much closer to the baseline (R_f = 0.06). Regardless, this solvent mixture was effective at significantly separating detergents and phospholipids, so the experiment was repeated for the TLC with MscL extract (Fig. 3.3E-H).

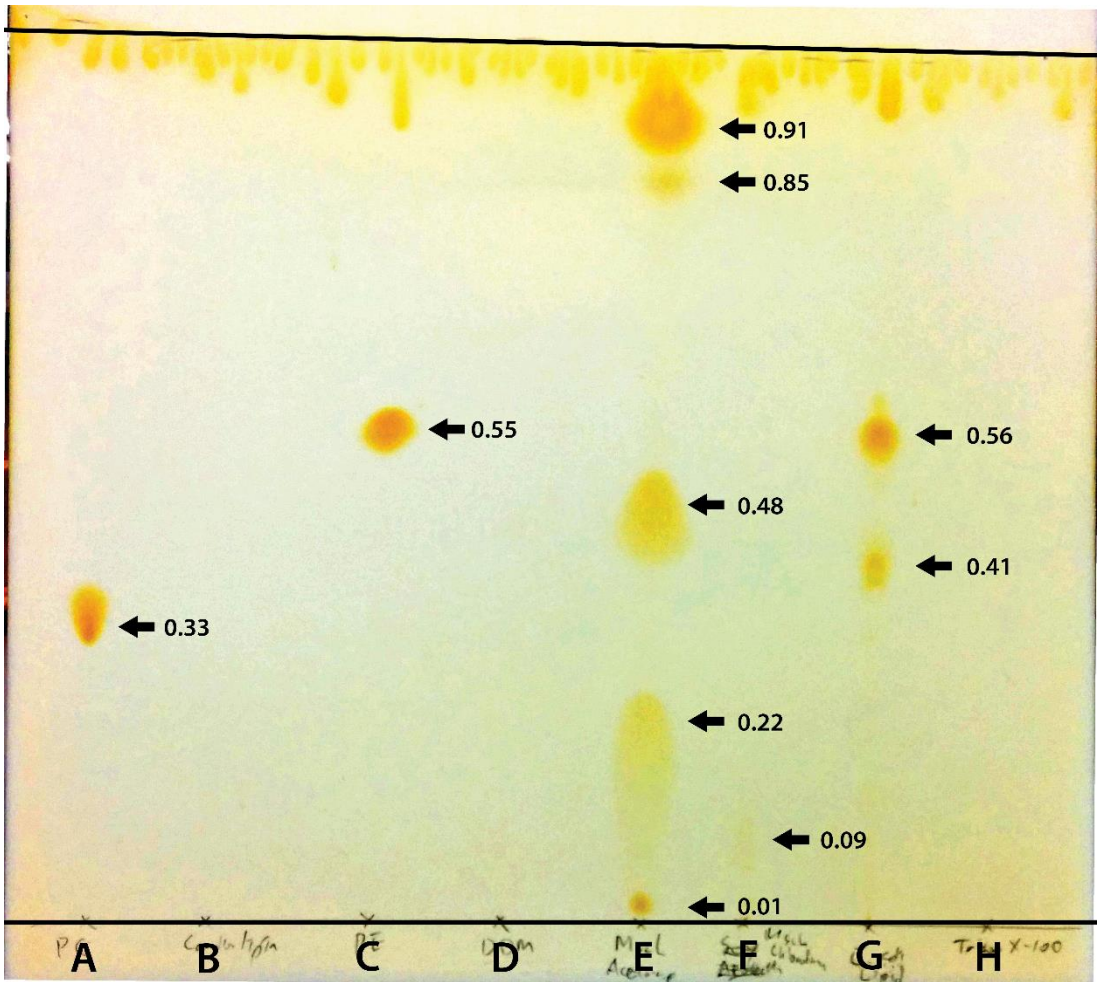

Figure 3.4. TLC of MscL and reference samples. The numbers next to arrows are R_f values of the bands. **A)** DOPC; **B)** Cardiolipin; **C)** DOPE; **D)** β-DDM; **E)** Acetone MscL extract (2 mg**); F)** Chloroform MscL extract (2 mg); **G)** *E. coli* lipid; **H)** Triton X-100.

Again, three components extracted from the purified MscL sample were able to be separated by TLC (Fig. 3.3E). One component again did not migrate up the plate at all ($R_f = 0$), and was hypothesised to be residual protein as in the earlier experiment. There was still the possibility that other organic molecules could also be present in this band, since most compounds in the soy azolectin sample remained on the baseline as well.

The second component ($R_f = 0.06$) migrated a similar distance compared to DOPE standard ($R_f = 0.07$), leading to further speculation that this could indeed be PE lipid. Interestingly, there was a band at the same location for the soy azolectin sample as well. PE is a major constituent of soy cell membranes (Erdahl *et al.*, 1973). The third component ($R_f = 0.50$) closely matched the migration distance of β-DDM ($R_f = 0.52$), and also to a faint band in soy azolectin. Hence, while it was hypothesised to be β-DDM band, there was also a possibility of additional compounds being present.

In addition to the three bands corresponding with the MscL sample, a number of additional bands were seen in the reference lane for the soy azolectin sample (Fig. 3.4E, H). While those with lower R_f than detergents were likely minor phospholipids in soy azolectin, the two bands with high R_f values could have been compounds with significantly different structures such as sterols. As bands with such high R_f values were not detected in the MscL sample, it was assumed that compounds co-purifying with MscL were mainly phospholipids. Hence, it was decided that the solvent for the next trial would be changed for better separation between different types of phospholipid.

In the third experiment, a chloroform-based solvent system with the chloroform:methanol:water (C:M:W, v/v) ratio of 13:5:1 was used. This was based on a TLC solvent system chart published by Avanti® Polar Lipids, Inc. (U.S.A.) (Avanti Polar Lipids), where the C:M:W ratio was simplified from 65:25:4. There were a total of five, well-separated bands for MscL samples (Fig. 3.4E). Apart from the lowest band (R_f = 0.01), which was likely residual protein, it was difficult to identify the stained compounds. However, the second lowest band (R_f = 0.05 – 0.23) was estimated to be β-DDM as its smeared locus significantly overlapped with that detected for the chloroform-extraction sample (R_f = 0.09).

The third band (R_f = 0.48) was speculated to be a phospholipid due to its position in the middle, but it neither matched PC nor PE. Interestingly, it did not match any major phospholipids in the *E. coli* lipid either, indicating that MscL might have an affinity for a less-abundant phospholipid in the native environment. Unfortunately, there was no stained band for cardiolipin sample – a minor constituent of *E. coli* cell membrane and also known to influence MscL channel gating (Andrew R. Battle *et al.*, 2011) – to help with identification.

The fourth and fifth bands (R_f = 0.85; 0.91) did not appear to be phospholipids due to their high R_f values. The high position suggested that they might be hydrophobic lipids such as triglycerides or products of degradation such as free fatty acids (Erdahl *et al.*, 1973; Fuchs *et al.*, 2011), however it was difficult to confirm this without reference samples. At this point, free fatty acid was not considered likely because there was no strongly-staining band which should have accounted for lysolipids (phospholipids with a fatty acid removed). It was also unlikely that there would be significant amount of triglyceride in *E. coli* membrane, or that triglycerides would have significant levels of interaction with MscL since it needs interaction with phospholipid bilayer for function.

Due to the failure of some of the control lanes and the emergence of an additional two bands, the previous TLC experiment was repeated. This time stained bands were seen in all references samples (Fig. 3.5). There were six bands for the MscL sample in total, with the lowest one (R_f = 0.01) likely residual protein (Fig. 3.5C). The second lowest band (R_f = 0.12) matched with one of the bands from the DOPC sample (R_f = 0.12), suggesting that it could be lysolipids, one of the products of

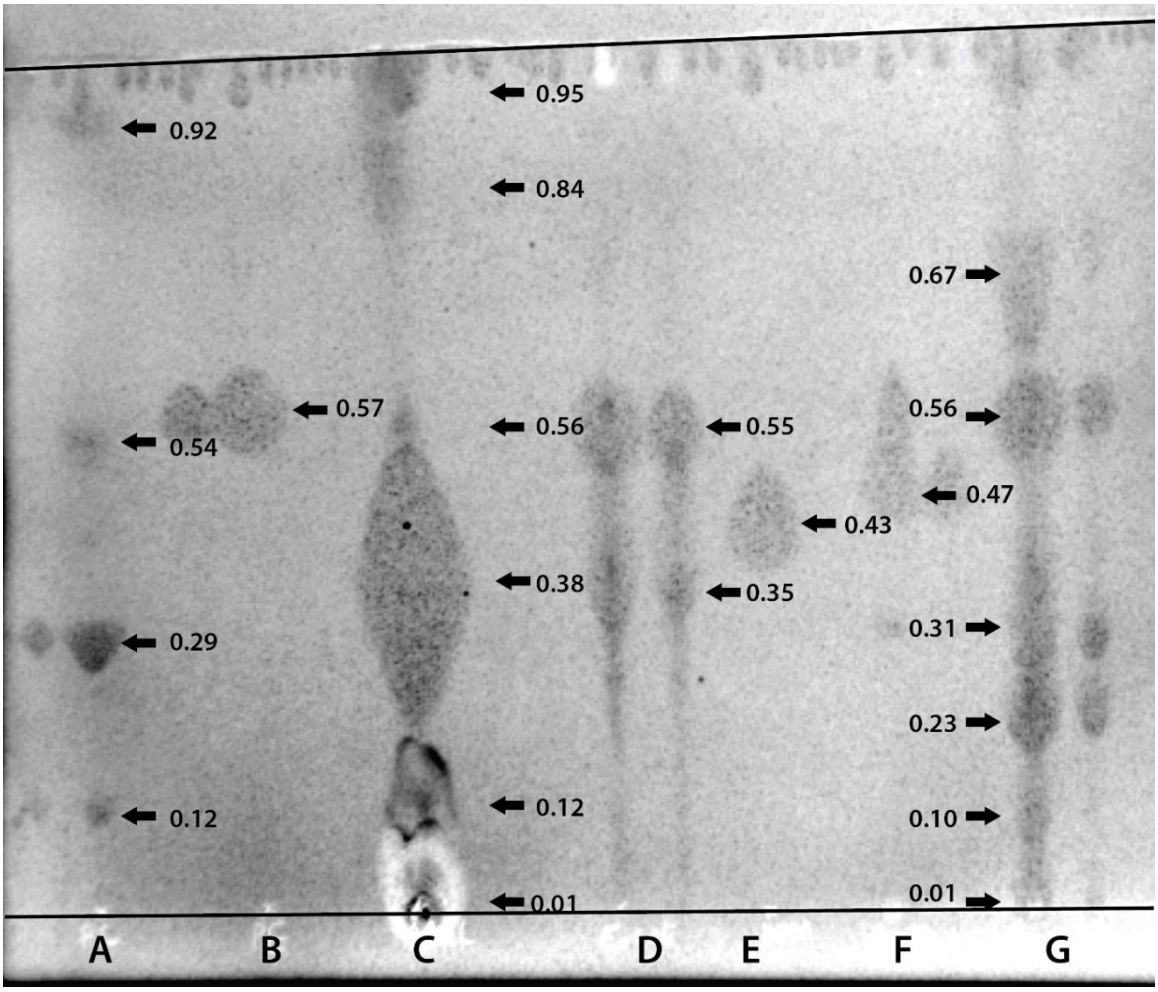

Figure 3.5. TLC of MscL and reference samples. The numbers next to arrows are R_f values. **A)** DOPC; **B)** DOPE ; **C)** MscL (5 mg); **D)** *E. coli* lipid (1 mg on the left, 0.5 mg on the right); **E)** β-DDM ; **F)** Cardiolipin; G) Soy Azolectin (1 mg on the left, 0.5 mg on the right)

phospholipid degradation during the MscL purification/extraction steps. Likewise, the bands at the top of the TLC plate (R_f = 0.84; 0.95) might be free fatty acids given the similar R_f value to a peak in the DOPC sample (R_f = 0.92).

It was difficult to identify the compound responsible for the third band (R_f = 0.25 – 0.50) due to the smear. The band appeared overloaded, and its R_f range was broad enough to overlap with those of the main band of DOPC, one of the bands in the *E. coli* lipid reference sample (likely PG), cardiolipin, and β-DDM. While the large load suggested that most of it could be β-DDM, the probability of other compounds also being present could not be discounted.

The fourth band of the MscL sample (R_f = 0.56) matched well with the DOPE sample band (R_f = 0.57) and the upper band of *E. coli* lipid sample (R_f = 0.55). The presence of this compound, which is likely PE, correlates well with the results from the first and the second TLC experiments, where faint bands with matching R_f to PE were also detected. Interestingly, such a band was absent in the third trial. There are two possible explanations for this discrepancy: first, as this PE band was very

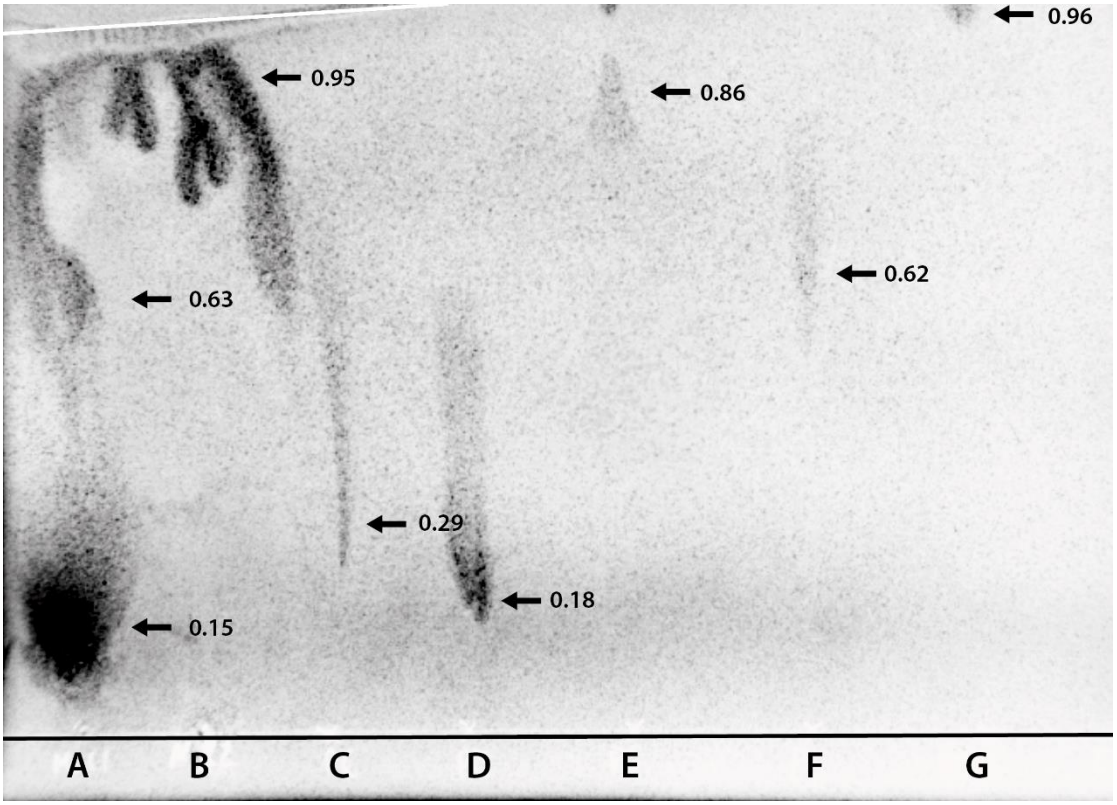

Figure 3.6. TLC of MscL and various reference samples. The numbers next to arrows are R_f values. **A**) MscL (3 mg); **B**) MscL (0.3 mg); **C**) DOPC; **D**) DOPE; **E**) POPG; **F**) DOPS; **G**) β-DDM

faint in all other experiments, sample load in the third TLC trial may have been too low to see the band with naked eye. The second explanation is that the third band in the third trial was actually PE which did not run to the same height as reference DOPE for an unidentified reason. In order to validate the two hypotheses, another TLC experiment was performed with a more hydrophilic mobile phase used to separate β-DDM from the phospholipids (C:M:W = 10:5:1, Fig. 3.6). Although the quality of the chromatogram was too poor for a definitive assessment, it seemed to validate the second hypothesis as the main band of MscL lane (Fig. 3.6A) had a similar R_f value (0.15) to the PE standard (0.18).

3.3.1.2. Mass Spectrometry of Isolated Lipid

As TLC had the limitation of not being able to provide clear identification of the observed band, extraction of compounds from the plate was attempted for reverse-phase high performance liquid chromatography (RP-HPLC) and mass spectrometry. In order to achieve this, a trial extraction of reference phospholipids was carried out. However, the rate of recovery was less than 10 % even for the most successful sample (Fig. 3.7) despite copious attempts, making it difficult for mass spectrometry to be carried out with the samples.

In a collaboration with Prof. Stephen Blanksby (Queensland University of Technology, Australia),

Figure 3.7. TLC of Reference Samples after a round of extraction with Bligh-Dyer method. **A**) DOPE extract; B) DOPC Extract; **C**) Cardiolipin extract; **D**) *E. coli* lipid; **E**) DOPE (100, 50, 20m and 10 mg/mL); **F**) DPPC; **G**) Cardiolipin

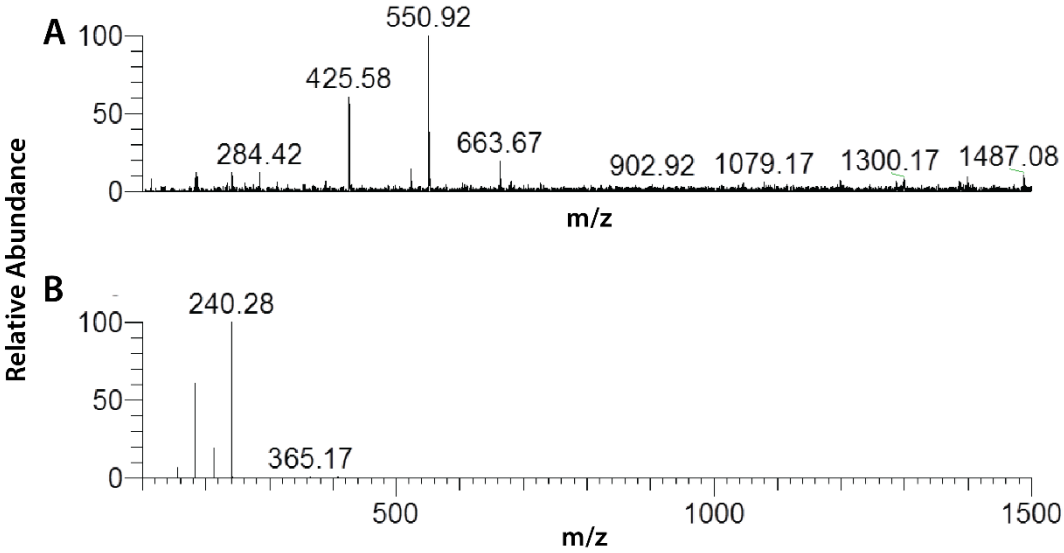

Figure 3.8. Mass spectrometry trace of silica containing MscL sample. **A**) Scanning mass spectrometry. Molecular weight (Mr) of 551 and 426 are too small to be phospholipids. **B**) Second ESI-MS of the peak with Mr of 551.

we sought to identify the lipids by mass spectrometry. One of Prof. Blanksby's MS/MS mass spectrometers was set up so that compound extraction from silica matrix was automated and coupled to the mass spectrometer, bypassing the need for manual extraction which had not been successful. Therefore, mass spectrometry was performed on the fourth TLC band of the MscL sample (R_f = 0.56) in the fourth TLC experiment (Fig. 3.5C). A number of compounds were detected from the trial run (Fig. 3.8). There were two compounds with significant amount identified in the experiment, but their molecular weights were too small to be phospholipids. While phospholipids were not positively identified in this trial, it was shown from the abundance of peaks that automated compound extraction and mass spectrometry from silica gel was successful. An explanation for the failure of this run to conclusively identify a lipid species was the relatively low sample load and the age of the sample, which had been stored at -80 ℃ for eight months.

3.3.1.3. Discussion

While this project was not progressed further due to time constraints, it has provided valuable information on the relationship between MscL and phospholipids in the native membrane environment. First, the presence of native *E. coli* membrane compounds with strong affinity to MscL was confirmed from thin layer chromatography. At least one of them was suspected to be PE lipid with reasonable certainty.

One of the outcomes of the TLC experiments was the confirmation of the hypothesis that some phospholipids in the native *E. coli* cell membrane have high enough affinity for MscL that they co-purify with the protein. Moreover, it may have a net neutrally charged phosphatidylethanolamine (PE) head group, which is present in both *E. coli* and *M. tuberculosis* membranes. This is a significant difference to *M. tuberculosis* MscL, which interacts with net negatively charged phosphatidylinositol (PI) head group lipids (Zhong & Blount, 2013). *M. tuberculosis* MscL has an altered gating property in the presence of PI, one of the major phospholipid components in *M. tuberculosis*, showing that its MscL had functionally significant interaction with PI. As the *E. coli* equivalent to PI in *M. tuberculosis* is phosphatidylglycerol (PG), it was predicted that *E. coli* MscL might interact with PG. However, *E. coli* MscL's apparent affinity for PE suggested that the two homologues may have significant differences in terms of their functional relationship with phospholipids.

The apparent difference in phospholipid affinity between *E. coli* and *M. tuberculosis* MscL may be due to the sequence variation in the residues thought to interact with phospholipid head groups. The sequence is especially poorly conserved on the periplasmic side formed by the TM1/TM2 interhelical loop between the two species (Fig. 1.10). *E. coli* MscL contains three aspartate residues

in this region, and the large number of negative charges may have resulted in the repulsion of negatively charged head groups (e.g. PG) in favour of neutral ones (e.g. PE). On the other hand, *M. tuberculosis* MscL has only one aspartate in the equivalent region, making it more receptive to negatively charged head groups (e.g. PI), although it would not necessarily lead to strong affinity for anionic lipids either (Elmore & Dougherty, 2003; Powl *et al.*, 2003).

The two MscL homologues' differing phospholipid preference likely has a functional significance. Anionic lipids favour the open conformation and net neutral phospholipids have stabilising effect on the closed conformation of both *E. coli* and *M. tuberculosis* MscL (Powl *et al.*, 2008a; Zhong & Blount, 2013). The TLC experiments in this section suggest that *E. coli* MscL has been evolved for increased affinity to PE, in which MscL has a higher gating threshold than even PC, another zwitterionic lipid (Powl *et al.*, 2008a). This in turn suggests the preference for a higher gating threshold and reduced pore size in *E. coli*. On the other hand, *M. tuberculosis* MscL has evolved in an opposite direction to require PI for lowered channel gating threshold.

While this appears to be divergent evolution at first glance, it can actually be explained as a case of convergent evolution. In a neutral phospholipid environment consisting mainly of PC and PE head groups, *E. coli* MscL's pressure threshold is already well within a physiologically relevant range (i.e. low enough to be induced by hyposmotic environment) in neutral phospholipid environment (Zhong & Blount, 2013). Given the redundancy of protective channels for hyposmotic shock (Martinac *et al.*, 2014), it would have been preferable for *E. coli* MscL to have higher gating threshold to reduce the collateral damage it can cause through the large channel pore, and this could have been facilitated by increased affinity for PE, the predominant a neutral phospholipid in the membrane. On the other hand, *M. tuberculosis* MscL has a pressure threshold that is too high to be useful as an osmotic emergency valve in neutral phospholipid environment. Hence, lowering the threshold to achieve a similar gating profile to *E. coli* MscL would have been necessary for *M. tuberculosis* MscL, and this could have been facilitated by increased affinity to PI (Zhong & Blount, 2013).

E. coli MscL's high affinity for PE is somewhat unusual from a structural perspective. Unlike MscS, which has phospholipid-sensing clefts between the transmembrane and cytoplasmic domains (Pliotas *et al.*, 2015), MscL is a much smaller protein lacking pockets for high-affinity binding. However, *E. coli* MscL's affinity for certain phospholipids, likely PE, has been observed in this study, and there is also an anecdotal observation of MscL resisting separation from β-DDM in mass spectrometry by Dr. Armagen Koçer (Konijnenberg *et al.*, 2014). These indicate that MscL is capable of strong interaction with phospholipids and lipid-like molecules.

One explanation for this is that MscL structure in the native phospholipid environment is more fluid

than is commonly accepted. Currently most structural studies (Corry *et al.*, 2010; Deplazes *et al.*, 2012; Gullingsrud & Schulten, 2003; Meyer *et al.*, 2006; Perozo, Cortes, *et al.*, 2002; Sawada *et al.*, 2012) are based on the crystal structure of *M. tuberculosis* MscL (G. Chang *et al.*, 1998), which has a compact and symmetric structure. However, MscL as a protein is dynamic enough that a significant proportion may exist as monomers *in vivo* (Hase, Minchin, *et al.*, 1997), and *S. aureus* MscL has been shown to switch between tetrameric and pentameric states depending on the detergent used (Dorwart *et al.*, 2010). Hence, unlike in crystal structures, MscL in a bilayer environment may exist in a more fluid state with an increased surface area available for stronger interaction with phospholipids.

While this section of the chapter was not progressed further, this has provided enough results to suggest further investigation is warranted. More specifically, additional TLC experiments and mass spectrometry can be reasonably expected to yield sufficient data for a publication similar to Pliotas et al. (2015) that identifies native phospholipids co-purifying with MscL. The main challenges lie in obtaining enough high purity MscL (and hence associating phospholipids) and successfully extracting the phospholipids. It is likely that the inconclusive result from the mass spectrometry experiment in this section are due to the poor recovery of lipids from the TLC silica. One of the methods in discussion at the time of writing this thesis was to perform the extraction in situ on the mass spectrometry equipment. This would in theory bypass the loss of lipids from manual extraction and handling, not only increasing the efficiency of extraction but also resulting in more pure samples. With this thesis having provided exciting preliminary data and directions for future experiments, this strategy has the potential to more conclusively identify phospholipids interacting with MscL.

3.3.2. MscL Behaviour in a Mixed Liposomal Environment

The main objective of this experiment was to study the difference in function and other properties of MscL in various liposomal environments. This was based on the hypothesis that liposomes formed from a heterogeneous mix of phospholipids would be varied in both composition and size, which would provide a quick and affordable way to test a range of variables for their influence on MscL function and other properties. With the identification of membrane lipids preferentially associating with MscL (Section 3.3.1.), one of the aims of this experiments was to see if MscL would also show a preferential incorporation to certain liposomes/phospholipid membranes, and if MscL channel function would be affected by such environments.

The proteoliposomes were produced from soy azolectin in this section for two reasons. First, a number of publications previously used soy azolectin to study the biophysical properties not only of

MscL (Chi *et al.*, 2015; A. Foo *et al.*, 2015; Kocer, 2015; Powl *et al.*, 2008a; Yoshimura *et al.*, 2008; Zhong & Blount, 2013) but also of other mechanosensitive channels (Coste *et al.*, 2012; Liao *et al.*, 2013; Petrov *et al.*, 2013). Therefore, using the same lipid environment would enable a more direct comparison of the data to previously published work. In addition, soy azolectin consists mostly of PC, which is the most commonly used phospholipid in MscL studies (Abdine *et al.*, 2012; Grage *et al.*, 2011; Iscla *et al.*, 2013; Konijnenberg *et al.*, 2014), and PE, which is suspected of associating with *E. coli* MscL (section 3.3.1.). The protocols for producing MscL/soy azolectin proteoliposomes and size-fractionation of the liposomes with sucrose gradient had already been largely established using soy azolectin by Dr. Alexander Foo (IMB) prior to the commencement of this project (Alexander Foo, 2014). Cost was also a consideration here since the costs of working with pure lipids was between 200 and 2,000 times more expensive, potentially reducing the scope and replicate of possible experiments that could be performed for a comparable cost.

Size fractionation by sucrose gradient was used as the main method of separating the liposomes by a primary variable (liposome size), which would in turn encompass underlying variables such as membrane curvature and phospholipid composition. The effect of varying protein-to-lipid (P:L) ratio was also visualised with carboxyfluorescein reporter molecules in this step. Dynamic light scattering was used to measure size and size distribution of the liposomes, which were indirect markers for the membrane curvature (a major potential influence on MscL function), and the trend was confirmed with electron microscopy. MscL distribution within and between the proteoliposomes was visualised by electron microscopy, which provided insights to the channel aggregation pattern. Lipid mass spectrometry was carried out in collaboration with Prof. Stephen Blanksby (QUT, Australia) to analyse phospholipid composition in each fraction and to study its potential effect on MscL incorporation and behaviour, which was a continuation of the experiments in section 3.3.1. and 3.3.3. Fluorescence-based cargo release assay was also performed to study MscL channel gating properties in these environments, but they were not included in the result section as these were primarily performed by Dr. Alexander Foo as part of his thesis (Alexander Foo, 2014). The results are discussed in section 3.3.2.1. as part of a wider discussion on the influence of the studied variables on MscL function.

3.3.2.1. Size-based Fractionation of MscL Proteoliposome by Sucrose Gradient

Sucrose gradients were performed on MscL/soy azolectin proteoliposome samples of P:L ratios of 1:40 and 1:10 (Fig. 3.9), and two main differences emerged between them. Compared to the negative control (Fig. 3.9A), there were additional orange-coloured bands in proteoliposome samples (Fig. 3.9B, C). Carboxyfluorescein is a self-quenching fluorescent dye, with its absorption wavelength of 495 nm giving it an orange-colour at high concentration and its fluorescent emission

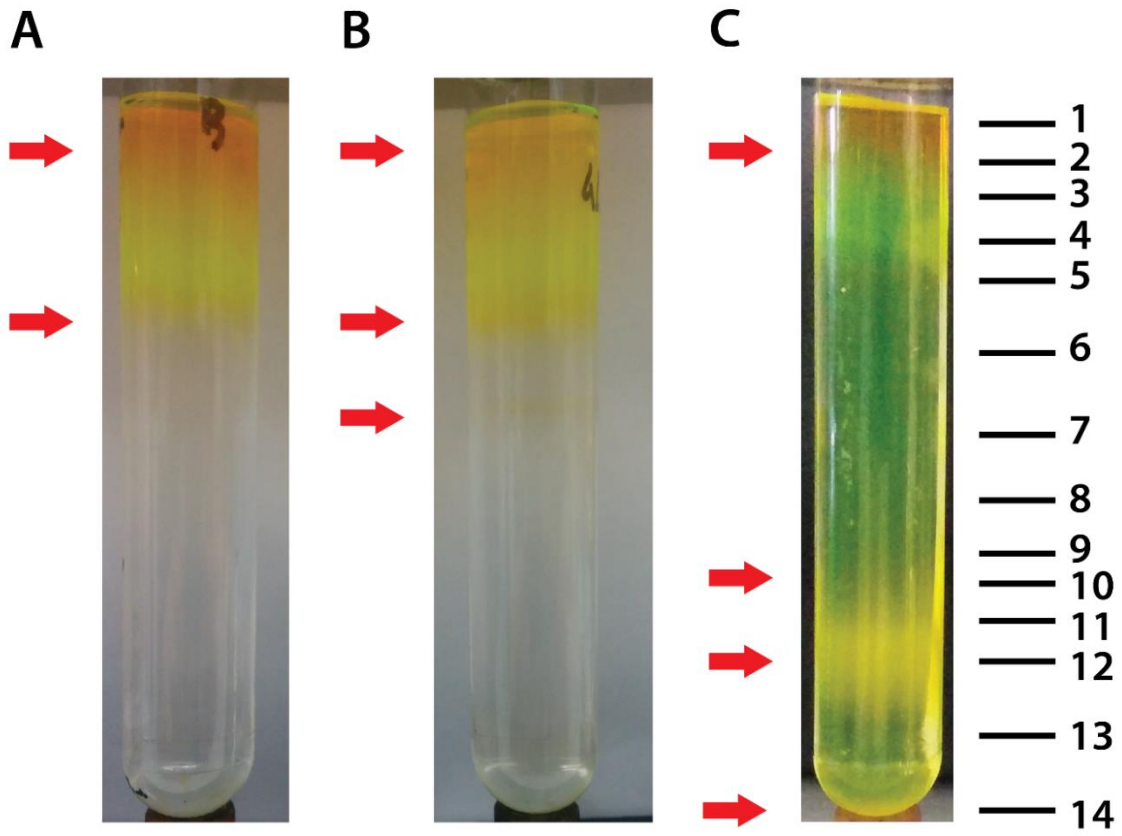

Figure 3.9. Fractionation of MscL/Soy azolectin proteoliposome. **A**) Control tube with only soy azolectin. There are two orange-coloured bands. **B**) Proteoliposome with P:L of 1:40. Three bands can be seen. **C**) Proteoliposome with P:L of 1:10. Four bands can be seen. Fractions were collected from this tube and labelled according to their fraction locations.

maximum at 517 nm wavelength giving it a yellow-green colour at low concentration. The faint orange colours of the bands indicated that carboxyfluorescein in the fractions was mostly contained within liposomes with little leakage. In the 1:10 (P:L) sample, however, there was a yellow smear across the entire gradient, indicating that some of the liposomes burst and released carboxyfluorescein as they travelled down the gradient.

The migration pattern of bands within the sucrose gradient was influenced by the P:L reconstitution ratio. For example at a P:L ratio of 1:40 (Fig. 3.9B), the two main bands appeared in the upper half of the sucrose gradient, but all three bands were located in the bottom half of the 1:10 sample (Fig. 3.9C). Generally, larger species migrate further down a sucrose gradient in experiments of this type, however, the migration patterns may have possibly been influenced by the higher MscL concentrations in the liposomes in the 1:10 sample. Since proteins are denser than lipids, increasing the amount of MscL in the liposomes would be expected to increase the overall density. Moreover, as the liposomes travelled down the gradient, fractionation over a wider range of sucrose gradient fractions would have made them better separated. This is probably responsible for the separation of two bands at fractions 10 and 12 in the 1:10 sample (Fig. 3.9C), which may not be adequately

separated in the 1:40 sample.

3.3.2.2. Electron Microscopy of Fractionated Liposomes

Proteoliposomes in each fraction were analysed by negative stain electron microscopy to visually identify their characteristics (Fig. 3.10 – 3.13). Negative stain EM has several advantages over cryo-EM in this experiment. First, much less optimisation is required for negative stain EM compared to cryo-EM. Second, negative stain EM allows screening larger area in shorter time than cryo-EM, which is beneficial not only for the high throughput required in semi-quantitative analysis but also for reducing sampling bias by viewing more liposomes than cryo-EM would allow.

His-MscL was labelled with Ni-NTA-Nanogold prior to negative staining to aid with its visualisation. The top fraction (Fraction 1) mostly contained liposomes of varying sizes, many of them between 200 nm and 400 nm in diameter (Fig. 3.10). There were few Nanogold particles throughout the micrographs, indicating that these liposomes did not contain MscL. The appearance of these liposomes despite their relatively large size suggests that the change in density by the presence of either protein and/or lipid composition of the liposomes was having a greater influence on the liposome sedimentation than the size.

Fractions 2, 3, and 4 were extracted from a region of the sucrose gradient that featured intense yellow colour. These contained a mix of small liposomes of less than 50 nm in size and lipid agglomerates of less than 10 nm in size (Fig. 3.10, 3.11). While most liposomes did not associate with Nanogold, the few which did had relatively large numbers of Nanogold particles bound. This suggests that MscL incorporated with high efficiency into some liposomes but not at all into others. The two possible explanations, not necessarily exclusive of each other, were that 1) the liposomes had high variability in their phospholipid composition, some of which MscL preferentially incorporated into; and that 2) MscL particles showed strong clustering patterns in the liposomes they incorporated into. As these particles were still significantly larger than the size of MscL/detergent micelles (approx. 10 nm), they were unlikely to be unincorporated MscL.

Interestingly, fractions 2 and 4 contained both liposomes and small lipid globules, whereas only lipid aggregates were visible in fraction 3. In addition, the lipid globules could be seen throughout the micrographs in fractions 3 and 4, but their density was not as high in the micrographs of fraction 2. This suggested that, on average, the sedimentation rate of the lipid globules was roughly equal to the sucrose concentration at fraction 3. Fraction 2 was likely at the transition interface between large liposomes (fraction 1) and small lipid agglomerates (fraction 3), hence featuring small liposomes. Likewise, fraction 4 would have been at the transition or overlap between lipid

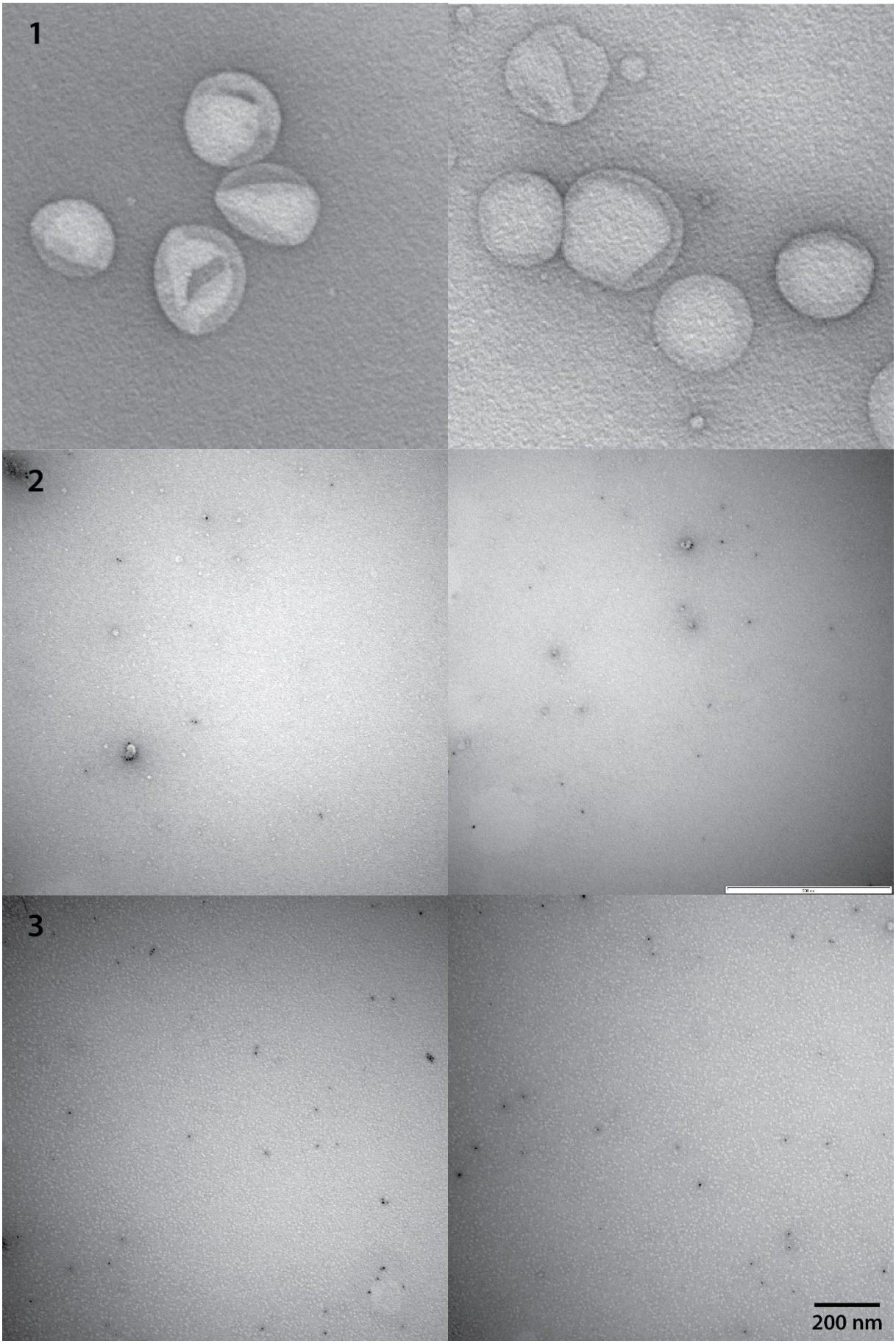

Figure 3.10. Electron micrographs of proteoliposome fractions from sucrose gradient. The numbers in the top left corner represent the fraction number (Fig. 3.9). The black dots are Nanogold particles with His-tags, presumably bound to His-MscL.

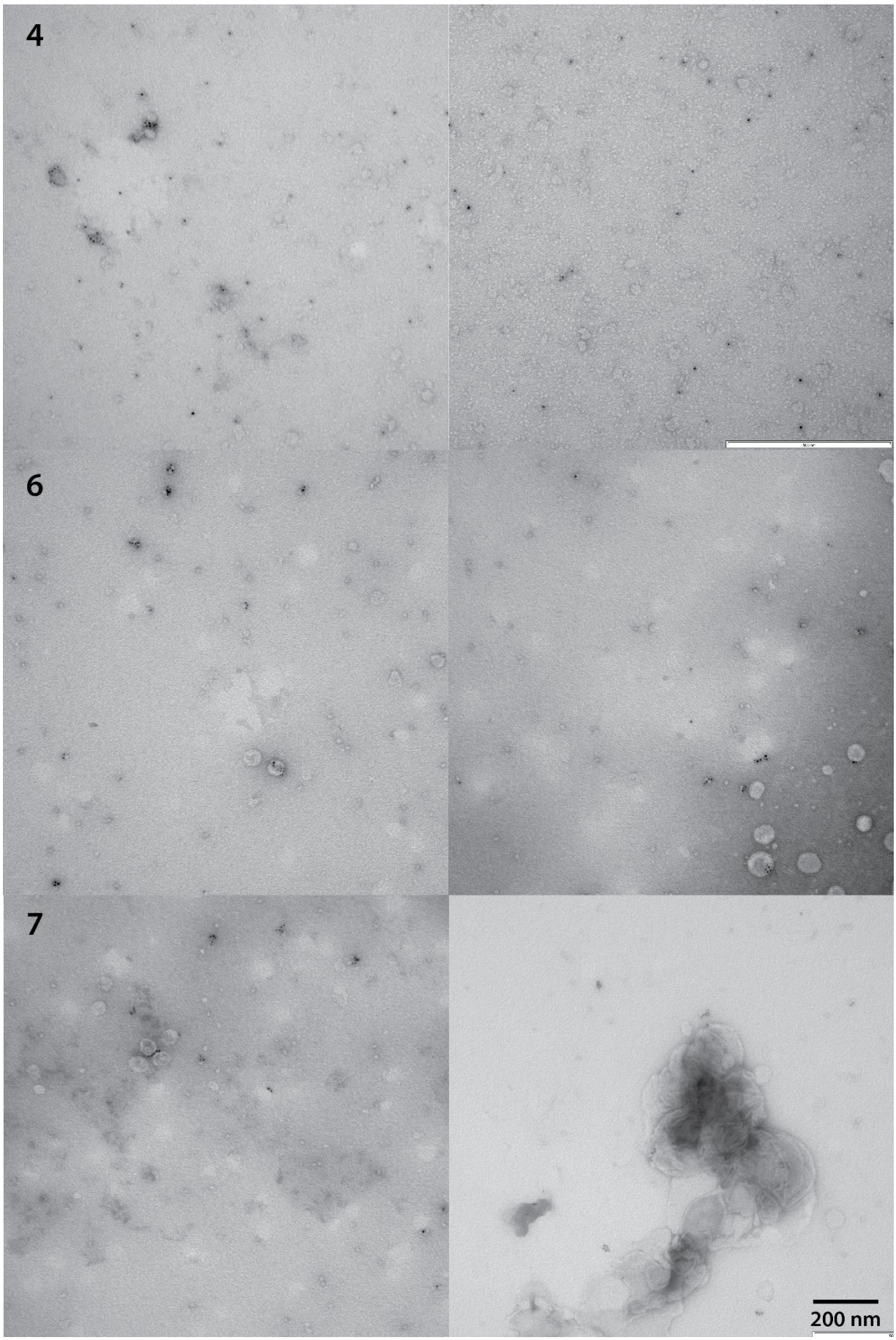

Figure 3.11. Electron micrographs of proteoliposome fractions from sucrose gradient. The numbers in the top left corner represent the fraction number (Fig. 3.9)

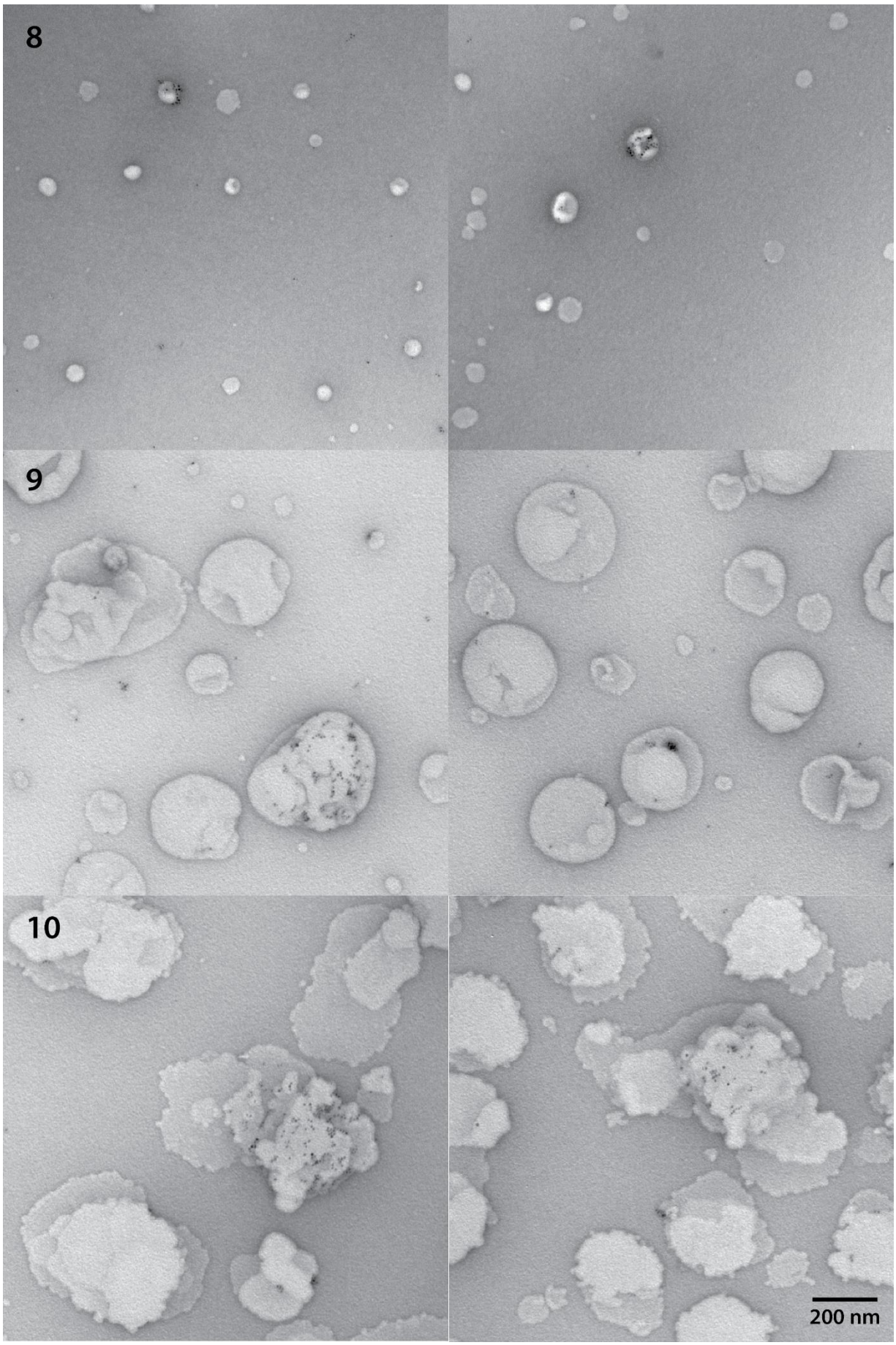

Figure 3.12. Electron micrographs of proteoliposome fractions from sucrose gradient. The numbers in the top left corner represent the fraction number (Fig. 3.9)

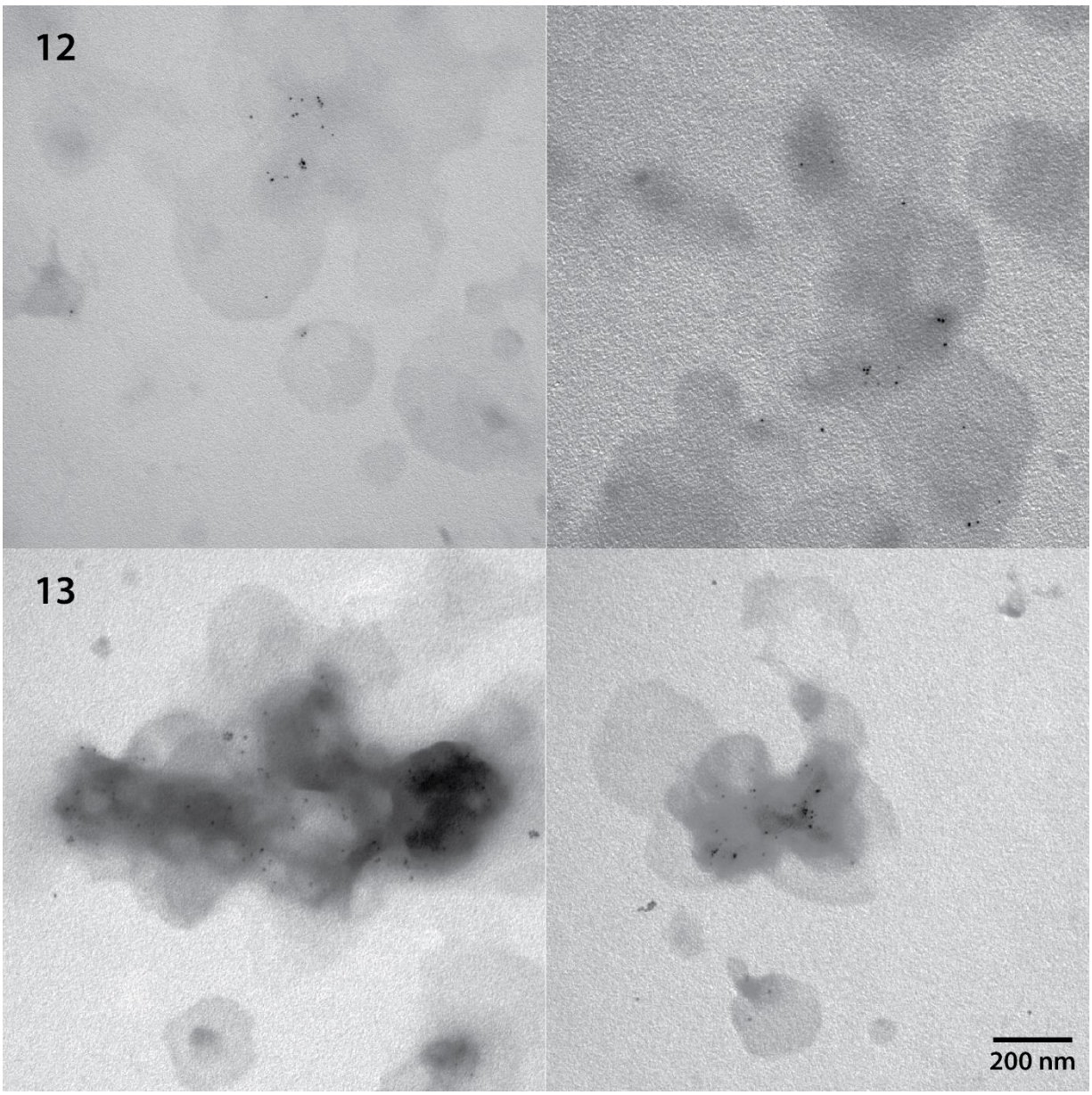

Figure 3.13. Electron micrographs of proteoliposome fractions from sucrose gradient. The numbers in the top left corner represent the fraction number (Fig. 3.9)

agglomerates and small proteoliposomes.

Although fractions 5, 6, 7, and 8 were all located in the part of the sucrose gradient with weak carboxyfluorescein intensity, the liposome profiles recorded by EM were considerably different (Fig. 3.11, 3.12). There was no visible lipid particle or Nanogold in fraction 5. In contrast, fractions 6, 7, and 8 contained small liposomes of 50 nm to 100 nm in diameter. The average liposome size appeared to increase with increasing sucrose concentration (i.e. lower fractions in the gradient). While the majority of liposomes did not associate with Nanogold, a small but a significant proportion contained Nanogold clusters of 5 – 10 particles. While this was similar to fractions 2 and 4, due to the larger liposome size, it could be clearly seen in these fractions that the Nanogold particles (by extension MscL molecules) were forming clusters instead of being randomly

distributed throughout the liposome.

Fraction 7 differed from 6 and 8 in that it was also populated by aggregated liposomes with highly variable sizes (100 nm to 500 nm). A few of them contained small Nanogold clusters, but most did not associate with any Nanogold despite the large surface area, indicating that MscL incorporation into them was poor.

A faint orange band about two thirds of the way down the sucrose gradient was separated into the upper (fraction 9) and lower (fraction 10) portions (Fig. 3.12). Although the two fractions were from the same band, the liposome morphology was significantly different between them. Whereas intact liposomes populated fraction 9 micrographs, fraction 10 mostly featured flat phospholipid bilayers with irregular edges. However, the sizes of these structures were similar (200 nm – 500 nm). In both fractions, Nanogold particles appeared largely randomly distributed, with only minor signs of clustering along the curved edge/grooves of the liposomes. These indicated that, despite the different appearance of the liposomes, they were still composed of similar species of phospholipid. In addition, the different MscL clustering pattern between fractions 6 – 8 and 9 – 10 suggested that the membrane environment for MscL was different between the two groups.

In fractions 12 and 13, which accounted for the large opaque band in the bottom quarter of the gradient, both the liposome size and MscL clustering pattern were significantly different (Fig. 3.13). The liposomes were variable in size (200 – 500 nm), often formed aggregates, and were positively stained instead of negative stains. There was also little sign of MscL clustering, with singular Nanogold particles randomly distributed on the liposomes. The further shift away from the MscL's propensity to aggregate indicated that the hypothesised cluster-inducing factor was further weakened in these liposomes.

Fraction 14, which contained an opaque precipitate at the bottom of the tube, mostly featured a mixture of large unstructured lipid and liposomes of various sizes and shapes. This indicated that the precipitate consisted of phospholipids which did not form liposomes and those which are heavier than the highest density provided by this sucrose gradient. There were few Nanogold particles throughout the micrograph, which suggested that MscL would not incorporate into these non-bilayer-forming lipid masses.

A semiquantitative analysis on the clustering pattern was carried out on fractions 1, 4, 6, and 13 to find if the observations made with the images could be quantified (Table 3.2). The Nanogold particle distribution and liposome diameter were manually measured due to the gradient staining of liposomes making the automated method described in *3.2.3.3*. inaccurate for images for fraction 13.

From these experiments, two trends were observed. First, the average liposome size, especially

those with Nangold-tagged MscL, generally increased down the sucrose gradient, with the notable exception of Fraction 1. This suggests that the sucrose gradient successfully separated the proteoliposomes according to their sizes as expected. Dynamic light scattering was performed in a follow-up experiment to confirm this observed trend.

Second, MscL's propensity to form clusters gradually decreased down the gradient, with MscL in fractions 2 – 8 showing the highest level of clustering and those in fractions 12 – 13 being largely monodispersed. At this stage, this could be explained by either the membrane curvature or lipid composition of the liposomes in each fraction influencing the clustering of MscL. To test the two hypotheses, lipid mass spectrometry was carried out to study the lipid composition of each fraction.

3.3.2.3. Liposome Size Measurement with Dynamic Light Scattering

The liposome samples were additionally assessed by dynamic light scattering with the assistance of Dr. Alexander Foo (Table 3.3) in order to quantitatively confirm the liposome size trend observed with electron microscopy. The overall trend in liposome size distribution throughout the gradient was consistent with what was observed by electron microscopy (Fig. 3.10 – 3.13). The liposome size decreased from fraction 1 to fraction 4, and then trended upward from fraction 4 to fraction 14. The aggregation observed in fractions by electron microscopy was consistent with the higher polydispersity index in this fraction, which was the highest of all fractions analysed by dynamic light scattering.

Table 3.2. Average Liposome Size and MscL Clustering Size Estimated from Electron Microscopy Images

Fraction	**1**	**4**	**6**	**13**
Total Liposomes	21	17	17	18
Mean Diameter (nm)	259	50	56	164
Standard Deviation (nm)	36	21	18	78
Standard Error (nm)	8	5	4	18
Liposomes with Nanogold-tagged MscL	0	5	2	14
Mean Diameter (nm)	N/A	66	96	112
Standard Deviation (nm)	N/A	12	9	44
Standard Error (nm)	N/A	5	4	20
Mean Nanogold-tagged MscL Cluster Size	0	9.8	5.0	1.4
Standard Deviation	N/A	7.4	5.7	0.9
Standard Error		2.0	2.0	0.1

The key difference between the light scattering data and the observations by negative-stained electron microscopy was that all fractions had average liposome sizes between 100 nm and 200 nm when measured by dynamic light scattering. This was in contrast with the electron microscopy where the average size varied from less than 50 nm in fraction 2 to over 300 nm in fraction 14. This discrepancy might be due to the interference with dynamic light scattering by carboxyfluorescein, which had been added to the liposome sample for band visualisation in sucrose gradient and potentially for follow-up experiments such as cargo release assay and total liposome volume analysis. Its emission spectrum ranges from approximately 450 nm to 650 nm, which overlaps with the wavelengths of the equipment's both primary (633 nm) and secondary (532 nm) lasers. As it was not equipped with an optical filter to remove this interference, carboxyfluorescein could have been a significant source of background light level. While this would introduce a degree of inaccuracy to the data, it would not affect the observed trend as the same bias would be present across all samples.

Table 3.3. Average Liposome Diameter Measured by Dynamic Light Scattering Equipment

Sample Number	Average Diameter (nm)		Polydispersity Index
	Mean	Mode	
1	141	147	0.03
2	114	124	0.09
4	90	106	0.13
6	102	120	0.14
8	136	150	0.07
10	140	147	0.03
12	156	158	0.09
14	188	191	0.19

3.3.2.4. Mass Spectrometry of Sucrose Gradient Fractionated Liposomes

Mass spectrometry was used to determine the phospholipid composition of the fractionated liposomes (Fig. 3.S1 – 3.S9; see section 3.6). Experiments were carried out in collaboration with Prof. Stephen Blanksby (QUT). Fractions 2 to 12 were scanned for the presence of phosphatidylcholines (PC), phosphatidylethanolamines (PE), and phosphatidylinositols (PI).

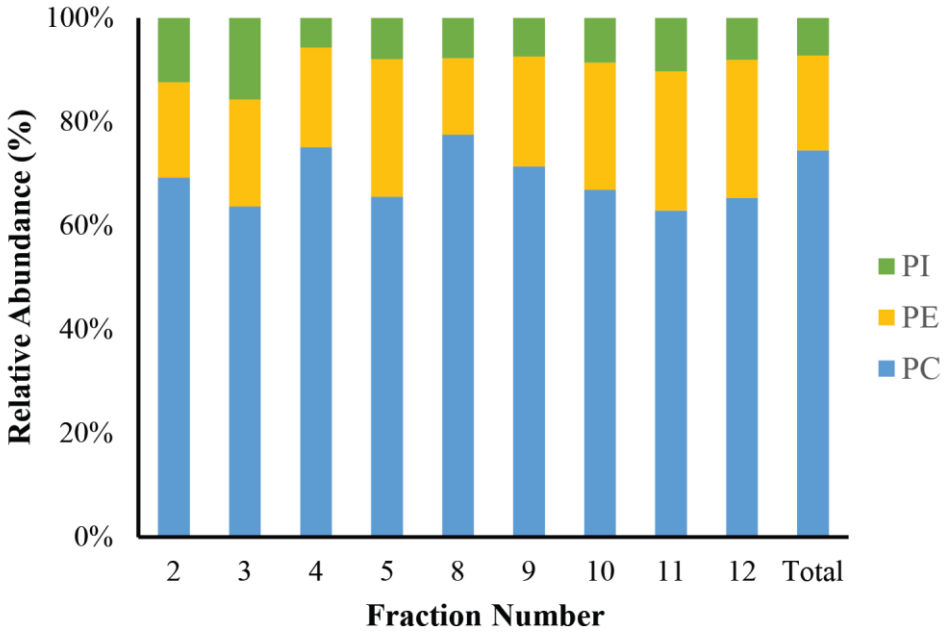

Figure 3.14. Relative abundance of phospholipid head groups estimated from mass spectrometry. Note that quantity estimation from mass spectrometry data has a large margin of error.

Across all fractions, PC was the most abundant phospholipid, followed by PE and PI respectively (Fig. 3.14). This is not unexpected since PC and PE are the most abundant phospholipids in soy azolectin. Their roughly even ratios across the fractions suggested that the phospholipid head groups did not have significant influence on the liposome size. By extension, this also indicated that MscL clustering was not directly dependent on the phospholipid head groups.

Unlike the head groups, there was a considerable variation in the tail group composition between fractions. In fractions 2 and 3, there were a wide range of fatty acid tail groups for all three phospholipids (Fig. 3.S1, 3.S4, 3.S7). There was a roughly even distribution of phospholipids with 34 and 36 carbon atoms in the tail group, with significant amounts of PC and PI with 38 carbon atoms as well (Table 3.4).

Phospholipid profiles of fractions 4 – 12 were similar for all three lipid head groups (Table 34). The tail groups were less heterogeneous than in fractions 2 and 3, with most containing 34 and 36 carbons. With PE, there were roughly even ratios of 34 and 36-carbon tail groups; with PC, there were more 36-carbon tail groups than 34-carbon; and with PI, there were more 34-carbon tail groups than 36-carbon (Table 3.4). Given the significant difference in MscL clustering patterns of fractions 4 – 8, 9 – 10, and 12 – 13, it appeared that the tail groups of these phospholipids were not main determinants either. From these results, it was concluded that lipid composition were similar across fractions, making this variable unlikely to be responsible for differential MscL clustering observed between fractions.

Table 3.4. The relative abundance of each phospholipid with 34-carbon hydrophobic tails compared to those with 36-carbon hydrophobic tails. The ratio for PI is less accurate than PC or PE because there were generally less of them in all fractions.

Fraction	Ratio of Tail Length Abundance (34/36)			
	PC	PE	PI	Total
2	1.45	2.00	1.91	1.58
3	1.26	2.53	1.31	1.45
4	0.59	0.89	5.54	0.72
5	0.61	1.01	2.73	0.79
8	0.58	0.90	4.94	0.72
9	0.55	0.97	4.24	0.72
10	0.61	0.98	3.25	0.78
11	0.58	1.07	2.55	0.80
12	0.65	1.07	2.76	0.83

3.3.2.5. Discussion

The main aim of this experiment was to investigate the potential influence of phospholipid bilayer environment on MscL function. This experiment was carried out in conjunction with a related project by Dr. Alexander Foo (IMB), where the relationship between liposome size and MscL channel gating properties was investigated.

While there was a clear relationship between the liposome size and MscL clustering pattern, phospholipid composition did not appear to be the underlying factor. Liposomes of all sizes consisted mainly of 34 and 36-carbon tail group phospholipids, and the ratios of PE, PC, and PI head groups were also similar. While fractions 2 and 3 were exceptions with the presence of 38-carbon tail group phospholipids, it is likely that the long-chain phospholipids formed lipid globules seen in the electron micrograph rather than liposomes. These observations are unlikely to be artefacts of high protein to lipid ratio, since mass-to-mass protein-to-lipid ratio of 1:10 represents a molar ratio of approximately 1:1000.

Taken together, these observations have major implications for understanding MscL function in that membrane is a major influence on its channel gating properties and clustering pattern. The mass spectrometry results indicated that the phospholipid composition was similar across the fractions, leaving intrinsic membrane curvature as the main plausible explanation for differences observed in MscL clustering. There is a similar precedent with a voltage-gated potassium channel (KvAP),

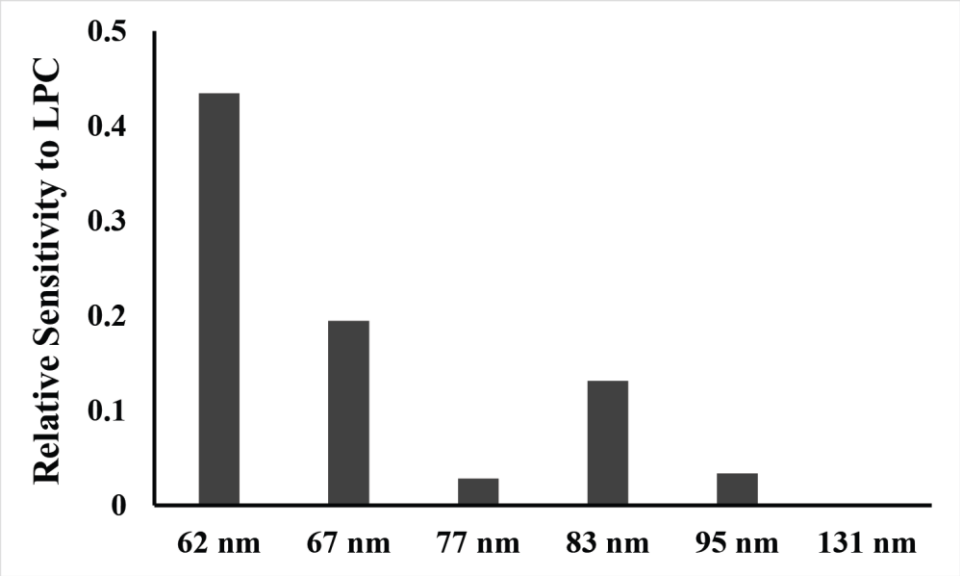

Figure 3.15. MscL channel activation sensitivity to LPC calculated by the percentage cargo release at 0.05 mM LPC (12:0) divided by cargo release at 0.5 mM LPC (12:0). The P:L ratio of the proteoliposome sample used in this experiment was 1:100.

where global curvature of membrane was shown to directly induce protein clustering without secondary factors such as phospholipid composition (Aimon *et al.*, 2014).

The MscL channel gating function also appears affected by the liposome size (Fig. 3.15), hence potentially by membrane curvature. Recently, a cargo release assay was developed in which MscL's sensitivity to the concentration of lysophosphatidylcholines (LPC), which induces membrane stress, could be used as an indirect measure of its channel gating threshold (A. Foo *et al.*, 2015). Carboxyfluorescein efflux from small liposomes was generally higher than larger liposomes, which could be explained by the reduce channel gating threshold of MscL (Dr. Alexander Foo, unpublished) (Fig. 3.15). The mass spectrometry result confirms that this relationship is primarily due to the membrane curvature rather than phospholipid composition. It was predicted with molecular dynamics simulations that curvature at global level such as that of small liposomes could affect MscL channel gating threshold (Meyer *et al.*, 2006), followed by more in-depth discussion with mathematical analyses and further simulations recently (Bavi, Cox, *et al.*, 2016; Bavi *et al.*, 2014). However, due to the practical limitation of performing patch clamp experiments on small liposomes, it was difficult to experimentally confirm this. By measuring a different but related parameter (sensitivity to LPC) to patch clamp (physical pressure across the membrane), the cargo release assay provided an alternative way of confirming the hypothesis.

This experiment to the best of my knowledge is the first to document the influence of membrane curvature on MscL clustering. It was shown from the electron microscopy experiments that MscL tends to cluster in smaller liposomes but not in larger ones (i.e. MscL's clustering tendency and

liposome size are inversely correlated). Since there is little variance in lipid composition between the fractions, it can be concluded that the clustering may be mediated by increased curvature of smaller liposomes. Previously, the effect of membrane curvature on MscL channel gating function was studied only in the context of the stress acting on singular channels (Meyer *et al.*, 2006; Tang *et al.*, 2008a; Zhu *et al.*, 2016) although MscL gating threshold had been reported to be affected by clustering (Grage *et al.*, 2011). A recent study investigated whether membrane curvature influences MscL aggregation *in silico*, but this was found to have a negligible effect (Bavi, Vossoughi, *et al.*, 2016). In contrast to this, the results presented here clearly indicate that clustering of MscL is dependent on liposome size, suggesting that intrinsic membrane curvature may indeed influence the propensity of MscL to aggregate.

MscL clustering in the membranes of small liposomes may be the result of energetic factors. The lowered channel gating threshold postulated for MscL in small liposomes might reflect an energetically less stable system, which has been confirmed in molecular dynamics studies (Bavi, Cox, *et al.*, 2016; Bavi *et al.*, 2014). In such small liposomes, aggregation of MscL may become energetically favourable. Generally, protein aggregation can theoretically confer increased energetic stability in certain conditions (Patro & Przybycien, 1996). Combined molecular dynamics and patch clamp experiment have suggested that the clustering of MscL positively correlates with an increased channel gating threshold (Grage *et al.*, 2011), confirming increased energetic stability in such environments. Therefore, the clustering of MscL particles might have partially compensated for the reduced energetic stability induced by membrane curvature. This phenomenon has also been experimentally observed with MscS, where MscL-induced clustering increased the membrane tension required for its activation, suggesting increased stability of the closed-state conformation (Nomura *et al.*, 2012).

A relationship between membrane protein function and membrane curvature has been documented with other proteins as well (Davies *et al.*, 2012; Draper & Liphardt, 2017; Hahn *et al.*, 2016; Jiko *et al.*, 2015; Pliotas *et al.*, 2015). Some membrane proteins such as chemoreceptors tend to passively cluster on the curved edges of membranes due to the energetic favourability (Draper & Liphardt, 2017) whereas in others such as MscS (Pliotas *et al.*, 2015) and ATP synthases (Daum *et al.*, 2013; Davies *et al.*, 2012; Dudkina *et al.*, 2005; Hahn *et al.*, 2016) the proteins actively induce localised membrane curvature, which can then lead to higher global curvature and clustering in the case of the latter. Molecular dynamics simulations have shown MscL capable of inducing local curvature as well (Bavi, Vossoughi, *et al.*, 2016), so an interesting area of future study would be to identify if MscL indeed has an active role in influencing membrane curvature and how this affects its clustering pattern and function..

Experiments performed in this chapter could be improved with better statistical models. While the results clearly demonstrate curvature-induced clustering of MscL, the analysis was semi-quantitative and there are uncontrolled variables which need to be measured in case they influenced the clustering behaviour. One such variables was phospholipid composition, which was studied by mass spectrometry in this chapter (section 3.3.2.4.) and confirmed not to be an influence, however there could still be other variables such as local protein-to-lipid ratio in liposomes with proteins only. While protein-to-lipid ratio is unlikely to be a factor as previously stated in this section, a measurement would have been helpful. Unfortunately, no experimental method was available at the time of writing that would allow MscL clustering to be quantitatively measured to the standard required for this thesis, although establishing a method to overcome this issue might be possible in the future.

This property of membrane curvature-induced MscL clustering has implications in the development of MscL as a nanovalve for liposomal drug delivery system. Two of the challenges in this regard were that 1) the channel gating threshold of wild type MscL is too high to open the pore with external force only (Nakayama *et al.*, 2015), and 2) liposomes for drug delivery systems need to be smaller than 200 nm to be able to filter through physiological barriers such as blood vessels (Sawant & Torchilin, 2012). Reducing the average size of liposomes will have the dual benefit of poising MscL channels to be more receptive to external triggers, improving its prospect as a nanovalve candidate. However, the propensity of MscL to self-associate in small liposomes prevents even incorporation of nanovalves across liposome surface, which would lead to mix populations of drug-carrying liposomes with large numbers of clustered MscL and those without MscL. One potential solution to this is using phospholipids (or a mixture of phospholipids) which do not cause MscL clustering in liposome production. The influence of phospholipids on MscL clustering was investigated and detailed in the next section.

3.3.3. MscL Distribution Pattern in Pure and Mixed Phospholipid Environments

The main aim of this experiment was to study the relationship between MscL and phospholipids with respect to its clustering pattern. It was previously shown that MscL forms clusters in membranes consisting solely of DOPC (Grage *et al.*, 2011) and even crystallises in this environment (Saint *et al.*, 1998). However, there is limited information on the influence of phospholipids on MscL clustering beyond this. Therefore, this aspect of MscL channel function was explored by visualising the Nanogold-tagged proteins with electron microscopy.

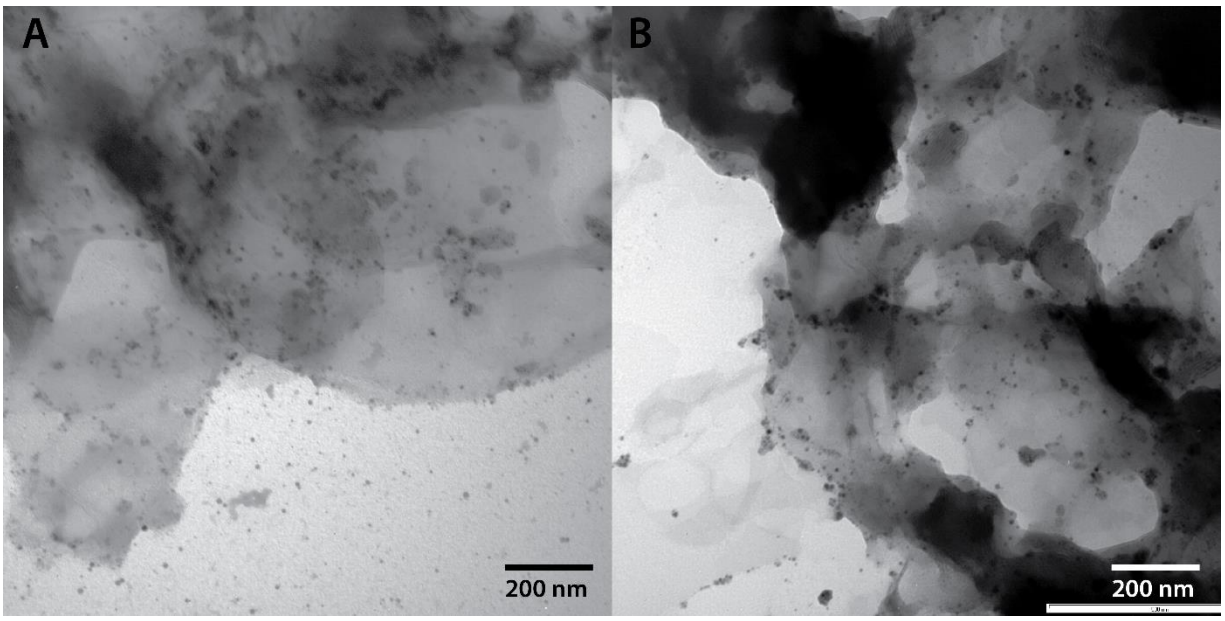

Figure 3.16. Electron micrographs (**A, B**) of Nanogold-tagged MscL in *E. coli* lipid liposome

3.3.3.1. Electron Microscopy of Negatively Stained Liposomes

His-MscL was reconstituted into pure lipid liposomes using the protocol optimised for MscL crystallisation attempts described in section 4.3.1. In the first attempt, DOPC and *E. coli* lipid (heterogeneous phospholipid mixture) were used to replicate the result described by Grage *et al.* (Grage *et al.*, 2011).

A large number of Nanogold-tagged MscL molecules in *E. coli* lipid liposomes contained large aggregates. While MscL did not form large clusters, they were not completely randomly distributed either. It appeared that the proteins would often localise to the curved edges of the liposomes. It is possible that this is a genuine feature of *E. coli* lipid liposomes, but it is more likely that this is an artefact of negative staining process. While liposomes are approximately spherical/ovoid in solution, the negative staining process flattens the liposomes and creates local curvature along the edges where the flattened liposome surfaces fold. Once the flat and curved interfaces form on the membrane, MscL would tend to form small clusters at the curved edges due to the effect discussed in section 3.3.2. On the other hand, monodisperse MscL particles have sufficient kinetic energy to diffuse away from the curved edges, hence leading to most Nanogold-tagged MscL particles still remaining on the flat surface.

Along the liposomal edges, the proteins were partially clustered, with both small clusters and single particles present (Fig. 3.16). On the flattened area of the liposomal membrane, there were occasionally singular MscL particles, but clusters were not observed. This result was in conflict with Grage *et al.* (Grage *et al.*, 2011), where MscL aggregation in *E. coli* spheroplasts was observed

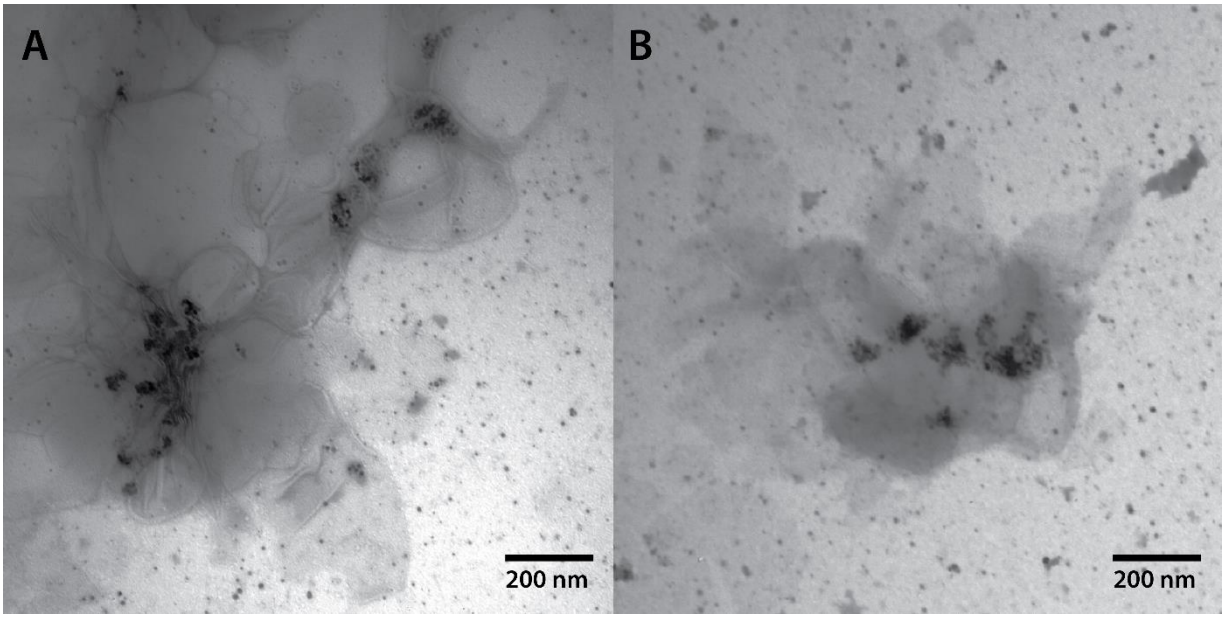

Figure 3.17. Electron micrographs (**A, B**) of Nanogold-tagged MscL in DOPC liposome

by confocal fluorescence microscopy, but in agreement with another publication (Romantsov *et al.*, 2010) where MscL showed an even distribution across *E. coli* membrane *in vivo*.

Additionally, it appeared that the rate of MscL incorporation was relatively high. Aggregated liposomes often had patches of very deeply-stained regions where very few features could be seen. The electron micrographs also became blurry when viewing these regions as if the focus had suddenly been lost. This is thought to be due to the large number of Ni-NTA-Nanogold particles bound to the membrane. Since the Nanogold particles carry Ni^{+} ions, having a very large number of them has the potential to distort the electron beam. As the liposome aggregates offered large membrane surface areas, MscL molecules, hence Ni-NTA-Nanogold particles, could be stacked in high enough concentration to significantly alter the course of incident electrons in random directions and make the images appear unfocused. As this phenomenon was observed and replicated only with *E. coli* lipid samples, it was determined to be a qualitative confirmation of the influence of phospholipid on MscL incorporation observed by Grage *et al.* (Grage *et al.*, 2011).

In contrast, MscL formed large clusters of up to hundreds of particles in DOPC liposomes (Fig. 3.17). There were few single particles, and their levels were similar to the background. Similar to the *E. coli* lipid sample, the clusters were usually located at the edges or aggregating surfaces of liposomes, further confirming this localisation as an artefact of negative staining. This also confirmed the MscL clustering in DOPC liposomes reported by *Grage et al.* (Grage *et al.*, 2011). Since MscL molecules showed a very distinct pattern of clustering in DOPC and did not pose the challenge with electron microscopy which it did in *E. coli* lipid. MscL/DOPC proteoliposome

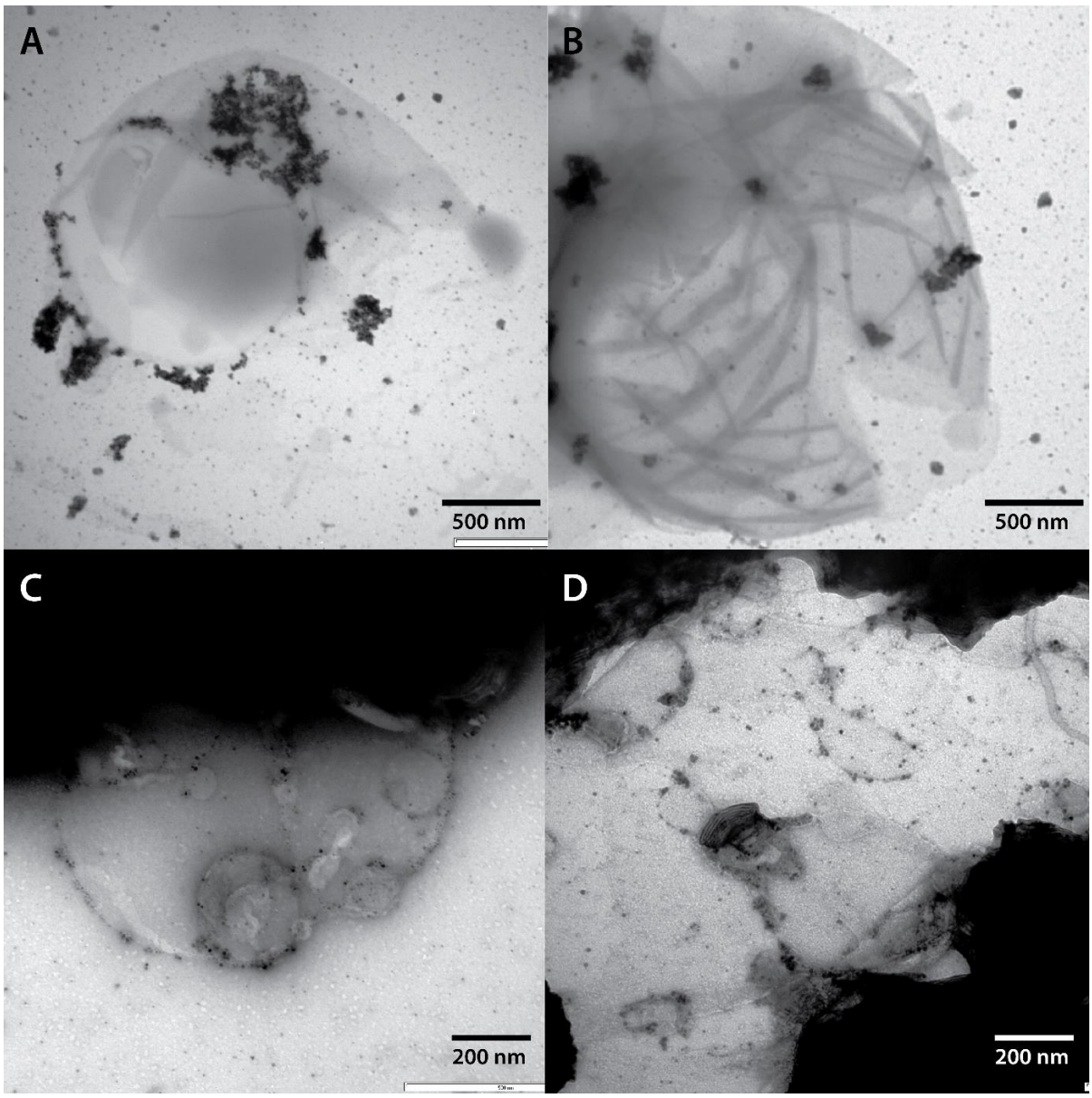

Figure 3.18. Electron micrographs of Nanogold-tagged MscL in DOPC (**A, B**) and *E. coli* lipid (**C, D**) liposomes.

samples were prepared in all subsequent experiments as reference samples to check if the results were consistent between trials.

In the second trial, a wider range of phospholipids were screened for MscL clustering, mainly with respect to the head groups. MscL formed large clusters in DOPC samples, and were roughly randomly distributed with minor clustering along the liposomal edges in *E. coli* lipid samples (Fig. 3.18). Both of these observations are identical to the results in the first trial.

As pure DOPE does not form liposomes, its influence on MscL clustering pattern was studied via mixed DOPC/DOPE liposomes. In samples with the DOPC:DOPE ratios of 3:1 and 1:1, Nanogold-tagged MscL appeared to cluster in a similar pattern to pure DOPC liposomes (Fig. 3.19A-D). In samples with the DOPC:DOPE ratio of 1:3 and pure DOPE lipid, liposomes did not form and no

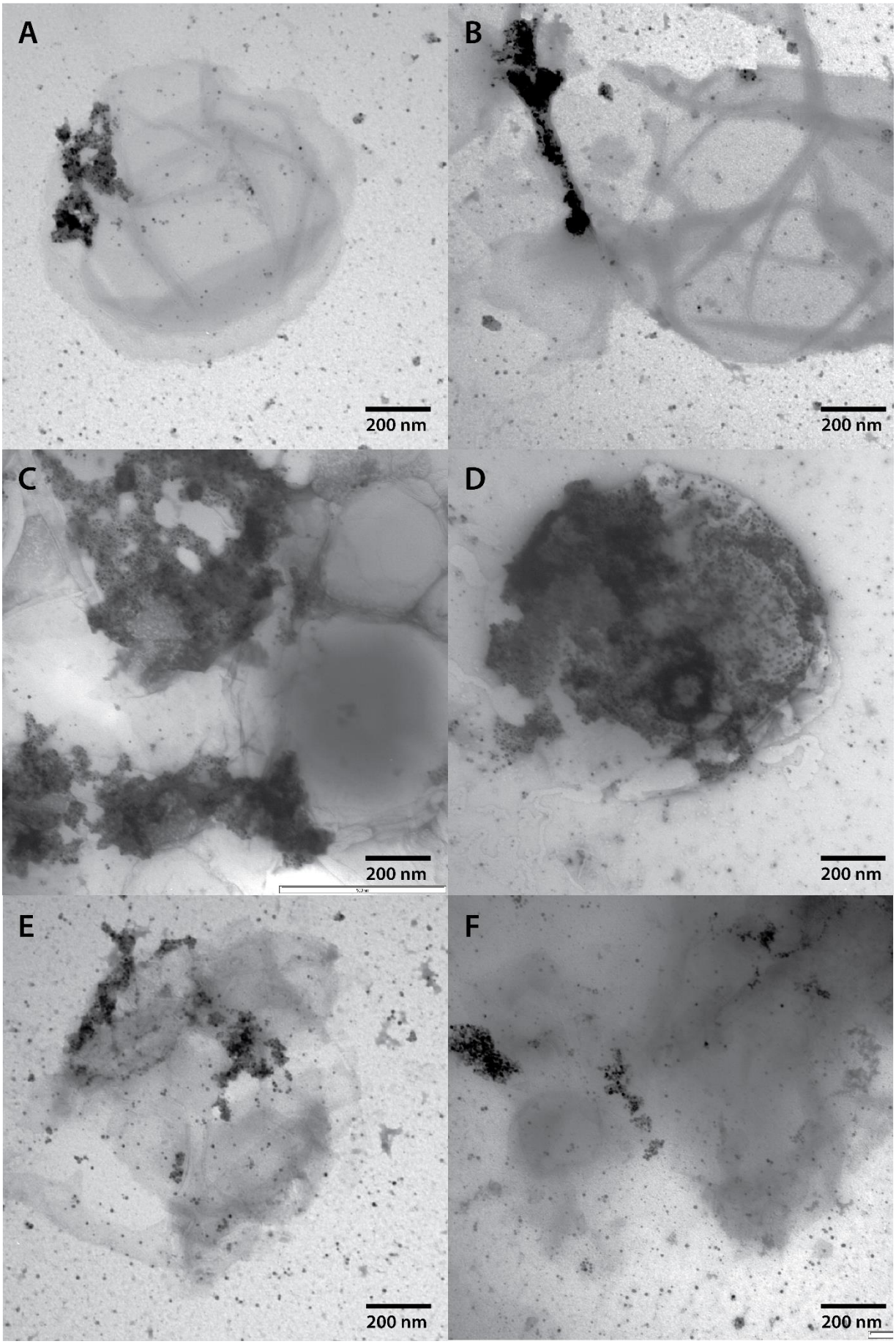

Figure 3.19. Electron micrographs of Nanogold-tagged MscL in mixed DOPC/DOPE liposomes at ratios of 3:1 (**A, B**) and 1:1 (**C, D**), and DOPC/cardiolipin liposomes at the ratio of 1:1 (**E, F**).

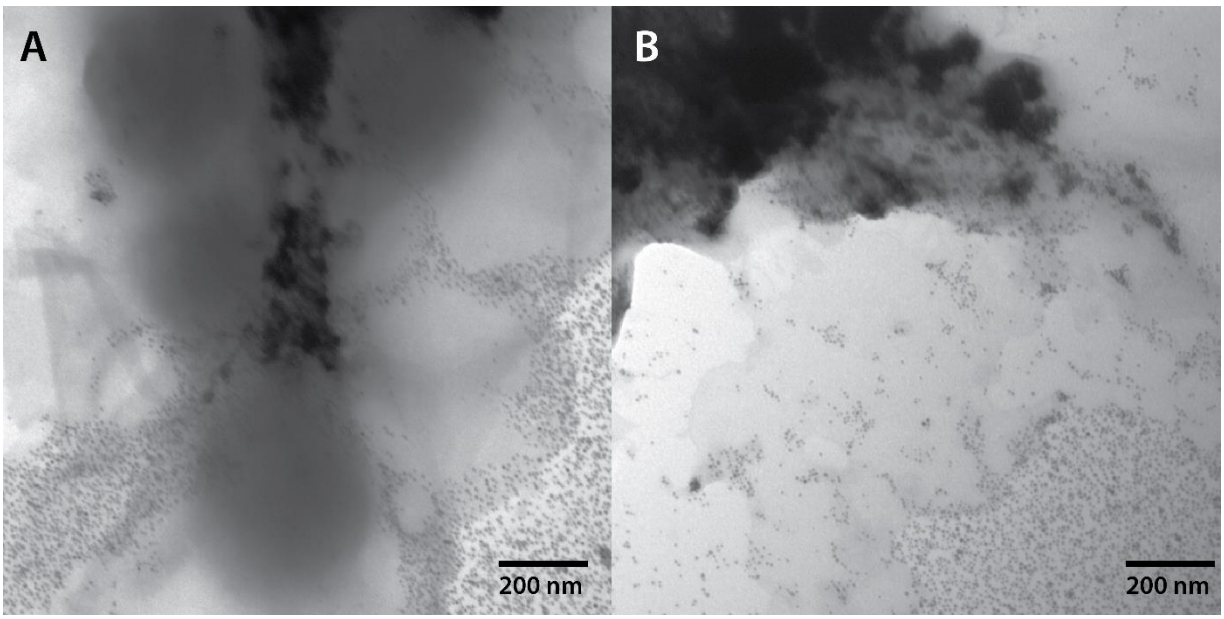

Figure 3.20. Electron micrographs of Nanogold-tagged MscL in DOPC (**A**) and *E. coli* lipid (**B**) liposomes. High level of background Nanogold can be seen in the bottom corners of both images.

image could be taken. There were two explanations for the MscL clustering in the DOPC/DOPE mixed liposome. First, DOPE might have little influence on MscL aggregation or even have a positive influence (hence reinforcing MscL's tendency to cluster in DOPC). The latter was possible since MscL appeared to form even larger clusters in liposomes with the DOPC:DOPE ratio of 1:1 than in 3:1. The second explanation was that the pro-clustering influence of DOPC could be overwhelming DOPE's negative influence. This hypothesis could not be experimentally tested in this trial because pure DOPE liposomes could not be produced.

Likewise, cardiolipin (18:1) appeared to have little influence on MscL clustering, as the large clusters similar to those in pure DOPC liposomes were seen in the sample with the DOPC:cardiolipin ratio of 1:1 (Fig. 3.19E-F). For an unknown reason, the sample with DOPC:cardiolipin ratio of 3:1 did not produce liposomes.

MscL proteoliposome formation was attempted with DOPC/DPPC mixed lipids in order to test if hydrophobic tails had any influence on MscL clustering. However, liposomes did not form, likely due to the high transition temperature of DPPC, which has saturated fatty acid tails. The transition of DPPC's state from gel (i.e. solid) phase to liquid crystalline (i.e. fluid) phase occurs at the temperature range of 42 – 52 ℃, and significant changes to its ability to form phospholipid bilayers occurs in this range (Leonenko *et al.*, 2004). However, the liposomes were prepared at room temperature (22 ℃), which would have kept DPPC firmly in the gel phase and prevent liposome formation. Since it was practically impossible to repeat this experiment at 55 ℃, which would not only introduce temperature as a major confounding factor but also risk heat denaturation of MscL, this condition was not further pursued in the subsequent trials.

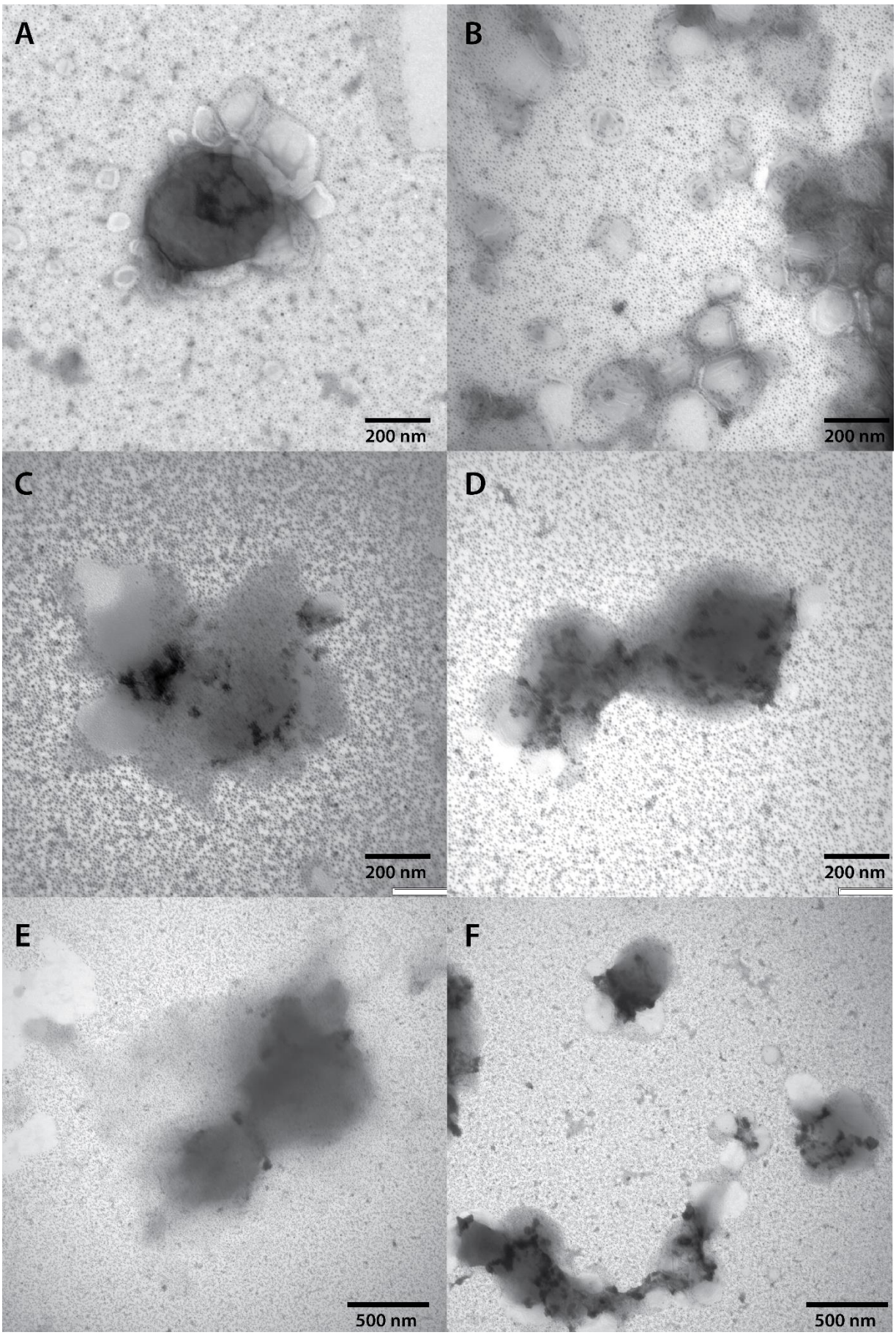

Figure 3.21. Electron micrographs of Nanogold-tagged MscL in pure POPC liposomes (**A**), DMPC liposomes (**B**), mixed DOPC/DMPC liposomes at ratios of 2:1 (**C**) and 1:1 (**D**), and DOPC/POPC liposomes at the ratios of 2:1 (**E**) and 1:1 (**F**).

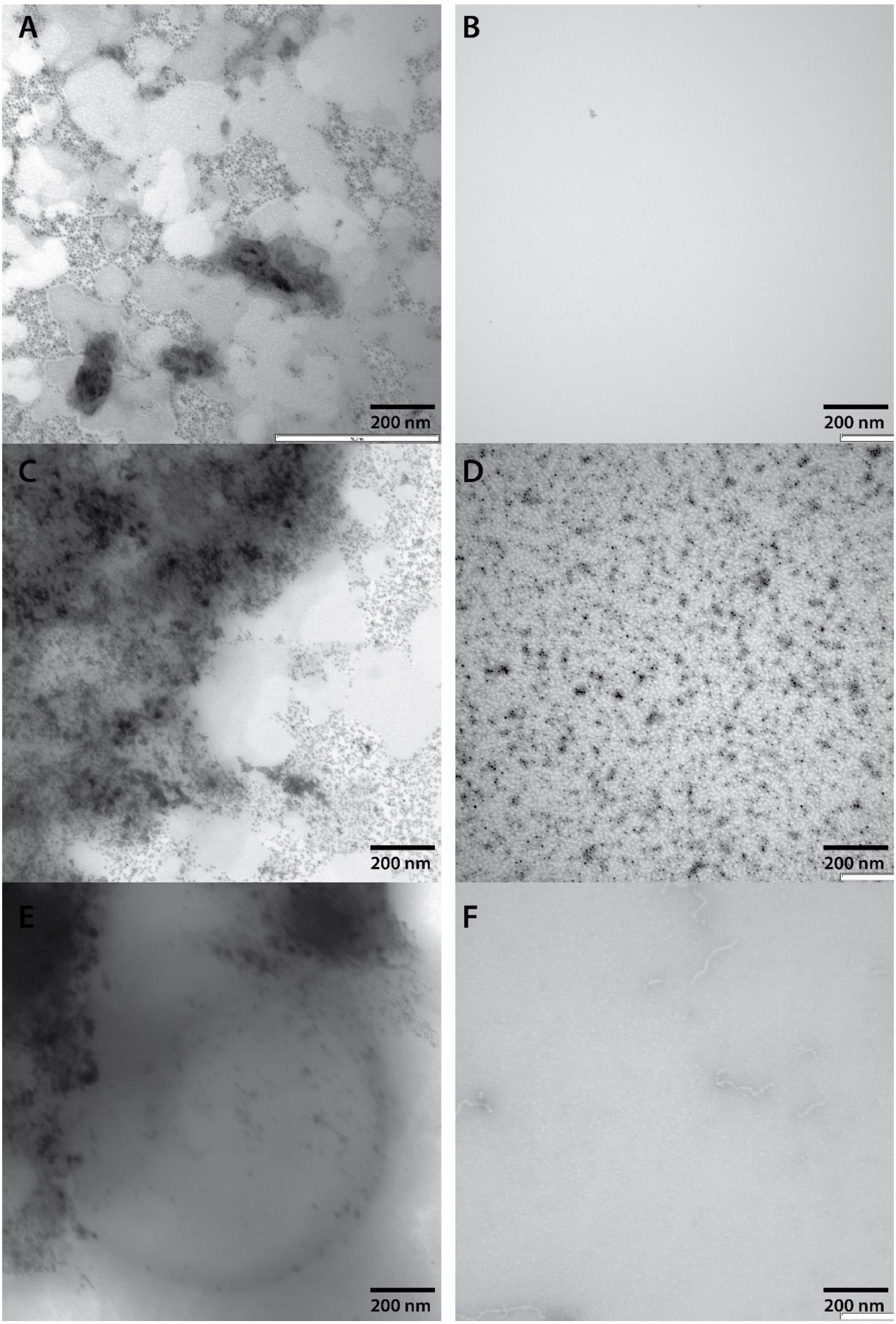

Figure 3.22. Left – Electron micrographs of Nanogold-tagged MscL in mixed DOPC/*E. coli* liposomes at the ratios of 1:3 (**A**), 1:1 (**C**), and 3:1 (**E**). Right – Electron micrographs of Nanogold only (**B**), Nanogold and MscL (**D**), and Nanogold and bovine serum albumin (**F**).

In the third trial, a range of phospholipid tail groups were screened for MscL clustering. Unfortunately, using a new batch of Nanogold led to a very high background level of Nanogold, making it difficult to properly analyse the micrographs (Fig. 3.20). As a result, MscL clustering pattern could not be identified in DOPC/DOPE mixed liposomes. However, the sample conditions were still good enough for analysis in other samples.

MscL did not incorporate into pure POPC and DMPC liposomes, suggesting that the saturation of both fatty acid chains might be important in MscL incorporation efficiency (Fig. 3.21A-B). Unlike DPPC, DMPC formed liposomes in this trial, which indicated that either 1) phase transition might not have been the sole explanation for the failure of DPPC to form liposomes, or 2) the room temperature environment (22 ℃) in which these experiments were carried out was sufficiently close to DMPC's transition temperature (23 °C) to allow liposome formation. In mixed DOPC/POPC and DOPC/DMPC samples, however, MscL aggregation could be observed, confirming that hydrophobic tail did not have a significant influence on MscL clustering (Fig. 3.21C-F).

MscL's tendency to cluster appeared to weaken in mixed DOPC/*E. coli* lipid liposomes with increasing levels of DOPC (Fig. 3.22A, C, E). Although the high background Nanogold made it difficult to make a definitive observation, MscL seemed to form only small clusters of approximately ten particles in 1:1 DOPC/*E. coli* lipid mixture. In contrast, MscL formed much larger clusters in the sample with 3:1 ratio. While this showed that some of the phospholipids in *E. coli* lipid samples negatively influenced MscL clustering, these phospholipids could not be identified with this experiment alone.

Since the high background Nanogold level interfered with electron microscopy, troubleshooting experiments were performed (Fig. 3.22B, D, F). The grid incubated with only Ni-NTA-Nanogold appeared largely featureless (Fig. 3.22B). Another with Ni-NTA-Nanogold and bovine serum albumin (BSA) did not show significant load of Nanogold either (Fig. 3.22F). On the other hand, Nanogold particles were observed throughout the grid incubated with MscL (in β-DDM) and Nanogold (Fig. 3.22D). From these, it was deduced that the background Nanogold level seen in the third trial was not due to nonspecific binding, and likely because there was a significant amount of MscL which did not incorporate into liposomes. A possible explanation was that MscL and β-DDM interacted strongly enough to resist detergent adsorption by Biobeads, which had previously been reported (Konijnenberg *et al.*, 2014).

With the source of the problem identified, additional experiments with modified protocols were set up in which phospholipid head groups were screened. The protein-to-lipid ratio was lowered from 1:1 to 1:10, and this successfully reduced the level of unincorporated MscL, which in turn led to

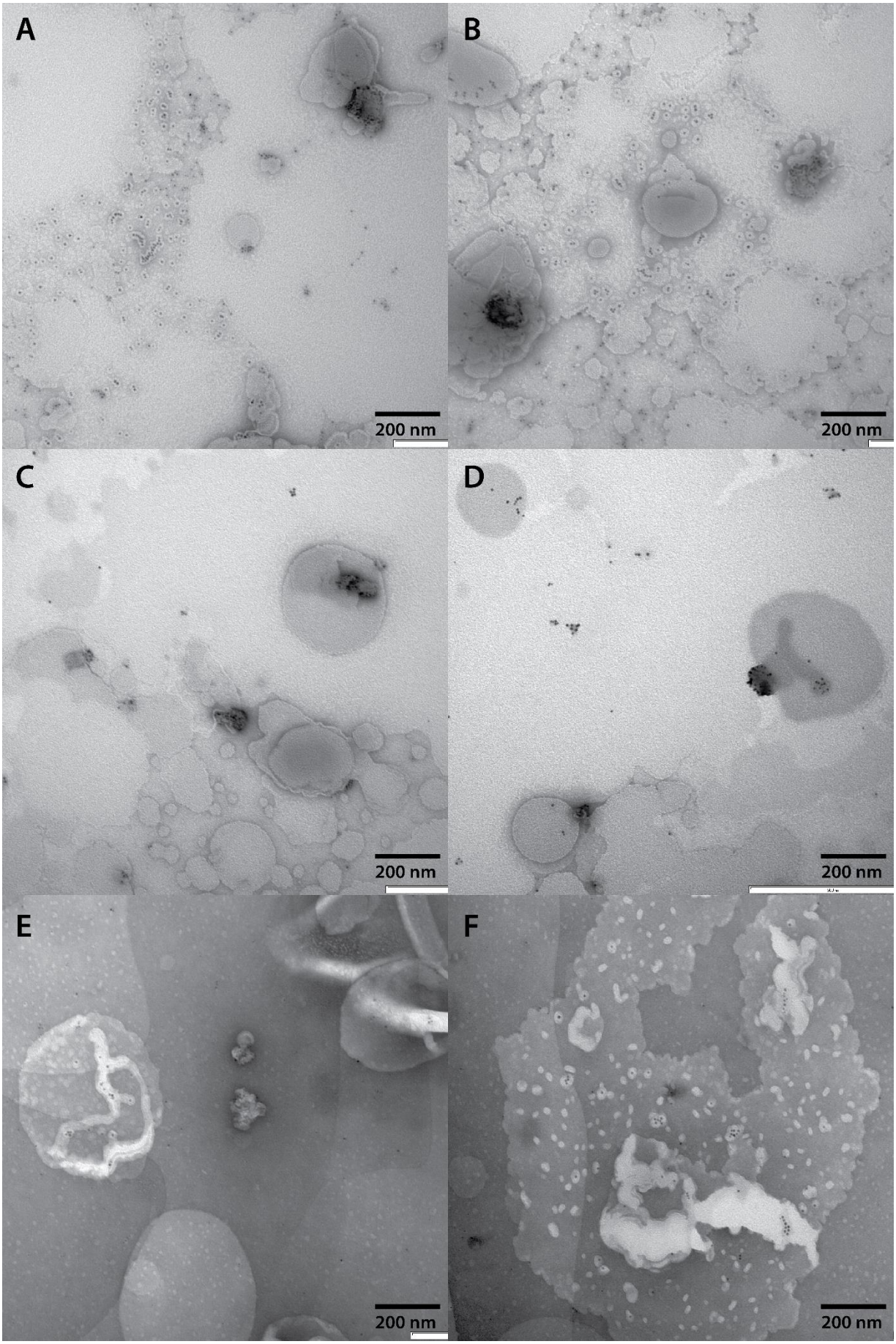

Figure 3.23. Electron micrographs of Nanogold-tagged MscL in mixed DOPC/POPG liposomes at ratios of 3:1 (**A, B**) and 1:1 (**C, D**), and DOPE/POPG liposomes at 3:1 ratio (**E, F**).

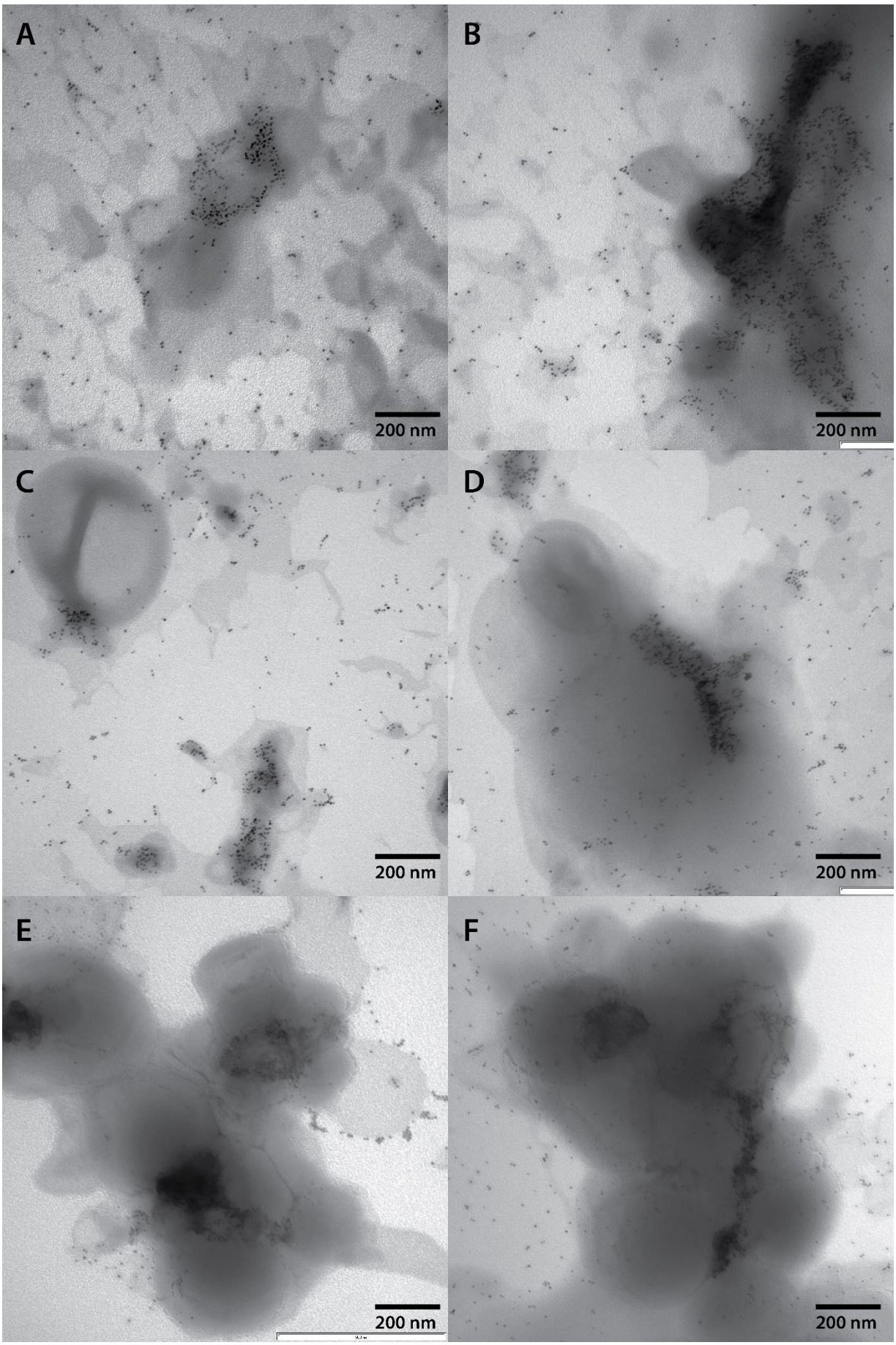

Figure 3.24. Electron micrographs of Nanogold-tagged MscL in mixed DOPC/DOPE liposomes at ratios of 3:1 (**A, B**) and 1:1 (**C, D**), and DOPC/POPC liposomes at 3:1 ratio (**E, F**).

lower background Nanogold level (Fig. 3.23 – 3.24). Liposomes did not form in mixed DOPC/DOPS samples at both 3:1 and 1:1 ratios.

Both MscL aggregation and incorporation appeared to be negatively influenced by the presence of POPG (Fig. 3.23A-D). In the sample with DOPC/POPG at the 3:1 ratio, the dominant species appeared to be singular MscL in equilibrium with small linear clusters. In addition, it looked as if the particles were surrounded by a raft of phospholipids on the membrane. Most of these singular MscL particles were located in flat membranes, and those in liposomes formed large clusters in a similar pattern to pure DOPC lipid (Fig. 3.23C, D). In the sample with DOPC/POPG ratio of 1:1, there were fewer Nanogold particles in general, indicating that MscL did not incorporate well into membrane with high proportion of PG lipid. However, similar to the ones with 3:1 ratio, some of the liposomes featured well-clustered MscL particles.

MscL particles were mostly monodisperse in the 3:1 DOPE/POPG phospholipid sample (Fig. 3.23E-F). Similarly to the 3:1 DOPC/POPG sample, most of the membrane formed flat surfaces rather than liposomes. Most of the Nanogold-MscL particles were co-located with what looked like curved protrusions from the flat surface. Interestingly, large MscL clusters could not be found in this sample, which suggested that MscL clustering seen in other samples may have been largely driven by the phosphatidylcholine (PC) head group.

DOPC/DOPE and DOPC/POPC phospholipid conditions were also tested in this trial to check for the reproducibility of the observations made in the previous trials (Fig. 3.24A-F). The outcome was similar to the past experiments, with Nanogold-MscL particles forming large clusters in the liposomes in DOPC/DOPE and DOPC/POPC phospholipids. With the 3:1 DOPC/POPC mixture sample, however, there were occasionally areas with singular MscL particles (Fig. 3.24E, F), indicating that POPC might be less likely to produce clusters than DOPC.

3.3.3.2. Semi-quantitative Analysis of MscL Clustering Pattern

In this experiment, a semi-quantitative analysis was carried out on the electron microscopy images to assess if correct observations were made with the relationship between MscL clustering and phospholipids. Two approaches were developed to test the hypothesis that MscL formed clusters in some samples but not in others.

First, a Gaussian distribution cluster analysis was carried out on the Nanogold-MscL particle images using the Matlab program to test whether this approach could identify MscL clusters and segregate them from singular species. The function identified large clusters in DOPC samples, which was in agreement with the visual observation. Similarly, it failed to reach convergence in *E. coli* lipid samples, indicating that MscL did not form clusters (Fig. 3.25). However, it could not

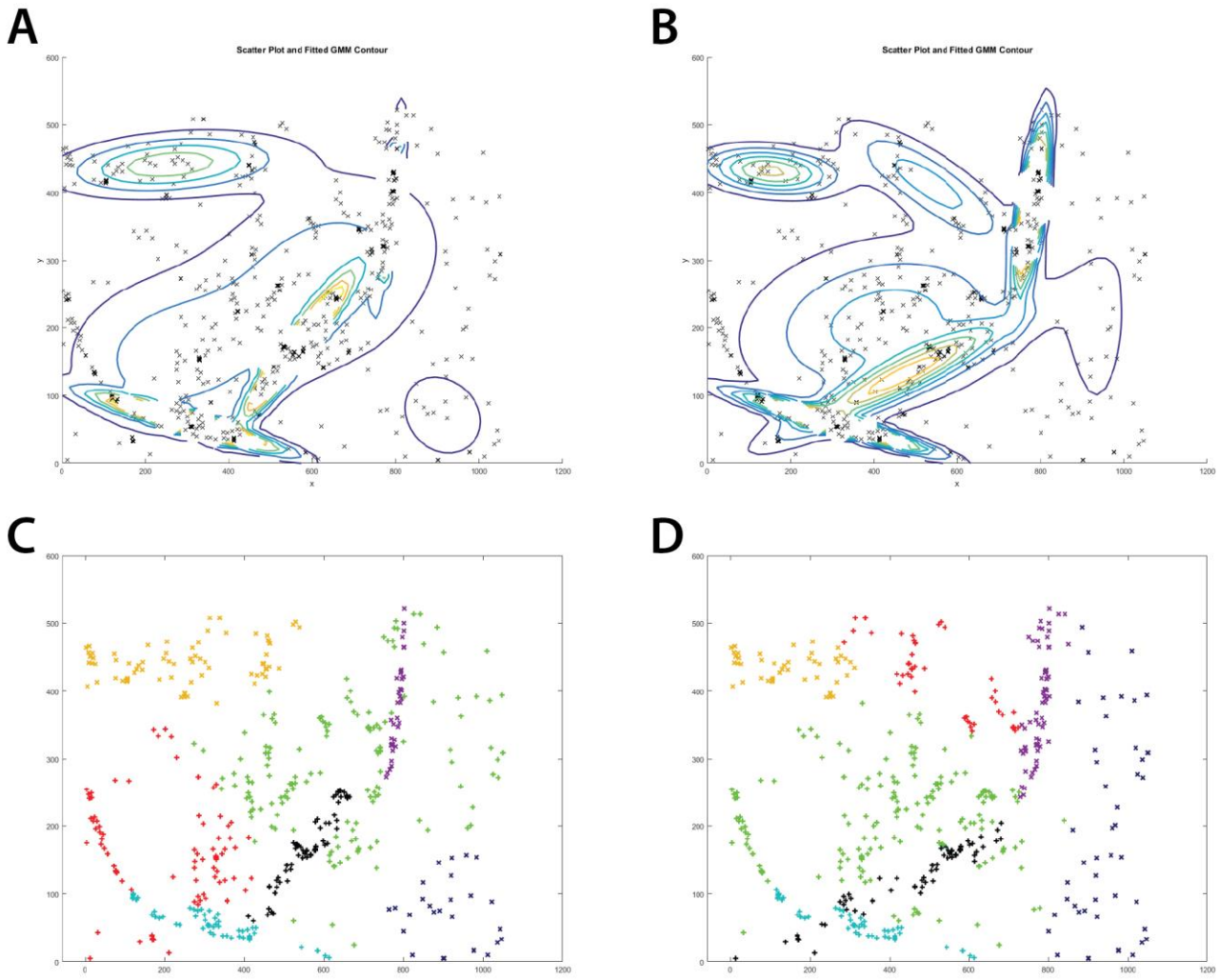

Figure 3.25. Gaussian distribution cluster analysis of Fig. 3.18C (MscL/*E. coli* lipids) with Matlab. Two runs were performed on the same micrograph. In the first step (**A, B**), potential clusters were identified with the Gaussian function. Two identical runs reaching different conclusions can be seen. In the second step (**C, D**), particles were assigned to each cluster. While some of the actual MscL clusters along the edge of the liposomes (light blue, black, purple, and orange) could be reliably classed, it was common for other clusters (red and green in C, green in D) to contain both clustered and scattered particles. In both instances, Matlab failed to reach convergence after 50 iterations, indicating that Matlab could not assign particles into cluster groups with high level of confidence.

segregate scattered (i.e. singular) MscL particles from clustered ones, often placing them in the same group (Fig. 3.25C, D). This was likely due to the nature of the Gaussian function, which would only form oval-shaped contours in two-dimensional space. On the other hand, the MscL clusters often formed arcs around the edges of the liposomes, making this approach incompatible. As a result, this method was ultimately determined unsuitable for cluster analysis.

The second approach estimated the size of clusters by measuring their areas. This was based on the assumption that the Nanogold particles were similar in size, and that Nanogold particles would not stack on top of each other due to the flattening effect of the negative staining process. By

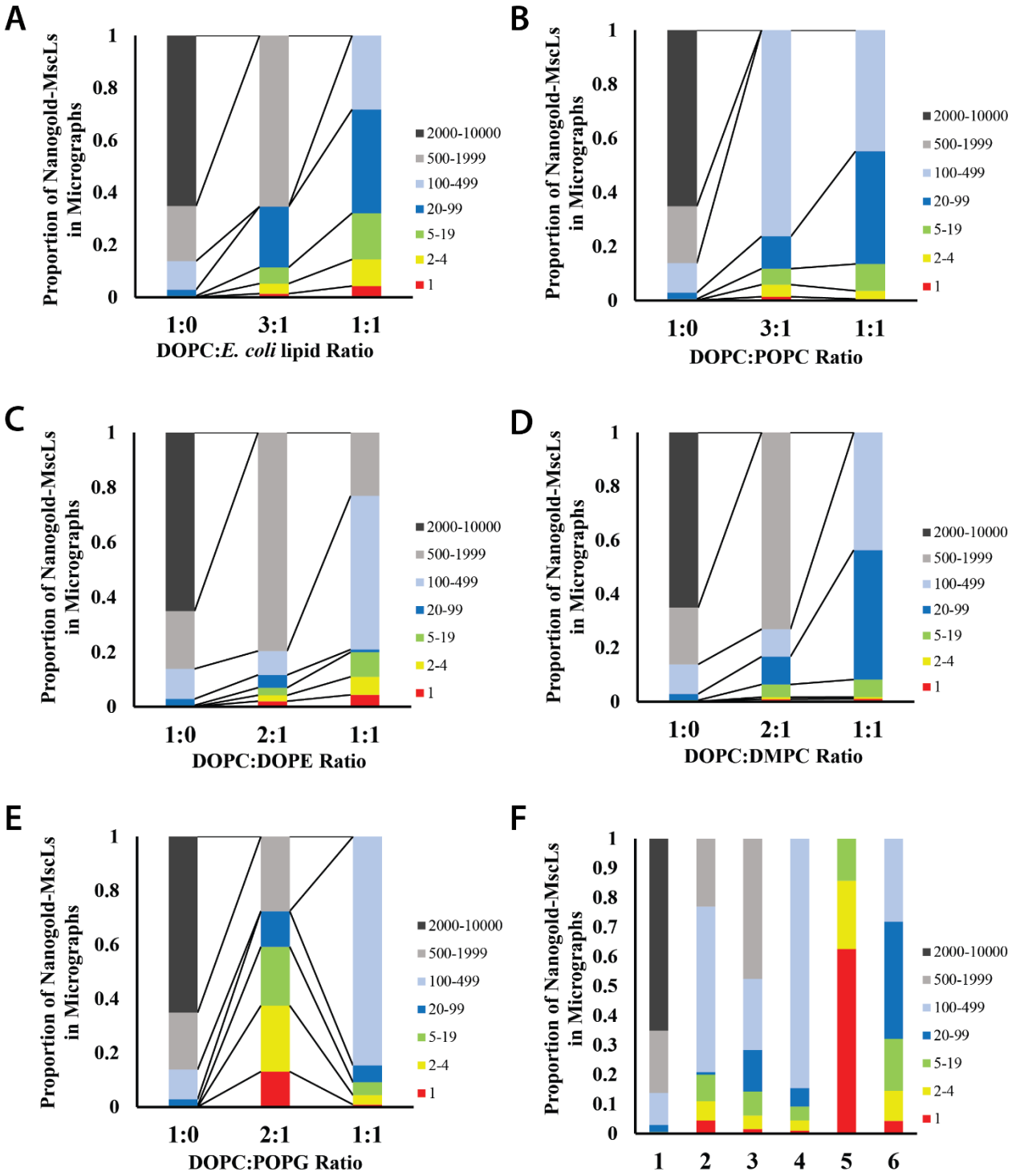

Figure 3.26. Proportion of particles in each cluster grouped by the number of particles. All ratios are w/w. **A**) DOPC/*E. coli* lipid liposome; **B**) DOPC/POPC Liposome; **C**) DOPC/DOPE liposome; **D**) DOPC/DMPC Liposome; **E**) DOPC/POPG liposome. **F**) **1** – DOPC liposome; **2** – 1:1 DOPC/DOPE liposome; **3** – 1:1 DOPC/cardiolipin lipid liposome; **4** – 1:1 DOPC/POPG liposome; **5** – 3:1 DOPE/POPG liposome; **6** – *E. coli* lipid liposome. Grey – large clusters; Blue – medium-sized clusters; Green/yellow – small clusters; Red – monodisperse particles.

performing statistical analysis on the sizes of the clusters, it could be quantitatively measured if the MscL particles were randomly distributed or preferred cluster formation.

This analysis confirmed many of the observations made in the previous section, and revealed additional details on the clustering pattern. First, hydrophobic tails had a minor influence on MscL clustering pattern (Fig. 3.26B, D). Clusters larger than 20 particles were the dominant species in samples with DOPC, DOPC/POPC, and DOPC/DMPC phospholipids. However, clusters were the largest on average in the pure DOPC sample, and smaller clusters of 20 – 500 particles became more dominant with decreasing DOPC levels.

The influence of phospholipid head groups on MscL clustering pattern was more pronounced. Whereas MscL formed large clusters in DOPC liposomes, it remained largely singular in mixed

DOPE/POPG lipid (Fig. 3.26F-5). In 3:1 DOPC/POPG mixed liposomes, there was an even distribution of cluster sizes, suggesting that POPG's strong anti-clustering influence was balancing DOPC's pro-clustering force (Fig. 3.26E). Although the proportion of large clusters increased in the 1:1 DOPC/POPG sample, this was likely explained by the poor incorporation of MscL into flat membranes which were speculated to have a relatively higher proportion of POPG.

On the other hand, DOPE and cardiolipin did not appear to have an active role in MscL clustering (Fig. 3.26C, F-3). In mixed DOPC/DOPE and DOPC/cardiolipin samples, smaller cluster size seemed to be preferred but the proportion of singular MscL particles remained small. This indicated that, while both phospholipids were not strongly cluster-inducing, they had much smaller influence than DOPC. A similar pattern was observed with MscL in DOPC/*E. coli* mixed environment, which was an expected result, since PE is the most abundant head group in *E. coli* lipid.

3.3.3.3. Discussion

The influence of phospholipid on MscL aggregation was investigated in this section, and a causative relationship was clearly established. The phospholipid head group was found to be the main influence on MscL clustering: PC head groups strongly favoured MscL aggregation, PE and cardiolipin head groups did not have significant involvement in MscL clustering, and PG head groups strongly favoured dissociation of MscL clusters (Fig. 3.26). This was an interesting result since this indicated that, while the head groups of phospholipids were important in MscL clustering, this was not due to their net charge. Both PC and PE head groups are net neutral, with the only difference being the amine group (PC has a quaternary amine, whereas PE has a primary one). However, PC was strongly cluster-inducing whereas PE was not, suggesting that this was driven by very specific interaction involving the amine group. In contrast, both PG and cardiolipin are net negatively charged head groups – cardiolipin effectively consists of two PG molecules linked by a

glycerol group (this is in fact how bacteria synthesise cardiolipin from PG and glycerol (Guo & Tropp, 2000)). That PG actively prevented MscL from clustering while cardiolipin did not indicates the possibility of another specific interaction with the protein which may be distinct from that of PC.

It is difficult to speculate on the MscL residues involved in the clustering – and by extension, interaction with phospholipids – or even the nature of the interactions from this experiment alone, especially with the discovery that charges of their head groups are not the main factor. In general, proteins can be induced to aggregate if their interaction with the environment is less favourable than interaction between the proteins themselves. While this can be a possible explanation for MscL clustering in the presence of PC head groups, this is contradicted by a mass spectrometry result showing MscL's increased structural stability in the presence of PC (Kocer, 2015). However, another common pathway where the strong affinity for intermediary molecules cause proteins to aggregate around them is unlikely in this case. PC molecules outnumbered MscL by a factor of 20 in the experiments even if 100 % incorporation rate at 1:1 P:L ratio (w/w) were assumed, so there would have been no relative shortage of PC head groups required for aggregation to occur. Moreover, MscL formed small clusters when the proportion of PC lipid in the membrane was reduced, contradicting this hypothesis.

Likewise, it is difficult to identify the interaction between PG and MscL responsible for interfering with the latter's cluster formation. This is possible if MscL has high affinity to PG, effectively "coating" itself with PG. However, the thin layer chromatography experiment carried out in section 3.3.1. showed that PG did not have high enough affinity to co-purify with MscL, whereas PE did. Moreover, MscL appeared to have a reduced rate of incorporation into membrane containing PG, which would be very unusual if they had high affinity for each other.

MscL's resistance to cluster formation in the presence of PG and the lack of influence by PE or cardiolipin may have functional significance *in vivo*. In an environment with little PG, MscL forms co-clusters with MscS and raises the gating threshold of the latter (Nomura *et al.*, 2012). However, unlike MscS, which usually localises to cardiolipin-rich regions, MscL is generally evenly distributed across *E. coli* membranes, suggesting that there is a counteracting factor to prevent MscL from co-clustering with MscS *in vivo*. The results described in this Chapter suggest that PG, which account for approximately five percent of *E. coli* membranes (Oliver *et al.*, 2014), might be this counteracting factor. Moreover, it is possible that *E. coli* might use the level of PG in the membrane to control the gating threshold of MscS by facilitating co-clustering with MscL in low-PG environment. The PG level in *E. coli* membranes can fluctuate between 4 – 7 % in routine cell cycle alone (Furse *et al.*, 2015), and *E. coli* is known to alter phospholipid composition to influence

membrane protein function (Vitrac *et al.*, 2015), giving further credence to this hypothesis. In addition, the lack of preference for either clustered or singular state of MscL by PE lipids, which it has a high affinity for (section 3.3.1.), will possibly moderate the transition between the two states to avoid inducing an unwanted physiological shock to the bacteria.

One of the potential confounding factors was the curvature of the membrane indirectly influencing the clustering of MscL. MscL tends to form clusters in small liposomes (section 3.3.2.), likely due to the increased curvature. In the experiments in this section, however, liposomes generally had sizes larger than 500 nm in diameter, hence making the effect of global curvature on MscL clustering negligible.

Phospholipid-mediated clustering properties of MscL can be used for nanovalve development as well. As discussed in section 3.3.2, MscL cluster formation in small liposomes can present a unique challenge for its use in a liposomal drug delivery system. A potential solution to this problem is adding small amounts of PG to the liposome preparation so that clustering can be minimised to allow for more even MscL incorporation across small liposomes.

In the near term, the findings from this section will aid with the design and analysis of other experiments on MscL. For example, phospholipid composition in patch clamp experiments could be designed to control the level of MscL clustering, which is a major confounding factor in analysing the channel gating function (Grage *et al.*, 2011; Nomura *et al.*, 2012). Additionally, molecular dynamics simulation can be designed to analyse the clustering effect of the phospholipids used, and assist with the investigation of the interaction between MscL and phospholipids. Pure phospholipids, especially those with PC head groups, are commonly used in such studies (Bavi, Vossoughi, *et al.*, 2016; Rui *et al.*, 2011; Sawada *et al.*, 2012; Zhu *et al.*, 2016). Results from this section can therefore be used to improve the experimental design such as using multiple MscL particles in the simulation instead of single particles suspended in the membrane, which has been put forward as necessary to properly study MscL channel function (Phillips *et al.*, 2009).

3.4. Summary

In this chapter, various aspects of the relationship between MscL and phospholipids were investigated. The general strategy was to identify variables which affect the MscL channel gating and clustering and to understand the results in the context of MscL's affinity to certain lipids. From thin layer chromatography experiments, phosphatidylethanolamine (PE) was identified as potentially having high enough affinity to co-purify with MscL. There have been experiments pointing to PE as an active participant in MscL channel function instead of being just a bulk lipid,

such as marked increase in MscL channel gating threshold when used to replace PC (Powl *et al.*, 2008b), and this result is the direct confirmation of such observations.

Sucrose gradient fractionation experiment has identified membrane curvature as a major variable affecting MscL function. While it was initially suspected that phospholipid composition was the underlying factor behind the observed dependence of channel gating properties and aggregation on liposome size, this was disproven by mass spectrometry, which showed similar phospholipid composition across liposome size. This has two implications in understanding the dynamics of MscL function in liposomes. First, small liposomes have enough membrane curvature to affect MscL channel gating and aggregation. Second, MscL passively incorporates into liposomes rather than actively "shaping" their properties during or after incorporation. This has both positive and negative implications for the evaluation of MscL as a nanovalve candidate for liposomal drug delivery system, which generally requires small liposomal size for improved penetration to target tissues (van den Hoven *et al.*, 2011).

Lastly, MscL distribution in various pure phospholipid liposomes was visualised with electron microscopy and analysed to conclusively establish the causative relationship between the two variables. It was determined from these experiments that phospholipid head groups are the main determinants of MscL aggregation, with tail groups potentially having minor influence (Fig. 3.26). The anti-clustering properties of phosphatidylglycerols (PG) may be used to address the MscL clustering problem in small liposomes. The findings from this study can also be used for better molecular dynamics simulation design, improved analysis of patch clamp experiments, and potentially structural studies of MscL in membranes, which are discussed in Chapter 4.

3.5. Future Directions

A worthwhile experiment in the near term would be the completion of follow up experiments to confirm the identity of the phospholipid natively associating with MscL by mass spectrometry. While thin layer chromatography is useful for quick identification of lipids, it is limited in not being conclusive evidence for phospholipid identification and specifically its inability to identify the tail group. Mass spectrometry, while being a more complicated process, will be able to provide these data, which will greatly improve the understanding of MscL channel function in the native environment. This is also a more cost-effective way of identifying phospholipid head groups than comparing MscL's TLC trace to reference lipids. Preliminary mass spectrometry experiments have already been performed, albeit unsuccessfully, so the main challenge will be in optimising the protocol. In addition, reconstituting MscL into liposomes with various pure lipid composition and

re-extracting the protein will yield a much more direct evidence of MscL's relative affinity to specific lipids.

It will be interesting to see if the sucrose gradient result can be replicated with *E. coli* lipids as well. Although soy azolectin is a commonly used phospholipid mixture, it is rich in PC and other lipids (such as phytosterols) which are not native to *E. coli*. Moreover, it was found from the pure phospholipid studies that the MscL clustering pattern is significantly different between PE (main head group of *E. coli* lipid) and PC (main head group of soy azolectin). As such, it is likely that MscL will have a different clustering and channel gating threshold in *E. coli* lipid, and it will be interesting to study the effect of membrane curvature on such properties in the context of a more native phospholipid environment.

Lastly, future work should include the repetition of some of the studies on the clustering of MscL pure phospholipids. The results for the DOPC/cardiolipin condition were time-consuming to reproduce, and there was only one attempt at producing DOPC/DOPS liposomes. Both cardiolipin and DOPS are minor constituents of *E. coli* lipid, and they are also negatively charged phospholipids, so observing their influence on MscL clustering pattern will help with better understanding the anti-clustering influence of PG lipid.

3.6. Supplementary Information

3.6.1. Mass Spectrometry of Size-fractionated MscL Proteoliposome

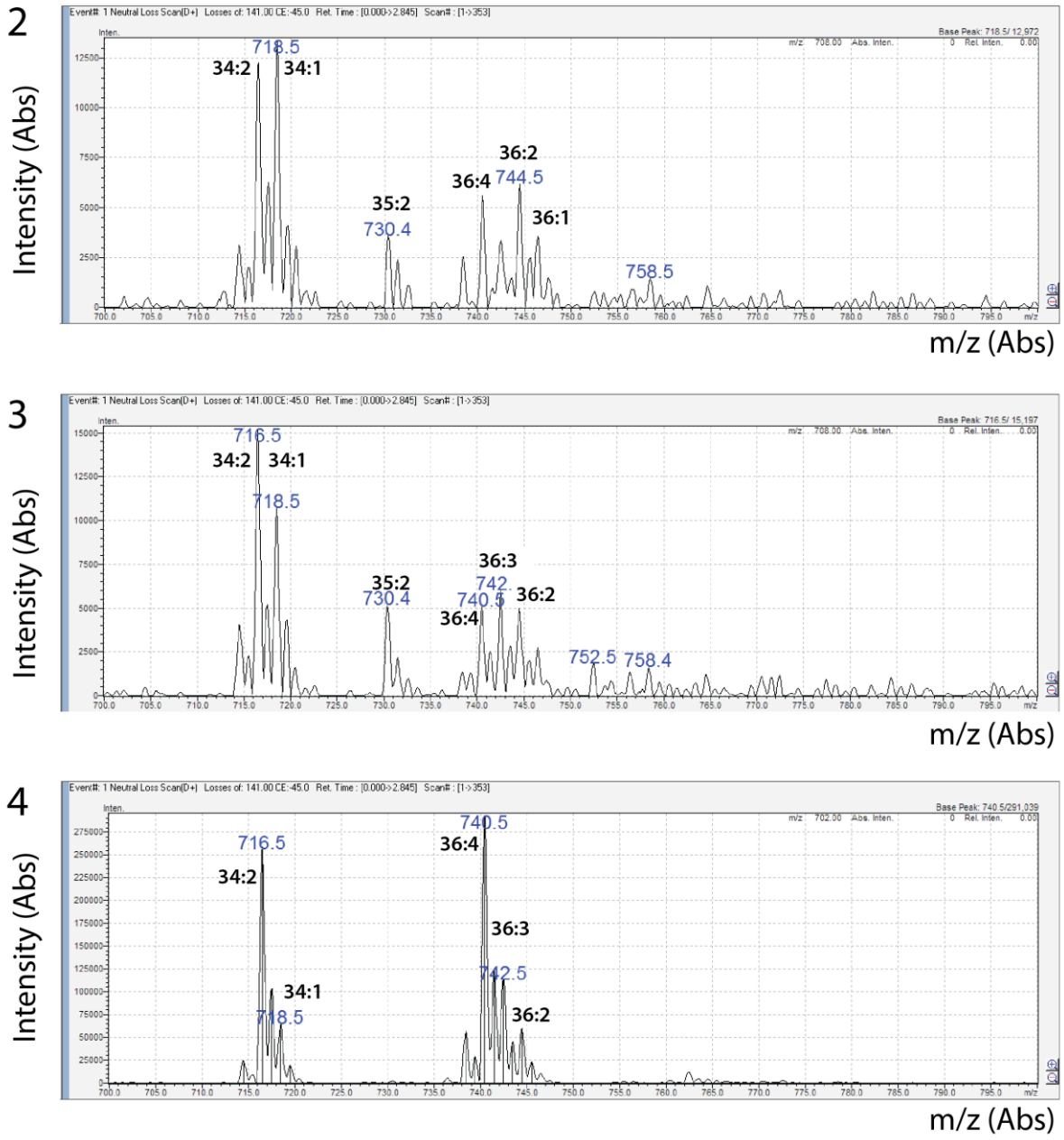

Figure 3.S1. Mass spectrometry of PE lipid region of MscL/Soy azolectin proteoliposomes size-fractionated by sucrose gradient. Numbers in the top left corner represents the fraction number (Fig. 3.9). Blue numbers in the trace indicate the estimated molecular mass of the peak compounds, and black numbers indicate the likely tail group configurations of the phospholipids.

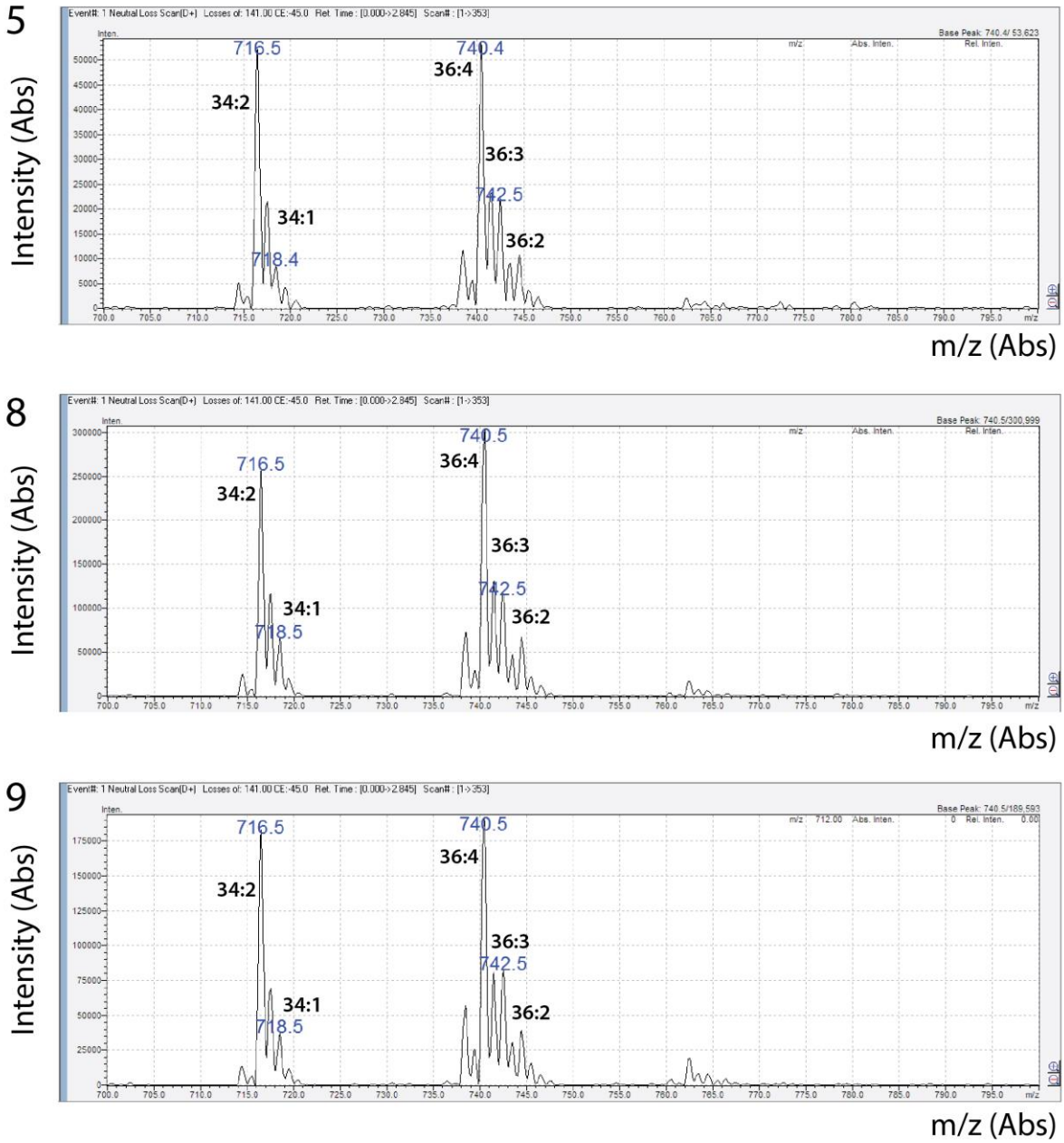

Figure 3.S2. Mass spectrometry of PE lipid region of MscL/Soy azolectin proteoliposomes size-fractionated by sucrose gradient. Numbers in the top left corner represents the fraction number (Fig. 3.9). Blue numbers in the trace indicate the estimated molecular mass of the peak compounds, and black numbers indicate the likely tail group configurations of the phospholipids.

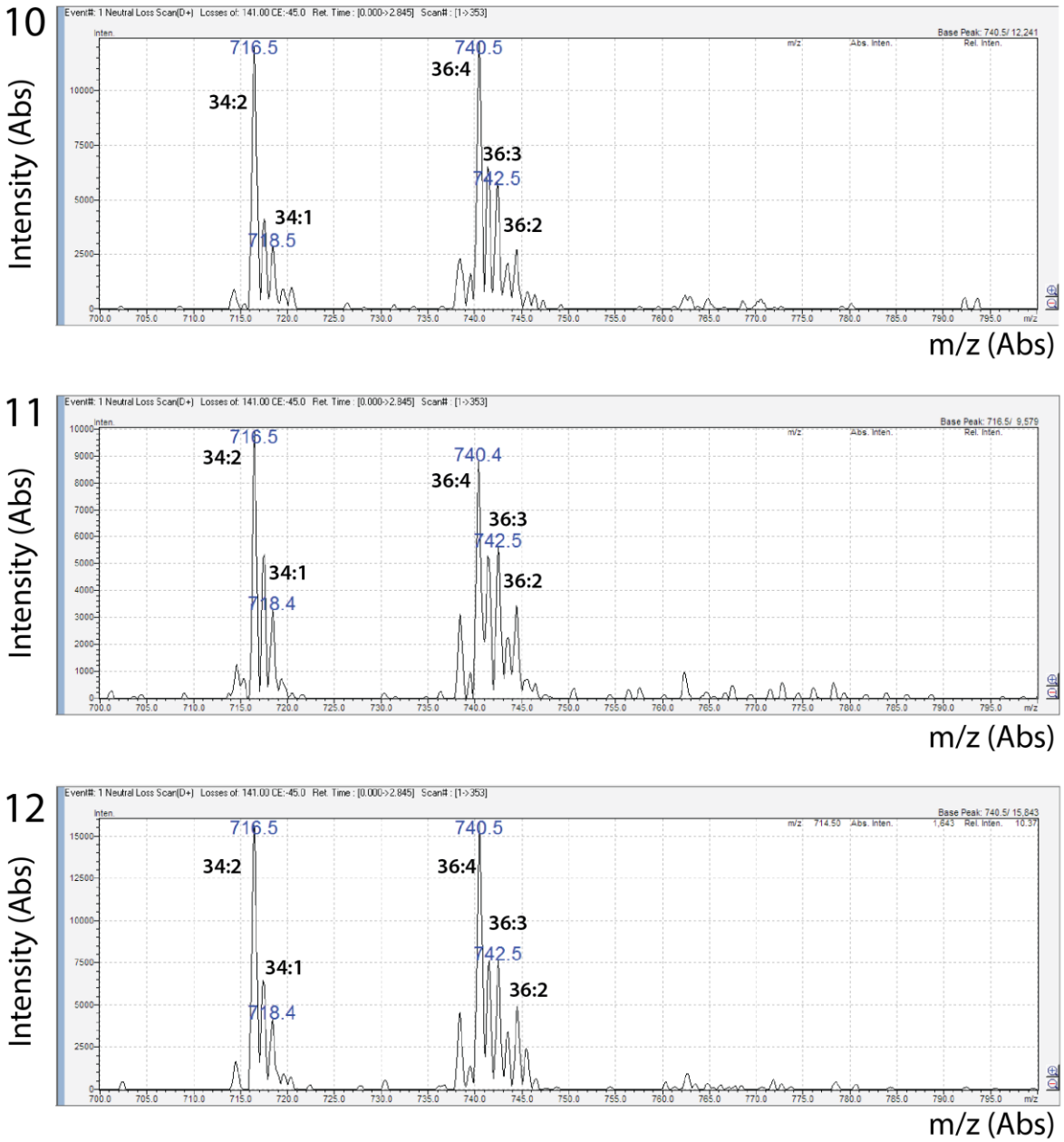

Figure 3.S3. Mass spectrometry of PE lipid region of MscL/Soy azolectin proteoliposomes size-fractionated by sucrose gradient. Numbers in the top left corner represents the fraction number (Fig. 3.9). Blue numbers in the trace indicate the estimated molecular mass of the peak compounds, and black numbers indicate the likely tail group configurations of the phospholipids.

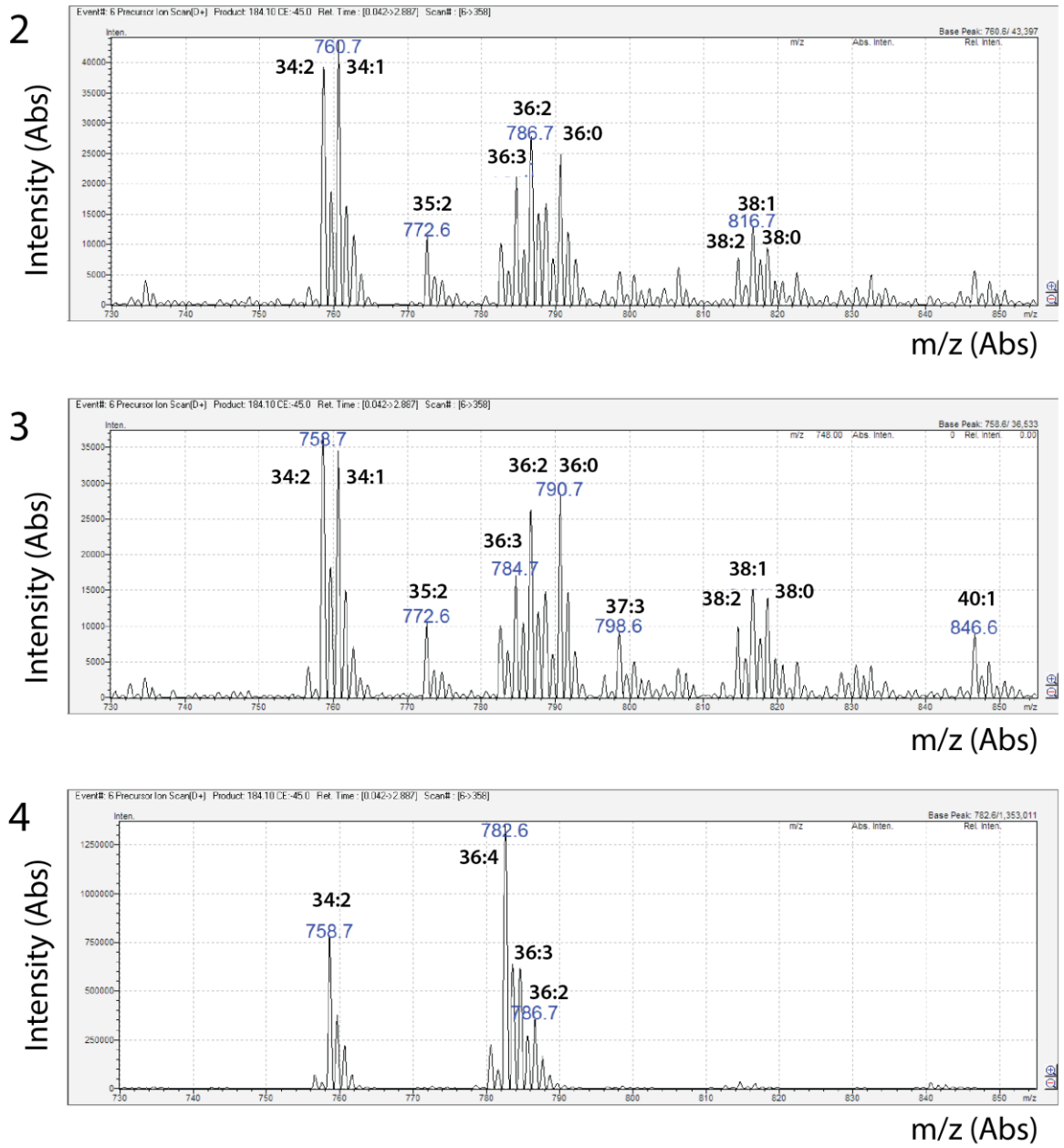

Figure 3.S4. Mass spectrometry of PC lipid region of MscL/Soy azolectin proteoliposomes size-fractionated by sucrose gradient. Numbers in the top left corner represents the fraction number (Fig. 3.9). Blue numbers in the trace indicate the estimated molecular mass of the peak compounds, and black numbers indicate the likely tail group configurations of the phospholipids.

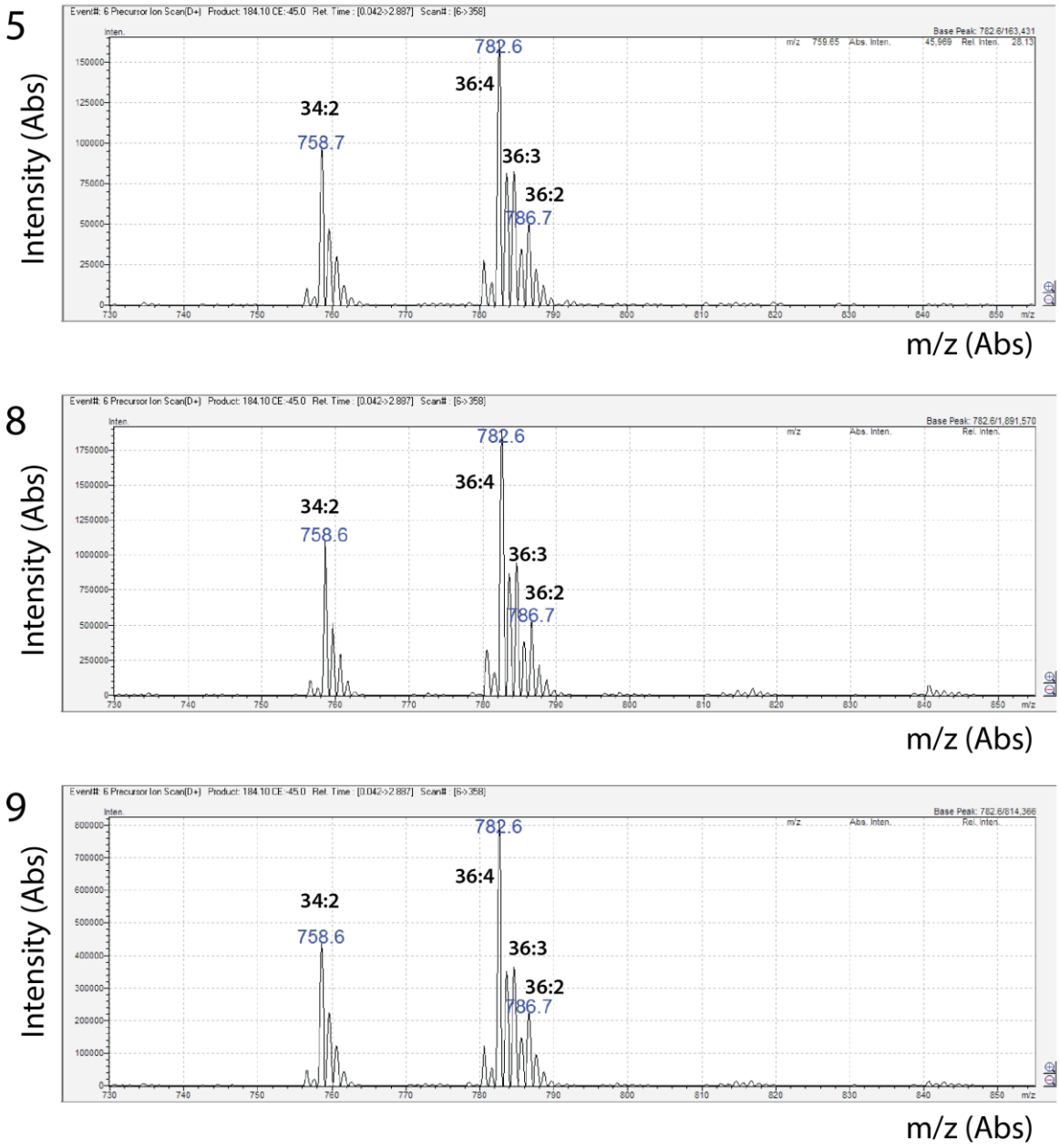

Figure 3.S5. Mass spectrometry of PC lipid region of MscL/Soy azolectin proteoliposomes size-fractionated by sucrose gradient. Numbers in the top left corner represents the fraction number (Fig. 3.9). Blue numbers in the trace indicate the estimated molecular mass of the peak compounds, and black numbers indicate the likely tail group configurations of the phospholipids.

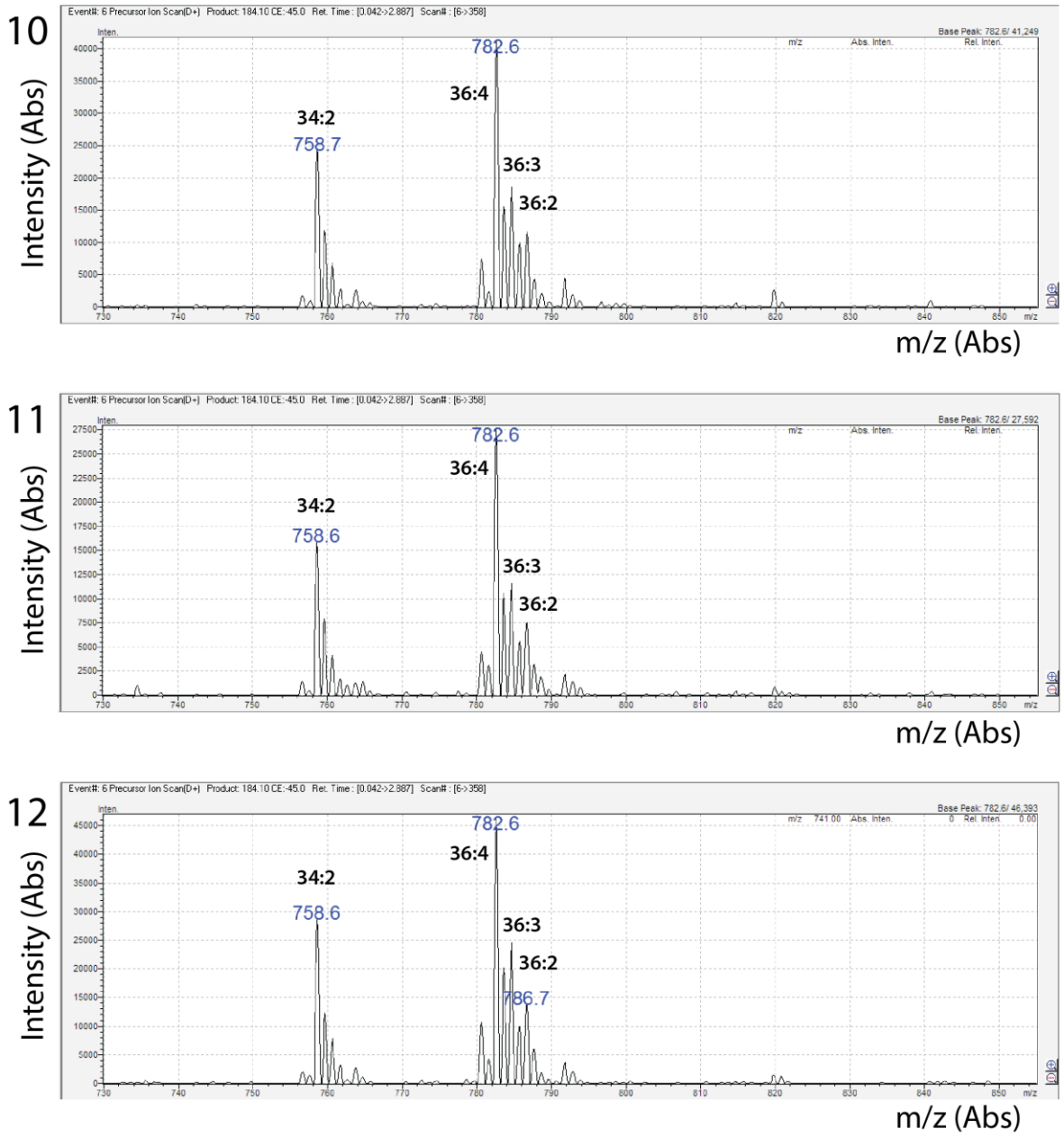

Figure 3.S6. Mass spectrometry of PC lipid region of MscL/Soy azolectin proteoliposomes size-fractionated by sucrose gradient. Numbers in the top left corner represents the fraction number (Fig. 3.9). Blue numbers in the trace indicate the estimated molecular mass of the peak compounds, and black numbers indicate the likely tail group configurations of the phospholipids.

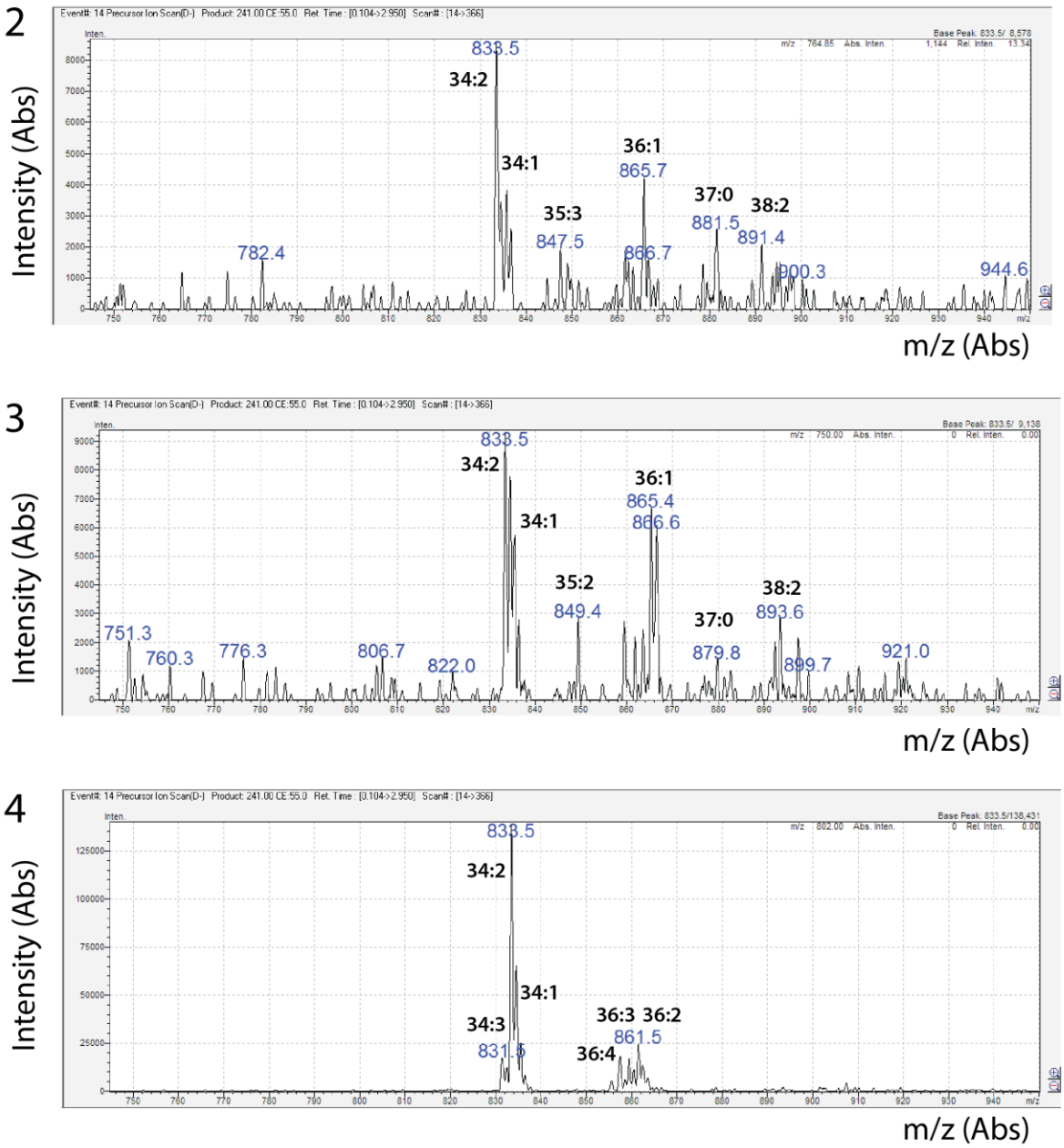

Figure 3.S7. Mass spectrometry of PI lipid region of MscL/Soy azolectin proteoliposomes size-fractionated by sucrose gradient. Numbers in the top left corner represents the fraction number (Fig. 3.9). Blue numbers in the trace indicate the estimated molecular mass of the peak compounds, and black numbers indicate the likely tail group configurations of the phospholipids.

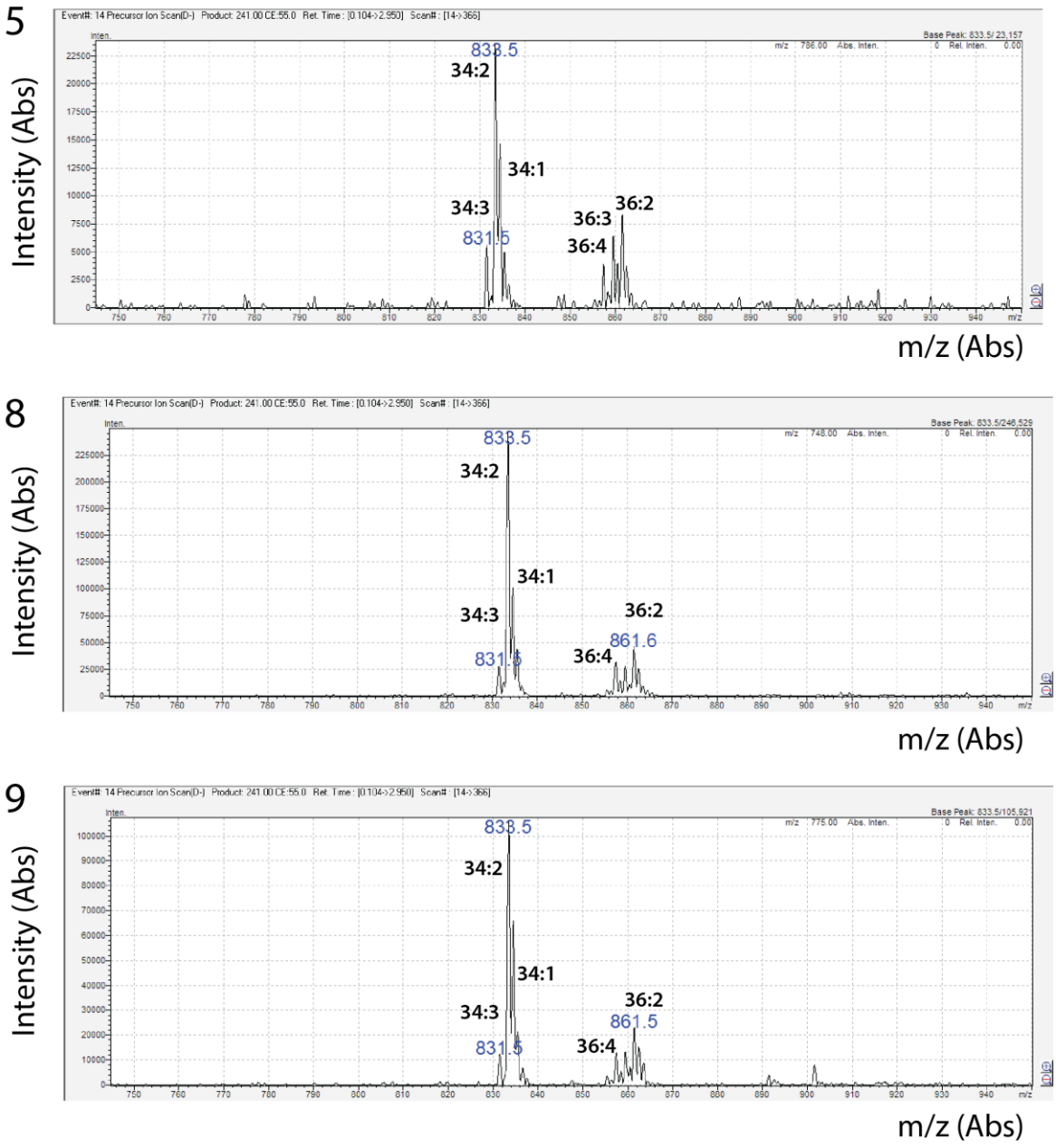

Figure 3.S8. Mass spectrometry of PI lipid region of MscL/Soy azolectin proteoliposomes size-fractionated by sucrose gradient. Numbers in the top left corner represents the fraction number (Fig. 3.9). Blue numbers in the trace indicate the estimated molecular mass of the peak compounds, and black numbers indicate the likely tail group configurations of the phospholipids.

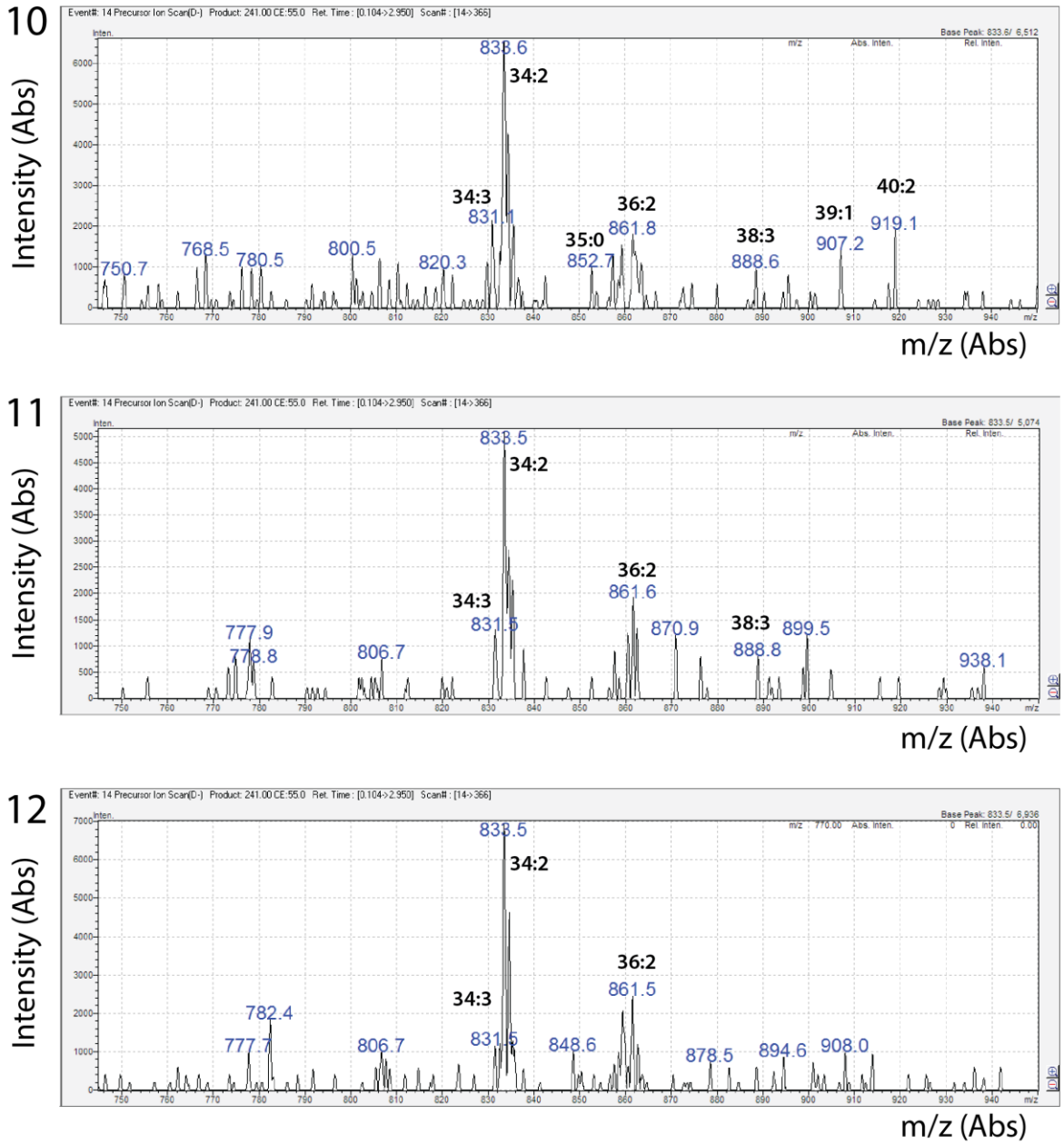

Figure 3.S9. Mass spectrometry of PI lipid region of MscL/Soy azolectin proteoliposomes size-fractionated by sucrose gradient. Numbers in the top left corner represents the fraction number (Fig. 3.9). Blue numbers in the trace indicate the estimated molecular mass of the peak compounds, and black numbers indicate the likely tail group configurations of the phospholipids.

3.6.2. Matlab Plot for the Electron Microscopy of MscL reconstituted in DOPC/DOPE (3:1) membrane

```
clear all

close all

clc


%% Import image

I = imread('bd.jpg'); % imports your file

imshow(I);  % shows image in a figure

title('Gammas original dot image')


%%

% Create a binary matrix - this assigns all non-white pixels as black;

idx_a  = I <45;

idx = flipdim(idx_a,1);


figure

contour (idx)  % produces a contour plot of the index values


% Finds the centre of your 'dots' to assign x,y coordinates

B = zeros(length(I(:,1)),length(idx)-6);

C = length(B(:,1))-1;

D = length(B)-1;

for i = 1:C

   for j = 1:D

   B(i,j) = (idx(i,j)+idx(i,j+1)+idx(i,j+2)+idx(i,j+3)+idx(i,j+4)+idx(i,j+5));

   end
```

```
end

% This part tries to pick out the centre of your protein based on a 6x6 dot
BB = transpose(B);
BBB = zeros(size(BB));
CC = length(BBB);
DD = length(BBB(1,:))-8;
for i = 1:CC
   for j = 1:DD
   BBB(i,j) = (BB(i,j)+BB(i,j+1)+BB(i,j+2)+BB(i,j+3)+BB(i,j+4)+BB(i,j+5));
   end
end

idx2 = BBB > 20, BBB < 30;  % Logical index, finds summed binary values of 32, which is pixel size of your dots
idx2 = transpose(idx2);

[x, y] = find(idx2==1);
xy = [x, y];



%%

%feature extraction - size distribution (area, pixels)
NG = regionprops(idx);
AA = [NG.Area];
```

```
AK = transpose(AA);
figure
hist(AA)
xlabel('Area (pixels)')
ylabel Popularity
title('Size Distribution')

%statistical measurements
mean(AA)
mode(AA)
std(AA)
median(AA)
```

3.6.3. Excel workflow and commands used for data processing

Conversion of area (imported from Matlab) to the number of Nanogold particles

```
=IF(C12>10,ROUNDDOWN(C12,-1)/10,"")
```

Table 3.S1. (Next page) Number and proportion of Nanogold-MscL particles in each cluster grouped by the number of particles in reconstituted pure phospholipid-MscL membrane

Number	***E. coli***	**DOPC**	**DOPC/DOPE 1:1**	**DOPC/DOPE 2:1**	**DOPC/POPC 1:1**	**DOPC/POPC 3:1**	**DOPC/Card 1:1**	**DOPC/DMPC 2:1**	**DOPC/DMPC 1:1**	**DOPC/Eco 3:1**	**DOPC/POPG 3:1**	**DOPC/POPG 1:1**	**DOPE/POPG 3:1**
1	28	5	106	53	5	42	49	18	8	16	266	11	92
2-4	67	0	160	55	26	136	153	14	5	44	495	42	34
5-19	116	32	217	71	85	182	271	92	47	71	440	57	21
20-99	260	158	23	117	357	366	466	202	352	267	268	75	0
100-499	185	743	1362	224	384	2330	804	199	320	0	0	1018	0
500-1999	0	1430	559	2037	0	0	1583	1424	0	751	560	0	0
2000-10000	0	4416	0	0	0	0	0	0	0	0	0	0	0
Total	656	6784	2427	2557	857	3056	3326	1949	732	1149	2029	1203	147
Proportion	***E. coli***	**DOPC**	**DOPC/DOPE 1:1**	**DOPC/DOPE 2:1**	**DOPC/POPC 1:1**	**DOPC/POPC 3:1**	**DOPC/Card 1:1**	**DOPC/DMPC 2:1**	**DOPC/DMPC 1:1**	**DOPC/Eco 3:1**	**DOPC/POPG 3:1**	**DOPC/POPG 1:1**	**DOPE/POPG 3:1**
1	0.04	0.00	0.04	0.02	0.01	0.01	0.01	0.01	0.01	0.01	0.13	0.01	0.63
2-4	0.10	0.00	0.07	0.02	0.03	0.04	0.05	0.01	0.01	0.04	0.24	0.03	0.23
5-19	0.18	0.00	0.09	0.03	0.10	0.06	0.08	0.05	0.06	0.06	0.22	0.05	0.14
20-99	0.40	0.02	0.01	0.05	0.42	0.12	0.14	0.10	0.48	0.23	0.13	0.06	0.00
100-499	0.28	0.11	0.56	0.09	0.45	0.76	0.24	0.10	0.44	0.00	0.00	0.85	0.00
500-1999	0.00	0.21	0.23	0.80	0.00	0.00	0.48	0.73	0.00	0.65	0.28	0.00	0.00
2000-10000	0.00	0.65	0.00	0.00	0.00	0.00	0.00	0.00	0.00	0.00	0.00	0.00	0.00
Total	1	1	1	1	1	1	1	1	1	1	1	1	1

Table 3.S2. Statistics of the Nanogold-MscL particle negative stain electron microscopy for reconstituted pure phospholipid-MscL membrane

	E. coli	DOPC	DOPC/DOPE 1:1	DOPC/DOPE 2:1	DOPC/POPC 1:1	DOPC/POPC 3:1	DOPC/Card 1:1	DOPC/DMPC 2:1	DOPC/DMPC 1:1	DOPC/Eco 3:1	DOPC/POPG 3:1	DOPC/POPG 1:1	DOPE/POPG 3:1
Mean cluster size	8.6	357.1	12.1	27.5	28.6	23.2	22.6	51.3	29.3	25.0	4.0	30.1	1.4
Median cluster size	2	22	1	1	9.5	3	3	2	8	3	1	2	1
Total number of clusters	76	19	201	93	30	132	147	38	25	46	510	40	105
Total number of particles	656	6784	2427	2557	857	3056	3326	1949	732	1149	2029	1203	147
Standard deviation	23	1009	58	150	42	70	104	231	45	110	25	92	1

4. Structural Characterisation of *E. coli* MscL

4.1. Introduction

One of the main objectives of this thesis was to obtain crystals of *E. coli* MscL with a view to determining its 3D structure. The structures of *M. tuberculosis* MscL, *S. aureus*, and *M. acetivorans* MscL have all provided significant insight into MscL function (J. Li *et al.*, 2015; Liu *et al.*, 2009; Steinbacher *et al.*, 2007). However, no structure currently exists for *E. coli* which is the best characterised MscL channel biophysically. There are significant differences between *E. coli* MscL and *M. tuberculosis* MscL in sequence (36 % identity and 50 % similarity between them; pBLAST) and in the gating function in different phospholipid environments (Zhong & Blount, 2013), so extrapolation of results between the two has often been difficult. Finally, no experimentally determined open channel structure of MscL exists. This chapter describes the work conducted to progress MscL crystal production using both 2D and 3D crystallisation approaches.

4.1.1. 2D crystallisation Experiments of MscL

The first strategy taken was to develop 2D crystallisation protocols for MscL to enable structure determination in a lipid bilayer environment. 2D crystallisation is a method of membrane protein crystallisation in which the protein is induced to form ordered 2D crystalline arrays following reconstitution into a phospholipid bilayer. It has the advantage of membrane proteins being studied in a near-native phospholipid environment rather than in detergent micelles (common for 3D membrane protein crystallisation), which can force the protein into an unnatural conformation (Dorwart *et al.*, 2010). Notably, 3D crystals of *S. aureus* MscL were reported to have an unexpected, tetrameric conformation rather than the native pentamer (Liu *et al.*, 2009), which was subsequently shown to be a result of the detergent conditions employed for crystallisation (Dorwart *et al.*, 2010). 2D crystallisation was therefore trialled to avoid this problem.

Previous attempts to obtain a structure of *E. coli* MscL using 2D methods have been reported (Saint *et al.*, 1998), further suggesting that this was a reasonable strategy to pursue. These early attempts yielded a 2D projection map erroneously determined as a hexamer, likely due to the incorrect imposition of a six-fold pseudosymmetry resulting from a hexagonal close packing arrangement of

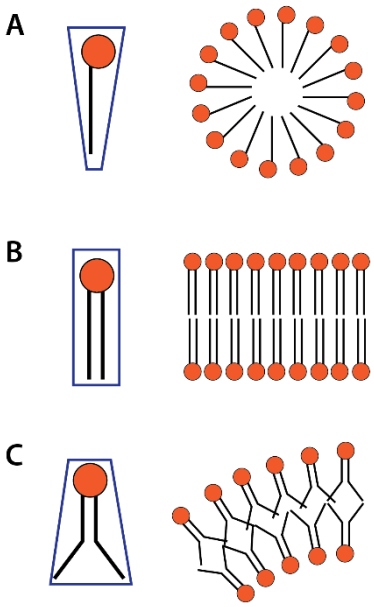

Figure 4.1. Schematic representation of lipid packing mediated by phospholipid geometry. Individual lipid molecules and their geometry are represented on the left, and the resulting membrane geometry are presented on the right. **A**) Positive curvature-inducing phospholipids. **B**) Curvature-neutral phospholipids. **C**) Negative curvature-inducing phospholipids.

the proteins rather than a true 2D crystal lattice. This necessitated identifying an improved crystallisation condition with reduced freedom for MscL in the crystal lattice.

In addition to protein and protein concentration, it is well established that a range of variables influence the propensity of membrane proteins to form 2D crystals.

Lipids: The type of lipid is a major factor in 2D crystallisation as it can determine the morphology of the bilayer (Lasala *et al.*, 2015). Depending on the relative cross-sectional areas of the lipid head and tail groups, the lipid molecules can induce the membrane to be either curved or flat, with the former potentially triggering tube and/or liposome formation (Fig. 4.1) (Alberts *et al.*, 2003). Lipids can also influence protein crystallisation via direct interaction with protein molecules. While there is no consensus on the principle behind this, it is believed to involve the general shift in the energetic favourability of the protein molecules toward the crystallised state. In certain cases, specific interactions between proteins and annular lipids might aid with crystallisation by increasing the protein's stability.

In general, 2D crystallisation has been most successful with phosphatidylcholines (PC) such as DMPC, POPC, and DOPC, and *E. coli* lipids, which together accounted for 85 % of published successful 2D crystallisation conditions (Lasala *et al.*, 2015; Schmidt-Krey, 2007). MscL was reported to crystallise in *E. coli* lipids as well (Saint *et al.*, 1998). Therefore, 2D crystallisation experiments outlined in this thesis focused on these lipids.

Protein-to-Lipid ratio: In 3D crystallisation, the solubility of proteins is predominantly controlled using a range of precipitants and precipitant concentrations (Lasala *et al.*, 2015). Precipitants draw water away from the proteins and force them to associate either into crystals or non-crystalline aggregates. An analogous approach in 2D crystallography is to screen a range of protein-to-lipid (P:L) ratios. At higher P:L ratios, there is less lipid bilayer available per protein to maintain its solubility, forcing proteins to pack more closely together, either into 2D arrays or non-crystalline aggregates.

Detergent: Stability of the target protein in the detergent used for extraction/purification is an important consideration in 2D crystallography, although ideally this would be optimised before a project advances to the stage of attempting to obtain protein crystals. Detergents can, however, have significant impact in the early phases of 2D crystallisation, as the interaction with proteins and phospholipids can affect the way protein molecules incorporate into the membrane (Lasala *et al.*, 2015). Nonionic glucoside detergents such as β-DDM as well as Triton X-100 are among the most commonly used detergents in 2D crystallisation.

MscL is reported to be relatively stable in both β-DDM and Triton X-100 (Price *et al.*, 2011; Yilmaz *et al.*, 2015). It has been suggested that β-DDM associates tightly with MscL (Konijnenberg *et al.*, 2014), making it potentially undesirable for 2D crystallisation since it might make complete detergent removal difficult. Furthermore, MscL was found to adopt non-native conformations in the presence of LDAO (Dorwart *et al.*, 2010), while in the early stages of this work it was observed that MscL solubility is negatively affected when stored in octylglucoside (data not shown) meaning that the choice of detergent had to be made carefully in these studies. In addition, the rate and extent of detergent removal can affect the morphology of reconstituted bilayers (Schmidt-Krey, 2007). Detergent chelators like Biobeads and cyclodextrins are most commonly used with microdialysis providing an alternative approach, albeit one that is limited by the long times required to completely remove detergents with low critical micelle concentration (Brent L. Nannenga *et al.*, 2013).

Anions and cations: As for 3D crystallisation, the type and concentration of inorganic salts can also affect 2D crystallisation. At high concentrations, solutes (which include ions) can "compete" with proteins for water molecules in solution to the point where a crystalline state is energetically favoured by the proteins (Majeed *et al.*, 2003; McPherson, 2004). An additional consideration for 2D crystallography is that ions can facilitate the fusion of lipid bilayers either by attracting liposomes which would otherwise electrostatically repel each other (Akashi *et al.*, 1998; Bentz & Duzgunes, 1985; Ruso *et al.*, 2003), or through Hofmeister ion effects where ions of inorganic salts indirectly influence the solubility of organic molecules (primarily proteins but also applicable to phospholipids) via weak interactions with bulk water molecules (Baldwin, 1996; Salis & Ninham,

2014; Z. Yang, 2009). Therefore, 2D crystallisation conditions were screened for various salt concentrations in this study.

A substantial amount of work in this chapter is focused on screening the influence of these parameters. Other variables which were screened in this study were pH, and freeze-thaw process. In particular, the freeze-thaw process can increase both the size of liposomes (Castile & Taylor, 1999), reduce the proportion of multilamellar vesicles (Traikia *et al.*, 2000), and incorporation of protein into the bilayer (Katzen *et al.*, 2009) through physical disruption of the membrane. It should be noted that automated screening methods that are commonplace in 3D crystallisation laboratories are not well-suited to 2D crystals and so the process is far more labour-intensive (Schmidt-Krey, 2007). Consequently a broad spectrum approach was initially taken to identify conditions of interest within this complex multi-dimensional space matrix.

4.1.1.1. Alternative crystallisation approaches

In this project, both the traditional 2D bilayer crystallography method introduced above and an approach that incorporated a phospholipid monolayer template were trialled in parallel. In the latter method, a mixture of phospholipids with and without affinity tags such as Ni-NTA was used to arrange the protein molecules in a specific orientation and to concentrate them at the water-template interface, both of which can promote crystallisation. This strategy is especially useful for membrane proteins, since proteins can be reconstituted into membranes in two orientations without such guidance.

One requirement of the monolayer-based method is that the protein's affinity tag should not to be cleaved off during purification to facilitate interaction with the template. Since additional linker residues or tags interfere with crystallisation (as these tend to have higher levels of freedom – i.e. are more flexible) this can be problematic. In the case of MscL, an important consideration is that the N-terminal peptide might be buried in the hydrophobic layer of micelles/membranes (see section 2.4.1.1.). Technically, this could be circumvented by the use of C-terminal hexahistidine tags. However, existing MscL constructs with C-terminal affinity tags had significantly different gating thresholds to both the wild-type MscL and the construct used in this study (Prof. Boris Martinac, personal communication), suggesting significant interference of the channel function and structure by the affinity tags, which in turn made its use in the crystallisation experiments undesirable.

4.1.2. 3D Crystallisation Experiments of MscL

In parallel, 3D crystallisation of MscL in the presence of detergents was attempted. X-ray diffraction from 3D crystals is the most common method of protein structure determination, and has been successfully used to determine the structures *of M. tuberculosis*, *S. aureus*, and *M. acetivorans* MscL (G. Chang *et al.*, 1998; J. Li *et al.*, 2015; Liu *et al.*, 2009). While this has the disadvantage of not being able to study MscL in the lipid bilayer environment, which is especially significant given its tight association with phosphatidylethanolamines (section 3.3.1.), the ability to perform high-throughput screening for a large number of crystallisation conditions and the less labour-intensive process have made this an approach worth exploring in this study.

An MscL construct with the N-terminal fusion tag uncleaved was intentionally used despite a potential drawback. It was hypothesised from publication records and personal communications that the difficulty with crystallising *E. coli* MscL could be in its native structure. Not only has the *E. coli* MscL structure remained undetermined despite its status as the most intensively studied species of MscL, there have been at least two unsuccessful attempts at crystallising *E. coli* MscL (Prof. Boris Martinac, personal communication). These suggested that using conventional methods of 3D crystallisation, one of which was using near-wild-type MscL in the experiments, would have a low chance of success.

Therefore, the N-terminal affinity tag was left uncleaved from MscL during the purification process to increase the solvent-facing surface of the protein. While there was a risk of the fusion tag interfering with crystallisation due to its high degree of freedom (as previously discussed), it was hypothesised that this might be outweighed by significantly increasing the solvent-facing surface of the protein, which generally has a positive effect on membrane protein crystallisation. Similar strategy was adopted to determine the structure of *M. acetivorans* MscL, where the pentameric riboflavin synthase is thought to have aided with crystallisation by creating a large solvent-facing surface for the fusion protein (J. Li *et al.*, 2015). Using a hexahistidine fusion-tag (His-tag) to aid with crystallisation also has precedents (Tajika *et al.*, 2004), and in some cases this is thought to be partly due to the interaction between histidine residues and organic buffer molecules such as HEPES (Majorek *et al.*, 2014).

4.2. Methods

4.2.1. 2D Crystallisation

4.2.1.1. 2D Crystallisation of MscL with Traditional Method

6 µL of 5 mg/mL liposome solution, 1.5 µL, 3µL or 7.5 µL of either PD1 buffer (PBS pH 7.4, 1 mM β-DDM), 200 mM $MgCl_2$ or 200 mM $MgSO_4$, and either 3 µL, 6 µL, 7.5 µL, or 12 µL of 10 mg/mL MscL were combined in a tube to yield protein-to-lipid ratios (w/w) of 1:1.5, 1:1, 1.5:1, 2:1, 3:1, and 5:1 respectively. PD1 buffer (pH 7.4 or 7.0) was added to a final volume of 30 µL. The solution was incubated on a rocker at room temperature for 30 min. The solution was then transferred to a new tube containing either 1 or 1.5 mg of Biobeads, and incubated on a rocker at room temperature for 1 h. The solution was then transferred to another tube containing another 1.5 mg of Biobeads, and further incubated on a rocker at room temperature for 3 h. For solutions undergoing freeze-thaw cycles, these were transferred to new tubes and flash-frozen in liquid nitrogen, followed by thawing at room temperature, and repeating three times. The samples were incubated for 12 h to facilitate crystallisation.

The samples were negatively stained on a mesh grid as described in section 3.2.3.2., and was analysed using a JEOL 1011 coupled to Morada CCD imaging system or Tecnai-12 (FEI, U.S.A.) coupled to FEI Eagle 4K x 4K CCD Imaging System (FEI). Images were recorded at a high-tension voltage of 100 keV and at magnifications of 5,000x, 25,000x, 50,000x, 80,000x and 100,000x.

4.2.1.2. 2D Crystallisation Assisted by Ni-NTA-coupled Phospholipid

This method was based on the protocol by Hussein *et al.* (2009) and Lévy *et al.* (1999).

40 µL of PBS (phosphate buffered saline) was placed in each well of a 12-well Teflon plate. 0.5 µL of chloroform solution containing 0.1 mg/mL Ni-NTA-DLPC and 4.9 mg/mL DOPC, or 1 mg/mL Ni-NTA-DLPC and 4 mg/mL DOPC were mixed and added to the top of the aqueous buffer reservoir. The chloroform was then left to evaporate at room temperature for 2 h. 5 µL of a 5 mg/mL liposome solution and 5 µL of 5 mg/mL MscL were combined and then added to the solution via a side port so as not to disturb the monolayer. The plate was incubated at room temperature for 30 min. 5 mg of Biobeads were added to the solution via the side port for each well for detergent removal, and the plate was further incubated at room temperature for 6 h to facilitate detergent depletion.

A glow-discharged 400-mesh copper grid (Electron Microscopy Sciences) was gently placed onto the solution, and then taken out after 15 s. It was blotted and negatively stained as described in

section 3.2.3.2., and analysed with JEOL 1011 coupled to Morada CCD imaging system. Images were recorded at high-tension voltage of 100 keV and at magnifications of 5,000x, 25,000x, 50,000x, and 100,000x.

4.2.2. 3D Crystallisation

4.2.2.1. Initial (Broad) Screen of MscL Crystallisation Conditions

Five commercial crystallisation screens were selected based on the properties of MscL (i.e. it being a membrane protein with a pI of 6.1). Specifically PEGRx1, PEGRx2, PEG/Ion, and PEG/Ion2 screens from Hampton Research (U.S.A.), and Clear Strategy™, Clear Strategy2™, MemGold2™, and MemSys™ screens from Molecular Dimensions (United Kingdom) were used.

A 96-well flat-bottom vapour diffusion plate (Hampton Research) containing the precipitants, a Viewdrop 96-well plate seal (TTP Labtech, United Kingdom), and 10 µL of 10 mg/mL His-MscL^{L-7Y} in PBS with 0.5 mM β-DDM were placed on a Mosquito® Crystal (TTP Labtech) system, and the crystallisation set up was performed with the hanging drops containing protein sample and precipitant at 1:1 (v/v) ratio. The sealed plated was placed in a Rock Imager (Formulatrix, U.S.A.) for a six-hour period of monitoring for eight days at 16 ℃.

Crystallisation progress was checked every day, and wells which appeared to contain crystals or relatively well-defined spherulites were identified and the crystallisation conditions recorded for further investigation.

4.2.2.2. Optimisation of MscL Crystallisation Conditions

2x stock solutions of the precipitant were placed into 200 µL aliquots. To change the pH of the precipitants, 2 M HCl, 2 M NaOH or 2 M KOH was added to the aliquots to create a range of pH screens with 0.2 increment. Precipitant concentration was controlled by diluting the aliquots with different volumes of water for 10% increment.

For the hanging drop method, 200 µL of the prepared precipitant solutions were placed in each reservoir well of 24-well hanging drop plate (Hampton Research). 2 µL of 10 mg/mL His-MscL^{L-7Y} was placed on one side of cover slip and 1 µL of the protein solution was placed on the other side, and 1 µL of the precipitant solution was added to each drop. The cover slips were quickly inverted and sealed onto the wells matching the precipitant solutions. The plates were stored at 4 ℃ until there was visible crystal growth or up to a maximum of two weeks.

For the sitting drop method, the protocol for the hanging drop method was largely repeated but using a 24-well sitting drop plate (Hampton Research). However, in this case 2 µL of protein

solutions were placed on the upper well instead of onto the cover slip. 10 µL of silicon oil was also added to some of the wells to control the rate of vapour diffusion.

For the microbatch method, 200 µL of either paraffin oil, Al's oil or a 1:1 (v/v) mix of both was added to each well of 96-well PCR plate (Thermo-Fisher). 2µL of 10 mg/mL His-MscL^{L-7Y} was mixed with either 1 µL or 2 µL of precipitant solution, and it was carefully placed at the bottom of each well (Chayen *et al.*, 1992). The plate was left on the bench for 10 min for the drop to adhere to the bottom of the well, and moved to a crystallisation bay for incubation at either 4 ℃ or room temperature until there was visible crystal growth, or up to two weeks.

20 µL of precipitant was gently added to the drop containing crystals. The solution was gently aspirated with a pipette. For this, the tip was cut to increase the diameter of the entrance and to minimise damage to the crystals. The solution was then mixed with 20 µL of precipitant and incubated for 10 s. Crystals were picked mount onto CryoLoops^{TM} (Hampton Research) and transferred to 20 µL of precipitant containing 10 % ethylene glycol as cryoprotectant, and incubated for 1 min. The crystals were mounted on CryoLoops again and were flash-frozen in liquid nitrogen. The crystals were analysed with the FR-E Superbright X-ray generator (Rigaku, Japan) coupled to Saturn 944 CCD area detector (Rigaku).

4.2.2.3. Preparation of Crystals for SDS-PAGE

Two frozen crystals were thawed and placed in 3 µL of water. 12 µL of 8M urea was added to the crystal solution to solubilise the crystals. This was followed by the addition of 5 µL of protein loading dye (50 mM Tris pH 6.8, 200 mM NaCl, 50 mM EDTA, 1 % SDS, 30 % glycerol (v/v)). The sample was run on SDS-PAGE and silver staining was performed as described in section 3.2.6.

4.3. Results/Discussion

4.3.1. 2D Crystallisation

For crystal screening of MscL, a broad incomplete factorial screen was conducted to cover a wide range of variables including phospholipid types, protein-to-lipid (P:L) ratio, rate of detergent removal, freeze-thaw process, pH, and the crystallisation method. This incomplete factorial-based approach (Fig. 4.2) was designed to identify promising ranges of conditions for more detailed investigation using a full factorial design (Page *et al.*, 2003). This is a favoured experimental design for 2D crystallisation than the more comprehensive, full factorial analysis, or a shotgun screen approach (Page *et al.*, 2003), while sacrificing minimal sampling space.

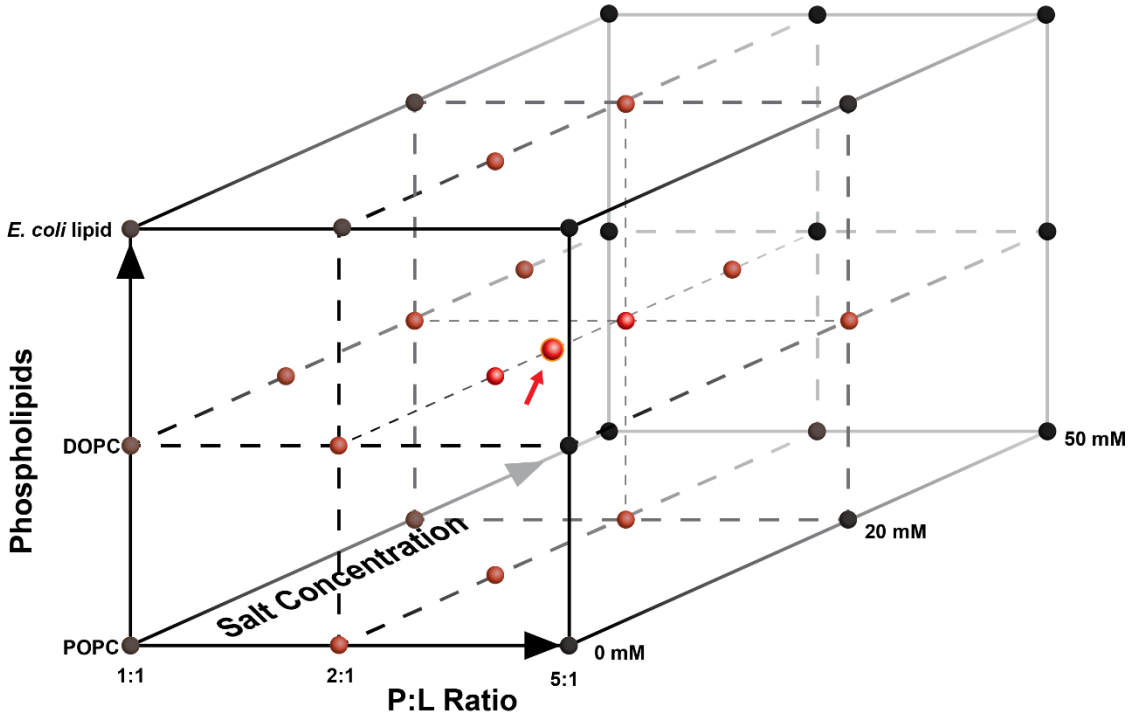

Figure 4.2. Schematic diagram of sparse/incomplete factorial approach to screen 2D crystallisation of MscL. Three of the screened factors (phospholipids, P:L ratio, and inorganic salt concentration) are featured. The quality of screened conditions, represented as spheres on the matrix, can be ranked (black – poor quality; red – high quality) to identify the best crystallisation environment (red arrow).

Such a multi-dimensional factorial screen relies on the use of one condition for evaluating multiple variables simultaneously. For example, one sample (MscL/*E. coli* lipid, 2:1 P:L ratio; 0 mM inorganic salt; 3 mg Biobeads used; no freeze-thaw; pH 7.5) was used to study the influence of both the rate of detergent removal and inorganic salt concentration (Fig. 4.6C, 4.7A). While this is advantageous for 2D crystallisation screens, which are often resource-intensive, it also means some micrographs had to be featured multiple times in this chapter.

4.3.1.1. The Influence of Phospholipid Types on 2D Crystallisation

The significance of phospholipids on MscL incorporation into lipid bilayers and potentially crystallisation was explored in this experiment first. Specifically, MscL and each of four phospholipids commonly used in 2D crystallography (POPC, DMPC, DOPC, and *E. coli* lipid) were mixed at the ratio (P:L ratio) of 1:1 (w/w) and the resultant proteoliposomes were compared to negative phospholipid controls. All four phospholipids changed morphologies with the addition of MscL, suggesting efficient MscL incorporation (Fig. 4.3). However, there were differences between them in detail.

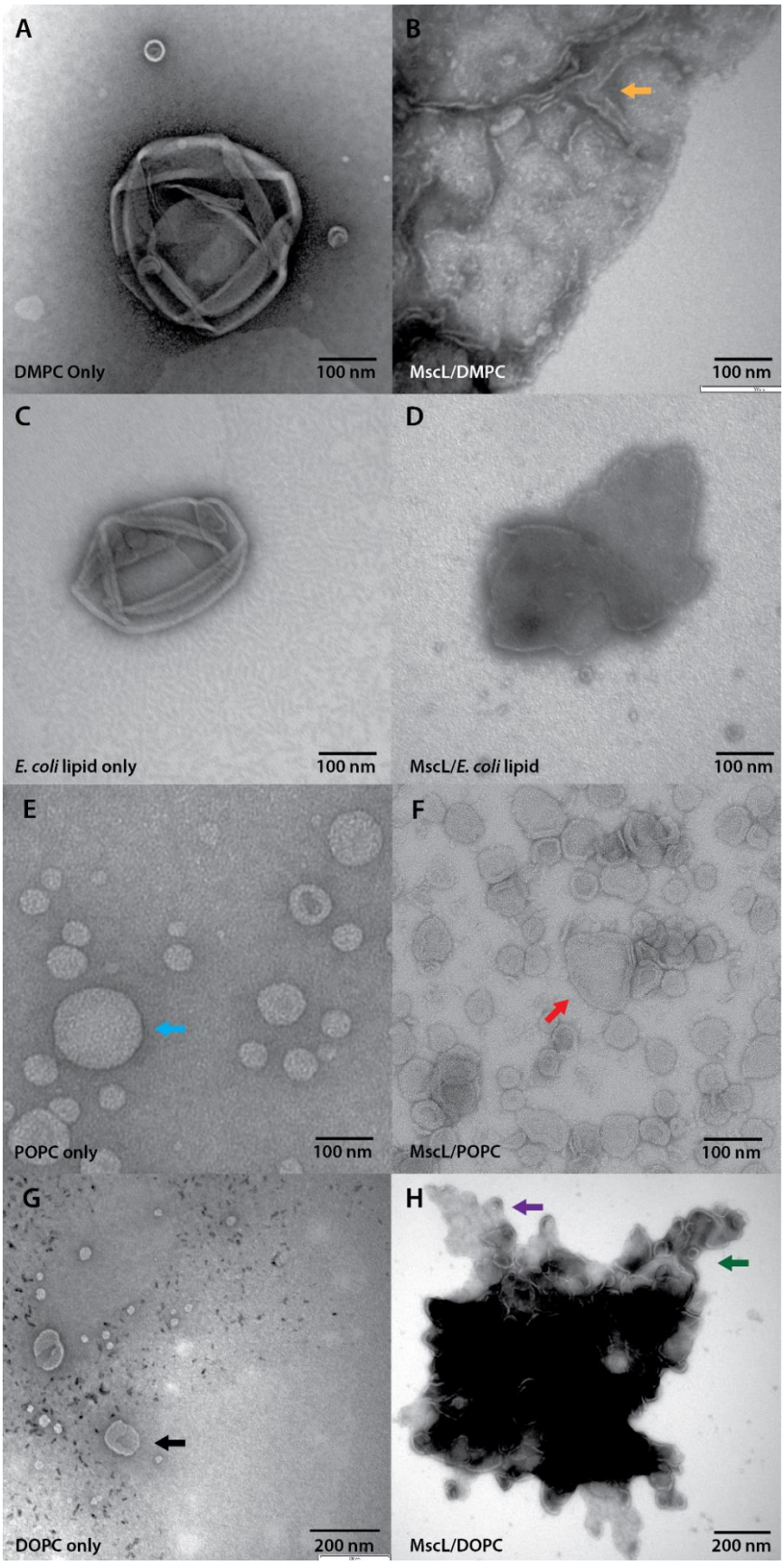

Figure 4.3. Electron micrographs of 2D crystallisation trials of MscL. Left column – lipid-only control samples; Right column – MscL/lipid samples (P:L = 1:1, 0 mM inorganic salt, 3 mg Biobeads, no freeze-thaw, pH 7.5). **B**) orange arrow – curved edge of the membrane; **E**) blue arrow – POPC vesicle; **F**) red arrow – small flat membrane with curved edge; **G**) black arrow – lysed DOPC vesicle; **H**) purple arrow – small flat membrane; green arrow – small flat membrane with curved edge

The negative controls for DMPC (PC 14:0/14:0) and *E. coli* lipid are shown in Figures 4.3A and 4.3C. Typically in these sample the vesicles had highly variable diameters of 20 nm to over 500 nm. On the other hand, in the negative control for POPC (PC 16:0/18:1, Fig. 4.3E), the vesicles were generally smaller and more consistent with diameters of 50 – 200 nm, and in the case of DOPC (PC 18:1/18:1, Fig. 4.3G), most vesicles were ~50 nm in diameter although a few vesicles with approximately 200 nm diameters could be seen. The larger liposome size of DMPC compared to smaller sizes for POPC and DOPC might be related to their lipid packing properties (Alberts *et al.*, 2003; Lasala *et al.*, 2015), where DMPC is a "cylindrical" phospholipid (i.e. curvature-neutral) preferring flatter membrane geometry, while DOPC and POPC have "inverted cone" shapes (i.e. negatively curvature-inducing) favouring curvature in general (Shearman *et al.*, 2006; Shinoda & Klein Michael, 2014; Vanni *et al.*, 2014).

With the addition of MscL, the MscL/DMPC samples formed sheet-like structures with high levels of curvature along the edges (Fig. 4.3B, orange arrow). MscL/*E. coli* lipid and MscL/DOPC membranes formed flatter bilayers with highly variable diameters from ~100 nm to over a few µm (Fig. 4.3D, H). This was in contrast to the intrinsic lipid packing properties of the phospholipids. This suggests that the transmembrane domain of MscL was counteracting DOPC's negative curvature-inducing properties, possibly by accommodating the unsaturated fatty acyl chains (Bavi, Vossoughi, *et al.*, 2016), whereas hydrophobic mismatch between MscL and DMPC (Bavi, Vossoughi, *et al.*, 2016) and curvature-inducing properties of the protein itself would have led to the membrane favouring curvature at certain points.

Since *E. coli* lipid (Fig. 4.3D) and DOPC (Fig. 4.3H) formed reasonably flat membranes upon incorporation of MscL, they were considered a sensible starting point for 2D crystallisation. While there were flat membrane structures present in the MscL/POPC sample as well (Fig. 4.3F), their low prevalence suggested relatively poor rates of incorporation. This is consistent with the result in section 3.3.3. (Fig. 3.21), where MscL (visualised by Ni-NTA-Nanogold) did not appear to incorporate well into POPC liposomes. The heterogeneous membrane morphology conditions (flat and highly curved areas) of MscL/DMPC membrane also made 2D crystallisation less possible in such a phospholipid bilayer. In addition to this experiment, it was reported that the majority of 2D crystallisation of alpha-helical membrane proteins – which MscL also belongs to – were successful with DOPC, POPC, and *E. coli* lipids (DMPC was favoured by beta-barrel proteins, which MscL does not belong to), making DOPC and *E. coli* lipid ideal phospholipids of choice for subsequent experiments.

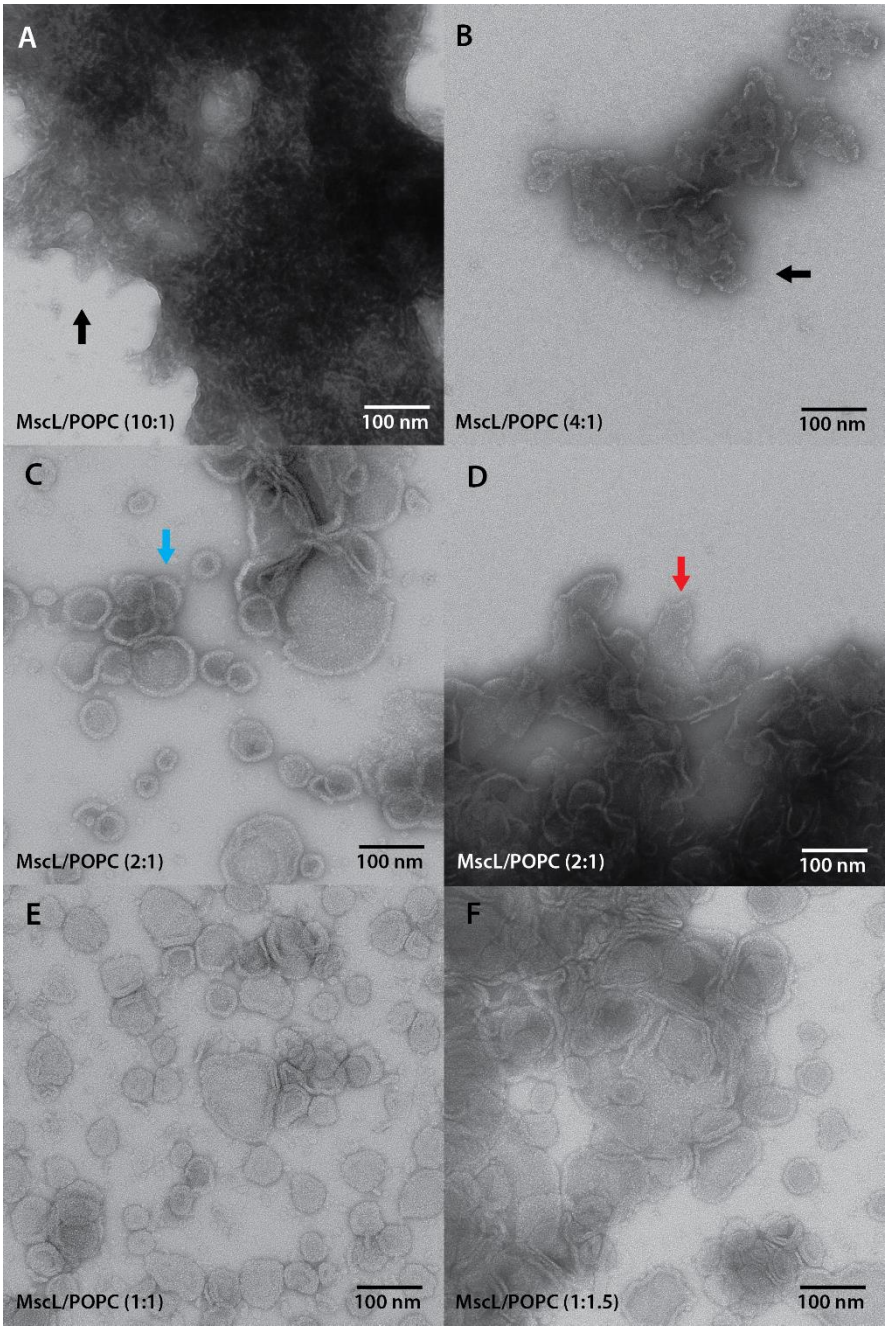

Figure 4.4. Electron micrographs of 2D crystallisation trials of MscL in POPC membrane with various P:L ratios (0 mM inorganic salt, 3 mg Biobeads, no freeze-thaw, pH 7.5). **A/B**) black arrow – small membranes with rough edges typically indicate insufficient phospholipids for continuous membrane formation; **C**) blue arrow – membrane in liposomal morphology; **D**) red arrow – membrane in flat surface morphology

4.3.1.2. The Influence of Protein to Lipid Ratio on 2D Crystallisation

With both MscL/DOPC and MscL/POPC samples, there was an approximate inverse correlation between the P:L ratio and the size of membrane structures. Samples with a higher P:L tended to exhibit smaller structures. This was especially noticeable in the MscL/POPC samples, for which P:L ratios of 10:1, 4:1, 2:1, 1:1, and 1:1.5 were trialled (Fig. 4.4A-D). The 10:1 and 4:1 samples appeared to contain fragments of sheets/vesicles with exposed edges which suggested insufficient

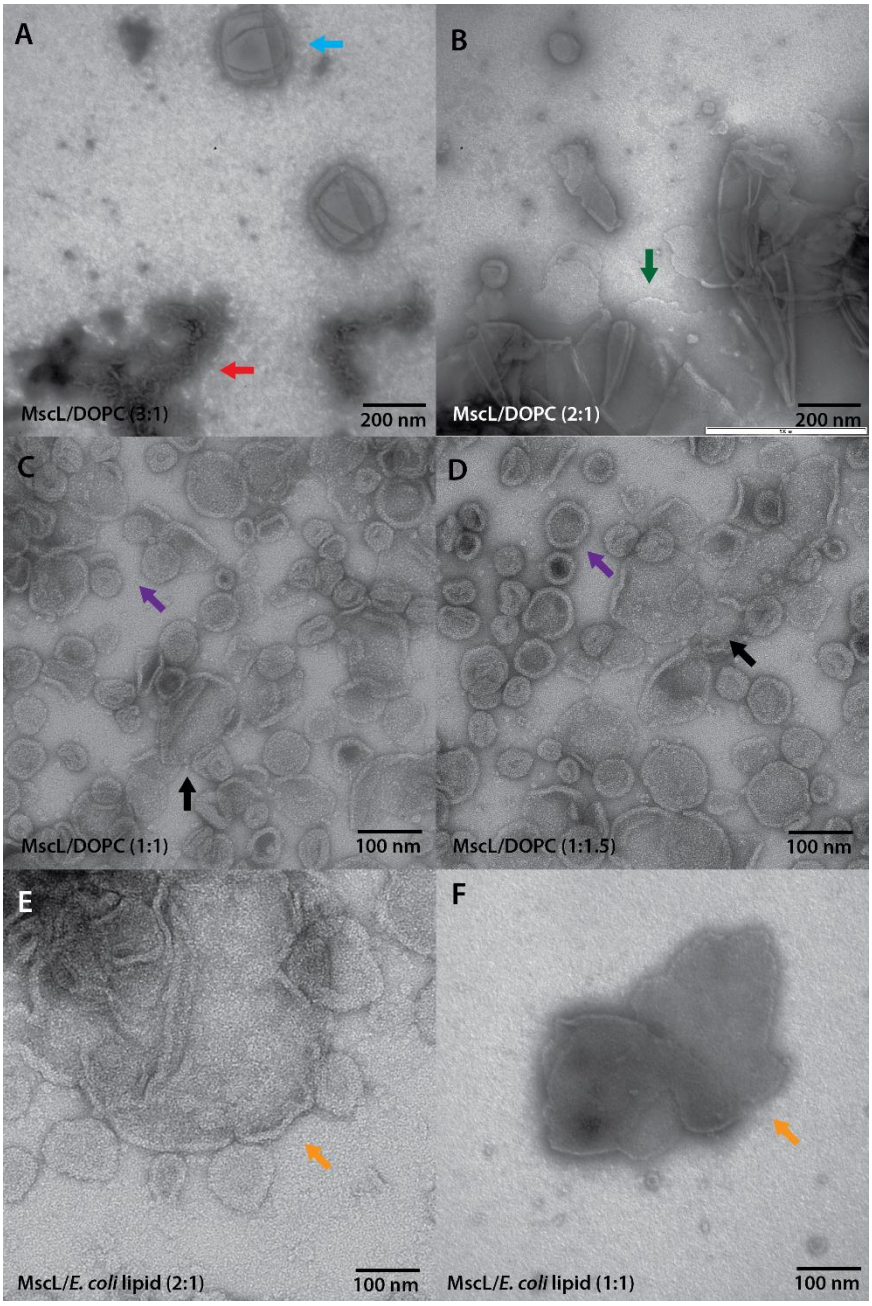

Figure 4.5. Electron micrographs of MscL reconstituted with DOPC (**A-D**) and *E. coli* lipid (**E, F**) lipids. The denoted P:L ratios were used in the presence of [3 mg Biobeads, no freeze-thaw, PBS pH 7.5]. **A**) blue indicates vesicular membranes; the red arrow – MscL aggregate; **B**) green arrow – flat sheet; **C/D**) – purple arrow – vesicular membrane, black arrow – small flat surface membrane with partially curved edges; **E/F**) orange arrow – flat surface membrane with partially curved edges

phospholipid to form continuous membrane (Fig. 4.4A, B). Although this can also be caused by incomplete detergent removal, it was noted that lower P:L ratios yielded complete vesicles, suggesting detergent removal was likely complete. At the 2:1 (P:L) ratio, both small protein packed vesicles (Fig. 4.4C) and flat bilayer regions similar to those in the higher P:L ratio samples but larger in size (Fig. 4.4D) were observed. This suggested that there was enough phospholipid to form continuous membranes but not so much that all membranes would form vesicles. At lower P:L ratios of 1:1 and 1:1.5, most membranes formed vesicles (Fig. 4.4E, F).

A similar trend was observed for MscL/DOPC samples (Fig. 4.5A-D), but with a key difference to the MscL/POPC trials. At the P:L ratio of 3:1 (Fig. 4.5A), liposomes with smooth surfaces and protein aggregates were observed, suggesting that MscL did not incorporate into the membrane. In the sample with 2:1 (P:L) ratio, flat membranes larger than 200 nm in width were regularly observed, often aggregated and/or folded (Fig. 4.5B). At lower P:L ratios of 1:1 and 1:1.5, vesicles dominated the samples, although there were still significant fractions

of flat membranes of approximately 100 nm in size (Fig. 4.5C, D). From these results, it was decided that 2:1 was the highest P:L ratio that could be used without negatively affecting the membrane morphology. This was also supported by the previous experiments of Saint *et al.*, who reported MscL crystals obtained in the 2:1 MscL:DOPC ratio environment (Saint *et al.*, 1998).

A narrower range of P:L ratios was trialled for MscL/*E. coli* lipid samples, and a slightly different pattern was observed. Both flat membranes and liposomes were observed in both 2:1 and 1:1 (P:L) samples (Fig. 4.5E, F). This suggested that a higher P:L ratio could be used with MscL/*E. coli* lipid, however for consistency most MscL/*E. coli* lipid samples were prepared with 2:1 P:L ratio.

4.3.1.3. The Influence of Detergent Types and Rate of Removal on 2D Crystallisation

Both the type of detergent and its rate of removal can significantly affect MscL stability and its reconstitution into a lipid bilayer, as well as crystallisation kinetics and potentially crystal size and morphology. To analyse the role of detergents in these respects, β-DDM and Triton X-100 were chosen as the detergents. The starting concentrations were 0.3 mM for β-DDM and 0.7 mM for Triton X-100, which were approximately 2.5-3 times their critical micellar concentrations (~0.12 mM for β-DDM and ~0.24 mM for Triton X-100). To induce crystallisation, the Biobeads were added to the MscL/phospholipid samples to induce detergent removal. As detergent adsorption by Biobeads is proportional to the total surface area of the Biobeads, the rate of detergent removal from the solution can be decreased simply by reducing the amount of Biobeads added from 2 x 1.5 mg to 2 x 1.0 mg (Lambert *et al.*, 1998). Since Biobeads have 7 % adsorption capacity (i.e. 1 mg Biobeads can adsorb 0.07 mg detergent), 2 mg of Biobeads are theoretically able to remove up to 0.14 mg of β-DDM, which was far in excess of the nominal β-DDM mass in each solution (0.005 mg).

As expected given that Biobeads were added in excess, little noticeable difference between the two treatments was observed in the case of the MscL/*E. coli* samples (Fig. 4.6C, D). In contrast, in the case of MscL/DOPC samples, lowering the amount of added Biobeads had a significant effect on the membrane morphology (Fig. 4.6B). Large flat sheets of several μm in diameter were dominant in the sample treated with 2 mg Biobeads, and the fusion of small liposomes with flat membranes

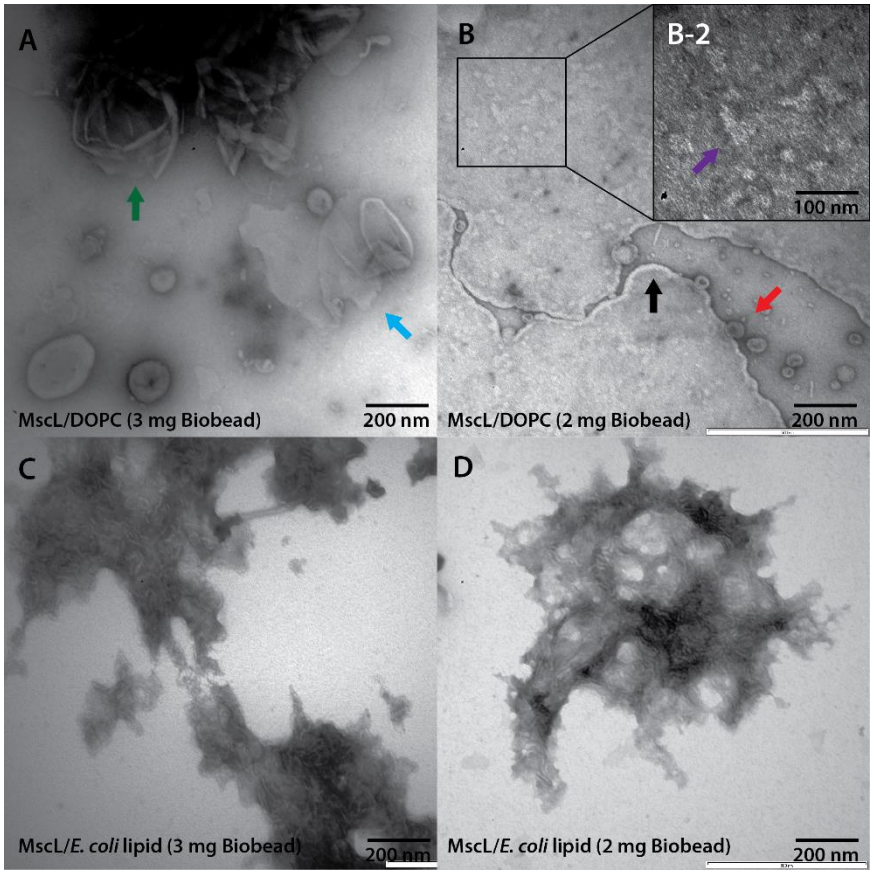

Figure 4.6. Electron micrographs of 2D crystallisation trials of MscL in DOPC (**A, B**) and *E. coli* lipid (**C, D**) membranes with variations in the amount of Biobeads added (2:1 P:L ratio, 0 mM inorganic salt, no freeze-thaw, pH 7.5). **A**) blue arrow – flat surface membrane, green arrow – vesicular membrane; **B**) red arrow – small liposomes fusing to large flat surface membrane, black arrow – round edge of the flat surface membrane; **B-2**) further 2x magnification of a section of the micrograph. Purple arrow – light-staining patch hypothesised to be MscL aggregating in membrane

was observed. There were also lightly-stained patches of 20 – 100 nm in size in the membrane (Fig. 4.6B-2), which might be MscL complexes aggregating in the membrane. These results were encouraging as the starting point for 2D crystallisation of MscL. However, the MscL density in the membrane (based on the relative area of the light-staining patches in the membrane) appeared to be too low to induce crystal formation, suggesting that, for this condition in particular, the P:L ratio could be increased (i.e. less phospholipid in sample). In addition, the membranes often had lightly stained round edges, which could be either a band of MscL along the peripheries of the membrane or residual β-DDM stabilising the edge.

Two starting β-DDM concentrations were trialled to investigate its effect on membrane formation. General destabilisation of the lipid bilayer with detergent has the potential to increase the rate of MscL incorporation into the membrane (A. Foo *et al.*, 2015; Kocer *et al.*, 2007; van den Bogaart *et al.*, 2007), making it a potentially important factor in 2D crystallisation. Therefore, an experiment was conducted in which the starting β-DDM concentration of the solution prior to Biobead addition

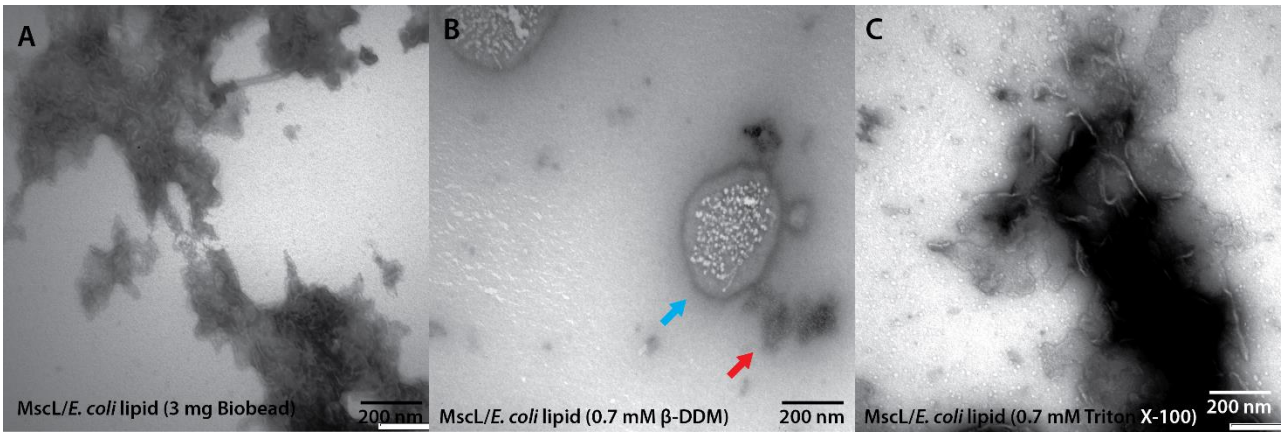

Figure 4.7. Electron micrographs of 2D crystallisation trials of MscL/*E. coli* lipid (2:1 P:L ratio, 3 mg Biobeads, no freeze-thaw, PBS pH 7.5). **A**) Reference sample where the starting β-DDM concentration was 0.3 mM, which was removed with Biobeads. **B**) The starting β-DDM concentration was 0.7 mM, which was removed with Biobeads. Blue arrow – large lipid aggregate, red arrow – MscL aggregate; **C**) 0.7 mM Triton X-100 was used throughout MscL purification instead of β-DDM.

was around twice (0.7 mM) that of the standard protocol (0.3 mM). Interestingly, this had a negative effect on the membrane formation instead, with the lipid and MscL aggregating separately (Fig. 4.7B). This was unlikely to be due to solubilisation of the phospholipids, since 0.7 mM β-DDM is still lower than the concentrations commonly used in biophysics studies (A. Foo *et al.*, 2015; Kocer *et al.*, 2007). A likely explanation is that the interaction between MscL and the phospholipid components is dependent on their molecular ratio. P:L ratios used in biophysics experiments generally do not exceed 1:100 (Anishkin *et al.*, 2005; A. R. Battle *et al.*, 2009; A. Foo *et al.*, 2015; Grage *et al.*, 2011; Kocer *et al.*, 2007; Yilmaz *et al.*, 2015), so MscL reconstitution would occur as MscL/detergent micelles incorporating into already formed large lipid bilayers (A. R. Battle *et al.*, 2009). In the 2D crystallisation trials, however, the mechanism of membrane formation is likely different due to the high concentration of MscL relative to lipids, as was observed in the P:L screen in section 4.3.1.2. (Fig. 4.4, 4.5). Therefore, it is possible that a higher detergent concentration would have interfered with membrane formation instead of assisting with it.

Replacing β-DDM with Triton X-100 as the detergent for MscL purification and 2D crystallisation did not lead to significant changes in the membrane morphology (Fig. 4.7C). This indicated that at least in the case of these two detergents their exchange had little influence on the size or shape of the MscL/lipid membranes formed under the conditions tested.

4.3.1.4. The Influence of Inorganic Ions on 2D Crystallisation

Counterions have a very significant effect both on the incorporation of membrane proteins into lipid bilayers and the formation of ordered 2D crystals. Consequently the influence of ion type and concentration on the size of the proteoliposomes was analysed next. To initiate this process

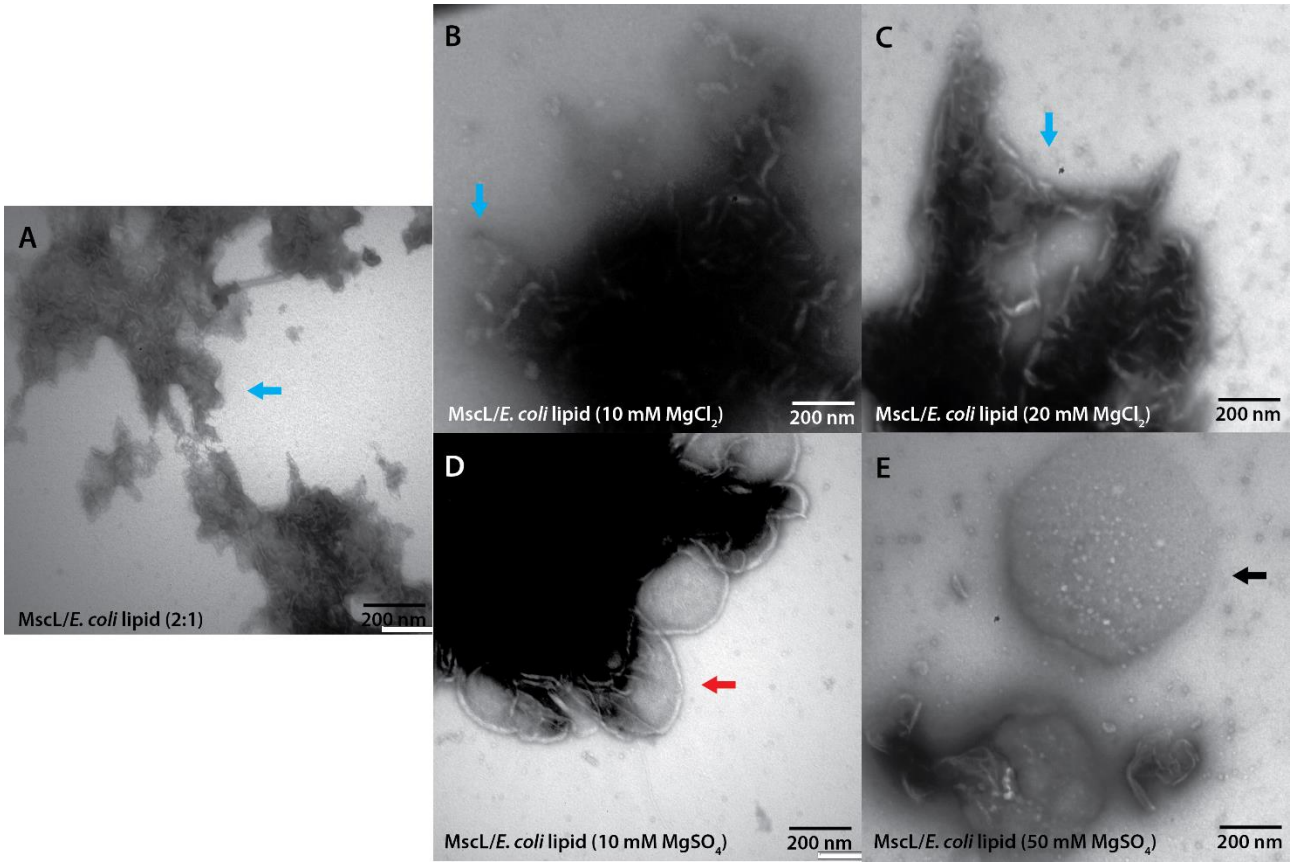

Figure 4.8. Electron micrographs of 2D crystallisation trials of MscL in *E. coli* lipid membrane with variations in the type and concentration of added inorganic salt in solution (2:1 P:L ratio, no freeze-thaw, pH 7.5). **A/B/C**) small flat membrane with partially curved edges; **D**) black arrow – larger membrane with better defined edges; **E**) black arrow – large lipid aggregate

MscL/*E. coli* lipid samples were supplemented with $MgCl_2$ (0 mM, 10 mM, and 20 mM) during reconstitution to measure the effect of divalent cations. No significant difference was observed, with the size and shape of the membrane remaining similar (Fig. 4.8A-C). In contrast, 10 mM $MgSO_4$ addition yielded larger MscL/*E. coli* lipid membranes (Fig. 4.8D), as well as aggregated lipid structures of over 500 nm in diameter with 50 mM $MgSO_4$ (Fig. 4.8E). The effect of $MgSO_4$ on MscL/DOPC was even more pronounced, with the 10 mM $MgSO_4$ treatment leading to large flat membrane formation (Fig. 4.9B) and 20 mM $MgSO_4$ inducing general lipid aggregation (Fig. 4.9C).

These results indicate that the fusion of membranes in this trial was largely induced by the anions ($SO4^{2-}$ in particular) (Baldwin, 1996; Z. Yang, 2009) rather than by cation-mediated electrostatic attraction (Mg^{2+}) (Akashi *et al.*, 1998; Bentz & Duzgunes, 1985; Ruso *et al.*, 2003). In general, divalent cations are believed to assist with 2D crystallisation by attracting net negatively charged surface of membranes and/or proteins, which would otherwise repel each other due to the electrostatic repulsion (Akashi *et al.*, 1998; Bentz & Duzgunes, 1985; Ruso *et al.*, 2003). This attraction could in turn induce the membrane fusion, which is favourable for large 2D crystal

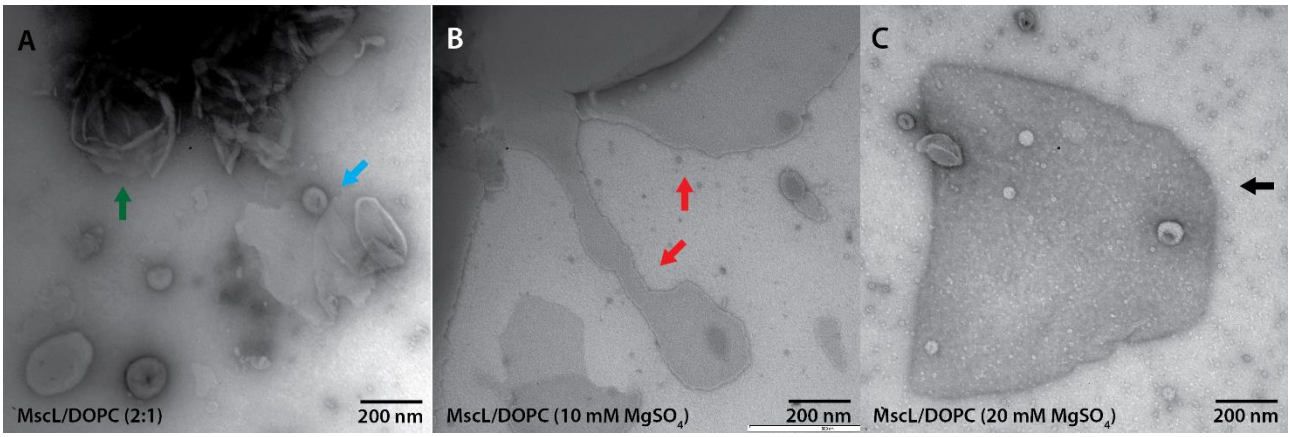

Figure 4.9. Electron micrographs of 2D crystallisation trials of MscL in DOPC membrane with variations in the concentration of added $MgSO_4$ in solution (2:1 P:L ratio, 3 mg Biobeads, no freeze-thaw, pH 7.5). **A**) green arrow – vesicular membrane, blue arrow – flat surface membrane; **B**) red arrows – large flat surface membrane, the elongated shape of the lower membrane suggests that the membrane's edge is stable; **C**) black arrow – large lipid aggregate

formation (Brent L. Nannenga *et al.*, 2013). However, many experiments studying this effect used net anionic phospholipids such as phosphatidylserine and phosphatidylglycerol rather than zwitterionic phospholipids used in this experiment (phosphatidylcholine and *E. coli* lipid, which is largely phosphatidylethanolamine) (Akashi *et al.*, 1998; Bentz & Duzgunes, 1985; Ruso *et al.*, 2003). Hence, for this experiment, it is probable that Mg^{2+} did not have significant influence on the membrane morphology.

In contrast, the differential effects of the anions Cl^- and $SO4^{2-}$ suggest that the observed changes may be driven by Hofmeister effect, where anions generally have stronger influence than cations (Z. Yang, 2009), on proteins. The position of ions in the Hofmeister series affects the solubility/aggregation of both proteins (Baldwin, 1996; Salis & Ninham, 2014) and phospholipids (Clarke & Lupfert, 1999; Petrache *et al.*, 2006; Z. Yang, 2009), but the effect of individual ions is more complicated. $SO4^{2-}$ has a higher ionic strength than Cl^- with respect to proteins (Baldwin, 1996; Salis & Ninham, 2014), but it has a weaker strength than Cl^- with respect to liposomes (Clarke & Lupfert, 1999; Petrache *et al.*, 2006). In this trial, $SO4^{2-}$ was shown to induce larger membrane formation (Fig. 4.8D), whereas Cl^- had little influence on the membrane morphology (Fig. 4.8B). This indicates that this was largely driven by the anions affecting MscL. This result is a positive outcome for MscL 2D crystallisation efforts, because 1) it suggests that MscL density in the membrane is high enough to overcome the opposing influence of phospholipids with respect to Hofmeister effect, and 2) this same effect is also thought to be the main driver for inorganic ion-mediated protein crystallisation in general (Majeed *et al.*, 2003). Therefore, 10 mM $MgSO_4$ was determined to be the optimal inorganic salt type and concentration for MscL 2D crystallisation

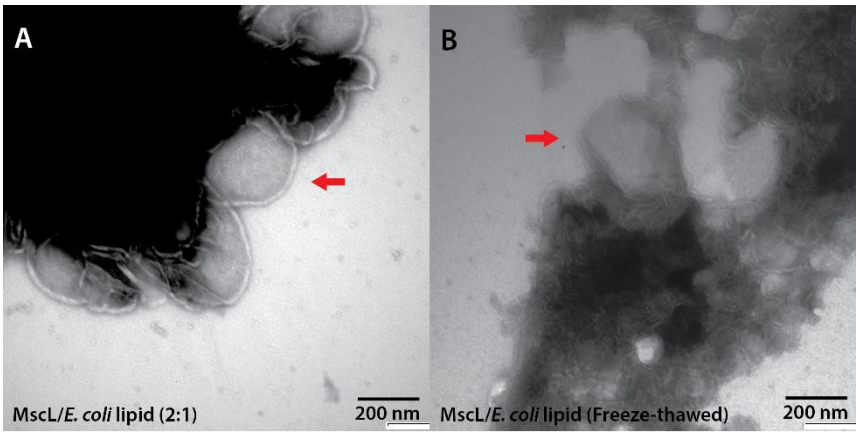

Figure 4.10. Electron micrographs of 2D crystallisation trials of MscL in *E. coli* lipid membrane plus/minus the use of freeze-thaw cycles (2:1 P:L ratio, 10 mM $MgSO_4$, 3 mg Biobeads, pH 7.5). **A/B**) Red arrow – flat membrane with curved edge

experiments, with potential for finer factorial screening around this ion concentration once other conditions have been further optimised.

4.3.1.5. The Influence of Freeze-Thaw Process on 2D Crystallisation

It is reported that, in some instances, the use of freeze-thaw cycles can increase the size of proteoliposomes/membranes, which can in turn assist with 2D crystallisation (Lasala *et al.*, 2015). The freeze-thaw process did not have significant effect on the MscL/*E. coli* lipid membrane morphology (Fig. 4.10). Although the sheet-like structures appeared to aggregate more often in freeze-thawed samples, there was no significant change in the size of the structures.

4.3.1.6. The Influence of pH on 2D Crystallisation

pH appeared to have little influence on the MscL/lipid membrane morphology and crystallisation (Fig. 4.11), although this might be due to the limited range tested (pH 7.0, 7.5). With the exception of synthetic lipids, net neutral phospholipids are generally not sensitive to such a small pH change (Phayre *et al.*, 2002), so it was expected that this would not significantly change the membrane formation. However, MscL has a pI of 6.1, so this experiment aimed to test whether lowering the pH to 7.0 from 7.5 would help induce MscL aggregation in the membrane without precipitating it in solution (observed at pH 6.0). While this parameter does not seem to be a major factor in promoting MscL aggregation/crystallisation, it may still be important in improving crystal quality once an otherwise optimal condition for MscL 2D crystallisation is identified.

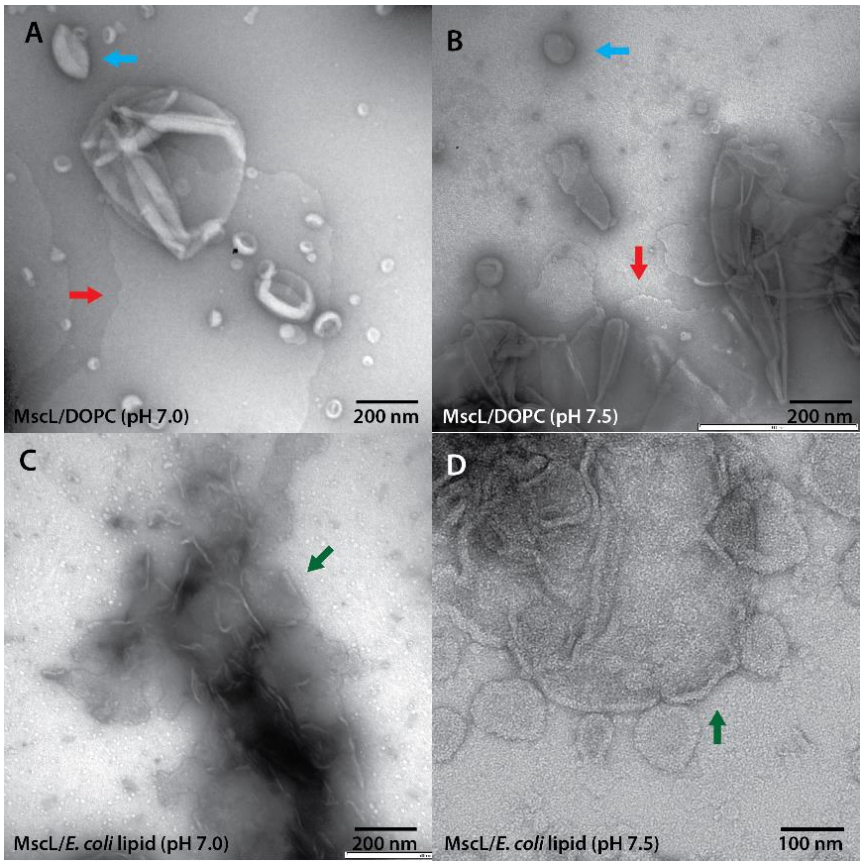

Figure 4.11. Electron micrographs of 2D crystallisation trials of MscL in DOPC (**A, B**) and *E. coli* lipid (**C, D**) membranes with variations in the pH of the solution (2:1 P:L ratio, 10 mM $MgSO_4$, 3 mg Biobeads, no freeze-thaw). **A/B**) Red arrow – flat membrane with sharp edge, blue arrow – vesicular membrane; **C/D**) green arrow – flat membrane with curved edge

4.3.1.7. Monolayer-assisted MscL 2D Crystallisation

2D crystallisation using phospholipid monolayer scaffolds is another method of 2D protein crystallisation related to the traditional method detailed in the previous sections. As it was learned from the previous trials that MscL and phospholipids could form large sheet-like structures, it was hypothesised that repeating this experiment in the presence of a monolayer scaffold might help with achieving high MscL density in the membrane, and that this coupled with aligning MscL molecules in the same orientation would assist with its crystallisation. Since the MscL/DOPC mixture could form large flat membranes with the least membrane curvature in the previous trials, DOPC was selected as the bilayer-forming phospholipid component in this experiment.

Small granular structures of approximately 10 nm in size could be seen in the MscL/β-DDM samples of both high (20 %) and low (2 %) Ni-NTA-DLPC densities in the monolayer (Fig. 4.12A, B). These were unlikely to be nonspecifically bound detergent micelles, since the negative control with only 1 mM β-DDM did not contain similar features (Fig. 4.12F). Instead, they are likely MscL/β-DDM micelles specifically bound to the Ni-NTA head groups of the lipid monolayer. In both samples, darkly stained MscL aggregates of 50 – 100 nm in size could also be seen (Fig. 4.12,

blue arrow), but these could simply be random aggregation of the protein on the scaffold rather than specific clustering of the protein. Additionally for the 2 % Ni-NTA-DLPC sample, the micelles appeared to merge to form larger continuous lightly stained areas throughout the grid (Fig. 4.12A). While such structures were occasionally present in the 20 % Ni-NTA-DLPC sample as well, they

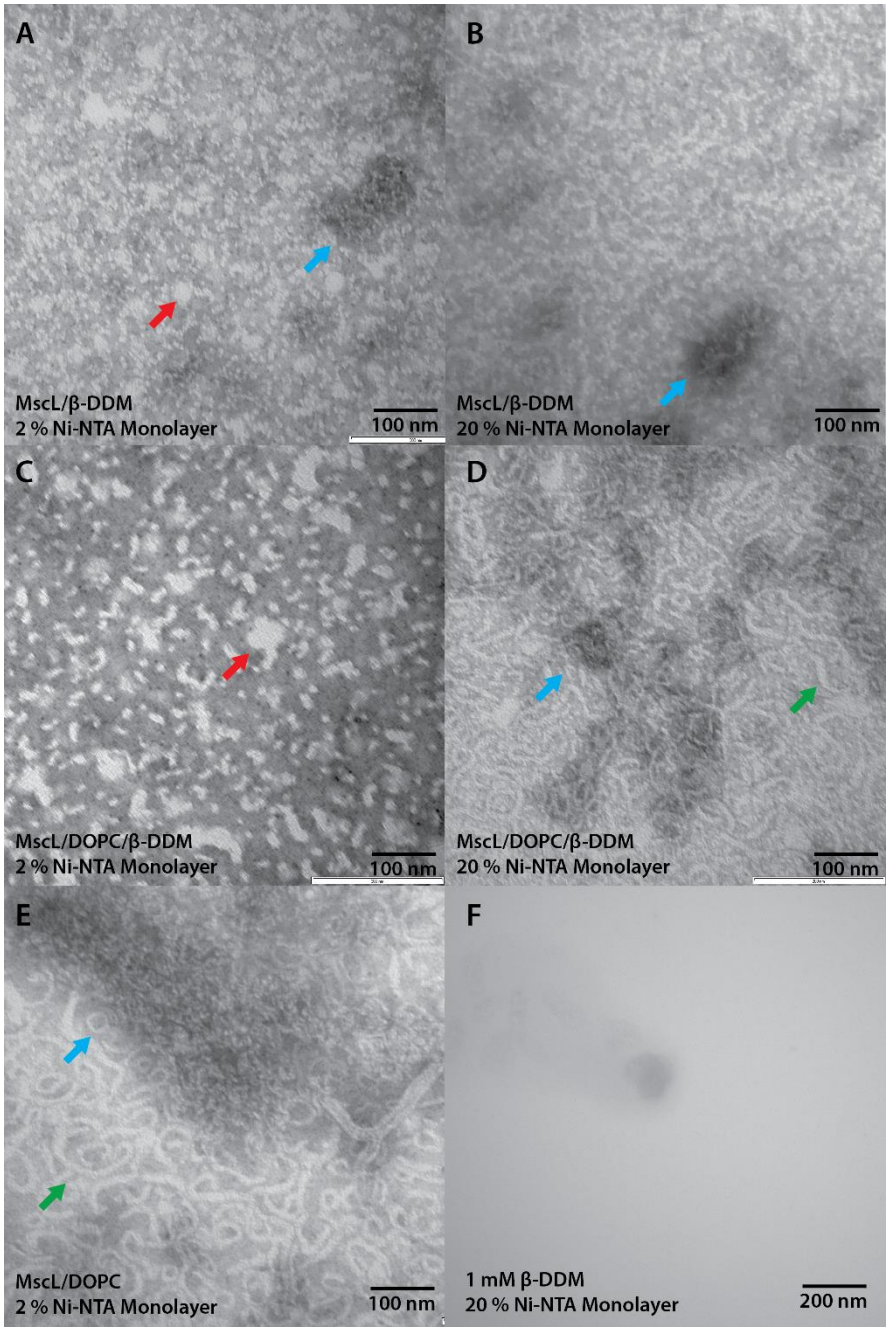

Figure 4.12. Electron micrographs of monolayer-assisted 2D crystallisation trials of MscL. Monolayer containing 2 % Ni-NTA-DLPC (w/w) was used for samples in the left column (**A, C, E**), and monolayer containing 20 % Ni-NTA-DLCP (w/w) was used for samples in the right column (**B, D, F**). **A/B**) MscL in 1 mM β-DDM, **C/D**) MscL in 1 mM β-DDM mixed with DOPC at the P:L ratio of 2:1. **E**) MscL in 1 mM β-DDM mixed with DOPC at the P:L ratio of 2:1, with the further addition of 3 mg Biobeads to each well. Red arrow – Fused MscL/β-DDM micelles; Blue arrow – MscL aggregate; Green arrow – string-like MscL/β-DDM/DOPC membrane. **F**) Negative control with only 1 mM β-DDM in solution.

were relatively rare in comparison and not present in the micrograph presented in this thesis (Fig. 4.12B). The high density of MscL/β-DDM micelles in the 2 % Ni-NTA-DLPC sample (Fig. 4.12A) was somewhat unexpected, since the lower density of Ni-NTA head group should have led to fewer particles binding to the monolayer. This could have been due to 2 % Ni-NTA-DLPC still being a high enough concentration to saturate the monolayer scaffold with MscL, but subsequent experiments showed significant differences between 2 % and 20 % samples, disproving this hypothesis.

The addition of DOPC to the MscL/β-DDM solution had different results for 2 % and 20 % Ni-NTA-DLPC samples. The density of the granular structures decreased, the lightly stained fused membrane/micellar structures became better defined (but not necessarily larger), and MscL aggregates became much less common in the 2 % Ni-NTA-DLPC sample (Fig. 4.12C). In contrast, string-like features largely replaced the granular structures in the 20 % Ni-NTA-DLPC sample (Fig. 4.12D). These might be one-dimensional aggregates (as opposed to 2D arrays) which can represent intermediates of curvature-inducing detergent-solubilised complexes and sheet-forming protein bilayers (Fig. 4.12C, D). These 1D aggregates appear flexible and this may explain MscL's orientation and the degree of freedom on the monolayer surface. MscL aggregates were also commonly present in this sample (Fig. 4.12D, blue arrow), but they were relatively small in size (50 – 100 nm), suggesting that these were random aggregates as well. Such differences in the two samples were in line with expectations, since they reflected the difference in the affinity tag density on the monolayer between them.

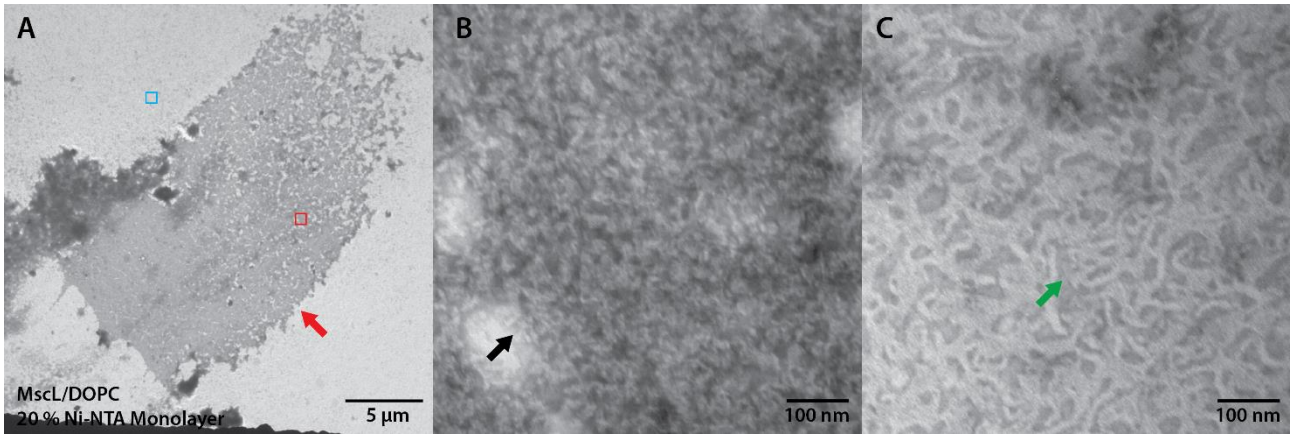

Figure 4.13. Electron micrographs of monolayer-assisted 2D crystallisation trials of MscL in 1 mM β-DDM mixed with DOPC at the P:L ratio of 2:1, with the further addition of 3 mg Biobeads to each well. The monolayer contained 20 % Ni-NTA-DLPC. **A**) Low-magnification image of the sample. The rectangular dark-staining structure (red arrow) is a large MscL aggregate. A section of the aggregate (red square) was further magnified in **B**), which shows unstructured MscL complexes (black arrow). **C**) is the light-staining region (blue square) of (A). Green arrow – fused string-like MscL/DOPC membrane

Removal of β-DDM from the solution with Biobeads had a significant impact on both samples (Fig. 4.12E, Fig. 4.13). String-like MscL/DOPC membranes also appeared in the 2 % Ni-NTA-DLPC sample (Fig. 4.12E), which was similar to the 20 % Ni-NTA-DLPC sample *before* detergent removal (Fig. 4.12D). This observed change suggests that the removal of detergent promoted partial organisation of MscL/DOPC membranes. In addition, large MscL aggregates up to a few µm in size could be seen (Fig. 4.12E, blue arrow). Given the relative lack of small aggregates, this could have been caused by the cluster-inducing effect of DOPC on MscL, which has been documented in Grage *et al.* (2011) as well as in section 3.3.3. of this thesis.

Detergent removal from the 20 % Ni-NTA-DLPC sample led to the formation of very large two-dimensional MscL aggregates (Fig. 4.13A, red arrow). Unlike smaller aggregates, they were well-defined at the global level and remained largely on the two-dimensional plane of the monolayer instead of forming a three-dimensional aggregate, suggesting some sort of order at the global level. However, at the local level, the MscL complexes were randomly oriented and did not form lattice structures (Fig. 4.13B, black arrow), indicating that they were still aggregates, not crystals. Light-staining "holes" were occasionally present in the sheet of MscL aggregate (Fig. 4.13B), indicating the presence of residual detergent (Ujwal & Bowie, 2011). Outside the large aggregate region, the sample was mostly dominated by string-like MscL/DOPC membranes which often fused to form slightly more continuous sheet-like structures (Fig. 4.13C). The failure of the membrane to form proper continuous sheets indicated that there was still a significant concentration of β-DDM in the solution, promoting 1D aggregate morphology and stabilising edges of the membrane. Hence, a strategy to more completely remove the detergent at a slower rate would likely help better organisation of both the MscL complex and the membrane.

4.3.1.8. Discussion

While further progress was hindered by time constraints, the results presented here identify a number of leads for further improvement of 2D crystallisation conditions. MscL/DOPC and MscL/*E. coli* lipid systems with P:L ratio of 2:1 were identified as producing planar membranes most conducive to 2D crystal formation. The addition of 10 mM $MgSO_4$ and slower detergent removal with Biobeads were factors also found to aid with the formation of larger, sheet-like membranes required for 2D crystallography. The experiments also identified factors which might not be critical for crystal formation at this stage of optimisation, such as the use of freeze-thaw cycles, pH, and the type of detergent used. It was also shown from the monolayer-assisted crystallisation trials that MscL was capable of forming nondenaturing 2D aggregates on the membrane, which are often precursors to crystallisation. Consequently these experiments have defined a region of interest within the complex multi-dimensional space analysed, which would

assist future crystallisation experiments.

However, the experiments have also revealed areas requiring further analysis. First, in larger planar membranes the edges were often smooth, suggesting that they were stabilised by the presence of residual detergents. Furthermore this was likely under relatively low local P:L ratio of the membrane as the membranes did not appear protein-packed. While the former possibility can be addressed by the inclusion of an extra Biobead addition step, it is more difficult to solve the latter problem since higher global P:L ratio of the solution would simply lead to reduction in membrane size as shown in Fig. 4.4 and Fig. 4.5. One potential way to overcome this might be through a stepwise addition of the protein component (i.e. MscL solution) so that the extra MscL added in later steps could incorporate into the preformed large membranes, raising its local P:L ratio. P:L ratio is recognised as one of the most important factors in 2D crystallisation (Kuang *et al.*, 2015; Lasala *et al.*, 2015; Lévy *et al.*, 1999; Brent L. Nannenga *et al.*, 2013; Stuart *et al.*, 2004), but strategies to control it, including the stepwise method proposed, are surprisingly sparse in the literature.

Another major challenge is controlling MscL aggregation in a way that will promote crystallisation instead of unstructured clustering as shown in the monolayer studies (Fig. 4.13). The MscL aggregation was likely mediated in two ways: a local over-concentration of MscL to the monolayer interface, and by the fact that it is energetically favourable for MscL to aggregate in DOPC membranes (see section 3.3.3.). The difference in the size of MscL aggregates observed on the 2 % and 20 % Ni-NTA-DLPC monolayers (Fig. 4.12E, 4.13B) suggests the importance of crowding factor, and MscL aggregation in DOPC is well-documented in Grage *et al.* (2011) and in section 3.3.3. While both factors can promote crystallisation under the right conditions (Majeed *et al.*, 2003; McPherson, 2004; Wiener, 2004), the aggregation needs to occur in an orderly progression for MscL to crystallise. One potential solution is to lower the rate of detergent removal, either by reducing the amount of Biobeads added per step (e.g. 6 x 0.5 mg Biobead addition instead of 2 x 1.5 mg) or by removing detergents by microdialysis instead. The reduced prevalence of MscL aggregates in the [MscL/β-DDM/DOPC; 2 % Ni-NTA-DOPC] sample suggests that detergents have a negative effect on MscL clustering. Hence, slower detergent removal may also make MscL aggregation occur at a slower pace, potentially leading to crystallisation.

Alternatively, DOPC-mediated MscL aggregation may be able to be controlled through the addition of other lipids and detergents. Section 3.3.3. showed phosphatidylglycerols (PG) to have a negative influence on MscL aggregation. While high concentrations of PG in the membrane might fully inhibit MscL aggregation (hence crystallisation), at lower concentrations, it may be a useful tool to control the energetic favourability of MscL to aggregate. While PG is by itself not a commonly

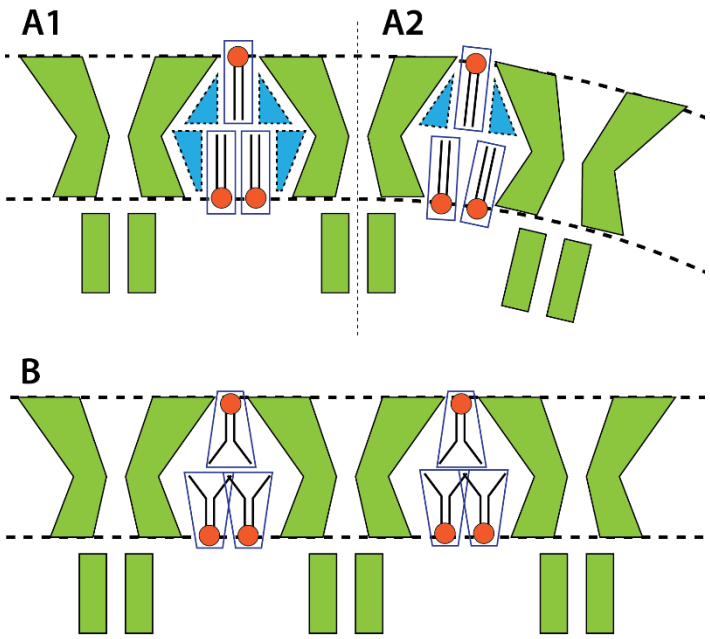

Figure 4.14. Schematic representation of MscL-induced membrane curvature. In MscL/DMPC membrane (**A1, A2**), curved membrane (**A2**) will be favoured to flat membrane (**A1**) due to the smaller void region (shaded in blue). In MscL/DOPC membrane (**B**), however, the negative curvature-inducing effect of DOPC will cancel out the positive curvature-inducing effect of MscL, leading to flat membrane.

used phospholipid for 2D crystallisation, it is one of two major components of *E. coli* lipid (Oursel *et al.*, 2007), a mixture which is commonly used (Lasala *et al.*, 2015), giving credence to this strategy.

Especially with MscL/*E. coli* lipid systems, membrane curvature may need to be controlled for a successful 2D crystallisation. Much of the membranes formed flat sheets, but there were also curved regions especially near the rim of the membranes. While this is apparently not critical to crystallisation since some 2D crystal structures were determined with tubular and vesicular membranes, flat membranes are still preferred this since it tends to yield higher-resolution structures (Lasala *et al.*, 2015). Solutions to this include adding small amounts of detergents such as HTG, which had success improving the quality of 3D Photosystem II crystals (Piano *et al.*, 2010), or phospholipids with specific lipid packing properties.

While the 2D crystallisation experiments are still a work in progress, the trials so far have produced significant results for studying the biophysical relationship between MscL and phospholipids. The most significant was the direct observation of MscL aggregation in DOPC membranes (Fig. 4.12, 4.13B). Section 3.3.3. indirectly visualised MscL clustering on membranes via Ni-NTA-Nanogold, and this experiment confirms the finding by showing MscL aggregation on the 2D plane. The resolution appears to be similar to that visualised by atomic force microscopy (AFM) in Grage et. al. (2011), which reinforces the findings of the study as well.

The second major finding is that MscL can directly influence the membrane curvature and/or stability. DMPC is generally a non-curvature-inducing phospholipid, whereas POPC and DOPC are negatively curvature-inducing phospholipids due to their molecular packing properties. However, in this trial MscL/DMPC membranes showed the highest level of curvature; MscL/POPC membranes had an intermediate level of curvature; and MscL/DOPC membranes showed the least. One of the major differences between DMPC and DOPC which could have affected membrane curvature in the presence of MscL is the hydrophobic mismatch. The length of the fatty acyl chains of DMPC is much shorter (14 carbons) than that of DOPC (18 carbons). This would have led to different levels of hydrophobic mismatch with the hydrophobic interface of MscL's transmembrane domain. The influence of hydrophobic mismatch on MscL channel function has been documented both experimentally and by molecular dynamics simulations (Bavi *et al.*, 2014; A. Foo *et al.*, 2015; Perozo, Kloda, *et al.*, 2002) and it has been correlated with local membrane curvature as well (Bavi, Vossoughi, *et al.*, 2016; Perozo, Kloda, *et al.*, 2002; Phillips *et al.*, 2009), giving further credence to the idea that the hydrophobic mismatch between MscL and the phospholipids could be affecting the observed membrane curvature.

Another difference between DMPC and DOPC which could affect the curvature of MscL/lipid membrane is the packing shape of both MscL and the phospholipids in the membrane. In this explanation, MscL has a positive curvature-inducing effect which can be negated by the negative curvature-inducing effects of DOPC but not by DMPC (which has a neutral curvature-inducing effect) (Fig. 4.14). Both this explanation and hydrophobic mismatch show that MscL can be an active factor influencing membrane curvature rather than merely being affected by it.

This result potentially has the significance of being an experimental observation of a mechanosensitive channel directly influencing membrane curvature. It has been hypothesised based on molecular dynamics studies that MscS can induce local curvature on the membrane (Phillips *et al.*, 2009; Pliotas *et al.*, 2015), but this has not been experimentally verified. Likewise, MscL and membrane curvature are hypothesised to influence each other (Phillips *et al.*, 2009), but most studies have generally focused on only one side of the relationship (i.e. curvature affecting MscL function) (Bavi, Cox, *et al.*, 2016; Bavi *et al.*, 2014; Bavi, Vossoughi, *et al.*, 2016; Tang *et al.*, 2008b). Despite its clear importance in both membrane protein biophysics and 2D crystallography, the relationship between the intrinsic shape of membrane proteins and membrane curvature is relatively little studied (McMahon & Boucrot, 2015; Svetina, 2015) apart from the observation of yeast and bovine ATPases inducing membrane curvature both *in vivo* (Davies *et al.*, 2012) and in attempted 2D crystallisation experiments (Jiko *et al.*, 2015). The experiments performed in this section have shown membrane proteins to be a potentially significant factor in membrane curvature,

and therefore presents an interesting starting point for further investigation into this relationship.

Lastly, the results from this section were also helpful for the design and interpretation of experiments in section 3.3.3. For example, early preparatory trials such as the suitable time for phospholipid sonication performed for this section were largely carried over to those in section 3.3.3., saving considerable time in this regard. One of the potential confounding factors in section 3.3.3. was liposome size influencing MscL clustering (instead of phospholipid composition). This could be addressed by adding 10 mM $MgSO_4$ to the samples (to make the liposomes larger in general), which are findings from this section. In addition, the observation of MscL clusters in the monolayer studies was a confirmation of the MscL clustering observed in DOPC liposomes seen in section 3.3.3., and it also supported the explanation that MscL clusters localising to the edges of liposomes was an artefact of the negative staining process (as opposed to being of biophysical relevance). Conversely, the improved understanding of MscL/phospholipid relationship from studies in section 3.3.3. will also be useful in guiding the future optimisation trials for 2D crystallography of MscL.

4.3.2. 3D Crystallisation

3D protein crystallisation is the most commonly used method to determine protein structure, and has been used to determine the structures of *M. tuberculosis*, *S. aureus*, and *M. acetivorans* MscL. While this had not been successful with *E. coli* MscL at the start of this project, it was considered as a potential approach to use in this thesis.

With the failure to cleave the linker region of $MscL^{TEVc}$ construct with both TEV protease and thrombin, it seemed likely that the linker region formed a structure partially embedded in the solubilising detergent micelle instead of being an unstructured strand located in solution. It was hypothesised from this observation that the linker region could aid with 3D crystallisation by 1) providing a more rigid and consistent structure to the micelles, which often sterically hinder crystallisation (Ghosh *et al.*, 2015); and 2) the soluble component of the linker region increasing the overall size of solution-facing surface. Increasing the soluble domain to aid with membrane protein crystallisation is commonly practiced with GPCR (Ghosh *et al.*, 2015). It has also been used to produce crystals of *M. acetivorans* MscL/riboflavin synthase fusion protein, where the latter is thought to have enabled crystallisation by significantly increasing the hydrophilic surface of the protein (J. Li *et al.*, 2015). Therefore, a crystallisation strategy where the full MscL construct with the linker region not cleaved was adopted.

Commercial broad screen conditions were chosen with the assistance of Dr. Suzanne Norwood

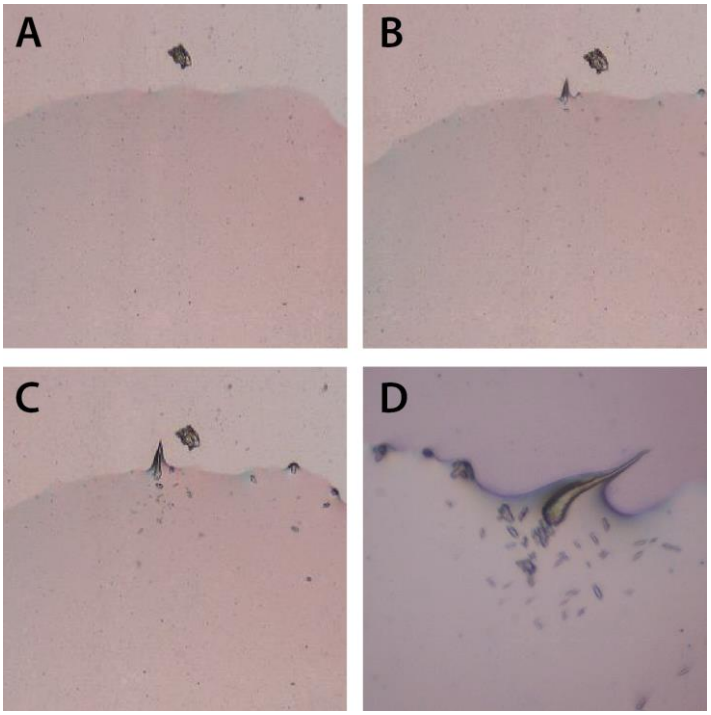

Figure 4.15. Crystallisation well of MscL in [0.1 M Tris pH 8.5, 1.8 M Li_2SO_4]. There were no crystals at the time of set up (**A**) However, crystal-like features appeared in Day 1 (**B**), and became larger in Day 5 (**C**). In Day 8 (**D**; magnified view), short rod-like precipitation can be seen.

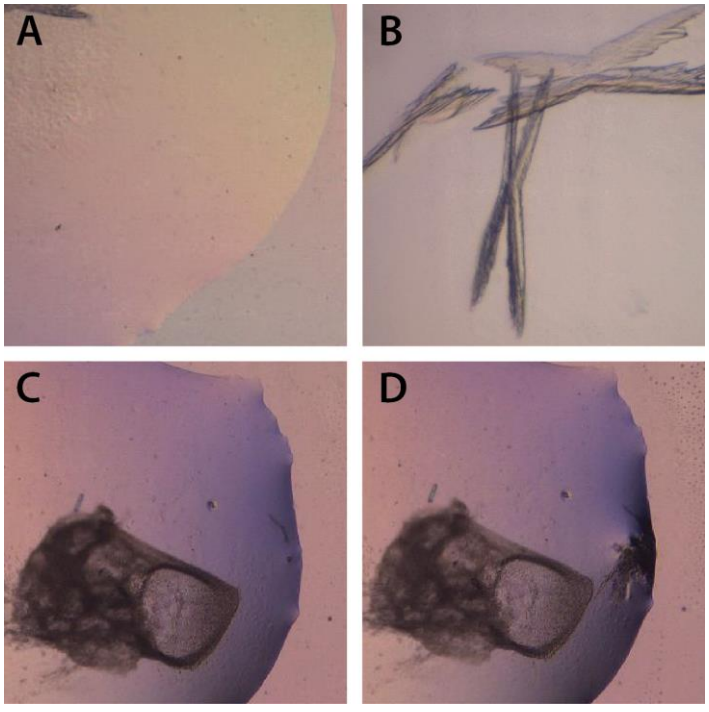

Figure 4.16. Crystallisation wells of MscL in [0.1 M Tris 8.5, 0.1 M $MgCl_2$, 0.1 M NaCl, 12 % PEG 4000] (**A-B**) and [0.2 M $MgCl_2$, 20 % PEG 3350] (**C-D**). With the first condition, large rod-like crystals showed up as soon as the well was set up (**A**), indicating that they could be inorganic salt crystals. With the second condition, there were only cloudy precipitates until Day 1 (**C**), but needle-like crystals started growing in Day 2 and reached peak size by Day 5 (**D**).

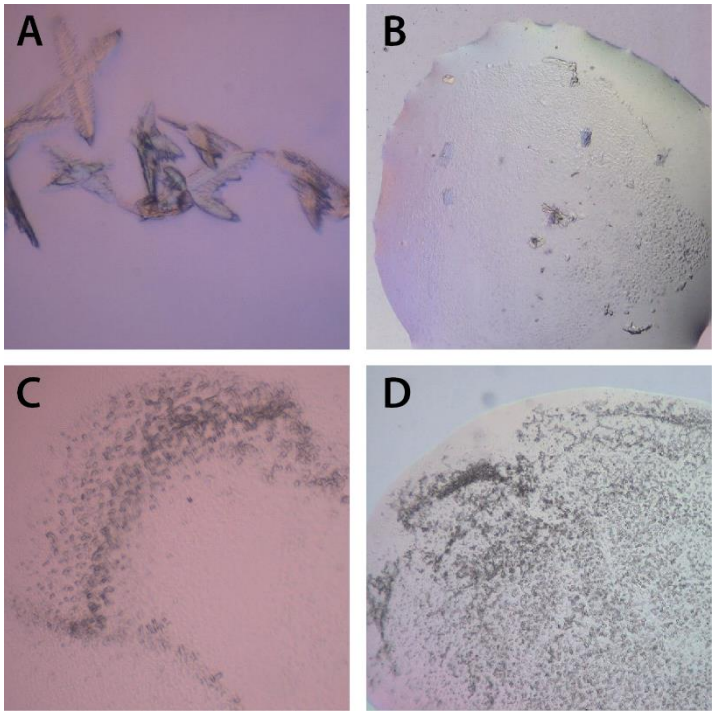

Figure 4.17. Crystallisation wells of MscL. **A**) Day 8, [0.1 M CAPSO pH 6.5, 0.1 M $MgCl_2$, 0.1 M NaCl, 12 % PEG 4000]; **B**) Day 8, [0.2 M CaCl2, 0.2 M CoCl2, 0.2 M CoCl2, 10 % PEG 3350]; **C**) Day 8, [0.1 M MES pH 6.5, 0.1 M NaCl, 0.1 M Li2SO4, 30 % PEG 400]; **D**) Day 8, [0.1 M MOPS pH 7.0, 0.1 M NaCl, 30 % PEG 400;]. Crystal-like features appeared in Day 0 in the first two conditions (A, B). Cloudy precipitates appeared in Day 0 in the latter two conditions (C, D), and they progressively became more organised over the next three days.

(IMB) to identify promising regions for refined investigation. The rationale for the selections were as follows:

- PEGRx sets screen for the polyethylene glycol's (PEG) length; PEG/Ion sets screen for a range
- of inorganic ions while keeping the PEG size constant;
- Clear Strategy sets have generally produced protein crystals in Dr. Brett Collins' group (oral communication; IMB);
- MemGold and MemSys sets are screens designed for the crystallisation of membrane proteins.

In addition, to reduce the possibility of detergent phase separation and detergent crystal formation, the buffer for MscL solution was exchanged to one with lower β-DDM concentration (0.5 mM) before the crystallisation experiments.

Once the broad screen was set up, the wells were checked every day for the next eight days and conditions ranked according to the morphology of the precipitate and/or crystals observed. X-shaped rod-like crystals appeared in two conditions (Condition 1 and 2; Fig. 4.16A/B, 4.17A) within 24 h. In addition, amorphous but still mildly defined clear precipitate appeared in five conditions between 12 h and 3 days, one of which produced a radiating bundle of needle-like crystals after three days (Condition 3, Fig. 4.16C/D). There were also a number of wells which

Table 4.1. MscL 3D crystallisation optimisation trials using hanging drop method. Appearance of crystallisation drops were labelled with colour shading. Light purple – clear; Light blue – amorphous precipitate (spherulite); Light orange – X-shaped crystals; Pink – phase separation; Yellow – needle-like crystals on spherulite; Light green – cloudy precipitate

	Tray 1					
	1-1	**1-2**	**1-3**	**1-4**	**1-5**	**1-6**
A	0.05 M Tris pH 8.5; 0.9 M Li_2SO_4	0.06 M Tris pH 8.5; 1.1 M Li_2SO_4	0.007 M Tris pH 8.5; 1.3 M Li_2SO_4	0.08 M Tris pH 8.5; 1.4 M Li_2SO_4	0.09 M Tris pH 8.5; 1.6 M Li_2SO_4	0.1 M Tris pH 8.5; 1.8 M Li_2SO_4
B	0.05 M MES pH 6.5; 0.05 M NaCl; 0.05 M Li_2SO_4; 15 % PEG 400	0.06 M MES pH 6.5; 0.06 M NaCl; 0.06 M Li_2SO_4; 18 % PEG 400	0.07 M MES pH 6.5; 0.07 M NaCl; 0.07 M Li_2SO_4; 21 % PEG 400	0.08 M MES pH 6.5; 0.08 M NaCl; 0.08 M Li_2SO_4; 24 % PEG 400	0.09 M MES pH 6.5; 0.09 M NaCl; 0.09 M Li_2SO_4; 27 % PEG 400	0.1 M MES pH 6.5; 0.1 M NaCl; 0.1 M Li_2SO_4; 30 % PEG 400
C	0.05 M MOPS pH 7.0; 0.05 M NaCl; 15 % PEG 400;	0.06 M MOPS pH 7.0; 0.06 M NaCl; 18 % PEG 400;	0.07 M MOPS pH 7.0; 0.07 M NaCl; 21 % PEG 400;	0.08 M MOPS pH 7.0; 0.08 M NaCl; 24 % PEG 400;	0.09 M MOPS pH 7.0; 0.09 M NaCl; 27 % PEG 400;	0.1 M MOPS pH 7.0; 0.1 M NaCl; 30 % PEG 400;
D	0.05 M Tris pH 8.5; 0.05 M $MgCl_2$; 0.05 M NaCl; 6 % PEG 4000	0.06 M Tris pH 8.5; 0.06 M $MgCl_2$; 0.06 M NaCl; 7 % PEG 4000	0.07 M Tris pH 8.5; 0.07 M $MgCl_2$; 0.07 M NaCl; 8 % PEG 4000	0.08 M Tris pH 8.5; 0.08 M $MgCl_2$; 0.08 M NaCl; 10 % PEG 4000	0.09 M Tris pH 8.5; 0.09 M $MgCl_2$; 0.09 M NaCl; 11 % PEG 4000	0.1 M Tris pH 8.5; 0.1 M $MgCl_2$; 0.1 M NaCl; 12 % PEG 4000
	Tray 2					
	2-1	**2-2**	**2-3**	**2-4**	**2-5**	**2-6**
A	0.05 M CAPSO pH 6.5; 0.05 M $MgCl_2$; 0.05 M NaCl; 6 % PEG 4000	0.06 M CAPSO pH 6.5; 0.06 M $MgCl_2$; 0.06 M NaCl; 7 % PEG 4000	0.07 M CAPSO pH 6.5; 0.07 M $MgCl_2$; 0.07 M NaCl; 8 % PEG 4000	0.08 M CAPSO pH 6.5; 0.08 M $MgCl_2$; 0.08 M NaCl; 10 % PEG 4000	0.09 M CAPSO pH 6.5; 0.09 M $MgCl_2$; 0.09 M NaCl; 11 % PEG 4000	0.1 M CAPSO pH 6.5; 0.1 M $MgCl_2$; 0.1 M NaCl; 12 % PEG 4000
B	0.1 M $MgCl_2$; 10 % PEG 3350	0.12 M $MgCl_2$; 11 % PEG 3350	0.14 M $MgCl_2$; 14 % PEG 3350	0.16 M $MgCl_2$; 16 % PEG 3350	0.18 M $MgCl_2$; 18 % PEG 3350	0.2 M $MgCl_2$; 20 % PEG 3350
C	0.1 M $CaCl_2$; 0.1 M $CoCl_2$; 0.1 M $CdCl_2$; 10 % PEG 3350	0.12 M $CaCl_2$; 0.12 M $CoCl_2$; 0.12 M $CoCl_2$; 11 % PEG 3350	0.14 M $CaCl_2$; 0.14 M $CoCl_2$; 0.14 M $CoCl_2$; 14 % PEG 3350	0.16 M $CaCl_2$; 0.16 M $CoCl_2$; 0.16 M $CoCl_2$; 16 % PEG 3350	0.18 M $CaCl_2$; 0.18 M $CoCl_2$; 0.18 M $CoCl_2$; 18 % PEG 3350	0.2 M $CaCl_2$; 0.2 M $CoCl_2$; 0.2 M $CoCl_2$; 10 % PEG 3350
D	Negative Control (1-6B)	Negative Control (1-6C)	Negative Control (1-6D)	Negative Control (2-6A)	Negative Control (2-6B)	Negative Control (2-6C)

Table 4.2. MscL 3D crystallisation optimisation trials using microbatch method. Appearance of crystallisation drops were labelled with colour shading. Light blue – amorphous precipitate (spherulite); Yellow – needle-like crystals on spherulite; Light green – cloudy precipitate

	Tray 4					
	4-1	**4-2**	**4-3**	**4-4**	**4-5**	**4-6**
A	0.1 M $MgCl_2$; 10 % PEG 3350; pH 6.0; Paraffin oil	0.12 M $MgCl_2$; 11 % PEG 3350; pH 6.0; Paraffin oil	0.14 M $MgCl_2$; 14 % PEG 3350; pH 6.0; Paraffin oil	0.16 M $MgCl_2$; 16 % PEG 3350; pH 6.0; Paraffin oil	0.18 M $MgCl_2$; 18 % PEG 3350; pH 6.0; Paraffin oil	0.2 M $MgCl_2$; 20 % PEG 3350; pH 6.0; Paraffin oil
B	0.1 M $MgCl_2$; 10 % PEG 3350; pH 7.5; Paraffin oil	0.12 M $MgCl_2$; 11 % PEG 3350; pH 7.5; Paraffin oil	0.14 M $MgCl_2$; 14 % PEG 3350; pH 7.5; Paraffin oil	0.16 M $MgCl_2$; 16 % PEG 3350; pH 7.5; Paraffin oil	0.18 M $MgCl_2$; 18 % PEG 3350; pH 7.5; Paraffin oil	0.2 M $MgCl_2$; 20 % PEG 3350; pH 7.5; Paraffin oil
C	0.1 M $MgCl_2$; 10 % PEG 3350; pH 6.0; Al's oil	0.12 M $MgCl_2$; 11 % PEG 3350; pH 6.0; Al's oil	0.14 M $MgCl_2$; 14 % PEG 3350; pH 6.0; Al's oil	0.16 M $MgCl_2$; 16 % PEG 3350; pH 6.0; Al's oil	0.18 M $MgCl_2$; 18 % PEG 3350; pH 6.0; Al's oil	0.2 M $MgCl_2$; 20 % PEG 3350; pH 6.0; Al's oil
D	0.1 M $MgCl_2$; 10 % PEG 3350; pH 7.5; Al's oil	0.12 M $MgCl_2$; 11 % PEG 3350; pH 7.5; Al's oil	0.14 M $MgCl_2$; 14 % PEG 3350; pH 7.5; Al's oil	0.16 M $MgCl_2$; 16 % PEG 3350; pH 7.5; Al's oil	0.18 M $MgCl_2$; 18 % PEG 3350; pH 7.5; Al's oil	0.2 M $MgCl_2$; 20 % PEG 3350; pH 7.5; Al's oil

produced poorly defined spherulites and/or clear precipitate, which were discarded as the chances of them being crystals were deemed too small.

Crystallisation conditions were then refined around the 8 selected conditions (Fig. 4.15, 4.16, 4.17), where precipitant concentration was varied for each condition (Table 4.1). Long rod-like crystals (>500 µm in length) with branches formed in both the control group (which did not contain MscL) and drops with MscL within 5 min in Conditions 1 and 2, which suggested that they were salt crystals. This was further confirmed by a quick experiment where the crystals were briefly treated with heat, which would destroy protein crystals but not salt crystals (Raghunathan *et al.*, 2010). The other five conditions (conditions 4 – 8) only produced spherulites and/or cloudy precipitate, which

Table 4.3. MscL 3D crystallisation optimisation trials using microbatch method. Appearance of crystallisation drops were labelled with colour shading. Light blue – amorphous precipitate (spherulite); Yellow – needle-like crystals on spherulite; Dark green – Hexagonal 3D crystals

	Tray 5					
	5-1	**5-2**	**5-3**	**5-4**	**5-5**	**5-6**
A	0.12 M $MgCl_2$; 14 % PEG 3350; PBS pH 7.5; Paraffin oil; 2 µL precipitant	0.16 M $MgCl_2$; 16 % PEG 3350; PBS pH 7.5; Paraffin oil; 2 µL precipitant	0.2 M $MgCl_2$; 20 % PEG 3350; PBS pH 7.5; Paraffin oil; 2 µL precipitant	0.12 M $MgCl_2$; 14 % PEG 3350; PBS pH 7.5; Paraffin oil; 1 µL precipitant	0.16 M $MgCl_2$; 16 % PEG 3350; PBS pH 7.5; Paraffin oil; 1 µL precipitant	0.2 M $MgCl_2$; 20 % PEG 3350; PBS pH 7.5; Paraffin oil; 1 µL precipitant
B	0.12 M $MgCl_2$; 14 % PEG 3350; PBS pH 6.0; Paraffin oil; 2 µL precipitant	0.16 M $MgCl_2$; 16 % PEG 3350; PBS pH 6.0; Paraffin oil; 2 µL precipitant	0.2 M $MgCl_2$; 20 % PEG 3350; PBS pH 6.0; Paraffin oil; 2 µL precipitant	0.12 M $MgCl_2$; 14 % PEG 3350; PBS pH 6.0; Paraffin oil; 1 µL precipitant	0.16 M $MgCl_2$; 16 % PEG 3350; PBS pH 6.0; Paraffin oil; 1 µL precipitant	0.2 M $MgCl_2$; 20 % PEG 3350; PBS pH 6.0; Paraffin oil; 1 µL precipitant
C	0.12 M $MgCl_2$; 14 % PEG 3350; PBS pH 7.5; Al's oil; 2 µL precipitant	0.16 M $MgCl_2$; 16 % PEG 3350; PBS pH 7.5; Al's oil; 2 µL precipitant	0.2 M $MgCl_2$; 20 % PEG 3350; PBS pH 7.5; Al's oil; 2 µL precipitant	0.12 M $MgCl_2$; 14 % PEG 3350; PBS pH 7.5; Al's oil; 1 µL precipitant	0.16 M $MgCl_2$; 16 % PEG 3350; PBS pH 7.5; Al's oil; 1 µL precipitant	0.2 M $MgCl_2$; 20 % PEG 3350; PBS pH 7.5; Al's oil; 1 µL precipitant
D	0.12 M $MgCl_2$; 14 % PEG 3350; PBS pH 6.0; Al's oil; 2 µL precipitant	0.16 M $MgCl_2$; 16 % PEG 3350; PBS pH 6.0; Al's oil; 2 µL precipitant	0.2 M $MgCl_2$; 20 % PEG 3350; PBS pH 6.0; Al's oil; 2 µL precipitant	0.12 M $MgCl_2$; 14 % PEG 3350; PBS pH 6.0; Al's oil; 1 µL precipitant	0.16 M $MgCl_2$; 16 % PEG 3350; PBS pH 6.0; Al's oil; 1 µL precipitant	0.2 M $MgCl_2$; 20 % PEG 3350; PBS pH 6.0; Al's oil; 1 µL precipitant
	Tray 6					
	6-1	**6-2**	**6-3**	**6-4**	**6-5**	**6-6**
A	0.12 M $MgCl_2$; 14 % PEG 3350; HEPES pH 7.5; Paraffin oil; 2 µL precipitant	0.16 M $MgCl_2$; 16 % PEG 3350; HEPES pH 7.5; Paraffin oil; 2 µL precipitant	0.2 M $MgCl_2$; 20 % PEG 3350; HEPES pH 7.5; Paraffin oil; 2 µL precipitant	0.12 M $MgCl_2$; 14 % PEG 3350; HEPES pH 7.5; Paraffin oil; 1 µL precipitant	0.16 M $MgCl_2$; 16 % PEG 3350; HEPES pH 7.5; Paraffin oil; 1 µL precipitant	0.2 M $MgCl_2$; 20 % PEG 3350; HEPES pH 7.5; Paraffin oil; 1 µL precipitant
B	0.12 M $MgCl_2$; 14 % PEG 3350; HEPES pH 7.5; Al's oil; 2 µL precipitant	0.16 M $MgCl_2$; 16 % PEG 3350; HEPES pH 7.5; Al's oil; 2 µL precipitant	0.2 M $MgCl_2$; 20 % PEG 3350; HEPES pH 7.5; Al's oil; 2 µL precipitant	0.12 M $MgCl_2$; 14 % PEG 3350; HEPES pH 7.5; Al's oil; 1 µL precipitant	0.16 M $MgCl_2$; 16 % PEG 3350; HEPES pH 7.5; Al's oil; 1 µL precipitant	0.2 M $MgCl_2$; 20 % PEG 3350; HEPES pH 7.5; Al's oil; 1 µL precipitant
C						
D		0.12 M $MgCl_2$; 14 % PEG 3350; HEPES pH 7.5; Al's oil+ Paraffin oil; 1 µL precipitant	0.16 M $MgCl_2$; 16 % PEG 3350; HEPES pH 7.5; Al's oil+ Paraffin oil; 1 µL precipitant	0.2 M $MgCl_2$; 20 % PEG 3350; HEPES pH 7.5; Al's oil+ Paraffin oil; 1 µL precipitant		

indicated that they were not suitable environments for MscL crystal growth. In two (60% and 80% precipitant concentrations) of the six conditions screened around condition 3 (Table 4.1, wells 2-3B, 2-4B), however, discrete needle-like crystals (too small for measurement) formed around well-defined spherulite-like mass after the fifth day, which made it a likely condition for MscL crystal growth.

In the second round of optimisation, both sitting drop and microbatch methods were trialled instead of the hanging drop method. The pH (6.0, 7.5), precipitant concentration (50 – 100 %), and in the case of microbatch plate, type of oil used (Paraffin oil, Al's oil) were varied (Table 4.2). Although only amorphous precipitates formed in the sitting drop plate, small discrete needles formed around such amorphous precipitates in the microbatch plate in eight conditions. However, the needle-like crystals were still too small for structural analysis and required further optimisation.

In a third round of optimisation, only the microbatch method was repeated. MscL buffer (PBS, 0.02 M HEPES), pH (6.0, 7.5), precipitant concentration (50 – 100 %), oil used (Paraffin oil, Al's oil, 1:1 mixture of Paraffin oil and Al's oil), and protein-to-precipitant ratio (2:1, 1:1) were varied (Table 4.3). The protein buffer was also varied as this precipitant condition did not contain its own buffer. Most conditions produced amorphous precipitates with tiny needles as before; however, one condition (20 mM HEPES pH 7.5; precipitant pH 6.0; 100 % precipitant; 1:1 paraffin oil and Al's oil mix; 2µL 10 mg/mL MscL; 1 µL precipitant) produced well-defined three-dimensional crystals of approximately 200 – 400 µm in diameter between the second and the third day (Fig. 4.18A). The crystals were harvested on the sixth day.

The crystals diffracted X-rays very poorly when tested at the UQ ROCX facility. While very poor diffraction patterns were seen around the beam stop and attempts at indexing with the Refmac program were unsuccessful. An important observation was that there was no strongly-diffracting spot in the high-resolution area of the detection plate, suggesting that the crystals were unlikely to be salt crystals.

There are two possibilities for the poor diffraction observed. First, protein molecules in the crystals might have been too poorly ordered to yield high resolution diffraction data. Second, the crystals might have been a β-DDM detergent-rich phase or detergent crystals, which are known to form crystals of various shapes. While the theoretical β-DDM concentration of the solution was too low for crystal formation and crystals of such large quantity, its actual concentration might have been higher due to its affinity for MscL. Given that 90 kDa His-MscLL-7Y molecules are in β-DDM micelles (which are normally 50 – 55 kDa in mass), it is reasonable to assume that the actual concentration of β-DDM in 10 mg/mL MscL solution could have been as high as 6 mg/mL. Although the solubility of β-DDM in water is over 200 mg/mL, the PEG-rich environment could

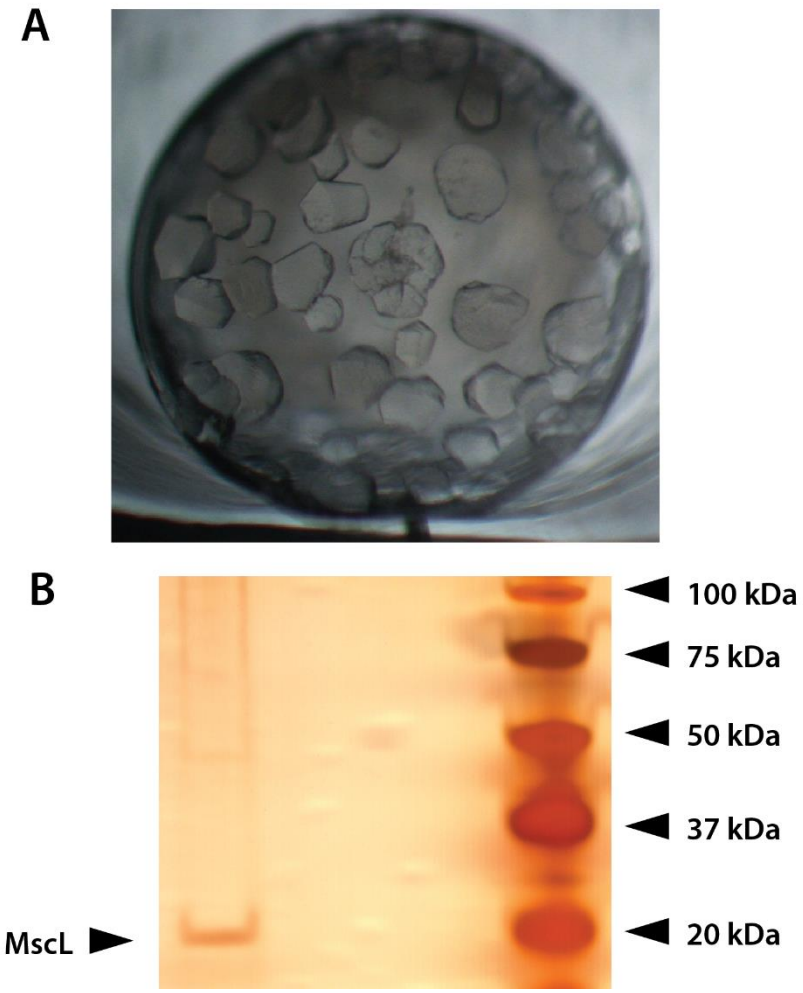

Figure 4.18. A) Crystals obtained in the well 6-4D, and **B**) Silver-stained SDS-PAGE of the crystals. The resolubilised crystal solution was loaded in the far left lane, where a band matching the size of His-MscL (19 kDa) can be seen.

have facilitated its crystallisation in this scenario.

In order to test the two possibilities, two frozen crystals were solubilised in 8M urea, and analysed using silver stained SDS-PAGE (Fig. 4.18B). The single band matching the size of MscL suggest that the crystals either contained significant amounts of MscL or were MscL protein crystals. In addition, the crystals did not dissolve in water but dissolved in 8M urea, suggesting that the crystals were largely made of protein rather than detergent. The hypothesis that these are protein crystals is supported by the fact that MscL should precipitate if significant amounts of β-DDM had crystallised, since the nominal concentration of the detergent was close to the critical micelle concentration. However, little precipitation was observed in this condition, indicating that MscL crystallised with the detergent micelles.

This leaves the second possibility of poor crystal quality as the likely cause of the diffraction problem. At least part of this could be attributed to the simple operational issues with the experiment such as not being able to quickly harvest the crystals due to equipment problems at the

time. Therefore, a repeat of the crystallisation trial with less damage to the crystals might increase the diffraction quality. There are also a number of techniques which can be used to improve the crystal quality. In addition to conventional optimisations such as finer screening for pH (only two pH conditions were trialled in this study) to find a condition for crystals with higher-resolution diffraction, microseeding and macroseeding techniques (Bergfors, 2003) can be used to produce better-ordered crystals. Since at least needle-like crystals can be reliably produced, microED, which is suitable for small 3D crystals, could also be trialled in the future studies (Rodriguez & Gonen, 2016).

4.4. Conclusion and Future Directions

I have detailed in this chapter my work conducted to crystallise *E. coli* MscL using 2D and 3D crystallography methods. The 2D crystallography experiments allowed me to identify conditions yielding sheet-like lipid bilayers containing MscL (Fig. 4.9B, 4.11A), which provide a solid basis for further refinement. Both optimised conditions and morphology of the MscL/phospholipid membrane were similar to that reported by Saint *et al.* (1998), but with several key improvements such as the addition of $MgSO_4$ and slower detergent removal with Biobeads leading to larger membrane formation, and the identification of DOPC as a potentially suitable lipid environment for crystallisation in addition to *E. coli* lipids. Additionally, monolayer-assisted 2D crystallisation allowed the direct visualisation of MscL complexes and aggregates in the native (i.e. not denatured) state in the presence of DOPC (Fig. 4.12, 4.13). These results indicate that it is possible for MscL to be crystallised in 2D lattice for future structure determination.

2D crystallisation experiments also provided valuable information for MscL aggregation experiments in Chapter 3 (section 3.3.3.). As the methods for these two projects were similar, the optimisation experiments carried out in this chapter could be applied to section 3.3.3. Moreover, the visualisation of MscL aggregation in the monolayer experiment confirmed the observation made in section 3.3.3.

3D crystallisation experiments also produced mixed but promising results. A suitable condition for 3D crystal formation was identified, and the observed quality was improved from spherulites and needle-like crystals to large discrete crystals through rationally designed optimisations. However, there still remains the challenge of improving the quality of diffraction, which was very poor to nearly absent when tested with an in-house X-ray source. As some of the identified problems such as late crystal harvesting can be easily rectified, there is a significant likelihood of improvement in crystal quality with further trials. Therefore, it will be worthwhile to continue this strategy for the determination of *E. coli* MscL structure.

An interesting alternative to conventional X-ray diffraction is an electron diffraction technique called MicroED (Brent L. Nannenga *et al.*, 2013; B. L. Nannenga *et al.*, 2014). The main advantage of this technique is that it requires the use of small protein crystals. Hence MicroED may allow bypassing one of the major bottlenecks in 3D crystallography, growing large crystals while maintaining crystallinity, for this project. In the 3D crystallisation trials of MscL, only one condition produced large crystals but small needle-like crystals were reproduced multiple times over a range of conditions (Tables 4.1, 4.2, 4.3). It is possible that the protein molecules are better ordered with these crystals, or at least that these crystals have larger windows for optimisation. An F30 electron microscope (FEI, USA) with a K2 direct electron detector camera (Gatan, USA), which is capable of MicroED, became operational at UQ at the time of writing this thesis, so this is an option with high potential for structure determination in the near future.

Although not described elsewhere in this chapter due to the lack of relevant data presented, single particle analysis is another potentially viable route to determine MscL structure. While this is theoretically limited by the small molecular weight of MscL (80 kDa), it could be overcome by either producing a fusion protein similar to that used by Li *et al.* (2015), or by using monoclonal antibodies (approx. 45 kDa). As MscL is a homopentamer, up to five antibodies will bind to MscL and bring the total molecular weight to ~300 kDa, which is large enough for single particle analysis if cryo-electron microscopy is employed. Moreover, these antibodies will bind to the cytoplasmic domain, which will further help with single particle analysis by reducing the relative influence of detergent micelles (heterogeneous in size and shape). This strategy was similarly employed for GPCRs to facilitate 3D crystallisation (Ghosh *et al.*, 2015), so it may also be applicable to technically challenging proteins such as MscL in order to determine their structures with electron microscopy.

Limited exploratory trials using anti-His monoclonal antibodies typically used in Western blots were carried out, however this could not be properly tested due to the formation of crystalline ice throughout the electron microscopy grids. Due to time and resource constraints, and to prevent distraction from more productive projects of the thesis, no further work was carried out as of the time of writing of the thesis. However, this still remains an interesting alternative method to determine MscL structure, albeit with less priority than crystallography approach due to technical and resource challenges.

5. Conclusion and Future Directions

5.1. Conclusion

Nanoparticle-based targeted drug delivery systems are rapidly being developed as therapeutic drug delivery systems with the potential to improve the safety and efficacy of both existing drugs and drug candidates by targeting these specific sites (Egusquiaguirre *et al.*, 2012; Torchilin, 2006). In the nanoparticle family, liposomes hold particular promise because they represent a proven technology already used in cosmetics and for medical applications, because it can be further improved for active targeting of the liposomal drugs to specific cells and tissues, and because externally controlled drug release mechanisms can be incorporated (Fan & Zhang, 2013; Levchenko *et al.*, 2012). To improve controlled drug release, a focused electromagnetic force can be used to open the nanovalves containing magnetic tags to release cargo molecules from liposomes in a site-specific manner (Nakayama *et al.*, 2015). Using this strategy, side effects resulting from non-specific drug release into healthy tissues could be greatly reduced. Drug doses could also be reduced to improve safety and cost. Nanovalves are therefore being actively researched, and successful proof-of-concept studies both *in vitro* and *in vivo* have been reported (Hughes *et al.*, 2008; Iscla *et al.*, 2013; Nakayama *et al.*, 2015).

The mechanosensitive channel of large conductance (MscL) in *Escherichia coli* is one of the best studied mechanosensitive channels both as a prototype for this class of protein channels and as a nanovalve candidate for liposomal drug delivery systems. The structures of its homologues in *Mycobacterium tuberculosis*, *Staphylococcus aureus*, and *Methanosarcina acetivorans* have been determined by protein 3D crystallography (G. Chang *et al.*, 1998; Liu *et al.*, 2009; Zhu *et al.*, 2016), and a wide range of biophysical studies to characterise the mechanism of channel gating have been reported (A. Foo *et al.*, 2015; Grage *et al.*, 2011; Petrov *et al.*, 2011; Y. Wang *et al.*, 2014; Yilmaz *et al.*, 2015; Zhu *et al.*, 2016). Despite this, a key point to be addressed in order to fully understand the mechanism of channel triggering and gating is to solve the channel structure in its open state in near native conditions. Therefore, this project commenced with the two main aims of biophysical characterisation of MscL in the membrane environment and its structural characterisation using crystallographic methods.

Chapter 2 focused on the development of new constructs for homogeneous MscL expression and improved quantification. The original MscL construct, used in a number of publications by several groups (Doerner *et al.*, 2012; Grage *et al.*, 2011; Hase, Le Dain, *et al.*, 1997; Kloda *et al.*, 2006; S. I. Sukharev *et al.*, 1994; Yoshimura *et al.*, 2001), had the problems of yielding two protein species

and inaccurate quantification due to the lack of tryptophan and tyrosine. To produce pure MscL which is also more readily detectable, a series of MscL constructs were designed and characterised, which eventually yielded the $MscL^{L-7Y}$ construct (Chi *et al.*, 2015).

In Chapter 3, MscL's relationship with the membrane environment was studied using various approaches. First, co-purifying lipids were analysed using thin layer chromatography to determine whether specific lipid constituents of *E. coli* membranes were tightly associated with the purified MscL complex. Phosphatidylethanolamine (PE), one of the main phospholipids of *E. coli* membrane, was identified as a molecule which associated with MscL with high enough affinity to co-purify.

In a separate set of experiments, MscL/soy azolectin proteoliposomes were size-fractionated by sucrose density gradient centrifugation to study if there were variables which could influence MscL function. It was found from this experiment that membrane curvature of liposomes can affect MscL channel gating and aggregation pattern even without changes in underlying factors such as phospholipid composition. This was a confirmation of the hypothesis that global membrane curvature is a significant influence on MscL function, and it has implications in the development of MscL for nanovalve since this factor will need to be considered when designing liposomal drug delivery system that incorporate MscL.

In the last set of experiments in this chapter, MscL's aggregation pattern in various phospholipid environments was studied to understand its relationship with phospholipids in the resting state. Phosphatidylcholine (PC) was found to have a positive influence on MscL clustering, whereas phosphatidylglycerol (PG) had a negative influence (Fig. 3.26). Interestingly, PE, which was found to have a relatively high affinity for MscL based on thin-layer chromatography analyses, did not appear to have a significant role in MscL clustering. The dependence of MscL aggregation on phospholipid composition provides another factor to consider in the design of liposomal drug delivery systems, since the phospholipid composition can significantly affect MscL distribution between liposomes. In summary, the key findings of Chapter 3 were that phospholipid type (especially its head groups) and membrane curvature influence MscL distribution in the membrane and its channel gating function, and that MscL clustering is influenced by phospholipids which do not associate with high affinity in the native *E. coli* membrane environment.

In Chapter 4, 2D and 3D crystallisation experiments were conducted with the objective of refining *E. coli* MscL crystallisation conditions. The 2D crystallisation experiments identified conditions yielding reasonably large sheet-like membrane structures which appear to be on the right rack in terms of 2D crystal formation. With monolayer-assisted crystallisation experiments, large two-dimensional MscL aggregates in the presence of DOPC were obtained, which was another

promising sign for 2D crystallisation. These experiments also yielded valuable information on the biophysical relationship between MscL and phospholipids, including the potential influence of MscL on membrane curvature and direct confirmation of MscL clustering in DOPC membranes. 3D crystallisation experiments also led to the identification of conditions for formation of 3D MscL crystals in detergent environment. Silver-stained SDS-PAGE confirmed these crystals to consist of MscL.

Collectively this project has made significant contributions both towards the biophysical understanding of MscL and to its development for nanovalve-based liposomal drug delivery systems. MscL's interaction with phospholipids, membrane curvature, and its aggregation state have been proposed as factors influencing its channel gating properties (Grage *et al.*, 2011; Meyer *et al.*, 2006; Pliotas *et al.*, 2015; Tang *et al.*, 2008b). This project has not only experimentally confirmed these speculations but also shown the factors to be correlated. This new information can be applied in the analysis of patch clamp data, improving the accuracy of fluorescence-based studies, and in the design of molecular dynamics simulations, hence helping with the biophysical characterisation of MscL in general. It is also a valuable finding of its own as it shows that the engineering of MscL into a protein-based nanovalve needs to be considered in the wider context of liposomal drug delivery system development to produce a nanovalve with desired channel gating properties and distribution.

5.2. Considerations for Advanced Nanovalve Design in the Context of Liposomal Drug Delivery Systems

Liposomal drug delivery systems, currently used in cosmetics and in medical therapies (particularly anticancer therapies), can be significantly improved for targeted drug delivery, which is part of the longer aim of developing MscL as nanovalves. A number of solutions for such improvement have been proposed, including antibody-mediated active targeting and externally triggered drug release at the target tissue. It is likely that a successful liposomal drug delivery system will incorporate many of these proposed features as there are both benefits and risks to most of them. For example, while antibodies provide highly specific targeting to the desired cells (Basile *et al.*, 2012), they also carry the risk of becoming ineffective e.g. if cancer cells have mutations which reduce their affinity for the receptors, as well as the documented safety concerns (Gabizon, 2001; Torchilin, 2006). Nanovalve-based liposomal drug delivery systems can circumvent these problems, but they are also limited by not enhancing deposition of the liposomes (which will likely be injected in very low concentrations) on their own. A successful approach will need to include both site-specific targeting and nanovalve-mediated drug release.

Figure 5.1 describes one such liposomal drug delivery system utilising the multiple strategies. Ideally, the liposomes will be small in size (less than 100 nm in diameter) to allow liposomes to pass through physiological barriers such as blood vessels and skin tissues (Egusquiaguirre *et al.*, 2012; Fan & Zhang, 2013; Tahover *et al.*, 2015). Accessory molecules on the liposomes such as polyethylene glycol and oligosaccharides will not only help with the immune system evasion by the liposomes but also actively target certain diseased tissues/cells with moderate specificity, allowing

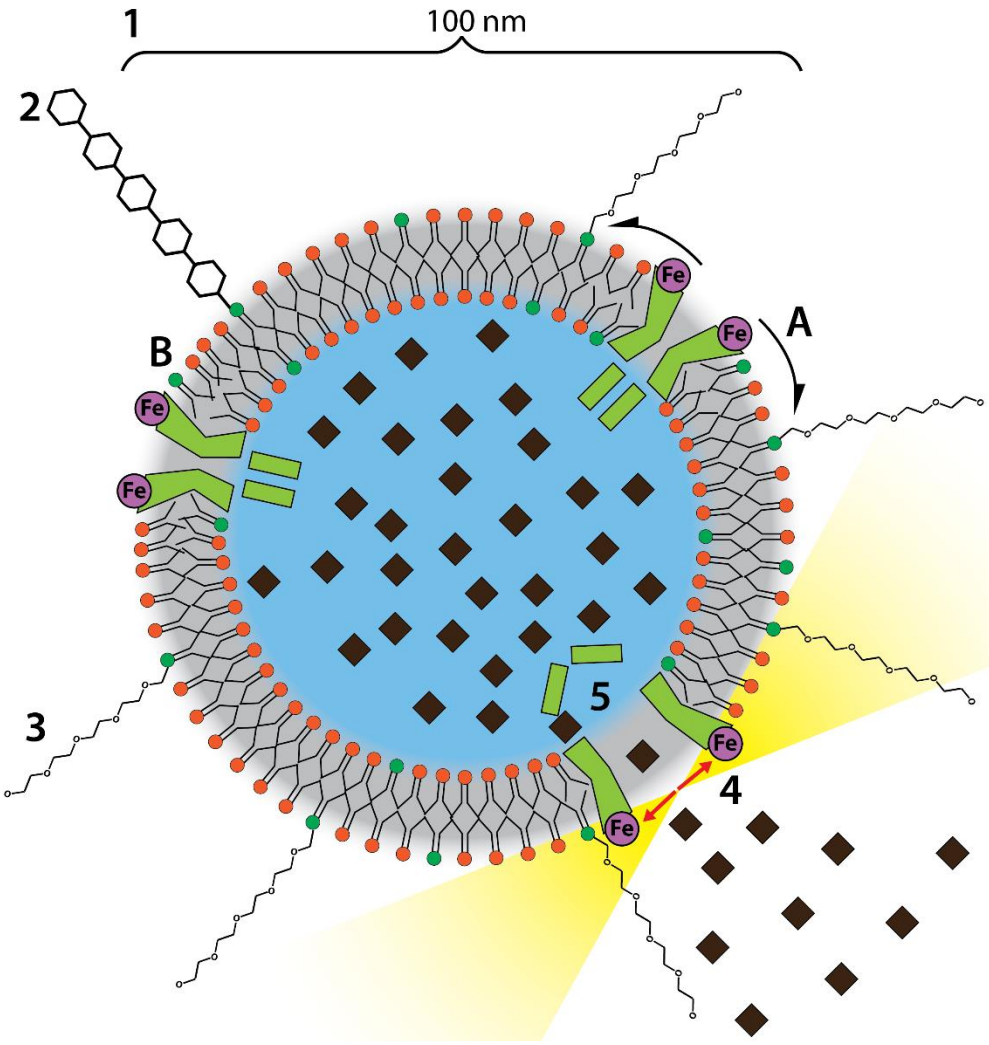

Figure 5.1. Schematic representation of a conceptual liposomal drug delivery system with externally activated nanovalves. **1** – Smaller liposomes (less than 100 nm in diameter) are generally preferred due to the permeability to physiological barriers such as the walls of blood vessels; **2,3** – The liposomal drug will need to contain glycolipids (**2**) or PEGylated lipids (**3**) to evade the immune system and for active targeting to targeted tissues; **4** – Magnetic nanoparticles attached to the nanovalves will provide the necessary mechanical force to open the channel pore – hence releasing the drug molecules (brown particles) from the liposomes – in the presence of focused electromagnetic field (yellow shading); **5** – If desired, the channel pore size can be controlled via the modification of the cytoplasmic domain of the nanovalve. **A**) In this thesis, the curvature of small liposomes was found to be significant enough to lower the channel gating threshold of MscL. Can be used to poise nanovalves close to their trigger point and to engineer them for modified gating threshold. **B**) Additionally, the curvature of small liposomes and lipid composition can trigger the clustering of MscL, which may in turn lead to the uneven distribution of MscL/nanovalves in the liposomal membranes. This can potentially be addressed by adding small amount of phospholipids with PG head group (lipids with green head group).

liposome deposition at the targeted site (H. I. Chang & Yeh, 2012; Immordino *et al.*, 2006; Slingerland *et al.*, 2012). The issue of depositing at non-target tissues can be circumvented by the use of site-specific triggering of nanovalve-based drug release system, which will ensure that the liposome-encapsulated drugs are released only at the target tissues and not in healthy ones. A promising strategy to facilitate the nanovalve opening is to engineer nanovalves to activate on the application of external triggers such as light or electromagnetic fields (Kocer *et al.*, 2005; Nakayama *et al.*, 2015).

In this thesis, a protocol was developed to isolate a range of size-fractionated liposomes from 50 nm to over 200 nm. The phospholipid composition of the liposome fractions were defined, and based on this and the electron micrographs of MscL proteoliposomes, lipid effects on MscL clustering and potentially gating threshold were identified. In order to engineer MscL into an externally triggered protein-based nanovalve, its gating threshold has to be controlled. This thesis has presented the experimental evidence that MscL channel gating threshold is sensitive to the membrane curvature of liposomes, providing an important factor to consider in the adjustment of the threshold (Fig. 5.1). From this thesis it was also learned that MscL can form self-associating clusters in curved membranes and in membranes with phosphatidylcholine head groups, currently the most commonly used lipid in liposomal drug formulations (H. I. Chang & Yeh, 2012; Fan & Zhang, 2013). Hence to ensure more even distribution of the MscL nanovalve in the liposomal populations, lipids with negative influence on the clustering such as phosphatidylglycerols also identified in this thesis will also need to be part of the liposomal formulations. The improved formulation of liposomes with nanovalves will therefore aid with the development of a novel liposomal drug delivery system with targeted drug delivery.

5.3. Future Directions

While this PhD project has significantly advanced the understanding of MscL function, there are still aspects which require further study. In the near term, some of the experiments which could not be performed due to time constraints will need to be carried out to confirm the discoveries made in this project.

First, the phospholipid found to have high affinity to MscL will need to be conclusively identified with mass spectrometry. This is currently in progress in collaboration with Prof. Stephen Blanksby (Queensland University of Technology). The protocol for this experiment is described in this thesis, and a similar experiment on MscS was recently performed by Pliotas et al. (2015), making it a project with high potential to yield results for publication.

Second, the crystallisation experiments using MscL will need to be continued for the structural characterisation of *E. coli* MscL. Significant progress has already been made in 2D crystallisation, and crystallisation conditions were found and optimised for 3D crystallography as well, so it is reasonable to expect the structure to be determined with further work. In particular, 3D crystallisation experiments look promising since the crystals obtained in this thesis was confirmed to be of protein and not of detergent or inorganic salt. However, it should be cautioned that it is common for membrane protein crystals to have poor diffraction, making this a still challenging project in general. Single particle analysis of cryo-electron microscopy of MscL may also be a viable route to determine its structure if the issue with protein size can be addressed.

Third, crystallisation trials with $MscL^{G22C}$ will be interesting experiments to carry out. MscLG22C can be locked in the open state with the addition of MTSET (L. M. Yang & Blount, 2011). Since MscL in the open state has a significantly different conformation to the closed state (Deplazes *et al.*, 2012), it will likely have a unique crystallising condition. While this was not carried out in this thesis as doing so would have spread the focus of the project even further, it will be a worthwhile project since this is probably a structural biology experiment with highest impact regarding MscL.

The aim for the structural biology experiments is not necessarily to obtain high-resolution structure. There are already a number of low-resolution structural information from FRET and EPR experiments (Corry *et al.*, 2010; Y. Wang *et al.*, 2014; Yilmaz *et al.*, 2015) as well as molecular dynamics simulations (Chen *et al.*, 2008; Corry *et al.*, 2010; Corry *et al.*, 2005; Deplazes *et al.*, 2012; Pliotas *et al.*, 2015; Rui *et al.*, 2011). These and the crystal structure of *M. tuberculosis* MscL will enable building an accurate atomic level structural model of *E. coli* MscL from a relatively low-resolution crystal or EM structure. Hence, while obtaining a high-resolution structure of this membrane protein may still be challenging, a publishable outcome is still a possibility with further experiments.

Fourth, additional quantitative analysis of the experiments discussed in sections 3.3.2. and 3.3.3. needs to be carried out. While the analyses described in this thesis successfully demonstrated the significance of membrane curvature and phospholipids in MscL clustering behaviour, there may be a better and more rigorous statistical method to validate this observation. This will likely bring the result of the section to the publishable quality without additional experiments.

In the medium term, the biophysical studies on MscL need to be expanded to include phospholipids as the main subject both to understand MscL channel function and for the development of nanovalve-assisted liposomal drug delivery systems. Prior to the start of this PhD project, most studies on MscL focused on the protein aspect of biophysics while comparatively little attention was paid to phospholipids. For example, most molecular dynamics studies use a model in which a

single MscL complex “floats” in a membrane consisting of a single species of phospholipid, which is more often than not phosphatidylcholine (which is not native to *E. coli* membrane) (Bavi, Vossoughi, *et al.*, 2016; Deplazes *et al.*, 2012; Meyer *et al.*, 2006; Sawada *et al.*, 2012). This project provides evidence that the relationship between MscL and phospholipids needs to be studied in the context of multiple proteins influencing the biophysics of phospholipid. These studies will contribute to our understanding of the mechanisms of the discoveries made in this project at the molecular level. Molecular dynamics simulation performed in this context not only will help to identify the protein residues and atoms in the phospholipids responsible for the aggregation and change in channel gating function, but also will be able to model the lipid and MscL structures more accurately and facilitate structure-guided nanovalve design.

A long term biotechnological goal of MscL studies is to develop these channels for use as protein-based nanovalves for new drug delivery systems. For example, there are already significant efforts to engineer MscL into light and magnetically activated nanovalves (Kocer *et al.*, 2005; Nakayama *et al.*, 2015), and this work will have to continue in tandem with liposome development to fast track the development of next generation liposomal drug delivery system. Significant work remains, but the work described here, together with conclusions from past experiments and future efforts, could collectively contribute to a new drug delivery system with improved safety, efficacy, and cost, which are among the main challenges facing modern medicine.

6. References

Abdine, A., Park, K. H., & Warschawski, D. E. (2012). Cell-free membrane protein expression for solid-state NMR. *Methods Mol Biol, 831*, 85-109. doi:10.1007/978-1-61779-480-3_6

Acosta, C., Djouhri, L., Watkins, R., Berry, C., Bromage, K., & Lawson, S. N. (2014). TREK2 expressed selectively in IB4-binding C-fiber nociceptors hyperpolarizes their membrane potentials and limits spontaneous pain. *J Neurosci, 34*(4), 1494-1509. doi:10.1523/jneurosci.4528-13.2014

Aimon, S., Callan-Jones, A., Berthaud, A., Pinot, M., Toombes, Gilman E. S., & Bassereau, P. (2014). Membrane Shape Modulates Transmembrane Protein Distribution. *Developmental Cell, 28*(2), 212-218. doi:http://dx.doi.org/10.1016/j.devcel.2013.12.012

Ajouz, B., Berrier, C., Besnard, M., Martinac, B., & Ghazi, A. (2000). Contributions of the different extramembranous domains of the mechanosensitive ion channel MscL to its response to membrane tension. *J Biol Chem, 275*(2), 1015-1022.

Akashi, K.-i., Miyata, H., Itoh, H., & Kinosita Jr, K. (1998). Formation of Giant Liposomes Promoted by Divalent Cations: Critical Role of Electrostatic Repulsion. *Biophysical Journal, 74*(6), 2973-2982. doi:http://dx.doi.org/10.1016/S0006-3495(98)78004-X

Al-Jamal, W. T., & Kostarelos, K. (2011). Liposomes: from a clinically established drug delivery system to a nanoparticle platform for theranostic nanomedicine. *Acc Chem Res, 44*(10), 1094-1104. doi:10.1021/ar200105p

Alberts, B., Johnson, A., Lewis, J., Raff, M., Roberts, K., & Walter, P. (2003). Membrane Structure *Molecular Biology of the Cell* (4th ed., Vol. 31): John Wiley & Sons Inc.

Allhenn, D., Boushehri, M. A., & Lamprecht, A. (2012). Drug delivery strategies for the treatment of malignant gliomas. *Int J Pharm, 436*(1-2), 299-310. doi:10.1016/j.ijpharm.2012.06.025

Anishkin, A., Chiang, C. S., & Sukharev, S. (2005). Gain-of-function mutations reveal expanded intermediate states and a sequential action of two gates in MscL. *J Gen Physiol, 125*(2), 155-170. doi:10.1085/jgp.200409118

Anishkin, A., Gendel, V., Sharifi, N. A., Chiang, C. S., Shirinian, L., Guy, H. R., & Sukharev, S. (2003). On the conformation of the COOH-terminal domain of the large mechanosensitive channel MscL. *J Gen Physiol, 121*(3), 227-244.

Arkin, I. T., Sukharev, S. I., Blount, P., Kung, C., & Brunger, A. T. (1998). Helicity, membrane incorporation, orientation and thermal stability of the large conductance mechanosensitive ion channel from *E. coli*. *Biochim Biophys Acta, 1369*(1), 131-140.

Avanti Polar Lipids, I. TLC Solvent Systems - Lipid Migration. Retrieved from https://avantilipids.com/tech-support/analytical-procedures/tlc-solvent-systems/

Bae, C., Gnanasambandam, R., Nicolai, C., Sachs, F., & Gottlieb, P. A. (2013). Xerocytosis is caused by mutations that alter the kinetics of the mechanosensitive channel PIEZO1. *Proc Natl Acad Sci U S A, 110*(12), E1162-1168. doi:10.1073/pnas.1219777110

Baldwin, R. L. (1996). How Hofmeister ion interactions affect protein stability. *Biophysical Journal, 71*(4), 2056-2063.

Balleza, D., & Gomez-Lagunas, F. (2009). Conserved motifs in mechanosensitive channels MscL and MscS. *Eur Biophys J, 38*(7), 1013-1027. doi:10.1007/s00249-009-0460-y

Baratchi, S., Almazi, J. G., Darby, W., Tovar-Lopez, F. J., Mitchell, A., & McIntyre, P. (2016). Shear stress mediates exocytosis of functional TRPV4 channels in endothelial cells. *Cell Mol Life Sci, 73*(3), 649-666. doi:10.1007/s00018-015-2018-8

Basile, L., Pignatello, R., & Passirani, C. (2012). Active targeting strategies for anticancer drug nanocarriers. *Curr Drug Deliv, 9*(3), 255-268.

Bass, R. B., Strop, P., Barclay, M., & Rees, D. C. (2002). Crystal structure of *Escherichia coli* MscS, a voltage-modulated and mechanosensitive channel. *Science, 298*(5598), 1582-1587. doi:10.1126/science.1077945

Battle, A. R., Nomura, T., & Martinac, B. (2011). Cardiolipin Effects on the Gating Behaviour and Reconstitution of MscL and MscS. *Biophysical Journal, 100*(3), 279a. doi:10.1016/j.bpj.2010.12.1730

Battle, A. R., Petrov, E., Pal, P., & Martinac, B. (2009). Rapid and improved reconstitution of bacterial mechanosensitive ion channel proteins MscS and MscL into liposomes using a modified sucrose method. *FEBS Lett, 583*(2), 407-412. doi:10.1016/j.febslet.2008.12.033

Bavi, O., Cox, C. D., Vossoughi, M., Naghdabadi, R., Jamali, Y., & Martinac, B. (2016). Influence of Global and Local Membrane Curvature on Mechanosensitive Ion Channels: A Finite Element Approach. *Membranes (Basel), 6*(1). doi:10.3390/membranes6010014

Bavi, O., Vossoughi, M., Naghdabadi, R., & Jamali, Y. (2014). The effect of local bending on gating of MscL using a representative volume element and finite element simulation. *Channels (Austin), 8*(4), 344-349. doi:10.1146/annurev-arplant-043014-114700

Bavi, O., Vossoughi, M., Naghdabadi, R., & Jamali, Y. (2016). The Combined Effect of Hydrophobic Mismatch and Bilayer Local Bending on the Regulation of Mechanosensitive Ion Channels. *PLoS One, 11*(3), e0150578. doi:10.1371/journal.pone.0150578

Bazykin, G. A., & Kochetov, A. V. (2011). Alternative translation start sites are conserved in eukaryotic genomes. *Nucleic Acids Research, 39*(2), 567-577. doi:10.1093/nar/gkq806

Becker, M., & Kramer, R. (2015). MscCG from Corynebacterium glutamicum: functional significance of the C-terminal domain. *Eur Biophys J, 44*(7), 577-588. doi:10.1007/s00249-015-1041-x

Bentz, J., & Duzgunes, N. (1985). Fusogenic capacities of divalent cations and effect of liposome size. *Biochemistry, 24*(20), 5436-5443.

Bergfors, T. (2003). Seeds to crystals. *J Struct Biol, 142*(1), 66-76.

Betz, G., Aeppli, A., Menshutina, N., & Leuenberger, H. (2005). In vivo comparison of various liposome formulations for cosmetic application. *Int J Pharm, 296*(1-2), 44-54. doi:10.1016/j.ijpharm.2005.02.032

Birkner, J. P., Poolman, B., & Kocer, A. (2012). Hydrophobic gating of mechanosensitive channel of large conductance evidenced by single-subunit resolution. *Proc Natl Acad Sci U S A, 109*(32), 12944-12949. doi:10.1073/pnas.1205270109

Bligh, E. G., & Dyer, W. J. (1959). A rapid method of total lipid extraction and purification. *Can J Biochem Physiol, 37*(8), 911-917. doi:10.1139/o59-099

Blount, P., Schroeder, M. J., & Kung, C. (1997). Mutations in a bacterial mechanosensitive channel change the cellular response to osmotic stress. *J Biol Chem, 272*(51), 32150-32157.

Blount, P., Sukharev, S. I., Schroeder, M. J., Nagle, S. K., & Kung, C. (1996). Single residue substitutions that change the gating properties of a mechanosensitive channel in *Escherichia coli*. *Proc Natl Acad Sci U S A, 93*(21), 11652-11657.

Bottcher, B., Prazak, V., Rasmussen, A., Black, S. S., & Rasmussen, T. (2015). The Structure of YnaI Implies Structural and Mechanistic Conservation in the MscS Family of Mechanosensitive Channels. *Structure, 23*(9), 1705-1714. doi:10.1016/j.str.2015.06.023

Brohawn, S. G. (2015). How ion channels sense mechanical force: insights from mechanosensitive K2P channels TRAAK, TREK1, and TREK2. *Ann N Y Acad Sci, 1352*(1), 20-32. doi:10.1111/nyas.12874

Brohawn, S. G., Campbell, E. B., & MacKinnon, R. (2013). Domain-swapped chain connectivity and gated membrane access in a Fab-mediated crystal of the human TRAAK K+ channel. *Proc Natl Acad Sci U S A, 110*(6), 2129-2134. doi:10.1073/pnas.1218950110

Brohawn, S. G., del Marmol, J., & MacKinnon, R. (2012). Crystal structure of the human K2P TRAAK, a lipid- and mechano-sensitive K+ ion channel. *Science, 335*(6067), 436-441. doi:10.1126/science.1213808

Cao, E., Liao, M., Cheng, Y., & Julius, D. (2013). TRPV1 structures in distinct conformations reveal activation mechanisms. *Nature, 504*(7478), 113-118. doi:10.1038/nature12823

Caracciolo, G., & Amenitsch, H. (2012). Cationic liposome/DNA complexes: from structure to interactions with cellular membranes. *Eur Biophys J, 41*(10), 815-829. doi:10.1007/s00249-012-0830-8

Castile, J. D., & Taylor, K. M. G. (1999). Factors affecting the size distribution of liposomes produced by freeze–thaw extrusion. *Int J Pharm, 188*(1), 87-95. doi:http://dx.doi.org/10.1016/S0378-5173(99)00207-0

Chang, G., Spencer, R. H., Lee, A. T., Barclay, M. T., & Rees, D. C. (1998). Structure of the MscL homolog from *Mycobacterium tuberculosis*: a gated mechanosensitive ion channel. *Science, 282*(5397), 2220-2226.

Chang, H. I., & Yeh, M. K. (2012). Clinical development of liposome-based drugs: formulation, characterization, and therapeutic efficacy. *Int J Nanomedicine, 7*, 49-60. doi:10.2147/ijn.s26766

Chayen, N. E., Shaw Stewart, P. D., & Blow, D. M. (1992). Microbatch crystallization under oil — a new technique allowing many small-volume crystallization trials. *Journal of Crystal Growth, 122*(1), 176-180. doi:http://dx.doi.org/10.1016/0022-0248(92)90241-A

Chen, X., Cui, Q., Tang, Y., Yoo, J., & Yethiraj, A. (2008). Gating mechanisms of mechanosensitive channels of large conductance, I: a continuum mechanics-based hierarchical framework. *Biophys J, 95*(2), 563-580. doi:10.1529/biophysj.107.128488

Chi, G., Rohde, P. R., Ridone, P., Hankamer, B., Martinac, B., & Landsberg, M. J. (2015). Functional similarities between heterogeneously and homogenously expressed MscL constructs. *Eur Biophys J, 44*(7), 589-598. doi:10.1007/s00249-015-1062-5

Clarke, R. J., & Lupfert, C. (1999). Influence of anions and cations on the dipole potential of phosphatidylcholine vesicles: a basis for the Hofmeister effect. *Biophys J, 76*(5), 2614-2624. doi:10.1016/s0006-3495(99)77414-x

Colombo, G., Marrink, S. J., & Mark, A. E. (2003). Simulation of MscL gating in a bilayer under stress. *Biophys J, 84*(4), 2331-2337. doi:10.1016/s0006-3495(03)75038-3

Corey, D. P. (2003). New TRP channels in hearing and mechanosensation. *Neuron, 39*(4), 585-588.

Corry, B., Hurst, A. C., Pal, P., Nomura, T., Rigby, P., & Martinac, B. (2010). An improved open-channel structure of MscL determined from FRET confocal microscopy and simulation. *J Gen Physiol, 136*(4), 483-494. doi:10.1085/jgp.200910376

Corry, B., Rigby, P., Liu, Z. W., & Martinac, B. (2005). Conformational changes involved in MscL channel gating measured using FRET spectroscopy. *Biophys J, 89*(6), L49-51. doi:10.1529/biophysj.105.072009

Coste, B., Xiao, B., Santos, J. S., Syeda, R., Grandl, J., Spencer, K. S., . . . Patapoutian, A. (2012). Piezo proteins are pore-forming subunits of mechanically activated channels. *Nature, 483*(7388), 176-181. doi:10.1038/nature10812

Daum, B., Walter, A., Horst, A., Osiewacz, H. D., & Kuhlbrandt, W. (2013). Age-dependent dissociation of ATP synthase dimers and loss of inner-membrane cristae in mitochondria. *Proc Natl Acad Sci U S A, 110*(38), 15301-15306. doi:10.1073/pnas.1305462110

Davies, K. M., Anselmi, C., Wittig, I., Faraldo-Gómez, J. D., & Kühlbrandt, W. (2012). Structure of the yeast F(1)F(o)-ATP synthase dimer and its role in shaping the mitochondrial cristae. *Proceedings of the National Academy of Sciences of the United States of America, 109*(34), 13602-13607. doi:10.1073/pnas.1204593109

Delcour, A. H., Martinac, B., Adler, J., & Kung, C. (1989). Modified reconstitution method used in patch-clamp studies of *Escherichia coli* ion channels. *Biophysical Journal, 56*(3), 631-636.

Deplazes, E., Louhivuori, M., Jayatilaka, D., Marrink, S. J., & Corry, B. (2012). Structural investigation of MscL gating using experimental data and coarse grained MD simulations. *PLoS Comput Biol, 8*(9), e1002683. doi:10.1371/journal.pcbi.1002683

Doerner, J. F., Febvay, S., & Clapham, D. E. (2012). Controlled delivery of bioactive molecules into live cells using the bacterial mechanosensitive channel MscL. *Nat Commun, 3*, 990. doi:10.1038/ncomms1999

Dominy, C., & Andrews, D. (2003). Site-Directed Mutagenesis by Inverse PCR. In N. Casali & A. Preston (Eds.), *E. coli Plasmid Vectors* (Vol. 235, pp. 209-223): Humana Press.

Dong, Y. Y., Pike, A. C., Mackenzie, A., McClenaghan, C., Aryal, P., Dong, L., . . . Carpenter, E. P. (2015). K2P channel gating mechanisms revealed by structures of TREK-2 and a complex with Prozac. *Science, 347*(6227), 1256-1259. doi:10.1126/science.1261512

Dorwart, M. R., Wray, R., Brautigam, C. A., Jiang, Y., & Blount, P. (2010). *S. aureus* MscL is a pentamer in vivo but of variable stoichiometries in vitro: implications for detergent-solubilized membrane proteins. *PLoS Biol, 8*(12), e1000555. doi:10.1371/journal.pbio.1000555

Draper, W., & Liphardt, J. (2017). Origins of chemoreceptor curvature sorting in Escherichia coli. *Nat Commun, 8*, 14838. doi:10.1038/ncomms14838

Dreaden, E. C., Austin, L. A., Mackey, M. A., & El-Sayed, M. A. (2012). Size matters: gold nanoparticles in targeted cancer drug delivery. *Ther Deliv, 3*(4), 457-478.

Duan, J., Yu, Y., Li, Y., Yu, Y., Li, Y., Zhou, X., . . . Sun, Z. (2013). Toxic effect of silica nanoparticles on endothelial cells through DNA damage response via Chk1-dependent G2/M checkpoint. *PLoS One, 8*(4), e62087. doi:10.1371/journal.pone.0062087

Dudkina, N. V., Heinemeyer, J., Keegstra, W., Boekema, E. J., & Braun, H. P. (2005). Structure of dimeric ATP synthase from mitochondria: an angular association of monomers induces the strong curvature of the inner membrane. *FEBS Lett, 579*(25), 5769-5772. doi:10.1016/j.febslet.2005.09.065

Egusquiaguirre, S. P., Igartua, M., Hernandez, R. M., & Pedraz, J. L. (2012). Nanoparticle delivery systems for cancer therapy: advances in clinical and preclinical research. *Clin Transl Oncol, 14*(2), 83-93. doi:10.1007/s12094-012-0766-6

El Karim, I., McCrudden, M. T., Linden, G. J., Abdullah, H., Curtis, T. M., McGahon, M., . . . Lundy, F. T. (2015). TNF-alpha-Induced p38MAPK Activation Regulates TRPA1 and TRPV4 Activity in Odontoblast-like Cells. *Am J Pathol*. doi:10.1016/j.ajpath.2015.07.020

Elmore, D. E., & Dougherty, D. A. (2003). Investigating lipid composition effects on the mechanosensitive channel of large conductance (MscL) using molecular dynamics simulations. *Biophys J, 85*(3), 1512-1524. doi:10.1016/s0006-3495(03)74584-6

Erdahl, W. L., Stolyhwo, A., & Privett, O. S. (1973). Analysis of soybean lecithin by thin layer and analytical liquid chromatography. *Journal of the American Oil Chemists Society, 50*(12), 513-515. doi:10.1007/bf02640522

Fan, Y., & Zhang, Q. (2013). Development of liposomal formulations: From concept to clinical investigations. *Asian Journal of Pharmaceutical Sciences, 8*(2), 81-87. doi:http://dx.doi.org/10.1016/j.ajps.2013.07.010

Fink, M., Lesage, F., Duprat, F., Heurteaux, C., Reyes, R., Fosset, M., & Lazdunski, M. (1998). A neuronal two P domain K+ channel stimulated by arachidonic acid and polyunsaturated fatty acids. *EMBO J, 17*(12), 3297-3308. doi:10.1093/emboj/17.12.3297

Foo, A. (2014). Development of Novel Nanovalves for Liposomal Drug Delivery Based on Bacterial Mechanosensitive Channel of Large Conductance: The University of Queensland, Institute for Molecular Bioscience.

Foo, A., Battle, A. R., Chi, G., Hankamer, B., Landsberg, M. J., & Martinac, B. (2015). Inducible release of particulates from liposomes using the mechanosensitive channel of large conductance and L-alpha-lysophosphatidylcholine. *Eur Biophys J, 44*(7), 521-530. doi:10.1007/s00249-015-1055-4

Frottin, F., Martinez, A., Peynot, P., Mitra, S., Holz, R. C., Giglione, C., & Meinnel, T. (2006). The proteomics of N-terminal methionine cleavage. *Mol Cell Proteomics, 5*(12), 2336-2349. doi:10.1074/mcp.M600225-MCP200

Fuchs, B., Suss, R., Teuber, K., Eibisch, M., & Schiller, J. (2011). Lipid analysis by thin-layer chromatography--a review of the current state. *J Chromatogr A, 1218*(19), 2754-2774. doi:10.1016/j.chroma.2010.11.066

Furse, S., Wienk, H., Boelens, R., de Kroon, A. I., & Killian, J. A. (2015). *E. coli* MG1655 modulates its phospholipid composition through the cell cycle. *FEBS Lett, 589*(19 Pt B), 2726-2730. doi:10.1016/j.febslet.2015.07.043

Gabizon, A. A. (2001). Pegylated liposomal doxorubicin: metamorphosis of an old drug into a new form of chemotherapy. *Cancer Invest, 19*(4), 424-436.

Gamini, R., Sotomayor, M., Chipot, C., & Schulten, K. (2011). Cytoplasmic domain filter function in the mechanosensitive channel of small conductance. *Biophys J, 101*(1), 80-89. doi:10.1016/j.bpj.2011.05.042

Garnier, B., Tan, S., Gounou, C., Brisson, A. R., Laroche-Traineau, J., Jacobin-Valat, M. J., & Clofent-Sanchez, G. (2012). Development of a platform of antibody-presenting liposomes. *Biointerphases, 7*(1-4), 11. doi:10.1007/s13758-011-0011-9

Gavila, J., Guerrero, A., Climent, M. A., Fernandez, A., Gozalbo, F., Carrascosa, M., . . . Ruiz, A. (2015). Efficacy and safety of neoadjuvant chemotherapy with concurrent liposomal-encapsulated doxorubicin, paclitaxel and trastuzumab for human epidermal growth factor receptor 2-positive breast cancer in clinical practice. *Int J Clin Oncol, 20*(3), 480-489. doi:10.1007/s10147-014-0727-x

Ge, J., Li, W., Zhao, Q., Li, N., Chen, M., Zhi, P., . . . Yang, M. (2015). Architecture of the mammalian mechanosensitive Piezo1 channel. *Nature, 527*(7576), 64-69. doi:10.1038/nature15247

Ghosh, E., Kumari, P., Jaiman, D., & Shukla, A. K. (2015). Methodological advances: the unsung heroes of the GPCR structural revolution. *Nat Rev Mol Cell Biol, 16*(2), 69-81. doi:10.1038/nrm3933

http://www.nature.com/nrm/journal/v16/n2/abs/nrm3933.html#supplementary-information

Gibson, C. T., Raston, C. L., Boulos, R. A., Booth, I. R., Miller, S., Muller, A., & Lehtovirta-Morley, L. (2015). The evolution of bacterial mechanosensitive channels. *J Antibiot (Tokyo), 57*(3), 140-150. doi:10.1038/ja.2015.4

10.1016/j.ceca.2014.12.011

Gottlieb, P. A., & Sachs, F. (2012). Piezo1: properties of a cation selective mechanical channel. *Channels (Austin), 6*(4), 214-219. doi:10.4161/chan.21050

Grage, S. L., Keleshian, A. M., Turdzeladze, T., Battle, A. R., Tay, W. C., May, R. P., . . . Martinac, B. (2011). Bilayer-mediated clustering and functional interaction of MscL channels. *Biophys J, 100*(5), 1252-1260. doi:10.1016/j.bpj.2011.01.023

Gullingsrud, J., Kosztin, D., & Schulten, K. (2001). Structural determinants of MscL gating studied by molecular dynamics simulations. *Biophys J, 80*(5), 2074-2081. doi:10.1016/s0006-3495(01)76181-4

Gullingsrud, J., & Schulten, K. (2003). Gating of MscL studied by steered molecular dynamics. *Biophys J, 85*(4), 2087-2099. doi:10.1016/s0006-3495(03)74637-2

Guo, D., & Tropp, B. E. (2000). A second Escherichia coli protein with CL synthase activity. *Biochim Biophys Acta, 1483*(2), 263-274.

Hahn, A., Parey, K., Bublitz, M., Mills, D. J., Zickermann, V., Vonck, J., . . . Meier, T. (2016). Structure of a Complete ATP Synthase Dimer Reveals the Molecular Basis of Inner Mitochondrial Membrane Morphology. *Mol Cell, 63*(3), 445-456. doi:10.1016/j.molcel.2016.05.037

Hamilton, E. S., Schlegel, A. M., & Haswell, E. S. (2015). United in diversity: mechanosensitive ion channels in plants. *Annu Rev Plant Biol, 66*, 113-137. doi:10.1016/j.ceca.2014.12.011

10.1146/annurev-arplant-043014-114700

Harley, C. B., & Reynolds, R. P. (1987). Analysis of *E. coli* promoter sequences. *Nucleic Acids Research, 15*(5), 2343-2361.

Hase, C. C., Le Dain, A. C., & Martinac, B. (1995). Purification and functional reconstitution of the recombinant large mechanosensitive ion channel (MscL) of *Escherichia coli*. *J Biol Chem, 270*(31), 18329-18334.

Hase, C. C., Le Dain, A. C., & Martinac, B. (1997). Molecular dissection of the large mechanosensitive ion channel (MscL) of *E. coli*: mutants with altered channel gating and pressure sensitivity. *J Membr Biol, 157*(1), 17-25.

Hase, C. C., Minchin, R. F., Kloda, A., & Martinac, B. (1997). Cross-linking studies and membrane localization and assembly of radiolabelled large mechanosensitive ion channel (MscL) of *Escherichia coli*. *Biochem Biophys Res Commun, 232*(3), 777-782. doi:10.1006/bbrc.1997.6370

Haswell, E. S., Phillips, R., & Rees, D. C. (2011). Mechanosensitive channels: what can they do and how do they do it? *Structure, 19*(10), 1356-1369. doi:10.1016/j.str.2011.09.005

Hay, M., Thomas, D. W., Craighead, J. L., Economides, C., & Rosenthal, J. (2014). Clinical development success rates for investigational drugs. *Nat Biotech, 32*(1), 40-51. doi:10.1038/nbt.2786

http://www.nature.com/nbt/journal/v32/n1/abs/nbt.2786.html#supplementary-information

Heneweer, C., Gendy, S. E., & Penate-Medina, O. (2012). Liposomes and inorganic nanoparticles for drug delivery and cancer imaging. *Ther Deliv, 3*(5), 645-656.

Hirel, P. H., Schmitter, M. J., Dessen, P., Fayat, G., & Blanquet, S. (1989). Extent of N-terminal methionine excision from *Escherichia coli* proteins is governed by the side-chain length of the penultimate amino acid. *Proceedings of the National Academy of Sciences of the United States of America, 86*(21), 8247-8251.

Ho, S. N., Hunt, H. D., Horton, R. M., Pullen, J. K., & Pease, L. R. (1989). Site-directed mutagenesis by overlap extension using the polymerase chain reaction. *Gene, 77*(1), 51-59.

Ho, T. C., Horn, N. A., Huynh, T., Kelava, L., & Lansman, J. B. (2012). Evidence TRPV4 contributes to mechanosensitive ion channels in mouse skeletal muscle fibers. *Channels (Austin), 6*(4), 246-254. doi:10.4161/chan.20719

Hu, C. M., & Zhang, L. (2012). Nanoparticle-based combination therapy toward overcoming drug resistance in cancer. *Biochem Pharmacol, 83*(8), 1104-1111. doi:10.1016/j.bcp.2012.01.008

Hughes, S., McBain, S., Dobson, J., & El Haj, A. J. (2008). Selective activation of mechanosensitive ion channels using magnetic particles. *J R Soc Interface, 5*(25), 855-863. doi:10.1098/rsif.2007.1274

Hussain, S. T. (2012). Local application of gentamicin-containing collagen implant in the prophylaxis and treatment of surgical site infection following vascular surgery. *Int J Surg, 10 Suppl 1*, S5-9. doi:10.1016/j.ijsu.2012.05.015

Huynh, K. W., Cohen, M. R., Chakrapani, S., Holdaway, H. A., Stewart, P. L., & Moiseenkova-Bell, V. Y. (2014). Structural Insight into the Assembly of TRPV Channels. *Structure, 22*(2), 260-268. doi:10.1016/j.str.2013.11.008

Immordino, M. L., Dosio, F., & Cattel, L. (2006). Stealth liposomes: review of the basic science, rationale, and clinical applications, existing and potential. *Int J Nanomedicine, 1*(3), 297-315.

Iscla, I., Eaton, C., Parker, J., Wray, R., Kovacs, Z., & Blount, P. (2013). Improving the Design of a MscL-Based Triggered Nanovalve. *Biosens Bioelectron, 3*(1), 171-184. doi:10.3390/bios3010171

Iscla, I., Levin, G., Wray, R., Reynolds, R., & Blount, P. (2004). Defining the physical gate of a mechanosensitive channel, MscL, by engineering metal-binding sites. *Biophys J, 87*(5), 3172-3180. doi:10.1529/biophysj.104.049833

Iscla, I., Wray, R., & Blount, P. (2008). On the structure of the N-terminal domain of the MscL channel: helical bundle or membrane interface. *Biophys J, 95*(5), 2283-2291. doi:10.1529/biophysj.107.127423

Iscla, I., Wray, R., & Blount, P. (2011). An in vivo screen reveals protein-lipid interactions crucial for gating a mechanosensitive channel. *FASEB J, 25*(2), 694-702. doi:10.1096/fj.10-170878

Iscla, I., Wray, R., Blount, P., Larkins-Ford, J., Conery, A. L., Ausubel, F. M., . . . Slattery, A. D. (2015). A new antibiotic with potent activity targets MscL. *J Antibiot (Tokyo), 68*(7), 453-462. doi:10.1038/ja.2015.4

Jiko, C., Davies, K. M., Shinzawa-Itoh, K., Tani, K., Maeda, S., Mills, D. J., . . . Gerle, C. (2015). Bovine F1Fo ATP synthase monomers bend the lipid bilayer in 2D membrane crystals. *Elife, 4*, e06119. doi:10.7554/eLife.06119

Kamaraju, K., & Sukharev, S. (2008). The Membrane Lateral Pressure-Perturbing Capacity of Parabens and Their Effects on the Mechanosensitive Channel Directly Correlate with Hydrophobicity†. *Biochemistry, 47*(40), 10540-10550. doi:10.1021/bi801092g

Katzen, F., Peterson, T. C., & Kudlicki, W. (2009). Membrane protein expression: no cells required. *Trends in Biotechnology, 27*(8), 455-460. doi:10.1016/j.tibtech.2009.05.005

Kim, D. (1992). A mechanosensitive K+ channel in heart cells. Activation by arachidonic acid. *J Gen Physiol, 100*(6), 1021-1040.

Kim, D. (1993). Novel cation-selective mechanosensitive ion channel in the atrial cell membrane. *Circ Res, 72*(1), 225-231.

Kloda, A., Ghazi, A., & Martinac, B. (2006). C-terminal charged cluster of MscL, RKKEE, functions as a pH sensor. *Biophys J, 90*(6), 1992-1998. doi:10.1529/biophysj.105.075481

Kocer-Sagiroglu, A., Bulten, E., Walko, M., Feringa, B., Robillard, G., & Meijberg, W. (2005). A sensory valve in liposomal drug delivery systems. *J Control Release, 101*(1-3), 374-376.

Kocer, A. (2010). Functional liposomal membranes for triggered release. *Methods Mol Biol, 605*, 243-255. doi:10.1007/978-1-60327-360-2_16

Kocer, A. (2015). Mechanisms of mechanosensing-mechanosensitive channels, function and re-engineering. *Curr Opin Chem Biol, 29*, 120-127. doi:10.1016/j.cbpa.2015.10.006

Kocer, A., Walko, M., & Feringa, B. L. (2007). Synthesis and utilization of reversible and irreversible light-activated nanovalves derived from the channel protein MscL. *Nat Protoc, 2*(6), 1426-1437. doi:10.1038/nprot.2007.196

Kocer, A., Walko, M., Meijberg, W., & Feringa, B. L. (2005). A light-actuated nanovalve derived from a channel protein. *Science, 309*(5735), 755-758. doi:10.1126/science.1114760

Konijnenberg, A., Yilmaz, D., Ingolfsson, H. I., Dimitrova, A., Marrink, S. J., Li, Z., . . . Kocer, A. (2014). Global structural changes of an ion channel during its gating are followed by ion mobility mass spectrometry. *Proc Natl Acad Sci U S A, 111*(48), 17170-17175. doi:10.1073/pnas.1413118111

Koprowski, P., Grajkowski, W., Balcerzak, M., Filipiuk, I., Fabczak, H., & Kubalski, A. (2015). Cytoplasmic Domain of MscS Interacts with Cell Division Protein FtsZ: A Possible Non-Channel Function of the Mechanosensitive Channel in Escherichia Coli. *PLoS One, 10*(5), e0127029. doi:10.1371/journal.pone.0127029

Koprowski, P., & Kubalski, A. (2003). C termini of the Escherichia coli mechanosensitive ion channel (MscS) move apart upon the channel opening. *J Biol Chem, 278*(13), 11237-11245. doi:10.1074/jbc.M212073200

Kuang, Q., Purhonen, P., & Hebert, H. (2015). Two-Dimensional Crystallization Procedure, from Protein Expression to Sample Preparation. *BioMed Research International, 2015*, 693869. doi:10.1155/2015/693869

Kubek, M. J., Domb, A. J., & Veronesi, M. C. (2009). Attenuation of kindled seizures by intranasal delivery of neuropeptide-loaded nanoparticles. *Neurotherapeutics, 6*(2), 359-371. doi:10.1016/j.nurt.2009.02.001

Kung, C., Martinac, B., & Sukharev, S. (2010). Mechanosensitive channels in microbes. *Annu Rev Microbiol, 64*, 313-329. doi:10.1146/annurev.micro.112408.134106

Lambert, O., Levy, D., Ranck, J. L., Leblanc, G., & Rigaud, J. L. (1998). A new "gel-like" phase in dodecyl maltoside-lipid mixtures: implications in solubilization and reconstitution studies. *Biophysical Journal, 74*(2 Pt 1), 918-930.

Lammers, T., Kiessling, F., Hennink, W. E., & Storm, G. (2012). Drug targeting to tumors: principles, pitfalls and (pre-) clinical progress. *J Control Release, 161*(2), 175-187. doi:10.1016/j.jconrel.2011.09.063

Landsberg, M. J., Ruggles, J. L., Hussein, W. M., McGeary, R. P., Gentle, I. R., & Hankamer, B. (2010). Molecular packing of functionalized fluorinated lipids in Langmuir monolayers. *Langmuir, 26*(24), 18868-18873. doi:10.1021/la103743e

Lasala, R., Coudray, N., Abdine, A., Zhang, Z., Lopez-Redondo, M., Kirshenbaum, R., . . . Ubarretxena-Belandia, I. (2015). Sparse and incomplete factorial matrices to screen membrane protein 2D crystallization. *J Struct Biol, 189*(2), 123-134. doi:10.1016/j.jsb.2014.11.008

Ledford, H. (2011). Translational research: 4 ways to fix the clinical trial. *Nature, 477*, 526 - 528. doi:10.1038/477526a

Lee, L. M., & Liu, A. P. (2015). A microfluidic pipette array for mechanophenotyping of cancer cells and mechanical gating of mechanosensitive channels. *Lab Chip, 15*(1), 264-273. doi:10.1039/c4lc01218f

Leonenko, Z. V., Finot, E., Ma, H., Dahms, T. E. S., & Cramb, D. T. (2004). Investigation of Temperature-Induced Phase Transitions in DOPC and DPPC Phospholipid Bilayers Using Temperature-Controlled Scanning Force Microscopy. *Biophysical Journal, 86*(6), 3783-3793. doi:10.1529/biophysj.103.036681

Levchenko, T. S., Hartner, W. C., & Torchilin, V. P. (2012). Liposomes for cardiovascular targeting. *Ther Deliv, 3*(4), 501-514.

Levin, G., & Blount, P. (2004). Cysteine scanning of MscL transmembrane domains reveals residues critical for mechanosensitive channel gating. *Biophys J, 86*(5), 2862-2870. doi:10.1016/s0006-3495(04)74338-6

Levina, N., Totemeyer, S., Stokes, N. R., Louis, P., Jones, M. A., & Booth, I. R. (1999). Protection of *Escherichia coli* cells against extreme turgor by activation of MscS and MscL mechanosensitive channels: identification of genes required for MscS activity. *EMBO J, 18*(7), 1730-1737. doi:10.1093/emboj/18.7.1730

Lévy, D., Mosser, G., Lambert, O., Moeck, G. S., Bald, D., & Rigaud, J.-L. (1999). Two-Dimensional Crystallization on Lipid Layer: A Successful Approach for Membrane Proteins. *J Struct Biol, 127*(1), 44-52. doi:http://dx.doi.org/10.1006/jsbi.1999.4155

Li, J., Guo, J., Ou, X., Zhang, M., Li, Y., & Liu, Z. (2015). Mechanical coupling of the multiple structural elements of the large-conductance mechanosensitive channel during expansion. *112*(34), 10726-10731. doi:10.1073/pnas.1503202112

Li, Y., Wray, R., Eaton, C., & Blount, P. (2009). An open-pore structure of the mechanosensitive channel MscL derived by determining transmembrane domain interactions upon gating. *FASEB J, 23*(7), 2197-2204. doi:10.1096/fj.09-129296

Liao, M., Cao, E., Julius, D., & Cheng, Y. (2013). Structure of the TRPV1 ion channel determined by electron cryo-microscopy. *Nature, 504*(7478), 107-112. doi:10.1038/nature12822

Liu, Z., Gandhi, C. S., & Rees, D. C. (2009). Structure of a tetrameric MscL in an expanded intermediate state. *Nature, 461*(7260), 120-124. doi:10.1038/nature08277

Ma, J., Campbell, A., & Karlin, S. (2002). Correlations between Shine-Dalgarno Sequences and Gene Features Such as Predicted Expression Levels and Operon Structures. *Journal of Bacteriology, 184*(20), 5733-5745. doi:10.1128/jb.184.20.5733-5745.2002

Majeed, S., Ofek, G., Belachew, A., Huang, C.-c., Zhou, T., & Kwong, P. D. (2003). Enhancing Protein Crystallization through Precipitant Synergy. *Structure, 11*(9), 1061-1070. doi:http://dx.doi.org/10.1016/S0969-2126(03)00185-0

Majorek, K. A., Kuhn, M. L., Chruszcz, M., Anderson, W. F., & Minor, W. (2014). Double trouble—Buffer selection and His-tag presence may be responsible for nonreproducibility of biomedical experiments. *Protein Science, 23*(10), 1359-1368. doi:10.1002/pro.2520

Martinac, B. (2001). Mechanosensitive channels in prokaryotes. *Cell Physiol Biochem, 11*(2), 61-76.

Martinac, B. (2011). Bacterial mechanosensitive channels as a paradigm for mechanosensory transduction. *Cell Physiol Biochem, 28*(6), 1051-1060. doi:10.1159/000335842

Martinac, B., Nomura, T., Chi, G., Petrov, E., Rohde, P. R., Battle, A. R., . . . Landsberg, M. J. (2014). Bacterial mechanosensitive channels: models for studying mechanosensory transduction. *Antioxid Redox Signal, 20*(6), 952-969. doi:10.1089/ars.2013.5471

Mathworks. (2016, 22-Feb-2016). Clustering Using Gaussian Mixture Models. Retrieved from http://au.mathworks.com/help/stats/clustering-using-gaussian-mixture-models.html

Maurer, J. A., & Dougherty, D. A. (2001). A high-throughput screen for MscL channel activity and mutational phenotyping. *Biochim Biophys Acta, 1514*(2), 165-169.

McMahon, H. T., & Boucrot, E. (2015). Membrane curvature at a glance. *Journal of Cell Science, 128*(6), 1065-1070. doi:10.1242/jcs.114454

McPherson, A. (2004). Introduction to protein crystallization. *Methods, 34*(3), 254-265. doi:10.1016/j.ymeth.2004.03.019

Meyer, G. R., Gullingsrud, J., Schulten, K., & Martinac, B. (2006). Molecular dynamics study of MscL interactions with a curved lipid bilayer. *Biophys J, 91*(5), 1630-1637. doi:10.1529/biophysj.106.080721

Moe, P., & Blount, P. (2005). Assessment of potential stimuli for mechano-dependent gating of MscL: effects of pressure, tension, and lipid headgroups. *Biochemistry, 44*(36), 12239-12244. doi:10.1021/bi0509649

Moe, P. C., Levin, G., & Blount, P. (2000). Correlating a protein structure with function of a bacterial mechanosensitive channel. *J Biol Chem, 275*(40), 31121-31127. doi:10.1074/jbc.M002971200

Montemurro, F., Rossi, V., Geuna, E., Valabrega, G., Martinello, R., Milani, A., & Aglietta, M. (2012). Current status and future perspectives in the endocrine treatment of postmenopausal, hormone receptor-positive metastatic breast cancer. *Expert Opin Pharmacother, 13*(15), 2143-2156. doi:10.1517/14656566.2012.725723

Mortz, E., Krogh, T. N., Vorum, H., & Gorg, A. (2001). Improved silver staining protocols for high sensitivity protein identification using matrix-assisted laser desorption/ionization-time of flight analysis. *Proteomics, 1*(11), 1359-1363. doi:10.1002/1615-9861(200111)1:11<1359::aid-prot1359>3.0.co;2-q

Nakayama, Y., Mustapic, M., Ebrahimian, H., Wagner, P., Kim, J. H., Hossain, M. S., . . . Martinac, B. (2015). Magnetic nanoparticles for "smart liposomes". *Proc Natl Acad Sci U S A, 44*(8), 647-654. doi:10.1073/pnas.1503202112

10.1007/s00249-015-1059-0

Nannenga, B. L., Iadanza, M. G., Vollmar, B. S., & Gonen, T. (2013). Overview of Electron Crystallography of Membrane Proteins: Crystallization and Screening Strategies Using Negative Stain Electron Microscopy. *Current protocols in protein science / editorial board, John E. Coligan ... [et al.], 0 17*, 10.1002/0471140864.ps0471141715s0471140872. doi:10.1002/0471140864.ps1715s72

Nannenga, B. L., Shi, D., Hattne, J., Reyes, F. E., & Gonen, T. (2014). Structure of catalase determined by MicroED. *Elife, 3*, e03600. doi:10.7554/eLife.03600

Nguyen, T., Clare, B., Guo, W., & Martinac, B. (2005). The effects of parabens on the mechanosensitive channels of *E. coli*. *Eur Biophys J, 34*(5), 389-395. doi:10.1007/s00249-005-0468-x

Nicolas, J., Mura, S., Brambilla, D., Mackiewicz, N., & Couvreur, P. (2013). Design, functionalization strategies and biomedical applications of targeted biodegradable/biocompatible polymer-based nanocarriers for drug delivery. *Chem Soc Rev, 42*(3), 1147-1235. doi:10.1039/c2cs35265f

Nomura, T., Cranfield, C. G., Deplazes, E., Owen, D. M., Macmillan, A., Battle, A. R., . . . Martinac, B. (2012). Differential effects of lipids and lyso-lipids on the mechanosensitivity of the mechanosensitive channels MscL and MscS. *Proc Natl Acad Sci U S A, 109*(22), 8770-8775. doi:10.1073/pnas.1200051109

Northfelt, D. W., Martin, F. J., Working, P., Volberding, P. A., Russell, J., Newman, M., . . . Kaplan, L. D. (1996). Doxorubicin encapsulated in liposomes containing surface-bound polyethylene glycol: pharmacokinetics, tumor localization, and safety in patients with AIDS-related Kaposi's sarcoma. *J Clin Pharmacol, 36*(1), 55-63.

Oliver, P. M., Crooks, J. A., Leidl, M., Yoon, E. J., Saghatelian, A., & Weibel, D. B. (2014). Localization of Anionic Phospholipids in Escherichia coli Cells. *Journal of Bacteriology, 196*(19), 3386-3398. doi:10.1128/jb.01877-14

Ou, X., Blount, P., Hoffman, R. J., & Kung, C. (1998). One face of a transmembrane helix is crucial in mechanosensitive channel gating. *Proc Natl Acad Sci U S A, 95*(19), 11471-11475.

Oursel, D., Loutelier-Bourhis, C., Orange, N., Chevalier, S., Norris, V., & Lange, C. M. (2007). Lipid composition of membranes of Escherichia coli by liquid chromatography/tandem mass spectrometry using negative electrospray ionization. *Rapid Communications in Mass Spectrometry, 21*(11), 1721-1728. doi:10.1002/rcm.3013

Page, R., Grzechnik, S. K., Canaves, J. M., Spraggon, G., Kreusch, A., Kuhn, P., . . . Lesley, S. A. (2003). Shotgun crystallization strategy for structural genomics: an optimized two-tiered crystallization screen against the Thermotoga maritima proteome. *Acta Crystallogr D Biol Crystallogr, 59*(Pt 6), 1028-1037.

Park, K. H., Berrier, C., Martinac, B., & Ghazi, A. (2004). Purification and functional reconstitution of N- and C-halves of the MscL channel. *Biophys J, 86*(4), 2129-2136. doi:10.1016/s0006-3495(04)74272-1

Park, K. S., Han, M. H., Jang, H. K., Kim, K. A., Cha, E. J., Kim, W. J., . . . Kim, Y. (2013). The TREK2 Channel Is Involved in the Proliferation of 253J Cell, a Human Bladder Carcinoma Cell. *Korean J Physiol Pharmacol, 17*(6), 511-516. doi:10.4196/kjpp.2013.17.6.511

Patro, S. Y., & Przybycien, T. M. (1996). Simulations of reversible protein aggregate and crystal structure. *Biophysical Journal, 70*(6), 2888-2902.

Paulsen, C. E., Armache, J.-P., Gao, Y., Cheng, Y., & Julius, D. (2015). Structure of the TRPA1 ion channel suggests regulatory mechanisms. *Nature, 520*(7548), 511-517. doi:10.1038/nature14367

Perozo, E., Cortes, D. M., Sompornpisut, P., Kloda, A., & Martinac, B. (2002). Open channel structure of MscL and the gating mechanism of mechanosensitive channels. *Nature, 418*(6901), 942-948. doi:10.1038/nature00992

Perozo, E., Kloda, A., Cortes, D. M., & Martinac, B. (2001). Site-directed spin-labeling analysis of reconstituted Mscl in the closed state. *J Gen Physiol, 118*(2), 193-206.

Perozo, E., Kloda, A., Cortes, D. M., & Martinac, B. (2002). Physical principles underlying the transduction of bilayer deformation forces during mechanosensitive channel gating. *Nat Struct Biol, 9*(9), 696-703. doi:10.1038/nsb827

Petrache, H. I., Zemb, T., Belloni, L., & Parsegian, V. A. (2006). Salt screening and specific ion adsorption determine neutral-lipid membrane interactions. *Proc Natl Acad Sci U S A, 103*(21), 7982-7987. doi:10.1073/pnas.0509967103

Petrov, E., Palanivelu, D., Constantine, M., Rohde, P. R., Cox, C. D., Nomura, T., . . . Martinac, B. (2013). Patch-clamp characterization of the MscS-like mechanosensitive channel from *Silicibacter pomeroyi*. *Biophys J, 104*(7), 1426-1434. doi:10.1016/j.bpj.2013.01.055

Petrov, E., Rohde, P. R., & Martinac, B. (2011). Flying-patch patch-clamp study of G22E-MscL mutant under high hydrostatic pressure. *Biophys J, 100*(7), 1635-1641. doi:10.1016/j.bpj.2011.02.016

Phayre, A. N., Vanegas Farfano, H. M., & Hayes, M. A. (2002). Effects of pH Gradients on Liposomal Charge States Examined by Capillary Electrophoresis. *Langmuir, 18*(17), 6499-6503. doi:10.1021/la025625k

Phillips, R., Ursell, T., Wiggins, P., & Sens, P. (2009). Emerging roles for lipids in shaping membrane-protein function. *Nature, 459*(7245), 379-385. doi:10.1038/nature08147

Piano, D., El Alaoui, S., Korza, H. J., Filipek, R., Sabala, I., Haniewicz, P., . . . Bochtler, M. (2010). Crystallization of the Photosystem II core complex and its chlorophyll binding subunit CP43 from transplastomic plants of Nicotianatabacum. *Photosynthesis Research, 106*(3), 221-226. doi:10.1007/s11120-010-9597-x

Pike, A. C. W., Dong, Y.Y., Tessitore, A., Goubin, S., Strain-Damerell, C., Mukhopadhyay, S., Kupinska, K., Wang, D., Chalk, R., Berridge, G., Grieben, M., Shrestha, L., Ang, J.H., Mackenzie, A., Quigley, A., Bushell, S.R., Shintre, C.A., Faust, B., Chu, A., Dong, L., von Delft, F., Arrowsmith, C.H., Edwards, A.M., Bountra, C., Burgess-Brown, N.A., Carpenter, E.P. (2014). Crystal structure of human two pore domain potassium ion channel TREK1 (K2P2.1). Protein Data Bank.

Pircher, M., Mlineritsch, B., Fridrik, M. A., Dittrich, C., Lang, A., Petru, E., . . . Greil, R. (2015). Lapatinib-plus-pegylated liposomal doxorubicin in advanced HER2-positive breast cancer following trastuzumab: a phase II trial. *Anticancer Res, 35*(1), 517-521.

Pivetti, C. D., Yen, M. R., Miller, S., Busch, W., Tseng, Y. H., Booth, I. R., & Saier, M. H., Jr. (2003). Two families of mechanosensitive channel proteins. *Microbiol Mol Biol Rev, 67*(1), 66-85, table of contents.

Pliotas, C., Dahl, A. C., Rasmussen, T., Mahendran, K. R., Smith, T. K., Marius, P., . . . Naismith, J. H. (2015). The role of lipids in mechanosensation. *Nat Struct Mol Biol, 22*(12), 991-998. doi:10.1038/nsmb.3120

Posner, R. (2002). Liposomes. *J Drugs Dermatol, 1*(2), 161-164.

Powl, A. M., East, J. M., & Lee, A. G. (2003). Lipid-protein interactions studied by introduction of a tryptophan residue: the mechanosensitive channel MscL. *Biochemistry, 42*(48), 14306-14317. doi:10.1021/bi034995k

Powl, A. M., East, J. M., & Lee, A. G. (2005). Heterogeneity in the binding of lipid molecules to the surface of a membrane protein: hot spots for anionic lipids on the mechanosensitive channel of large conductance MscL and effects on conformation. *Biochemistry, 44*(15), 5873-5883. doi:10.1021/bi047439e

Powl, A. M., East, J. M., & Lee, A. G. (2007). Different effects of lipid chain length on the two sides of a membrane and the lipid annulus of MscL. *Biophys J, 93*(1), 113-122. doi:10.1529/biophysj.107.105130

Powl, A. M., East, J. M., & Lee, A. G. (2008a). Anionic phospholipids affect the rate and extent of flux through the mechanosensitive channel of large conductance MscL. *Biochemistry, 47*(14), 4317-4328. doi:10.1021/bi702409t

Powl, A. M., East, J. M., & Lee, A. G. (2008b). Importance of direct interactions with lipids for the function of the mechanosensitive channel MscL. *Biochemistry, 47*(46), 12175-12184. doi:10.1021/bi801352a

Pradhan, P., Giri, J., Rieken, F., Koch, C., Mykhaylyk, O., Doblinger, M., . . . Plank, C. (2010). Targeted temperature sensitive magnetic liposomes for thermo-chemotherapy. *J Control Release, 142*(1), 108-121. doi:10.1016/j.jconrel.2009.10.002

Preiss, M. R., & Bothun, G. D. (2011). Stimuli-responsive liposome-nanoparticle assemblies. *Expert Opin Drug Deliv, 8*(8), 1025-1040. doi:10.1517/17425247.2011.584868

Price, C. E., Kocer, A., Kol, S., van der Berg, J. P., & Driessen, A. J. (2011). In vitro synthesis and oligomerization of the mechanosensitive channel of large conductance, MscL, into a functional ion channel. *FEBS Lett, 585*(1), 249-254. doi:10.1016/j.febslet.2010.11.057

Qi, Y., Cheng, X., Han, W., Jo, S., Schulten, K., & Im, W. (2014). CHARMM-GUI PACE CG Builder for Solution, Micelle, and Bilayer Coarse-Grained Simulations. *J Chem Inf Model*. doi:10.1021/ci500007n

Raghunathan, K., Harris, P. T., & Arvidson, D. N. (2010). Trial by fire: are the crystals macromolecules? *Acta Crystallogr Sect F Struct Biol Cryst Commun, 66*(Pt 5), 615-620. doi:10.1107/s1744309110012078

Rodriguez, J. A., & Gonen, T. (2016). Chapter Fourteen - High-Resolution Macromolecular Structure Determination by MicroED, a cryo-EM Method. In R. A. Crowther (Ed.), *Methods in Enzymology* (Vol. Volume 579, pp. 369-392): Academic Press.

Rohacs, T. (2014). Phosphoinositide regulation of TRP channels. *Handb Exp Pharmacol, 223*, 1143-1176. doi:10.1007/978-3-319-05161-1_18

Romantsov, T., Battle, A. R., Hendel, J. L., Martinac, B., & Wood, J. M. (2010). Protein localization in *Escherichia coli* cells: comparison of the cytoplasmic membrane proteins ProP, LacY, ProW, AqpZ, MscS, and MscL. *J Bacteriol, 192*(4), 912-924. doi:10.1128/jb.00967-09

Rowe, I., Elahi, M., Huq, A., & Sukharev, S. (2013). The mechanoelectrical response of the cytoplasmic membrane of *Vibrio cholerae*. *J Gen Physiol, 142*(1), 75-85. doi:10.1085/jgp.201310985

Rui, H., Kumar, R., & Im, W. (2011). Membrane tension, lipid adaptation, conformational changes, and energetics in MscL gating. *Biophys J, 101*(3), 671-679. doi:10.1016/j.bpj.2011.06.029

Ruso, J. M., Besada, L., Martínez-Landeira, P., Seoane, L., Prieto, G., & Sarmiento, F. (2003). Interactions Between Liposomes and Cations in Aqueous Solution. *Journal of Liposome Research, 13*(2), 131-145. doi:10.1081/LPR-120020316

Saint, N., Lacapere, J. J., Gu, L. Q., Ghazi, A., Martinac, B., & Rigaud, J. L. (1998). A hexameric transmembrane pore revealed by two-dimensional crystallization of the large mechanosensitive ion channel (MscL) of *Escherichia coli*. *J Biol Chem, 273*(24), 14667-14670.

Salis, A., & Ninham, B. W. (2014). Models and mechanisms of Hofmeister effects in electrolyte solutions, and colloid and protein systems revisited. *Chem Soc Rev, 43*(21), 7358-7377. doi:10.1039/C4CS00144C

Sawada, Y., Murase, M., & Sokabe, M. (2012). The gating mechanism of the bacterial mechanosensitive channel MscL revealed by molecular dynamics simulations: from tension sensing to channel opening. *Channels (Austin), 6*(4), 317-331. doi:10.4161/chan.21895

Sawant, R. R., & Torchilin, V. P. (2012). Challenges in development of targeted liposomal therapeutics. *AAPS J, 14*(2), 303-315. doi:10.1208/s12248-012-9330-0

Schmidt-Krey, I. (2007). Electron crystallography of membrane proteins: two-dimensional crystallization and screening by electron microscopy. *Methods, 41*(4), 417-426. doi:10.1016/j.ymeth.2006.07.011

Shahidullah, M., Mandal, A., & Delamere, N. A. (2015). Damage to lens fiber cells causes TRPV4-dependent Src family kinase activation in the epithelium. *Exp Eye Res, 140*, 85-93. doi:10.1016/j.exer.2015.08.013

Sharif-Naeini, R., Dedman, A., Folgering, J. H., Duprat, F., Patel, A., Nilius, B., & Honore, E. (2008). TRP channels and mechanosensory transduction: insights into the arterial myogenic response. *Pflugers Arch, 456*(3), 529-540. doi:10.1007/s00424-007-0432-y

Shearman, G. C., Ces, O., Templer, R. H., & Seddon, J. M. (2006). Inverse lyotropic phases of lipids and membrane curvature. *Journal of Physics: Condensed Matter, 18*(28), S1105.

Shinoda, W., & Klein Michael, L. (2014). Effective interaction between small unilamellar vesicles as probed by coarse-grained molecular dynamics simulations *Pure and Applied Chemistry* (Vol. 86, pp. 215).

Sievers, F., Wilm, A., Dineen, D., Gibson, T. J., Karplus, K., Li, W., . . . Higgins, D. G. (2011). Fast, scalable generation of high-quality protein multiple sequence alignments using Clustal Omega. *Molecular systems biology, 7*, 539. Retrieved from http://europepmc.org/abstract/MED/21988835

http://europepmc.org/articles/PMC3261699?pdf=render

http://europepmc.org/articles/PMC3261699

http://www.pubmedcentral.nih.gov/picrender.fcgi?tool=EBI&pubmedid=21988835&action=stream&blobtype=pdf

http://www.pubmedcentral.nih.gov/articlerender.fcgi?tool=EBI&pubmedid=21988835

http://dx.doi.org/10.1038/msb.2011.75 doi:10.1038/msb.2011.75

Slingerland, M., Guchelaar, H. J., & Gelderblom, H. (2012). Liposomal drug formulations in cancer therapy: 15 years along the road. *Drug Discov Today, 17*(3-4), 160-166. doi:10.1016/j.drudis.2011.09.015

Soattin, L., Fiore, M., Gavazzo, P., Viti, F., Facci, P., Raiteri, R., . . . Vassalli, M. (2016). The biophysics of piezo1 and piezo2 mechanosensitive channels. *Biophys Chem, 208*, 26-33. doi:10.1016/j.bpc.2015.06.013

Stano, M., & Klucar, L. (2011). phiGENOME: An integrative navigation throughout bacteriophage genomes. *Genomics, 98*(5), 376-380. doi:http://dx.doi.org/10.1016/j.ygeno.2011.07.004

Steinbacher, S., Bass, R., Strop, P., & Rees, D. C. (2007) Structures of the Prokaryotic Mechanosensitive Channels MscL and MscS. *Vol. 58* (pp. 1-24).

Stuart, M. C. A., Koning, R. I., Oostergetel, G. T., & Brisson, A. (2004). Mechanism of formation of multilayered 2D crystals of the Enzyme IIC-mannitol transporter. *Biochimica et Biophysica Acta (BBA) - Biomembranes, 1663*(1–2), 108-116. doi:http://dx.doi.org/10.1016/j.bbamem.2004.02.008

Sukharev, S., Durell, S. R., & Guy, H. R. (2001). Structural models of the MscL gating mechanism. *Biophys J, 81*(2), 917-936. doi:10.1016/s0006-3495(01)75751-7

Sukharev, S. I., Blount, P., Martinac, B., Blattner, F. R., & Kung, C. (1994). A large-conductance mechanosensitive channel in *E. coli* encoded by mscL alone. *Nature, 368*(6468), 265-268. doi:10.1038/368265a0

Sukharev, S. I., Martinac, B., Arshavsky, V. Y., & Kung, C. (1993). Two types of mechanosensitive channels in the *Escherichia coli* cell envelope: solubilization and functional reconstitution. *Biophys J, 65*(1), 177-183. doi:10.1016/s0006-3495(93)81044-0

Svetina, S. (2015). Curvature-dependent protein–lipid bilayer interaction and cell mechanosensitivity. *European Biophysics Journal, 44*(7), 513-519. doi:10.1007/s00249-015-1046-5

Tahover, E., Patil, Y. P., & Gabizon, A. A. (2015). Emerging delivery systems to reduce doxorubicin cardiotoxicity and improve therapeutic index: focus on liposomes. *Anticancer Drugs, 26*(3), 241-258. doi:10.1097/cad.0000000000000182

Tajika, Y., Sakai, N., Tamura, T., Yao, M., Watanabe, N., & Tanaka, I. (2004). Crystal structure of hypothetical protein PH0828 from Pyrococcus horikoshii. *Proteins, 57*(4), 862-865. doi:10.1002/prot.20255

Tang, Y., Yoo, J., Yethiraj, A., Cui, Q., & Chen, X. (2008a). Gating mechanisms of mechanosensitive channels of large conductance, II: systematic study of conformational transitions. *Biophys J, 95*(2), 581-596. doi:10.1529/biophysj.107.128496

Tang, Y., Yoo, J., Yethiraj, A., Cui, Q., & Chen, X. (2008b). Mechanosensitive channels: insights from continuum-based simulations. *Cell Biochem Biophys, 52*(1), 1-18. doi:10.1007/s12013-008-9024-5

Theodoulou, M., & Hudis, C. (2004). Cardiac profiles of liposomal anthracyclines: greater cardiac safety versus conventional doxorubicin? *Cancer, 100*(10), 2052-2063. doi:10.1002/cncr.20207

Thoppil, R. J., Adapala, R. K., Cappelli, H. C., Kondeti, V., Dudley, A. C., Gary Meszaros, J., . . . Thodeti, C. K. (2015). TRPV4 channel activation selectively inhibits tumor endothelial cell proliferation. *Sci Rep, 5*, 14257. doi:10.1038/srep14257

Tomalik-Scharte, D., Lazar, A., Meins, J., Bastian, B., Ihrig, M., Wachall, B., . . . Fuhr, U. (2005). Dermal absorption of permethrin following topical administration. *Eur J Clin Pharmacol, 61*(5-6), 399-404. doi:10.1007/s00228-005-0932-7

Torchilin, V. P. (2005). Recent advances with liposomes as pharmaceutical carriers. *Nat Rev Drug Discov, 4*(2), 145-160. doi:10.1038/nrd1632

Torchilin, V. P. (2006). *Nanoparticulates as Drug Carriers*: Imperial College Press.

Traikia, M., Warschawski, D. E., Recouvreur, M., Cartaud, J., & Devaux, P. F. (2000). Formation of unilamellar vesicles by repetitive freeze-thaw cycles: characterization by electron microscopy and 31P-nuclear magnetic resonance. *Eur Biophys J, 29*(3), 184-195.

Trajkovski, B., Petersen, A., Strube, P., Mehta, M., & Duda, G. N. (2012). Intra-operatively customized implant coating strategies for local and controlled drug delivery to bone. *Adv Drug Deliv Rev, 64*(12), 1142-1151. doi:10.1016/j.addr.2012.05.016

Tsai, I. J., Liu, Z. W., Rayment, J., Norman, C., McKinley, A., & Martinac, B. (2005). The role of the periplasmic loop residue glutamine 65 for MscL mechanosensitivity. *Eur Biophys J, 34*(5), 403-412. doi:10.1007/s00249-005-0476-x

Tuxen, M. K., Cold, S., Tange, U. B., Balslev, E., & Nielsen, D. L. (2014). Phase II study of neoadjuvant pegylated liposomal doxorubicin and cyclophosphamide +/- trastuzumab followed by docetaxel in locally advanced breast cancer. *Acta Oncol, 53*(10), 1440-1445. doi:10.3109/0284186x.2014.921727

Ujwal, R., & Bowie, J. U. (2011). Crystallizing membrane proteins using lipidic bicelles. *Methods (San Diego, Calif.), 55*(4), 337-341. doi:10.1016/j.ymeth.2011.09.020

Uriarte-Pinto, M., Escolano-Pueyo, A., Gimeno-Ballester, V., Pascual-Martinez, O., Abad-Sazatornil, M. R., & Agustin-Ferrandez, M. J. (2016). Trastuzumab, non-pegylated liposomal-encapsulated doxorubicin and paclitaxel in the neoadjuvant setting of HER-2 positive breast cancer. *Int J Clin Pharm, 38*(2), 446-453. doi:10.1007/s11096-016-0278-5

van den Bogaart, G., Krasnikov, V., & Poolman, B. (2007). Dual-color fluorescence-burst analysis to probe protein efflux through the mechanosensitive channel MscL. *Biophys J, 92*(4), 1233-1240. doi:10.1529/biophysj.106.088708

van den Hoven, J. M., Van Tomme, S. R., Metselaar, J. M., Nuijen, B., Beijnen, J. H., & Storm, G. (2011). Liposomal drug formulations in the treatment of rheumatoid arthritis. *Mol Pharm, 8*(4), 1002-1015. doi:10.1021/mp2000742

Vanni, S., Hirose, H., Barelli, H., Antonny, B., & Gautier, R. (2014). A sub-nanometre view of how membrane curvature and composition modulate lipid packing and protein recruitment. *Nat Commun, 5*. doi:10.1038/ncomms5916

Vasquez, V., Sotomayor, M., Cortes, D. M., Roux, B., Schulten, K., & Perozo, E. (2008). Three-dimensional architecture of membrane-embedded MscS in the closed conformation. *J Mol Biol, 378*(1), 55-70. doi:10.1016/j.jmb.2007.10.086

Vitrac, H., MacLean, D. M., Jayaraman, V., Bogdanov, M., & Dowhan, W. (2015). Dynamic membrane protein topological switching upon changes in phospholipid environment. *Proceedings of the National Academy of Sciences of the United States of America, 112*(45), 13874-13879. doi:10.1073/pnas.1512994112

Vitzthum, C., Clauss, W. G., & Fronius, M. (2015). Mechanosensitive activation of CFTR by increased cell volume and hydrostatic pressure but not shear stress. *Biochim Biophys Acta, 1848*(11 Pt A), 2942-2951. doi:10.1016/j.bbamem.2015.09.009

Walton, T. A., & Rees, D. C. (2013). Structure and stability of the C-terminal helical bundle of the *E. coli* mechanosensitive channel of large conductance. *Protein Sci, 22*(11), 1592-1601. doi:10.1002/pro.2360

Wang, C. X., Ge, H. X., Hou, X. P., & Li, Y. Q. (2007). Roles of larger conductance mechanosensitive channels (MscL) in sporulation and Act secretion in *Streptomyces coelicolor*. *J Basic Microbiol, 47*(6), 518-524. doi:10.1002/jobm.200700238

Wang, W., Black, S. S., Edwards, M. D., Miller, S., Morrison, E. L., Bartlett, W., . . . Booth, I. R. (2008). The structure of an open form of an *E. coli* mechanosensitive channel at 3.45 A resolution. *Science, 321*(5893), 1179-1183. doi:10.1126/science.1159262

Wang, Y., Liu, Y., Deberg, H. A., Nomura, T., Hoffman, M. T., Rohde, P. R., . . . Selvin, P. R. (2014). Single molecule FRET reveals pore size and opening mechanism of a mechano-sensitive ion channel. *Elife, 3*, e01834. doi:10.7554/eLife.01834

Weinberg, B. D., Blanco, E., & Gao, J. (2008). Polymer implants for intratumoral drug delivery and cancer therapy. *J Pharm Sci, 97*(5), 1681-1702. doi:10.1002/jps.21038

Wells, J. A., Vasser, M., & Powers, D. B. (1985). Cassette mutagenesis: an efficient method for generation of multiple mutations at defined sites. *Gene, 34*(2-3), 315-323.

Wiener, M. C. (2004). A pedestrian guide to membrane protein crystallization. *Methods, 34*(3), 364-372. doi:10.1016/j.ymeth.2004.03.025

Williamson, M. P. (1994). The structure and function of proline-rich regions in proteins. *Biochemical Journal, 297*(Pt 2), 249-260.

Wilson, M. E., Maksaev, G., & Haswell, E. S. (2013). MscS-like Mechanosensitive Channels in Plants and Microbes. *Biochemistry, 52*(34), 5708-5722. doi:10.1021/bi400804z

Wolff, A. C., Wang, M., Li, H., Pins, M. R., Pretorius, F. J., Rowland, K. M., . . . Davidson, N. E. (2010). Phase II trial of pegylated liposomal doxorubicin plus docetaxel with and without trastuzumab in metastatic breast cancer: Eastern Cooperative Oncology Group trial E3198. *Breast Cancer Res Treat, 121*(1), 111-120. doi:10.1007/s10549-010-0838-7

Yang, L. M., & Blount, P. (2011). Manipulating the permeation of charged compounds through the MscL nanovalve. *FASEB J, 25*(1), 428-434. doi:10.1096/fj.10-170076

Yang, L. M., Wray, R., Parker, J., Wilson, D., Duran, R. S., & Blount, P. (2012). Three Routes To Modulate the Pore Size of the MscL Channel/Nanovalve. *ACS Nano, 6*(2), 1134-1141. doi:10.1021/nn203703j

Yang, Z. (2009). Hofmeister effects: an explanation for the impact of ionic liquids on biocatalysis. *J Biotechnol, 144*(1), 12-22. doi:10.1016/j.jbiotec.2009.04.011

Yilmaz, D., Dimitrova, A. I., Walko, M., & Kocer, A. (2015). Study of light-induced MscL gating by EPR spectroscopy. *Eur Biophys J, 44*(7), 557-565. doi:10.1007/s00249-015-1063-4

Yoshimura, K., Batiza, A., & Kung, C. (2001). Chemically charging the pore constriction opens the mechanosensitive channel MscL. *Biophys J, 80*(5), 2198-2206. doi:10.1016/s0006-3495(01)76192-9

Yoshimura, K., Batiza, A., Schroeder, M., Blount, P., & Kung, C. (1999). Hydrophilicity of a single residue within MscL correlates with increased channel mechanosensitivity. *Biophys J, 77*(4), 1960-1972. doi:10.1016/s0006-3495(99)77037-2

Yoshimura, K., Nomura, T., & Sokabe, M. (2004). Loss-of-function mutations at the rim of the funnel of mechanosensitive channel MscL. *Biophys J, 86*(4), 2113-2120. doi:10.1016/s0006-3495(04)74270-8

Yoshimura, K., & Sokabe, M. (2010). Mechanosensitivity of ion channels based on protein-lipid interactions. *J R Soc Interface, 7 Suppl 3*, S307-320. doi:10.1098/rsif.2010.0095.focus

Yoshimura, K., Usukura, J., & Sokabe, M. (2008). Gating-associated conformational changes in the mechanosensitive channel MscL. *Proc Natl Acad Sci U S A, 105*(10), 4033-4038. doi:10.1073/pnas.0709436105

Zhong, D., & Blount, P. (2013). Phosphatidylinositol Is Crucial for the Mechanosensitivity of *Mycobacterium tuberculosis* MscL. *Biochemistry, 52*(32), 5415-5420. doi:10.1021/bi400790j

Zhu, L., Wu, J., Liu, L., Liu, Y., Yan, Y., Cui, Q., & Chen, X. (2016). Gating mechanism of mechanosensitive channel of large conductance: a coupled continuum mechanical-continuum solvation approach. *Biomech Model Mechanobiol*. doi:10.1007/s10237-016-0783-4

Zou, Y., Chintamanani, S., He, P., Fukushige, H., Yu, L., Shao, M., . . . Zhou, J. M. (2015). A gain-of-function mutation in Msl10 triggers cell death and wound-induced hyperaccumulation of JA in Arabidopsis. *J Integr Plant Biol*. doi:10.1111/jipb.12427